

~~CONFIDENTIAL~~

DECLASSIFIED

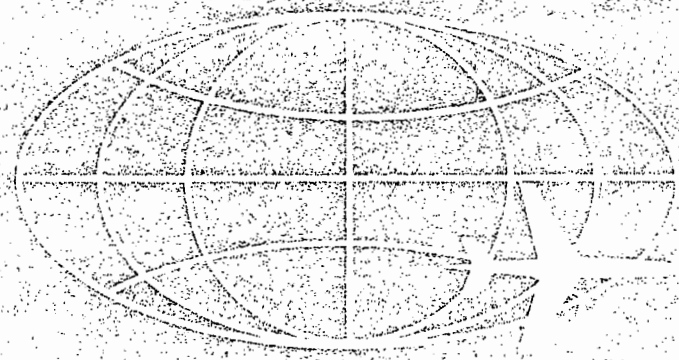
APEX - 573

AIRCRAFT
NUCLEAR
PROPULSION
DEPARTMENT

LOAN COPY
TECHNICAL LIBRARY

LC932

Cy 1



H. Peterson - 12-9-88

INTERIM REPORT
ON ADVANCED CORE TEST HAZARDS

Classification cancelled, or changed to
BY authority of
By

UNCLASSIFIED

MAY 20 1977

This Document/Material Has Been Reviewed
And determined to Contain
NO CLASSIFIED OR SENSITIVE INFORMATION
Classification Reviewer: K.C. Gerard

K.C. Gerard
Signature Date

CI 15378

DECLASSIFIED

GENERAL ELECTRIC

CONFIDENTIAL

CI 15378

LEGAL NOTICE

This report was prepared as an account of Government sponsored work. Neither the United States, nor the Commission, nor the Air Force, nor any person acting on behalf of the Commission or the Air Force:

- A. Makes any warranty or representation, express or implied, with respect to the accuracy, completeness, or usefulness of the information contained in this report, or that the use of any information, apparatus, method, or process disclosed in this report may not infringe privately owned rights; or
- B. Assumes any liabilities with respect to the use of, or for damages resulting from the use of any information, apparatus, method, or process disclosed in this report.

As used in the above "person acting on behalf of the Commission or Air Force" includes any employee or contractor of the Commission or Air Force to the extent that such employee or contractor prepares, handles, or distributes, or provides access to, any information pursuant to his employment or contract with the Commission or Air Force.

~~CONFIDENTIAL~~

~~SECRET~~

APEX - 573

Special Distribution

DECLASSIFIED

INTERIM REPORT ON ADVANCED CORE TEST HAZARDS

September 26, 1960

United States Air Force
United States Atomic Energy Commission

Contract No. AF33(600)-38062
Contract No. AT (11-1)-171

GENERAL  ELECTRIC
AIRCRAFT NUCLEAR PROPULSION DEPARTMENT
Cincinnati 15, Ohio

Classification Cancelled (or changed to)

by *J. H. Baker* of *SAIC* *6-24-61*

to *SECRET* *6-18-62*

~~CONFIDENTIAL~~

~~SECRET~~
RESTRICTED DATA

THIS DOCUMENT CONTAINS RESTRICTED DATA AS DEFINED BY THE ATOMIC ENERGY ACT OF 1954 AND (WHEN APPLICABLE) THE DISCLOSURE OF ITS CONTENTS IN ANY MANNER TO AN UNAUTHORIZED PERSON IS PROHIBITED.

~~CONFIDENTIAL~~

~~CONFIDENTIAL~~
~~SECRET~~

FORM 8-53

SECRET

CONFIDENTIAL

CONFIDENTIAL

CONFIDENTIAL

SECRET

~~CONFIDENTIAL~~
~~SECRET~~

~~CONFIDENTIAL~~

~~SECRET~~

DECLASSIFIED

DISTRIBUTION

EXTERNAL

- 1-30 AEC-LAROO
- 31 Idaho Test Division, AEC-LAROO

INTERNAL

- | | |
|-----------------------|----------------------------------|
| 32 S.W. Ahrends | 59 P.E. Lowe |
| 33 E.A. Aitken | 60 R.C. Mann |
| 34 F.A. Aschenbrenner | 61 L. Masson |
| 35 J.K. Baker | 62 H.F. Matthiesen |
| 36 R.E. Baker | 63 F.W. Mezger |
| 37 N. Bifano | 64 S.H. Minnich |
| 38 B. Blumberg | 65 T.R. Mitchell |
| 39 V.P. Calkins | 66 C.W. Moon |
| 40 C.B. Cannon | 67 J.W. Morfitt |
| 41 J.W. Conley | 68 J. Neuhoff |
| 42 A.R. Crocker | 69 G.W. Newton |
| 43 J. Epstein | 70 R.B. O'Brien |
| 44 L.C. Faupell | 71 J.D. Platt |
| 45 L.A. Feathers | 72 W.G. Root |
| 46 P.G. Fischer | 73 D.F. Shaw |
| 47 A.E. Focke | 74 C.L. Storrs |
| 48 D.L. Francis | 75 F.G. Tabb |
| 49 C.C. Gamertsfelder | 76 R. Tallman |
| 50 C.R. Gray | 77 G. Thornton |
| 51 W.J. Koshuba | 78 H.C. Towle |
| 52 J.M. Krase | 79 J. Trice |
| 53 R.K. Lane | 80 J.I. Trussell |
| 54 D.C. Layman | 81 J.E. VanHoomissen |
| 55 M.C. Leverett | 82 R.E. Wood |
| 56 S.J. Levine | 83 L.F. Yost |
| 57 F.C. Linn | |
| 58 W.H. Long | 84 Reports Library - Idaho |
| | 85-88 Reports Library - Evendale |

DECLASSIFIED

~~SECRET~~

~~CONFIDENTIAL~~

~~CONFIDENTIAL~~

~~SECRET~~

~~CONFIDENTIAL~~

ABSTRACT

This report contains a description of the Advanced Core Test assembly and an evaluation of the hazards associated with the operation of this assembly.

~~CONFIDENTIAL~~

~~SECRET~~

~~CONFIDENTIAL~~

~~CONFIDENTIAL~~

CONTENTS

	Page
1. Introduction	7
2. System Description	9
2.1 Component Description	11
2.1.1 Reactor	11
2.1.2 Engines	45
2.1.3 Shield	47
2.1.4 Controls and Instrumentation	52
2.1.5 Auxiliary Equipment	83
2.1.6 Effluent-Cleaning Equipment	84
2.2 Assembly Procedure	86
2.3 Disassembly Procedure	87
3. Test Requirements	89
3.1 Low-Power Operations at LPT	89
3.2 Cold-System Checkout	89
3.3 Chemical Operation at FET	90
3.4 Low-Power Nuclear Operation at FET	90
3.5 Full-Power-Range Operations at FET	91
4. Operating Procedures	93
4.1 Checkout	93
4.2 Operation	93
4.2.1 Operation on Chemical Power Only	93
4.2.2 Reactor Startup	94
4.2.3 Transfer from Chemical to Nuclear Power	94
4.2.4 All-Nuclear Operation	94
4.2.5 Transfer from Nuclear to Chemical Power	94
4.2.6 Nuclear Start	95
4.2.7 Power Plant Shutdown	95
5. Release Mechanism for Radioactive Materials	97
5.1 Normal Operations	97
5.1.1 Recoil	97
5.1.2 Diffusion	98
5.1.3 Water-Vapor Corrosion	98
5.1.4 Effect of Coating on Mechanism	98
5.1.5 Conclusions	99
5.1.6 Comparison of Laboratory Release Measurements With In-Pile Measurements	99
5.2 Operational Accidents	100
5.2.1 Startup Runaway	100
5.2.2 Power-Range Failures	109
5.2.3 Local Overheating	134
5.3 After-Shutdown Meltdown	147

100-200000

	Page
6. Hazards Calculations	157
6.1 Assumptions	157
6.2 Calculated Doses for Normal Operations	157
6.3 Estimated Off-Site Dose	174
6.3.1 General	174
6.3.2 Inhabitants and Dairy Cattle	175
6.3.3 Dose Distributions by Sectors	175
6.3.4 Estimation of Dose to Off-Site Personnel - Normal Operation	178
6.4 Calculated Doses for Major Accidents	183
6.5 Doses for Detectable Localized Melts	186
7. Conclusions	187
8. Appendix	189
8.1 Site and Facilities	189
8.1.1 General Description	189
8.1.2 Test Facilities	189
8.2 Geophysical Characteristics at NRTS	195
8.2.1 Hydrology and Disposition of Liquid Wastes	195
8.2.2 Geology	196
8.2.3 Seismology	196
8.2.4 Climatological Data	197
8.3 Area Surveys and Meteorological Control	220
8.4 Current Hazard Studies	221
8.4.1 Reactor Effluent Dilution	221
8.4.2 Limited-Melt Experiments	223
8.4.3 Sub-LIME Test	226
8.4.4 Air-Cleaning Measurements	226
8.4.5 TREAT Testing of Fuel Elements	227
8.4.6 Impact-Deformation Experiments	227
8.5 Methods and Formulae for Hazards Calculations	227
8.5.1 Hazards Formulae	227
8.5.2 Methods and Assumptions Used in Runaway Analysis	230
8.5.3 Reactivity Effects of Melted Fuel Redistributions	238
8.6 Reactor Physics	239
8.6.1 Introduction	239
8.6.2 Cross Sections	239
8.6.3 Spectra	245
8.6.4 Delayed Neutrons	245

~~CONFIDENTIAL~~
~~SECRET~~

DECLASSIFIED

1. INTRODUCTION

This report presents an evaluation of the radiological safety aspects of the testing planned for the D140E1 Advanced Core Test assembly. The test assembly is a prototype of a direct-cycle divided-shield aircraft power plant in which the engine air is directly heated by the reactor and the shielding is divided between the reactor and the crew compartment in order to minimize the total shield weight. The assembly consists of reactor, shield, X211 engine with chemical interburners, and accessory equipment. The reactor contains ceramic fuel-moderator elements consisting of beryllium oxide impregnated with a uranium oxide - yttrium oxide fuel additive.

The test program includes (1) preliminary operation with the chemical interburners, (2) low-power nuclear tests at powers to 10 megawatts to obtain aerothermal and nuclear data, and (3) operation at full power for 1000 hours to determine performance and endurance capabilities. The reactor power during most of these tests will be that required to simulate reactor conditions during cruise, about 50 megawatts; but some tests will be made at 110 megawatts to simulate emergency conditions. The energy accumulation used in the calculations of fission product inventory was based on a power level of 50 megawatts, whereas the analyses of potential system malfunctions are based on power levels near 100 megawatts. In normal service the temperature levels throughout the system are the same for both power levels, the difference in power being produced by the difference between the density of air at 35,000 feet altitude and air at 5,000 feet altitude, which are the design-point altitudes for the cruise and emergency conditions, respectively. Cruise conditions will be simulated in Idaho by restricting airflow to the compressor or by bypassing air around the reactor.

Both the continuous fission product release rates and the physical characteristics of the fuel that were used in the analyses reported herein are based on experimental data acquired from many laboratory and in-pile engineering tests of fuel elements and fuel assemblies.

Release of radioactive material during ACT operation occurs under the following circumstances.

1. Normal operation:
Acceptable low-level release of fission products from the fuel elements.
2. Abnormal operation:
 - a. Local overheating of one or more fuel tubes as a result of air blockage.
 - b. A meltdown caused by failure of afterheat-removal mechanism.
 - c. A nuclear excursion caused by control failures or core deformation resulting from meltdown.

The analysis provided in the report shows that the normal low-level release of fission products produces only a fraction of the tolerance dose for essentially unrestricted operations. The analysis also shows that by proper exercise of safety measures and operational control, the hazard involved with any of the abnormal situations discussed can be limited to acceptable levels.

7
~~SECRET~~

DECLASSIFIED

2. SYSTEM DESCRIPTION

The Advanced Core Test assembly, shown in Figure 2.1, is a single-engine integral in-line arrangement in which a compressor and turbine of the existing X211 design are used with a shielded ceramic reactor. The compressor and turbine are connected by a hollow, cooled shaft. The reactor, side shield, end shields, and chemical interburners are arranged concentrically around the shaft. Reactor control is accomplished with multiple poison rods in the reflector that are moved by actuators symmetrically distributed around the rear frame of the compressor.

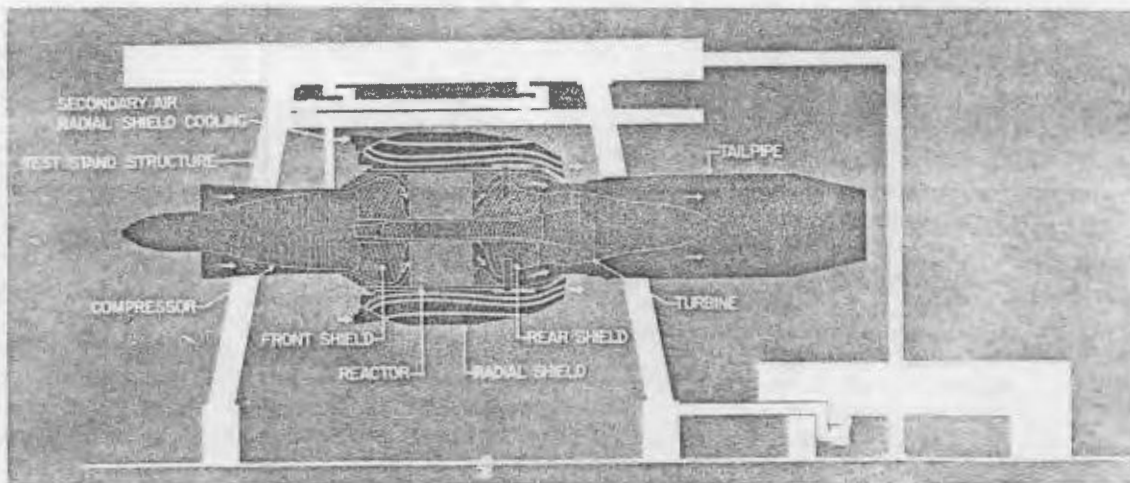


Fig. 2.1 - D140E1 Advanced Core Test assembly

Primary air flows from the compressor discharge annulus through an annular passage in the forward shield and into the reactor. Air, discharged from the reactor through a similar annular passage in the rear shield, flows through the chemical interburner section and then into the turbine. After expanding through the turbine, the air passes through the afterburner and tailcone and is exhausted through a stack to the atmosphere. A portion of the primary air bypasses the reactor core and provides cooling for the front shield, rear shield, reflector, control rods, and associated mechanical structure. Subsequently, this air is collected in the rear annular duct, where it is mixed with reactor discharge air. The mixture then enters the turbine. Turbine cooling air and seal leakage air are bled from the compressor. The hollow shaft is cooled by ninth-stage compressor bleed air.

The mechanical, thermodynamic, and nuclear characteristics of the assembly are listed in Table 2.1.

UNCLASSIFIED
SECRET

TABLE 2.1

ACT TEST ASSEMBLY
MECHANICAL, THERMODYNAMIC, AND NUCLEAR CHARACTERISTICS

<u>Mechanical</u>	
Engine type	X211
Engine speed (military), rpm	5000
Test assembly maximum diameter, inches	111
Test assembly length, inches	427
Test assembly design life, hours	1000
Reactor active core outside diameter, inches	45
Reactor active core inside diameter, inches	17.2
Reactor active core length, inches	30
<u>Fuel tubes</u>	
Base material	BeO
Fuel additive	55 Y ₂ O ₃ - 45 UO ₂
Number of tubes	170,000
Inside diameter, inches	0.167
Across flats, inches	0.249
Clad material	85 ZrO ₂ - 15 Y ₂ O ₃
Clad thickness, inch	0.003
<u>Control rods</u>	
Number	48
Material	Eu ₂ O ₃ -Ni
Length of stroke, inches	24
<u>Thermodynamic</u>	
Engine airflow, lb/sec	173
Reactor power, mw	50
Engine compressor ratio	12:1
Turbine inlet temperature, °F	1740
Turbine-to-compressor pressure ratio	0.75
Compressor discharge temperature, °F	583
Compressor discharge pressure, lb/in. ²	73.3
Reactor active core airflow area, in. ²	545
Reactor-outlet-to-inlet pressure ratio	0.857
Reactor inlet air temperature, °F	583
Reactor inlet pressure, psia	69.2
Total reactor flow, lb/sec	154.6
Fuel tube airflow Mach No.	0.121
Average fuel element discharge temperature, °F	1896
Average-fuel-channel maximum surface temperature, °F	2210
Maximum estimated fuel element surface temperature, °F	2500
Maximum estimated fuel element temperature, °F	2530
<u>Nuclear</u>	
Excess multiplication constant, % Δk	
Clean core at 68°F	+ 5.9
Poisoned, depleted core at 2000°F	+ 0.7
Control capacity	- 9.0
Fueled core composition	
Fuel loading (93.2% enriched uranium), lb	192
Volume fractions	
Void	0.418
Fuel elements	0.582
Reflector thicknesses, inches	
Front - Be	3.25
BeO	1.50
Rear - BeO	3.0
Radial - BeO	8.5
Fuel element average power density, Btu/in. ³ -sec	2.04
Active core average power density, Btu/in. ³ -sec	1.14

UNCLASSIFIED
SECRET

2.1 COMPONENT DESCRIPTION

2.1.1 REACTOR

2.1.1.1 General Description

The general configuration of the D140E1 reactor is shown in Figures 2.2, 2.3, and 2.4, and dimensions are given in Table 2.2. The reactor is composed of an active core, a central island, side and end reflectors, and external structure.

The active core is an annular cylindrical region containing beryllium oxide fuel elements. Each fuel element is a small hexagonal tube, 0.249 inch across flats and 4.28 inches long with an inside diameter of 0.167 inch. There are nearly 25,000 airflow passages through the reactor and approximately 170,000 separate fuel elements in the active core.

The central island, surrounded by the active core, provides a through-hole for the shaft of the turbomachinery. The island is composed of an annular region of aluminum oxide tubes and bars (with the same over-all dimensions as the fuel elements), a metal liner, and a metal shaft tunnel. The alumina tubes and bars provide thermal insulation

TABLE 2.2
SUMMARY OF D140E1 REACTOR DIMENSIONS
(Dimensions in inches)

Radial Dimensions	
Shaft OD	11.25
Tunnel ID	12.50
Tunnel OD	12.63
Liner ID	13.37
Inner reflector ID (equivalent)	13.64
Inner reflector thickness (Al_2O_3)	1.79
Active core ID	17.22
Active core OD	45.00
Radial reflector thickness (BeO)	8.50
Reflector OD	62.0
Pressure pad thickness (nominal)	0.25
Pressure pads OD	62.50
Spring gap thickness	1.625
Structural shell ID	65.75
Structural shell thickness	0.125
Over-all diameter of structural shell (nominal)	66.00
Longitudinal Dimensions	
Forward hardware (screen and instrumentation)	0.50
Front reflector (Be)	3.25
Expansion gap	0.20
Forward transition (BeO Adapter)	1.50
Active core	30.00
Rear reflector (BeO)	1.50
Rear support structure	2.50
Total reactor length (nominal)	39.45

~~CONFIDENTIAL~~
~~SECRET~~

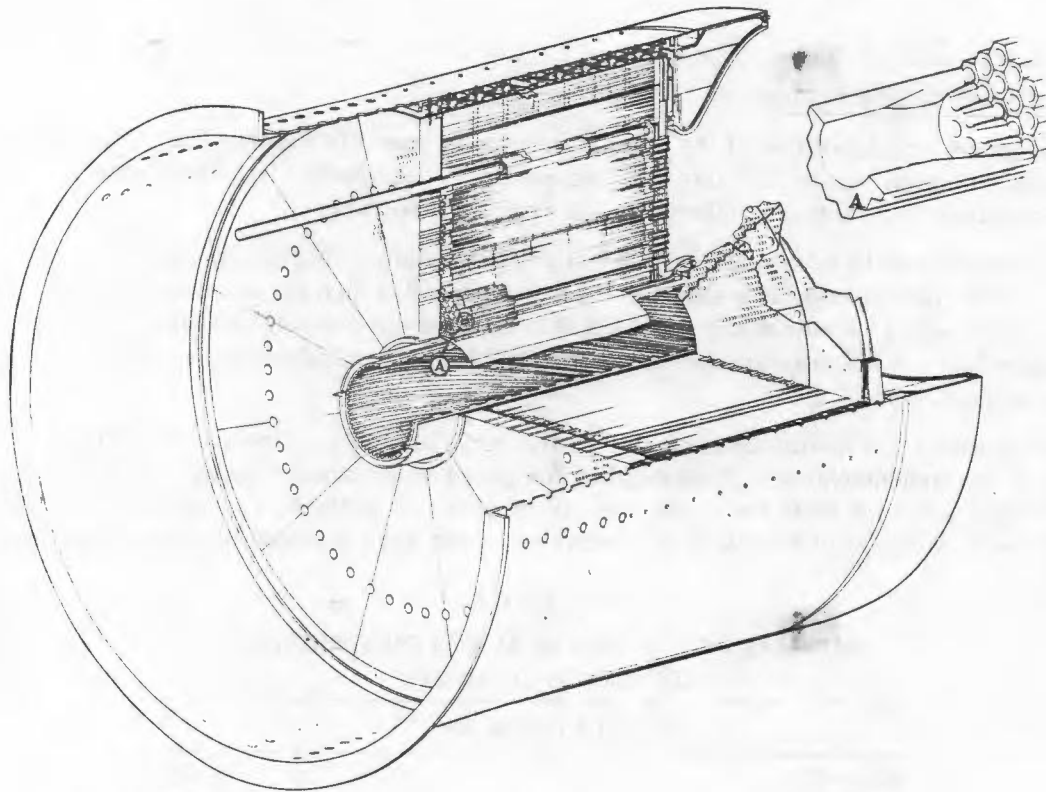


Fig. 2.2-D140E1 reactor

for the metallic components in the center of the island. The tubes also function as a gamma shield and reduce the heating rate in the metallic components. The liner functions as an arch so that the tubes can bridge the central hole. The tunnel is a structural component as well as part of the air-ducting system for the shield. It carries part of the longitudinal loads on the reactor from the aft retainer to the front shield. The tunnel and liner form an annular duct that channels cooling air from the front shield to the rear shield. The tunnel is kept concentric with the liner so that the airflow in the annular passage is not affected by deflections of the reactor under flight loads.

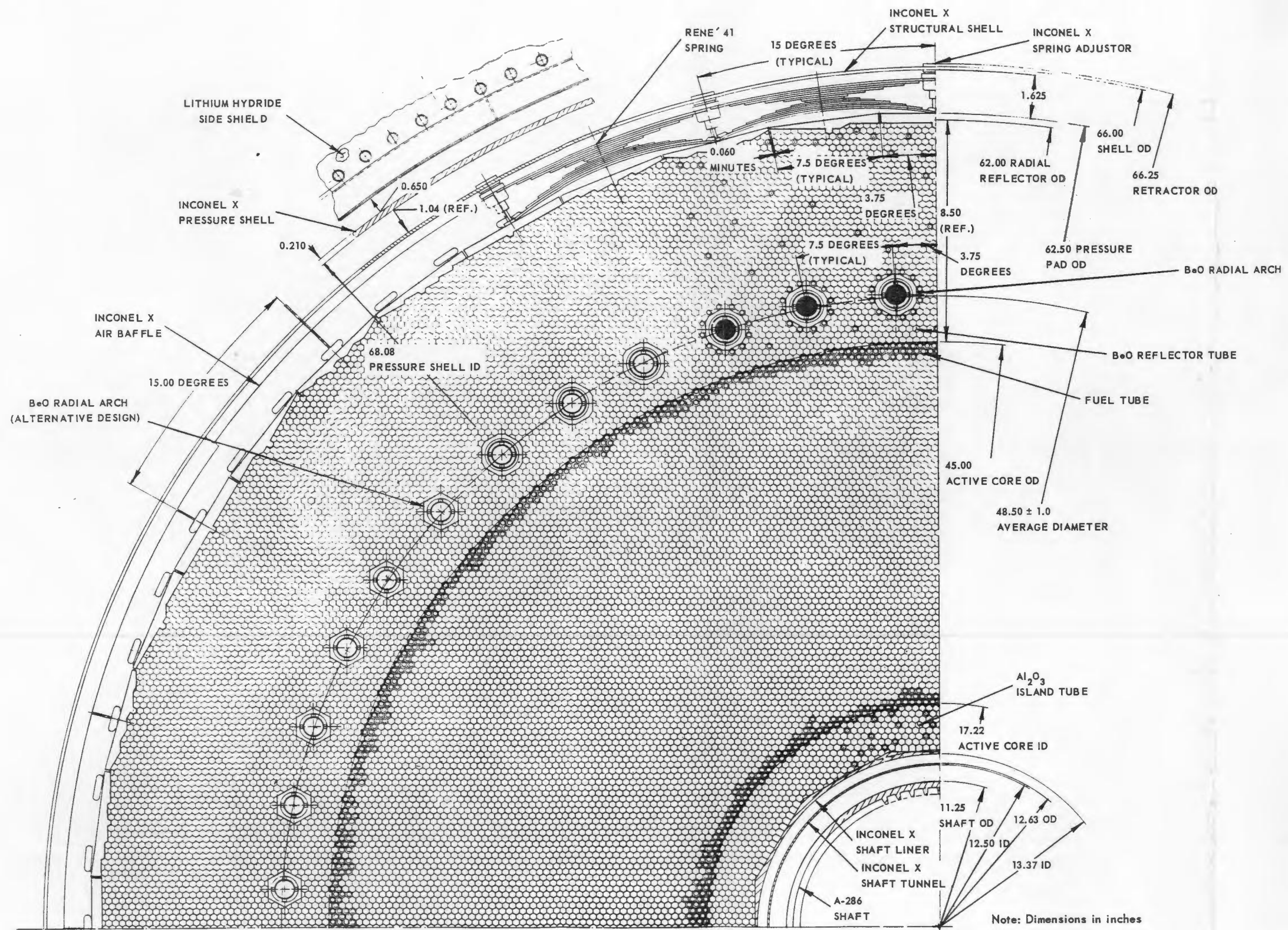
The side reflector is an 8.5-inch thickness of unfueled beryllium oxide tubes. Absorber rods are placed at 48 locations within the side reflector 1.75 inches from the boundary of the active core. These rods, which are Eu_2O_3 in a nickel matrix with an 80 Ni - 20 Cr cladding, are withdrawn or inserted for reactivity control. A larger BeO tube (1.5 inches across flats) provides the cavity for the control rod guide tube.

The rear reflector is a 1.5-inch thickness of unfueled beryllium oxide in the form of a transition segment that takes air from 19 fuel element tubes and collects it into a single large-diameter passage. Transition pieces are also used at the forward end of the reactor between the metallic reflector and the active core. The transition piece permits the use of larger-diameter holes in the forward and rear structural components and thus facilitates a better structural and aerodynamic design.

~~CONFIDENTIAL~~
~~SECRET~~

CONFIDENTIAL

~~SECRET~~



CONFIDENTIAL

~~SECRET~~

DECLASSIFIED

CONFIDENTIAL

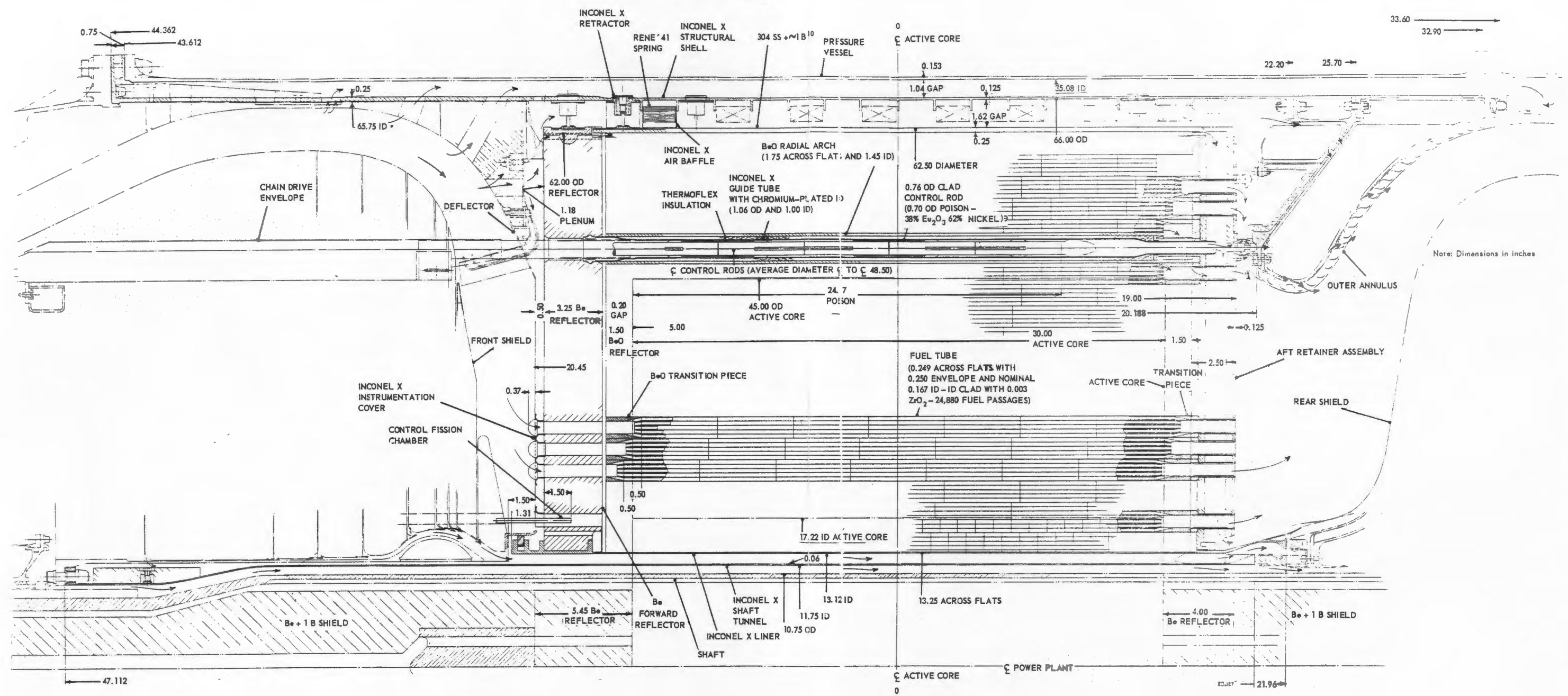


Fig. 2.4 - Longitudinal section of D140E1 reactor

DECLASSIFIED

CONFIDENTIAL

The front reflector is composed of a 3.25-inch thickness of beryllium metal and a 1.5-inch thickness of beryllium oxide. The beryllium slabs are divided into several segments and are perforated to admit cooling air to the active core. The front reflector also serves as a structural component to restrain fuel elements against forward motion.

The external structure of the reactor is composed of a radial support system and a longitudinal support system. The radial structure maintains the ceramic reactor components in a compressed unit assembly and resists lateral loads. The longitudinal structure resists aerodynamic drag on the reactor and axial inertial loads.

The radial structure is composed of a structural shell, leaf springs, and pressure pads. The structural shell, which envelops the reactor, is cantilevered from the flange connection to the shield at the forward end. The springs are loaded against the shell and impose a load that is transmitted through the pressure pads into the tube bundle. The pressure pads, which are borated (1 weight percent B¹⁰) to suppress neutron heating in the side shield, distribute the spring loads over several tubes.

The main component of the longitudinal support system is the aft retainer structure. This structure, which resists the aft loads on the reactor, is made in 30-degree segments that are supported near the center by the shaft tunnel and near the outside by the rear-shield outerbody.

The aft retainer is a fabricated structure of plates and tubes. The tubes act as shear ties and spacers for the parallel plates. The discharge air from the fuel elements passes through the tubes of the aft retainer, and the structure is cooled internally by air taken from the reflector region of the reactor.

2.1.1.2 Thermal Design

Performance Requirements

Reactor performance requirements tabulated in Table 2.3 correspond to power plant operation at an altitude of 35,000 feet (standard day) and a flight Mach number of 0.8.

Reactor Airflow Distribution

Estimates of reactor airflow distribution and associated air temperatures are shown in Table 2.4. Fuel element thermal design is based on the fuel element airflow and exit air temperature given in the table.

Current design proposals anticipate the use of air exhausted from the control rods and guide tubes, and from the outer portion of the radial reflector for cooling the aft retainer. Air exhausted from the springs, pressure pads, and shell is used to cool the outer body of the aft shield.

TABLE 2.3

REACTOR PERFORMANCE REQUIREMENTS

Reactor Flow Rate, lb/sec	154.6
Fuel Element Flow Rate, lb/sec	129.9
Core Inlet Pressure, psia	69.2
Core Pressure Ratio	0.857
Core Inlet Temperature, °F	582
Turbine Inlet Temperature, °F	1740
Total Reactor Power, mw	50.4

~~DECLASSIFIED~~
SECRET

TABLE 2.4
REACTOR AIRFLOW DISTRIBUTION

	Airflow lb/sec	Percent of Total Airflow	Exit Air Temperature, °F
Center Island	1.4	0.9	
Fuel Elements	129.9	84.0	1896 ^a
Reflector	7.1	4.6	1350 (inner portion) 900 (outer portion)
Control Rods and Guide Tubes	2.8	1.8	970
Springs, Pressure Pads, and Shell	2.0	1.3	750
Bypass for Shield Cooling	11.4	7.4	
Total	154.6	100.0	

^aFuel element power equals 96 percent of reactor total power.

Reactor Temperatures

A longitudinal temperature profile through the length of the reactor is shown in Figure 2.5. This temperature profile is calculated for an average channel. An average channel is defined as a channel that produces average power and that handles average airflow. As shown in Figure 2.5, the maximum temperature of this channel is 2210°F. This is referred to as the average-channel maximum temperature.

Figure 2.6 shows the temperature distribution in a radial cross section. The radial section through the reactor has been cut at the position of maximum temperature in the

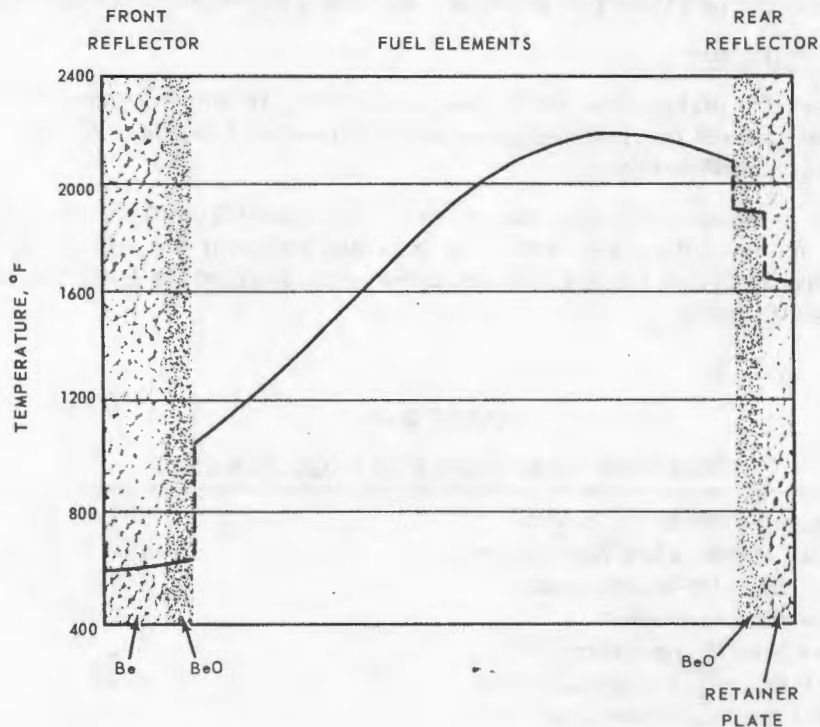


Fig. 2.5 - Average longitudinal temperature distribution, ACT assembly

~~DECLASSIFIED~~
SECRET

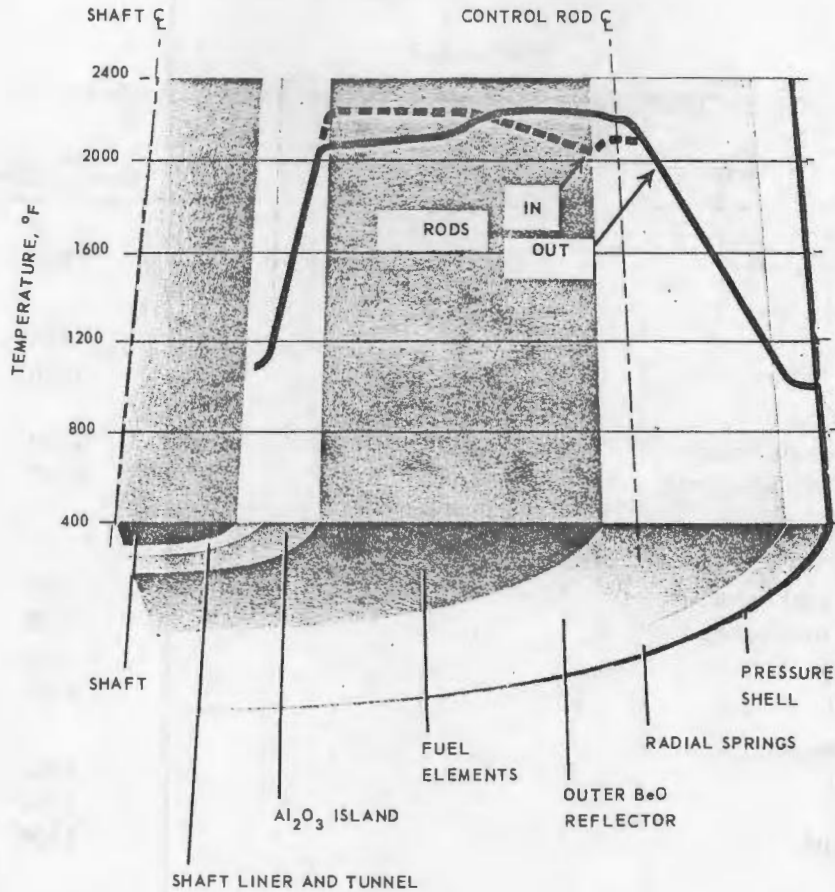


Fig. 2.6 - Radial temperature distribution, ACT assembly

longitudinal direction. The left edge of Figure 2.6 represents the shaft axis. Outward radially from the shaft axis the temperatures are relatively low in the shaft, tunnel, and liner. The temperature then rises through the aluminum oxide island in order to meet the active core temperatures. The temperature then decreases through the radial reflector to a relatively low value in the area of the springs and reactor shell. The fuel element temperatures shown in this figure indicate the gross effect of control rod movement. When the control rods are fully inserted early in core life, the power and consequently the temperatures are highest near the center of the core. As the control rods are removed, the power and temperatures shift gradually; the other curve shows the temperatures for the extreme position of the control rods, namely, completely withdrawn, which occurs at the end of core life. The average of these two curves is 2210°F, which is the average-channel maximum temperature mentioned previously. The fuel element temperatures shown in Figures 2.5 and 2.6 are predicted for ideal reactor behavior. Deviations from this ideal behavior are discussed later under "Fuel Element Thermal Predictions," where a fuel element maximum temperature of 2530°F is identified.

Predicted maximum design temperatures for the several reactor components are given in Table 2.5.

Fuel Element Thermal Design

Sizing of the fuel element flow passages required additional conditions and assumptions. Subsequent design modifications, such as changes in the area for flow of fuel element air

~~UNCLASSIFIED~~
SECRET

TABLE 2.5
PREDICTED COMPONENT MAXIMUM DESIGN TEMPERATURES
FOR ACT ASSEMBLY

	Temperature, °F
Active Core	
Fuel elements	2530
Central Island	
Shaft tunnel ^a	800
Shaft liner ^a	1200
Alumina tubes	
Adjacent to shaft liner	1200
Adjacent to fuel elements	2300
Side and End Reflectors	
Side reflector	
Adjacent to fuel elements	2300
Adjacent to pressure pads	1200
Front reflector	650
Rear reflector	2100
Radial Support System	
Pressure pads	1200
Leaf springs	1200
Pressure shell ^a	1100
Aft Retainer	
Structure ^a	1600
Insulation	2050
Poison Rod Group	
Poison rod - center of poison core	1800
Clad	1650
Guide tube	1500
Insulation	2000
Radial arch ^a	2300

^aThese temperatures are the maximum values used for design.

Operating temperatures may be adjusted to lower levels.

through the aft retainer, may later modify some of the assumptions. Data shown in Table 2.6 represent the assumptions associated with the thermal design data shown in Table 2.7, and are not necessarily consistent in all detail with configuration data shown elsewhere in this report.

Design requirements and assumptions listed above permit the determination of required fuel element free-flow area and hydraulic diameter. These data plus other thermal data are shown in Table 2.7.

Identification of fueled volume fractions for the active core together with coating assumptions and the above flow passage dimensions establishes the thermal characteristics of the fuel tubes as shown in Table 2.8.

Fuel Element Thermal Predictions

Radial temperature distributions in the active core are shown in Figure 2.7 in somewhat greater detail than was shown in Figure 2.6. The two curves shown in Figure 2.6,

~~UNCLASSIFIED~~
SECRET

TABLE 2.6
FUEL ELEMENT THERMAL DESIGN ASSUMPTIONS

Configuration	
Length of active core, in.	30
Length of forward reflector, in.	4
Length of aft reflector, in.	1.5
Aft retainer thickness, in.	1.0
Nuclear	
Longitudinal power distribution	Chopped cosine curve symmetrical about reactor midplane with maximum-to-minimum ratio of 2
Radial power distribution	Uniform
Thermal	
Heat transfer coefficient (Smooth tube, Subscripts b and f refer to bulk and film temperature, respectively. $T_f = (T_s + T_b)/2$)	$\frac{hD}{k_f} = 0.0205 \left(\frac{DG}{\mu_f}\right)^{0.8} \left(\frac{T_b}{T_f}\right)^{0.8} \left(\frac{C_p \mu}{k}\right)_f^{0.4}$
Friction factor	$f = 1.15 \times 0.046 N_{Re}^{-0.2}$ ($f = 1.15 \times f_{smooth\ tube}$)
Inlet Loss Coefficient (based on fuel dynamic head at fuel tube inlet)	0.36
Exit Loss Coefficient (based on fuel dynamic head at fuel tube exit)	0.40
Average-Channel Maximum Temperature	2210°F

the distribution for the case of control rods fully inserted and for the case of control rods fully removed, are reported in Figure 2.7. They were modified slightly to reflect an improved radial fuel distribution. A third curve for an intermediate rod insertion of 10 inches was added. The predicted radial power shifts due to control rod movements result in an average fuel element surface temperature within a radial region of about 2290°F, or 80°F in excess of the average maximum temperature of 2210°F.

Superimposed on these three curves are some of the fine detail expected in the temperature profiles. Since it is necessary to make discrete steps in fuel loading, power gradients will occur across regions of constant fuel loading. The local temperature deviations shown here correspond to those power gradients and indicate that a deviation from region average temperature of about 40°F will result. The concept of temperature flattening is best illustrated by the curves shown in Figure 2.7. Control rod insertion and removal to compensate for nuclear poisons produces variations in temperatures. At the beginning of core life the temperatures are highest in the inner regions of the core, and at the end of core life they are highest in the outer regions of the core. The aim of the temperature flattening is to equalize these two maximum temperatures and maintain temperatures in the remainder of the core as near to these temperatures as possible. These kinds of temperature deviations are built-in temperature deviations because they are known characteristics of the reactor design.

~~SECRET~~
DECLASSIFIED

TABLE 2.7

THERMAL CHARACTERISTICS OF AVERAGE
FUEL ELEMENT FLOW PASSAGE

Temperatures, °F	
Inlet air to forward reflector	582
Exit air from aft retainer	1896
Surface - average maximum	2210
Configuration	
Area for airflow, in. ²	545
Hydraulic diameter, in.	0.167
Length, in.	36.5
Forward reflector	4
Fuel elements	30
Aft reflector	1.5
Aft retainer	1.0
Number of passages	24,881
Heat transfer area, ft ²	2720
Mass Velocity, lb/sec-ft ²	34.3
Heat Flux, Average, Btu/hr-ft ²	64,700
Total Pressure, psia	
Reactor inlet	69.2
Reactor exit	59.3
Total Pressure Loss, psi	
Entrance loss	9.93
Friction and heat addition	0.25
Exit loss	8.95
Reynolds Number	
Fuel element inlet	2.37 x 10 ⁴
Fuel element exit	1.44 x 10 ⁴
Mach Number	
Fuel element inlet	0.121
Fuel element exit	0.214
Dynamic Head	
Fuel element inlet, psi	0.69
Fuel element exit, psi	1.79

TABLE 2.8

THERMAL CHARACTERISTICS OF FUEL TUBES

Configuration	
Hydraulic diameter, in.	0.167
Width across flats, in.	0.249
Coating thickness, in.	0.003
Inner diameter, fueled matrix, in.	0.173
Total length, in.	30
Volumetric Heating, Btu/sec-in. ³	
Average	2.04
Average maximum	2.49
Average Internal Temperature Rise, °F	
Coating	25.5
Fueled matrix	12.5
	13

~~SECRET~~
DECLASSIFIED

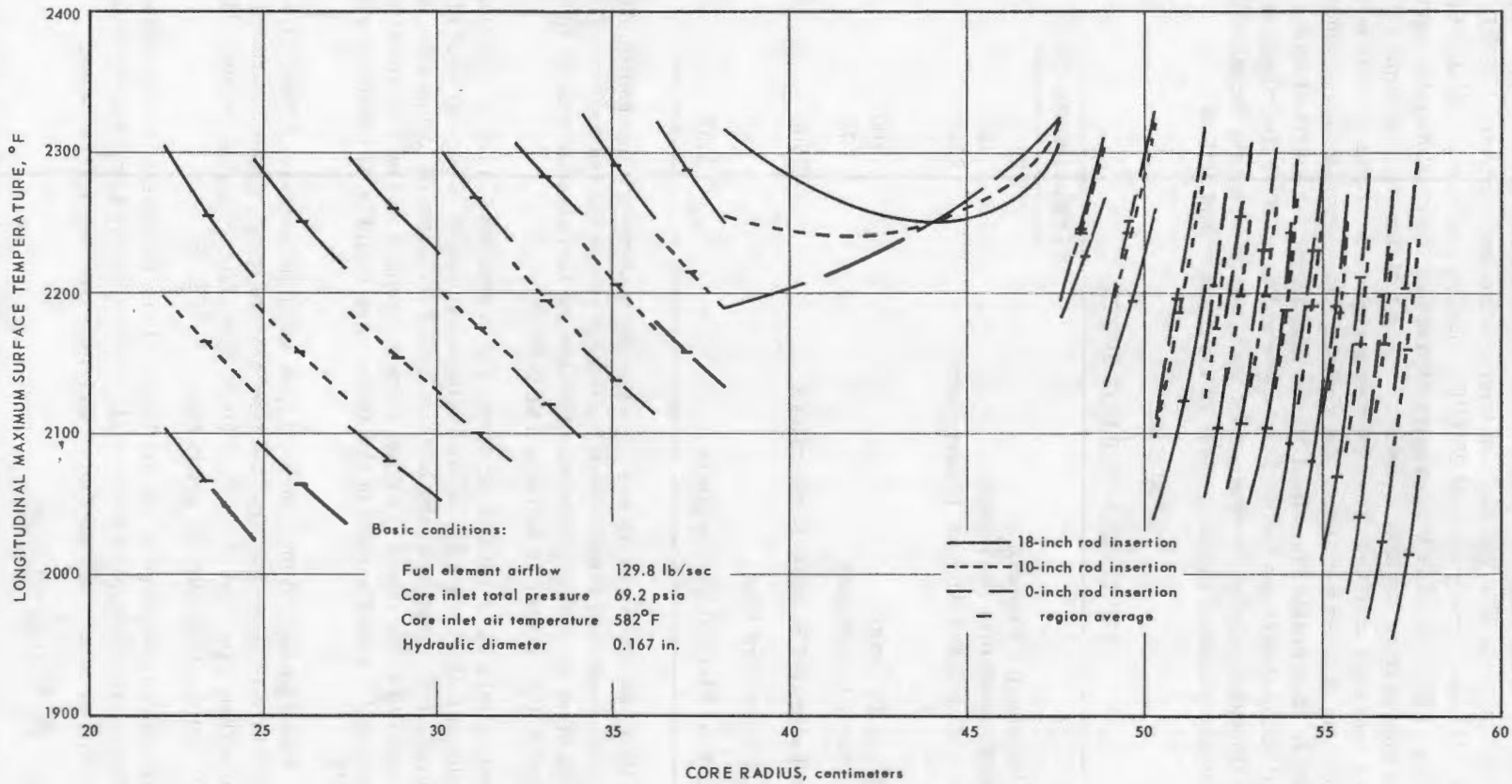


Fig. 2.7—Radial variation of longitudinal maximum surface temperature in D140E1 fuel elements

~~SECRET~~
~~DECLASSIFIED~~

Temperature allowances for the built-in deviations and added allowances for other variables were made in order to arrive at a hot-channel maximum temperature. These data are summarized in Table 2.9. The built-in temperature deviations total 120°F. Adding this to the reference temperature of 2210°F produces a maximum calculated surface temperature of 2330°F. This temperature represents the maximum temperature that can be predicted from the known power and flow distributions, assuming that power and flow are correctly matched. The next items represent allowances for possible statistical combinations of other variables. The allowance for dimensional tolerances assumes a completely unfavorable stackup of all the tolerances in a single channel. Since design practice will be to determine the nuclear power and the airflow distributions experimentally, the allowance labeled "measurement uncertainty" accounts for possible imprecisions in the experimental measurements of local power and airflow.

TABLE 2.9
FUEL ELEMENT HOT SPOTS

	Temperature, °F
Average Maximum Temperature	2210
Built-In Temperature Deviations	120
Maximum Calculated Surface Temperature	2330
Allowances	
Fabrication Tolerance	100
Measurement Uncertainty	70
Maximum Estimated Surface Temperature	2500
Internal Temperature Rise	30
Maximum Fuel Element Temperature	2530

The addition of these deviations to the average-channel maximum temperature produces an estimate of maximum surface temperature for the hot channel in the reactor. This estimate is 2500°F. Since the temperature rise through the fuel element wall is 30°F, the highest temperature in the reactor is estimated at 2530°F.

Longitudinal temperature distributions for three radial positions, 12.2, 21.02, and 22.28 inches, are shown in Figures 2.8, 2.9, and 2.10, respectively. Consideration of the longitudinal temperature distributions, the built-in radial temperature deviations, and the statistical temperature deviations resulting from tolerances and measurement uncertainties suggests that a small portion of the active core would be at temperatures approaching 2500°F.

This conclusion is demonstrated in Figure 2.11, in which percentage of the active core at any given temperature is plotted against the temperature itself. From this curve it was determined that less than 1 percent of the fuel element surface operates between 2400° and 2500°F and that the average surface temperature is 2000°F.

Radial distribution of temperature of the air issuing from the active core is shown in Figure 2.12. These data correspond to the built-in fuel element temperature deviations and do not include any allowance for tolerances and measurement uncertainties.

Advanced Core Test Thermal Predictions

Reactor thermal predictions in the preceding discussion have been for an aircraft cruise condition. The Advanced Core Test will require operation of the reactor at Idaho

~~SECRET~~
~~DECLASSIFIED~~

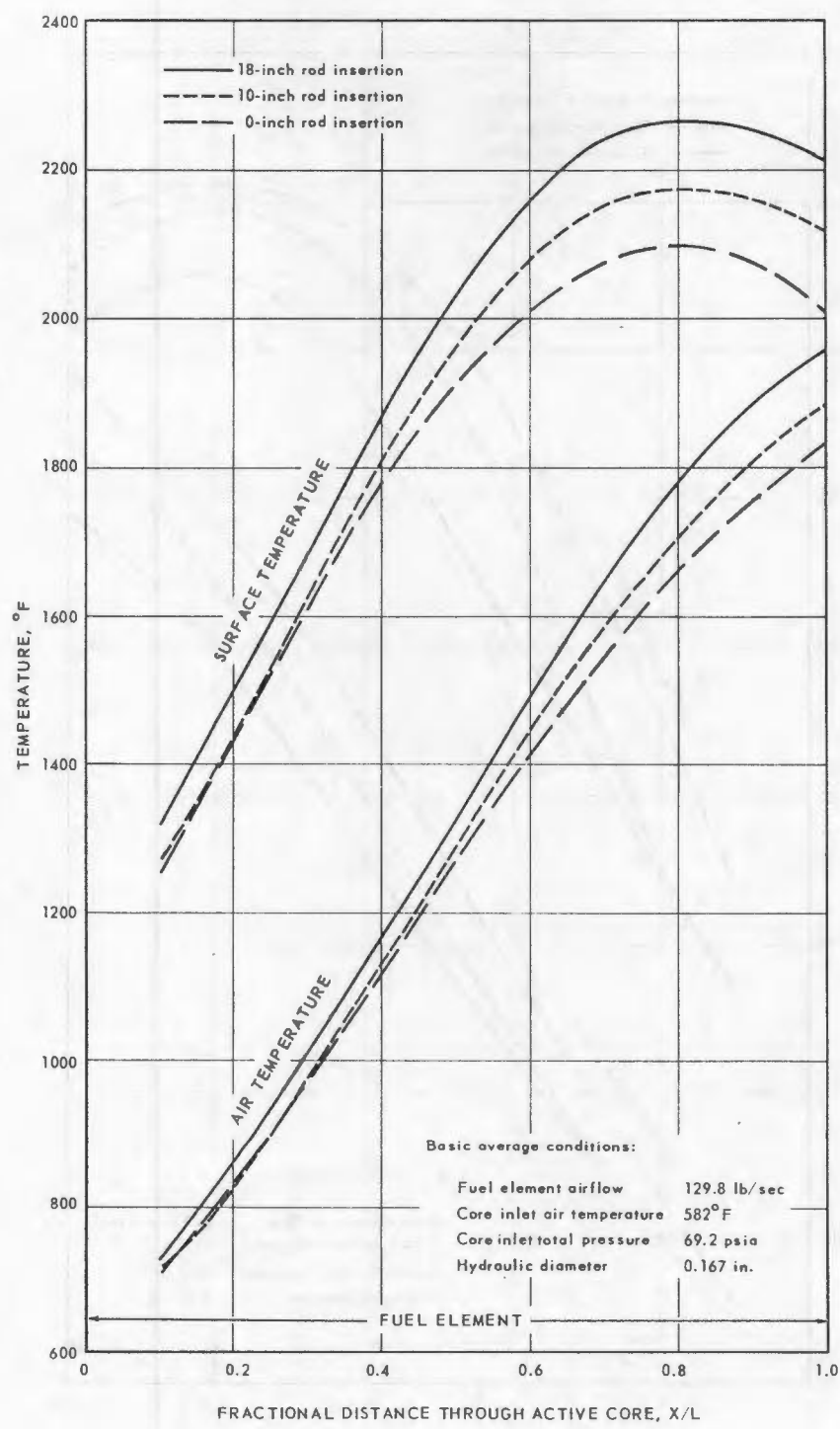


Fig. 2.8 - Longitudinal temperature distribution in D140E1 fuel elements at radial location 31 centimeters (12.2 in.) from core center

CONFIDENTIAL
SECRET

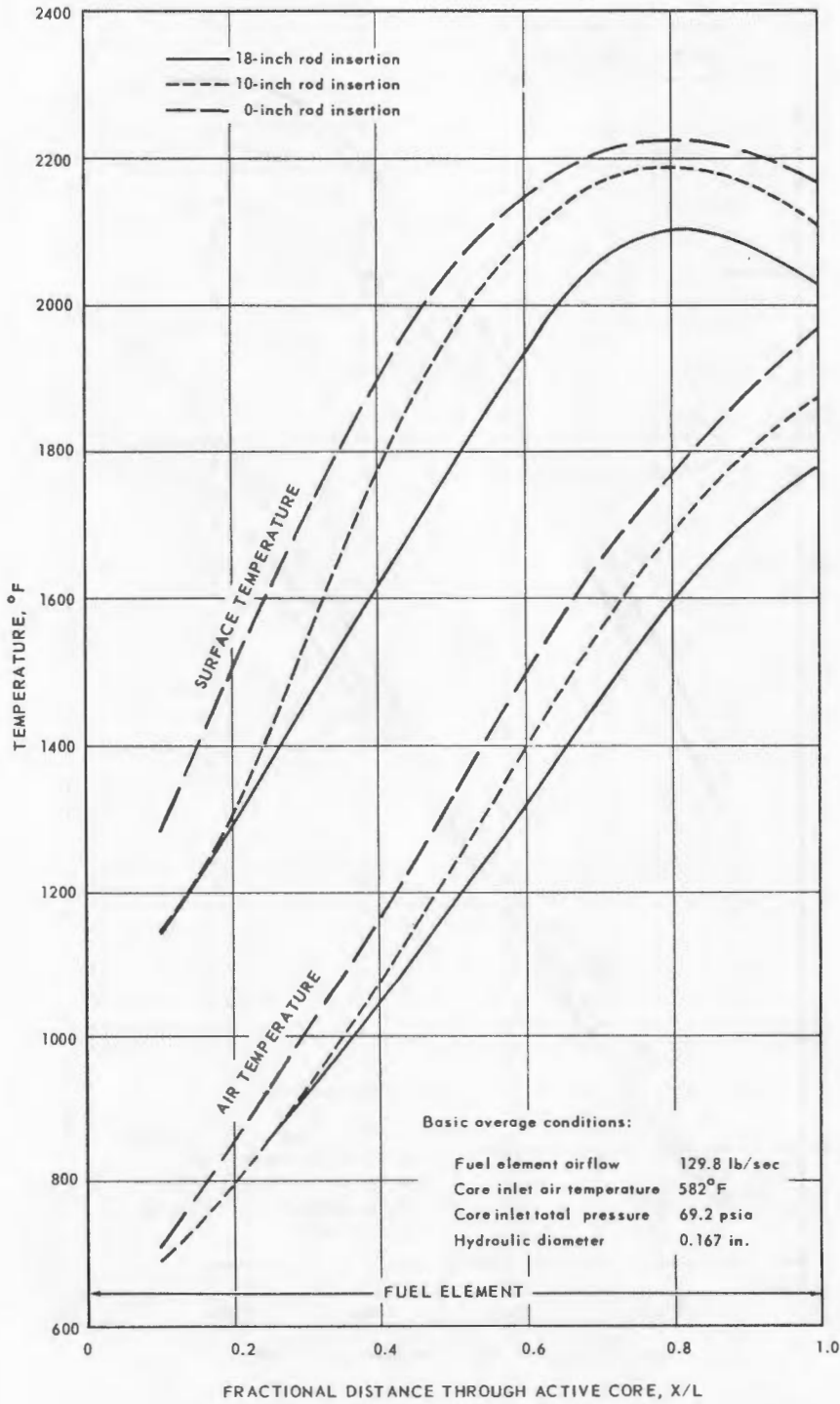


Fig. 2.9 - Longitudinal temperature distribution in D140E1 fuel elements at radial location 53.4 centimeters (21.02 in.) from core center

SECRET
DECLASSIFIED

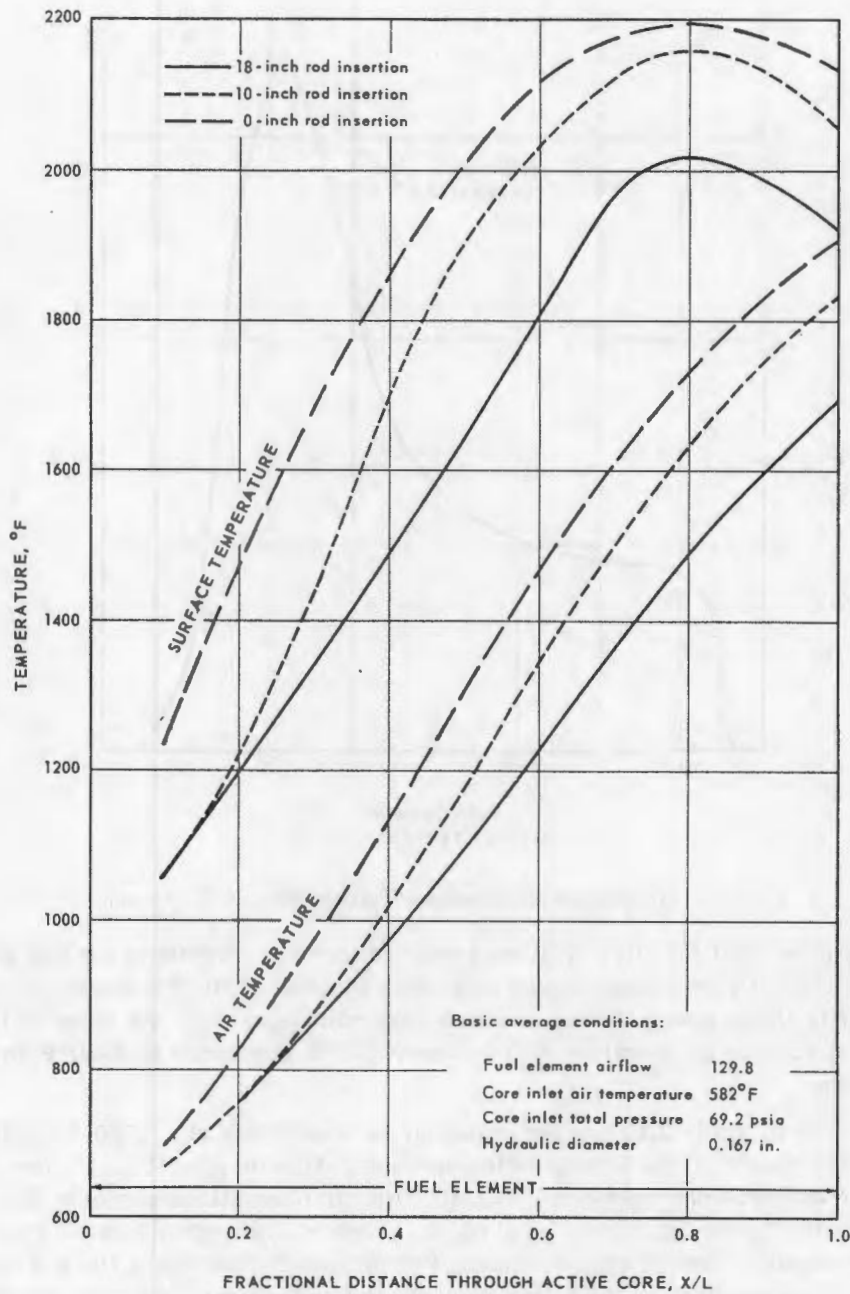


Fig. 2.10—Longitudinal temperature distribution in D140E1 fuel elements at radial location 56.6 centimeters (22.28 in.) from core center

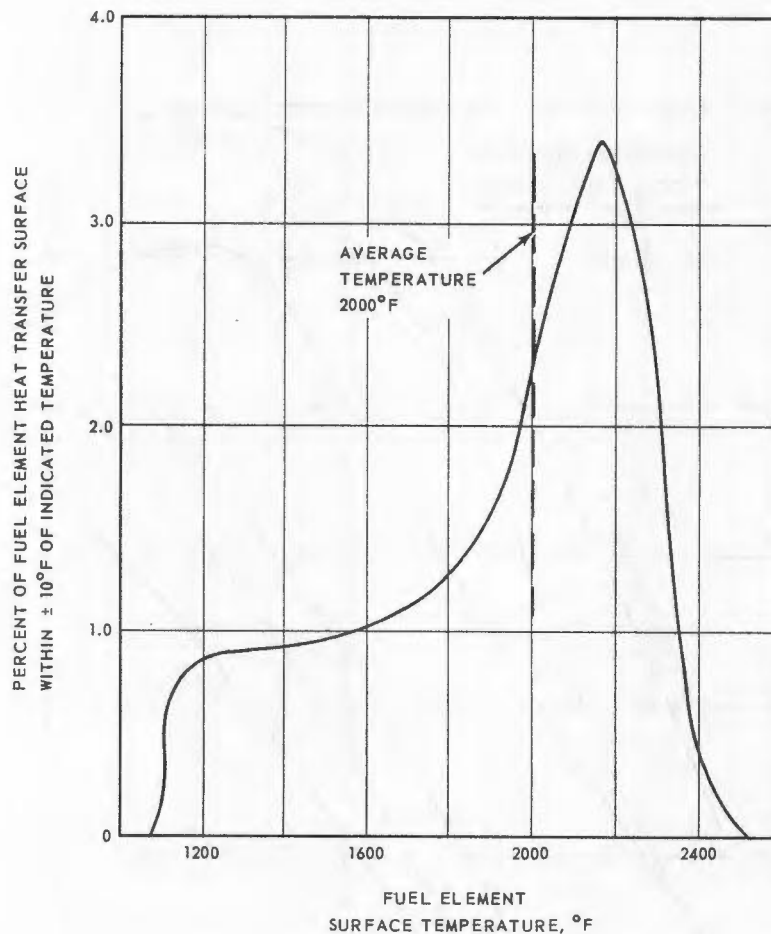
~~SECRET~~

Fig. 2.11 – Temperature distribution of fuel elements, ACT assembly.

in the Flight Engine Test facility. Predicted reactor thermal conditions for that operation are compared with the cruise design point data in Table 2.10. Temperature patterns will be similar to those shown for the cruise design point operation. As is noted in the table, maximum surface temperature will be less, 2450°F compared to 2500°F, for cruise operation.

ACT data shown in Table 2.10 are for standard day conditions at a 5000-foot altitude. Required reactor power levels for operation on colder days may be 10 to 15 percent higher than for standard day operation. The ACT thermal conditions shown in Table 2.10 impose about twice the design power level on the reactor. Consequently, it is planned to approximately simulate design reactor thermal conditions by modifying the power plant cycle for ACT. One possible modification involves the reduction of pressure levels in the compressor and reactor by placing a flow resistance forward of the compressor inlet. Reduction of pressure levels reduces the reactor air mass flow rate and hence for the same air temperature rise reduces the reactor power level. Although detailed data are not available for inclusion here, it is planned that the reactor design power level of 50.4 mw and the fuel element maximum surface temperature of 2500°F will be approximately duplicated. Other conditions, such as reactor inlet air temperature or engine speed, may not be duplicated. The ACT will be operated with thermal conditions approximating the design thermal conditions for most of its life and will be operated at the ACT conditions shown in Table 2.10 for only a small percentage of the total operating life.

~~SECRET~~

SECRET
DECLASSIFIED

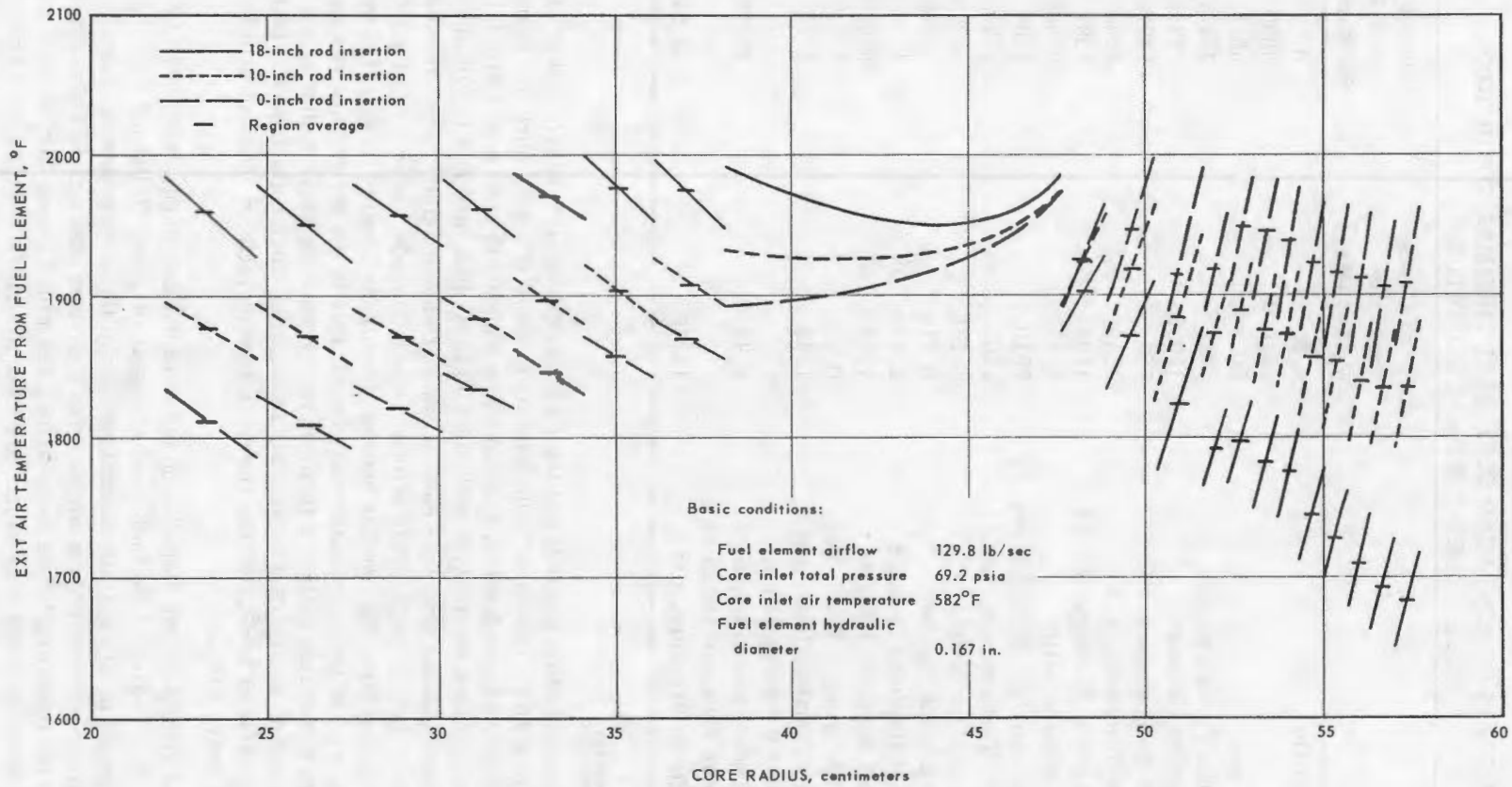


Fig. 2.12—Radial variation of exit air temperature from D140E1 fuel elements

SECRET
DECLASSIFIED

REF ID: A66531
 UNCLASSIFIED
 SECRET

TABLE 2. 10
 COMPARISON OF ADVANCED CORE TEST THERMAL CONDITIONS
 WITH DESIGN THERMAL CONDITIONS

Flight Condition	Aircraft Cruise on Station Standard Day	Advanced Core Test, Idaho Standard Day
Flight Mach Number	0. 8	0
Altitude, ft	35, 000	5000
Reactor Power, mw	50. 4	96. 2
Reactor Inlet Total Pressure, psia	69. 2	142. 7
Fuel Element Airflow, lb/sec	129. 9	273. 8
Reactor Inlet Air Temperature, °F	582	649
Turbine Inlet Air Temperature, °F	1740	1695
Fuel Element Exit Air Temperature, °F	1896	1837
Reactor Total Pressure Ratio	0. 857	0. 868
Average Maximum Surface Temperature, °F	2210	2186
Maximum Surface Temperature, °F	2500	2450
Fuel Element Inlet Mach Number	0. 121	0. 129
Fuel Element Exit Mach Number	0. 214	0. 213
Fuel Element Inlet Reynolds Number	$2. 37 \times 10^4$	$4. 79 \times 10^4$
Fuel Element Exit Reynolds Number	$1. 44 \times 10^4$	$3. 08 \times 10^4$
Fuel Element Inlet Dynamic Head, psi	0. 69	1. 59
Fuel Element Exit Dynamic Head, psi	1. 79	3. 70
Reactor Inlet Total Pressure Minus Reactor Exit Total Pressure, psi	9. 93	18. 75
Reactor Inlet Total Pressure Minus Reactor Exit Static Pressure, psi	11. 75	22. 54

2.1.1.3 Nuclear Design

The principal nuclear characteristics of the D140E1 reactor are determined by (1) the annular active core with its nuclearly homogeneous mixture of highly enriched uranium oxide fuel, beryllium oxide moderator, yttrium oxide stabilizer, and coolant air; (2) the relatively thick end reflectors and side reflectors of beryllium metal or beryllium oxide; and (3) the neutron resonance absorber rods arranged to move axially in the side reflector. The neutron energy spectrum is strongly space dependent because of the moderating effect of the reflectors. The median energy of neutrons causing fission is about 28 ev, but this parameter varies from a minimum of about 0.1 ev in the active core region immediately adjacent to the side reflector to about 100 ev near the mean radius of the annular active core and about 46 ev adjacent to the aluminum oxide inner reflector. The fuel inventory is 87 kilograms of U²³⁵, and the over-all atomic ratio of beryllium to U²³⁵ is about 110 for the active core.

The flattening of fission power distribution in the radial coordinate is effected by a particular radial distribution of the fuel. Fuel elements of about 17 distinct fuel concentrations distributed in 20 separate coaxial regions of the active core are expected to produce a radial power distribution within about 8 percent above and 15 percent below the average, over the operating life of the reactor. The radial power distribution referred to here is that derived by integrating in the direction of airflow and therefore corresponds to the power added to air flowing through the reactor. The fuel concentrations in the elements adjacent to the side reflector are relatively low to compensate for the sharp in-

SECRET
 UNCLASSIFIED

crease in power that the proximity of the reflector otherwise would cause. The higher fractional burnup here will help balance the increase in local power as the absorber rods are withdrawn to compensate for poisoning and burnup.

The longitudinal distribution of fission power density is somewhat forward peaked because of the relatively thick front reflector. The control rods have an appreciably, but not severe, effect upon longitudinal power distribution in the fuel channels near the reflector and in the outer active core region.

The homogeneous active core has a predicted, appreciable, negative temperature coefficient of reactivity when the reflectors are kept at ambient temperature. This negative coefficient is the result of increased probability of thermal leakage and thermal expansion as temperature is increased. Increasing the reflector temperature while keeping the active core at ambient temperature produces a positive reactivity-temperature coefficient, the magnitude of which decreases with increasing reflector temperature. The positive temperature coefficient of the reflectors is the result of increasing the thermal diffusion area and an associated increase in statistical weight of reflector neutrons with increasing temperature. In steady-state operation the reflector temperatures are functions of the reactor power level and compressor discharge air temperature and reach relatively high values. The result of these iterations is a steady-state reactivity-temperature coefficient that is positive for active-core temperatures from 68°F to nearly 1000°F; thereafter the coefficient becomes negative.

Experiment and Analysis

The D140E1 reactor nuclear characteristics presented here are based principally upon nuclear analysis using evaluated reactor theory and accepted neutron cross sections. A series of critical experiments that was performed with a good representation of the gross reactor dimensions and composition but a relatively crude approximation of fuel element arrangement, has either confirmed or indicated corrections for analytically derived room-temperature characteristics of reactors of this type.

As design of the D140E1 reactor progresses, increased emphasis will be placed upon critical experiment measurements. A room-temperature critical experiment designated the KEY matrix has been constructed. This assembly contains a 60-degree pie-shaped measurement sector in which an accurate mockup of the reactor with fueled or unfueled ceramic tubes is installed and the remainder of the core is mocked up with uranium foil and BeO pieces distributed appropriately. In addition, the KEY matrix is large enough to accommodate a nuclear mockup of a large part of the reactor shield. The measurement sector will be power mapped and compared with the analysis. The differences between the critical experiment analysis and the measurements will then be applied as corrections to the design reactor calculations. An iterative procedure of measurements, analysis, and modification of the critical experiment (primarily fuel redistribution) will be followed until a temperature-flattened design is achieved. Suitable approximations of poisoning and fuel depletion will be used to obtain the necessary power maps with rods withdrawn. The final power maps in this series will be made with production fuel elements and reflector pieces in the pie-shaped sector.

An elevated-temperature critical experiment designated the "zero-power test" will be performed in the Low Power Test facility at the Idaho Test Station. The active core and side reflectors will be heated independently to approximately uniform temperatures (maximum of 1000°F) for observation of the effects of temperature on reactivity and power distribution. The elevated-temperature observations will be translated to the expected full-power test conditions so that the final distributions of fuel concentrations for optimization of power distribution can be determined and full-power temperature distributions accurately predicted.

Composition - The regional composition and geometry of the D140E1 reactor-shield assembly as used in the combination of one-dimensional analyses is diagrammed in Figure 2.13. To simplify the figure, the active core is represented as a single region of average composition. In two-dimensional studies regions not on the principal coordinate axes have been used as well as the regional definition as shown.

Design Reactivity - The excess reactivity changes that the D140E1 reactor will experience in meeting the performance objectives of the Advanced Core Test and flight cruise condition are shown in Table 2.11. The data for a power level of 110 megawatts correspond to that for operation with standard inlet condition at the Idaho Test Station, whereas the 50-megawatt level corresponds to the aircraft cruise design point.

TABLE 2.11
DESIGN REACTIVITY CHANGES FOR THE D140E1 REACTOR

	Reactivity, % $\Delta k/k$	
	At 110 mw	At 50 mw
Equilibrium xenon	-2.0 ± 0.7	-1.5 ± 0.5
Fuel burnup, lithium buildup, and long-lived fission products, including U^{235} , U^{238} , Pu^{239} , Li^6 , Sm^{149} , and slag (other stable fission products) (55,000 mw-hr)	-2.9 ± 1.0	-2.9 ± 1.0
Reactivity change, ambient to operating temperature	0 ± 0.6	0 ± 0.6
Reactivity margin for error	-0.9	-0.8
Design reactivity (95 percent confidence level)	5.9	5.2

Equilibrium xenon was determined analytically by subdividing the core in 20 radial regions. The flux spectrum and power level from an 18-energy-level, multiregion, diffusion calculation was used to determine the regional equilibrium concentrations. These concentrations were then used in a three-energy-group, multiregion diffusion calculation in which an iterative procedure is used to establish consistent reflector savings in the radial and longitudinal coordinates.

The evaluation of fuel burnup, lithium buildup, and long-lived fission products including U^{235} , U^{236} , Pu^{239} , Li^6 , Sm^{149} , and "slag" (lumped stable fission products) was made using the flux spectrum and regional procedure described above. The slag cross sections used for the relatively stable low-cross-section fission products have an absorption resonance integral of 268 barns per fission and a capture cross section of 50 barns per fission for 2200-meter-per-second neutrons.

Results of the temperature-reactivity analysis are shown in Figure 2.14. The reactivity effect of temperature includes two contributions: a positive contribution due to the reduced absorption in the reflector at high temperatures and a negative contribution due to thermal expansion and increased thermal leakage. The steady-state analysis was based upon isothermal operation until the compressor discharge temperature of 600°F was reached; thereafter component temperatures were proportional to specific power levels. In a reactor runaway the core temperature rises rapidly while nonfueled components such as the reflectors experience little change. As a result the temperature-

UNCLASSIFIED
SECRET

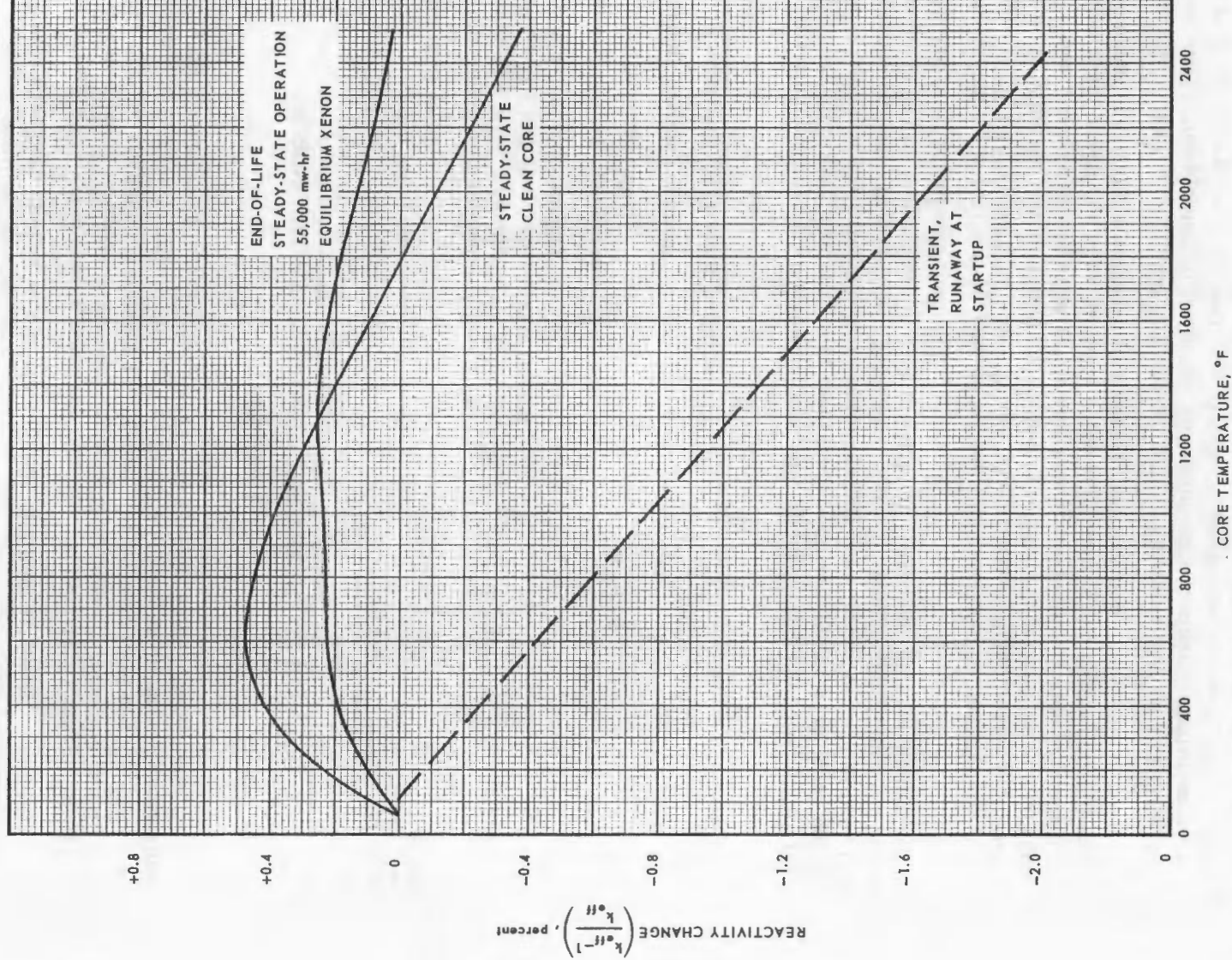


Fig. 2.14 - Calculated temperature-reactivity characteristics of the D140E1 reactor

UNCLASSIFIED
SECRET

reactivity curve for a runaway has a steeper negative slope than exists at any point on the steady-state curve.

In Table 2.11 the reactivity allowance for temperature is based upon the temperature-reactivity curve corresponding to end-of-life conditions. This curve varies from that of the clean core primarily because of the change in xenon cross section with temperature. Doppler effects have been neglected but are expected to be slightly negative, about -0.2 percent Δk_{eff} over the full temperature range.

The uncertainties listed with items in Table 2.11 correspond to the maximum ranges expected; σ_i , the standard deviation, is one-third this range. A 95 percent confidence level corresponds to $2\bar{\sigma}$ where $\bar{\sigma} = \sqrt{\sum \sigma_i^2}$.

Available Reactivity - The calculated reactivity has been corrected by a comparison of analysis with experiment in a critical mockup using materials identical to those assumed in the analysis and having similar geometry. The analysis shows that a system excess reactivity of 6.5 percent $\Delta k/k$ is available at the cold (68°F) clean condition. Final adjustment of system reactivity will be made during the final design period after the operation of the nuclear mockup.

Control Rod Worth - A total worth of 9 percent $\Delta k/k$ is expected for the 48 rods comprising the control system. This value is based upon an extrapolation of critical experiment measurements to values for the design configuration. Each rod that is worth 0.188 percent $\Delta k/k$ in the bank, for a 24-inch stroke would be worth approximately 0.25 percent $\Delta k/k$ if it were unshadowed. A longitudinal importance curve derived from a two-dimensional, three-energy-group analysis is shown in Figure 2.15.

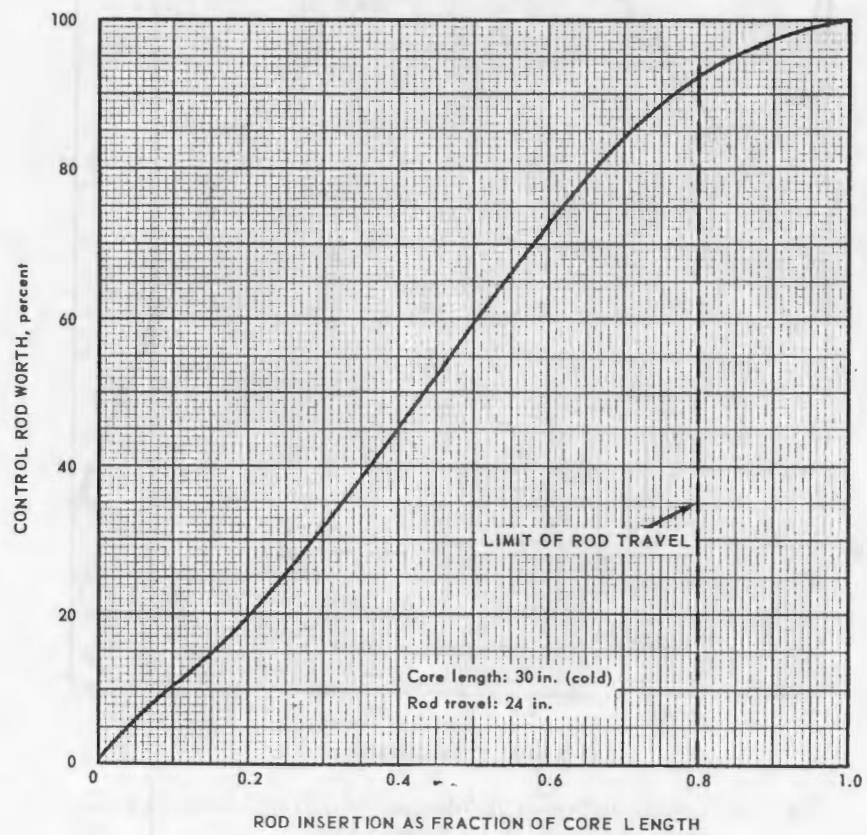


Fig. 2.15—Percentage of control rod worth versus fraction of longitudinal insertion

~~CONFIDENTIAL~~
SECRET

Power and Flux Distribution - The fission density distributions given below were derived by three-group diffusion theory analysis in cylindrical (R,Z) geometry. The relative power density is given on a volumetric basis and is directly interpretable in thermodynamic studies since the volume of fuel-bearing material per fuel element is a constant.

The longitudinal relative power distributions in Figures 2.16, 2.17, and 2.18 show the effect of control rod position in the hot clean reactor.

The radial distributions of relative power density in Figure 2.19 incorporate the combined effects of control position and composition changes due to 50-megawatt power for the operating histories indicated. The discontinuities in power distribution are due to changes in fuel concentration for the purpose of flattening the radial power distribution. The region between about the 38.2-centimeter radius and 47.6-centimeter radius has the peak fuel concentration of 10.0 weight percent highly enriched uranium dioxide in the fuel element; fuel concentration decreases toward both the side reflector and island reflector.

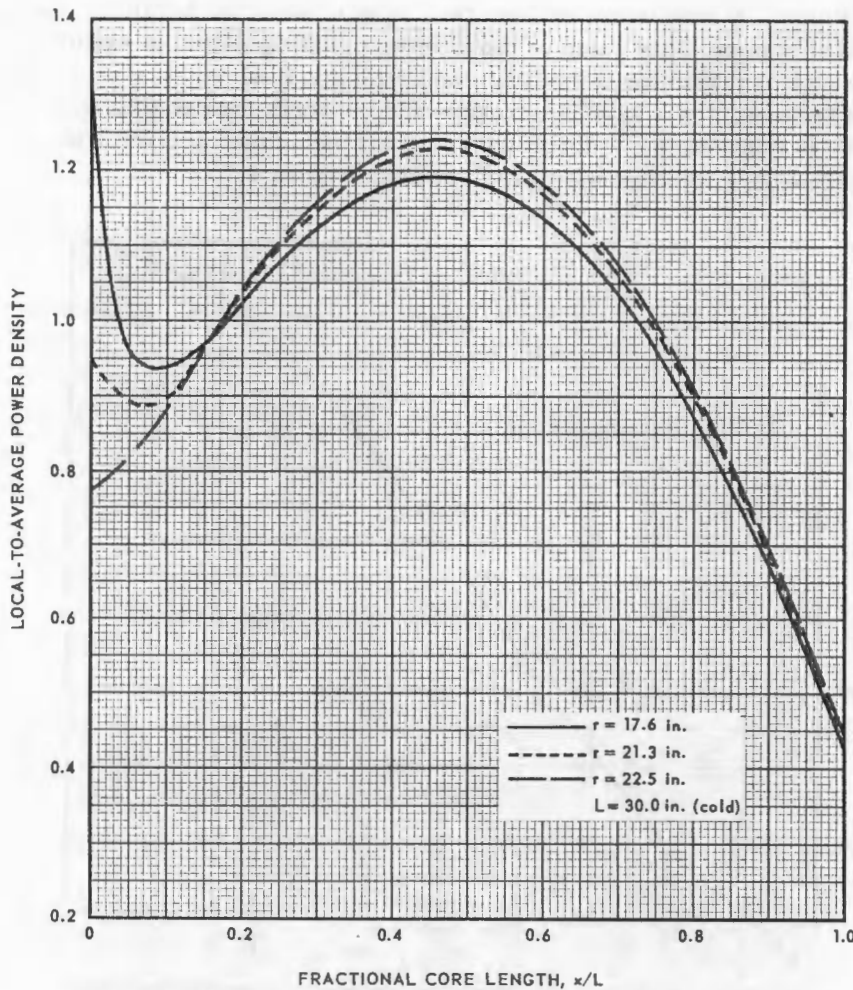


Fig. 2.16 - Longitudinal power distribution at three radial locations for no control rod insertion, hot clean reactor

SECRET
~~CONFIDENTIAL~~

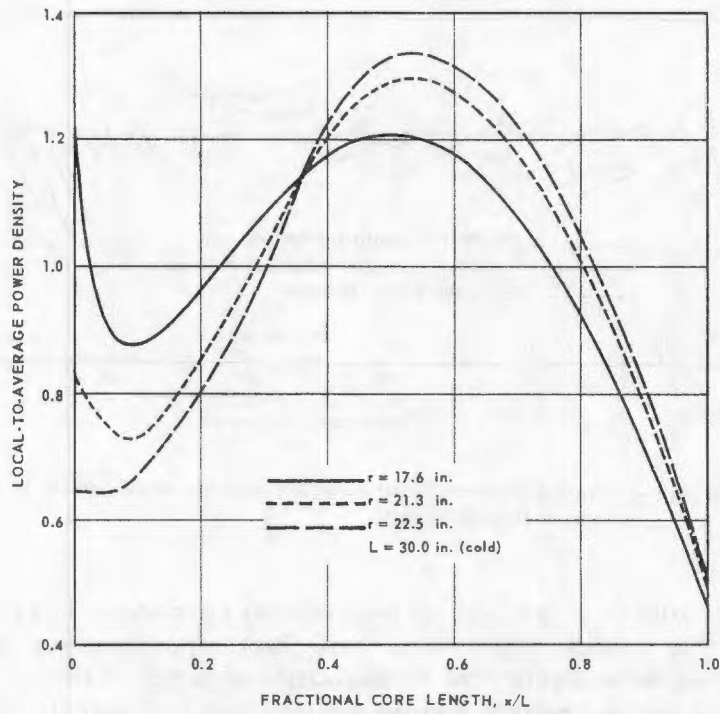


Fig. 2.17—Longitudinal power distribution at three radial locations for insertion of 48 control rods 10 inches, hot clean reactor

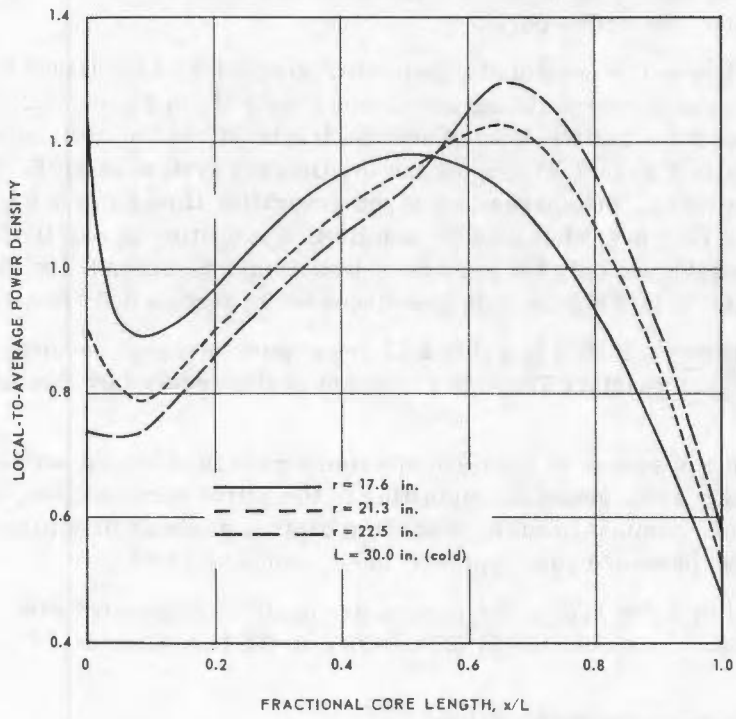


Fig. 2.18—Longitudinal power distribution at three radial locations for insertion of 48 control rods 18 inches, hot clean reactor

~~CONFIDENTIAL~~
SECRET

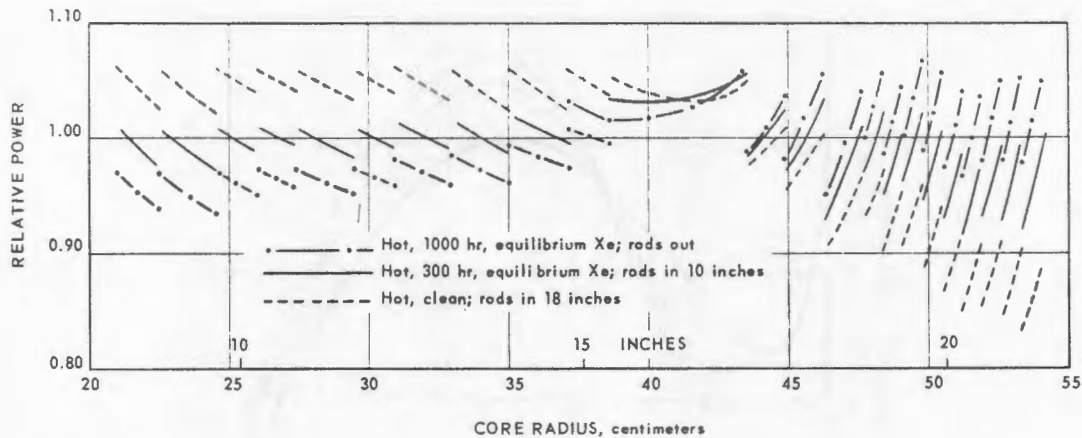


Fig. 2.19—Gross radial power distributions for three conditions during D140E1 operation at 50 megawatts

The radial distributions of three-group neutron fluxes are shown in Figure 2.20 for the hot clean reactor without control rods. These flux distributions were derived from 18-level, 1-dimensional analysis. The normalization of computed flux is such that the product of flux and fission-production cross section integrated over the full energy range and over core volume produces k_{eff} neutrons. The absolute flux levels for a power of 50 megawatts are 7.62×10^{15} n/cm²-sec times the relative values plotted. The peak total flux of about 8.5×10^{14} n/cm²-sec for 50 megawatts occurs at a radius of about 40 centimeters (15.75 inches from the power plant axis, and longitudinally at about the middle of the active core).

Reactor Kinetics - The predicted kinetic characteristics of the D140E1 reactor are shown by the plot of steady-state period versus reactivity in Figure 2.21 and by Table 2.12, which gives the effective delayed neutron fractions and the neutron generation times. The data in Figure 2.21 are for the multiregion system at 68°F. For elevated-temperature operation, the change in neutron generation time from 5.6×10^{-5} second at 68°F to 4.3×10^{-5} second at 2000°F results in a reduction in reactivity for a given period that is significant only for periods of less than 0.01 second. The delayed neutron data incorporated in this kinetic data are discussed in section 8.6 "Reactor Physics."

Secondary Heating - Listed in Table 2.13 are nominal average secondary heating rates in the D140E1 reactor. The data represent heating caused by gamma rays and neutrons.

About 18.5 Mev of energy in the form of gamma rays is released per fission, with most of the energy from gammas originating in the active core (prompt, decay, and nonfission capture gammas) and the rest from capture gammas originating in the shaft liner, reflectors, pressure pads, springs, shell, and rear grate.

Also included in Table 2.13 is the heating associated with neutron kinetic energy loss during slowing down and with the (n, α) reaction in the borated pads.

2.1.1.4 Fuel Element Characteristics

The fuel elements for the ACT consist of a mixture of beryllium oxide containing a solid solution of yttria-stabilized UO₂. The fuel element is a hexagonal tube with a circular bore. Air flows through the bore, which is coated with ZrO₂ to which about

~~CONFIDENTIAL~~
SECRET

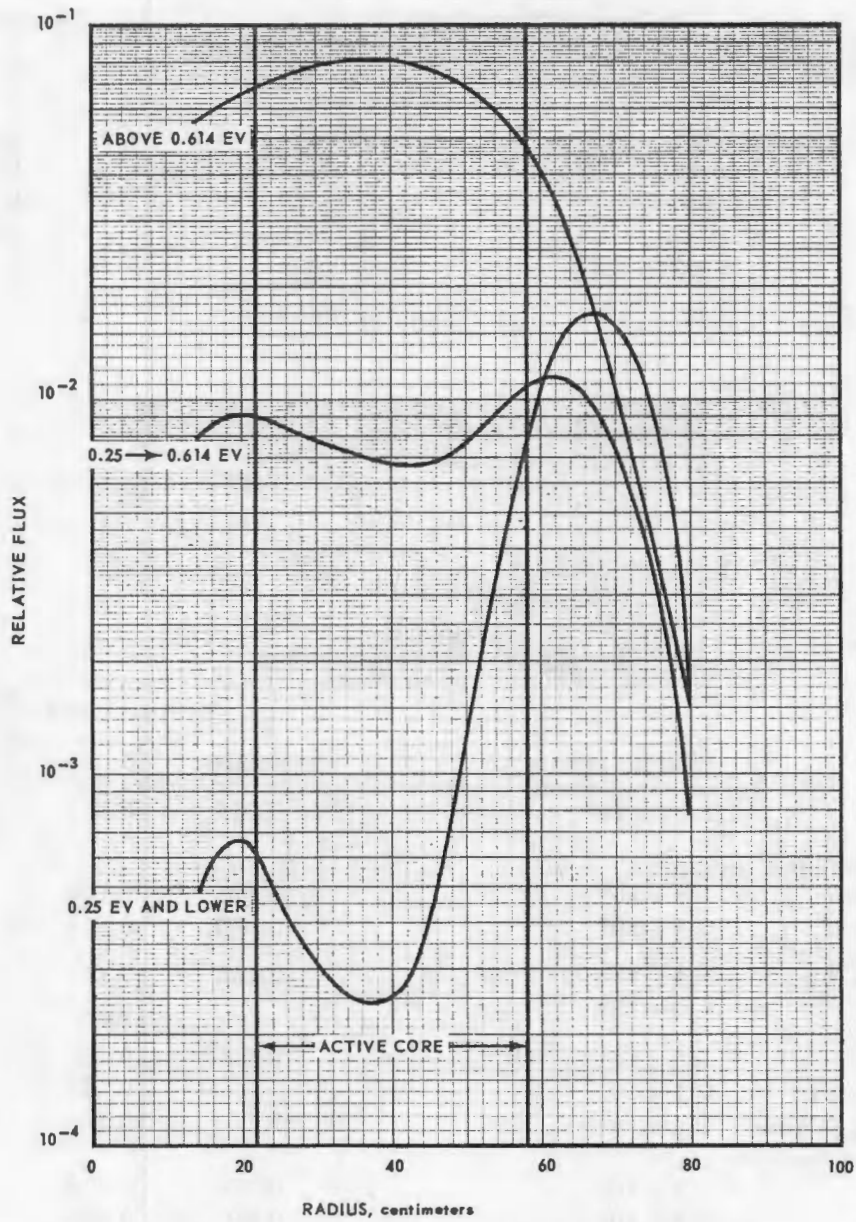


Fig. 2.20 - Relative three-group fluxes versus core radius

~~SECRET~~

TABLE 2. 12
D140E1 KINETIC CONSTANTS

Index	Delayed Neutron Data		Decay Constant, sec ⁻¹
	Actual Delay Fraction	Effective Delay Fraction	
1	0. 00023	0. 00025	0. 01260
2	0. 00142	0. 00149	0. 03110
3	0. 00126	0. 00135	0. 1134
4	0. 00264	0. 00280	0. 3060
5	0. 00080	0. 00086	1. 253
6	0. 00022	0. 00023	3. 381
	$\beta_{act} = 0. 00657$	$\beta_{eff} = 0. 00698$	

Neutron Generation Time

$$l = 5. 6 \times 10^{-5} \text{ sec at } 680^{\circ}\text{F}$$

$$l = 4. 3 \times 10^{-5} \text{ sec at } 2000^{\circ}\text{F}$$

TABLE 2. 13
D140E1
AVERAGE SECONDARY HEATING RATES

Component	Weight, grams	Heating Rates, $\frac{\text{watts}}{\text{g/mw}}$		
		Neutron	Gamma	Total
Core	$1. 36 \times 10^6$	0. 014	0. 047	0. 061
Forward reflector				
3. 25 in. Be	$8. 3 \times 10^4$	0. 006	0. 008	0. 014
1. 50 in. BeO	$5. 4 \times 10^4$	0. 006	0. 018	0. 024
BeO aft reflector	$5. 4 \times 10^4$	0. 005	0. 013	0. 018
Rear grate	$6. 0 \times 10^4$		0. 010	0. 010
Shaft	$4. 2 \times 10^4$	0. 0008	0. 022	0. 023
Tunnel and liner	$6. 1 \times 10^4$	0. 0009	0. 025	0. 026
1. 8 in. Al ₂ O ₃ island	$1. 4 \times 10^5$	0. 005	0. 030	0. 035
Be shaft shielding				
Front	$1. 1 \times 10^4$	0. 006	0. 010	0. 016
Rear	$8. 2 \times 10^3$	0. 005	0. 006	0. 011
Radial reflector	$1. 7 \times 10^6$	0. 002	0. 011	0. 013
Pressure pads (1% B ¹⁰)	$1. 7 \times 10^5$ (0.25 in nominal)	0. 018 ^a	0. 0026	0. 021
Springs	$3. 2 \times 10^5$		0. 0020	0. 0020
Shell	$1. 1 \times 10^5$		0. 0015	0. 0015
Absorber rod			0. 068	0. 068

^a(n, α) reaction in B¹⁰.

~~SECRET~~

SECRET
UNCLASSIFIED

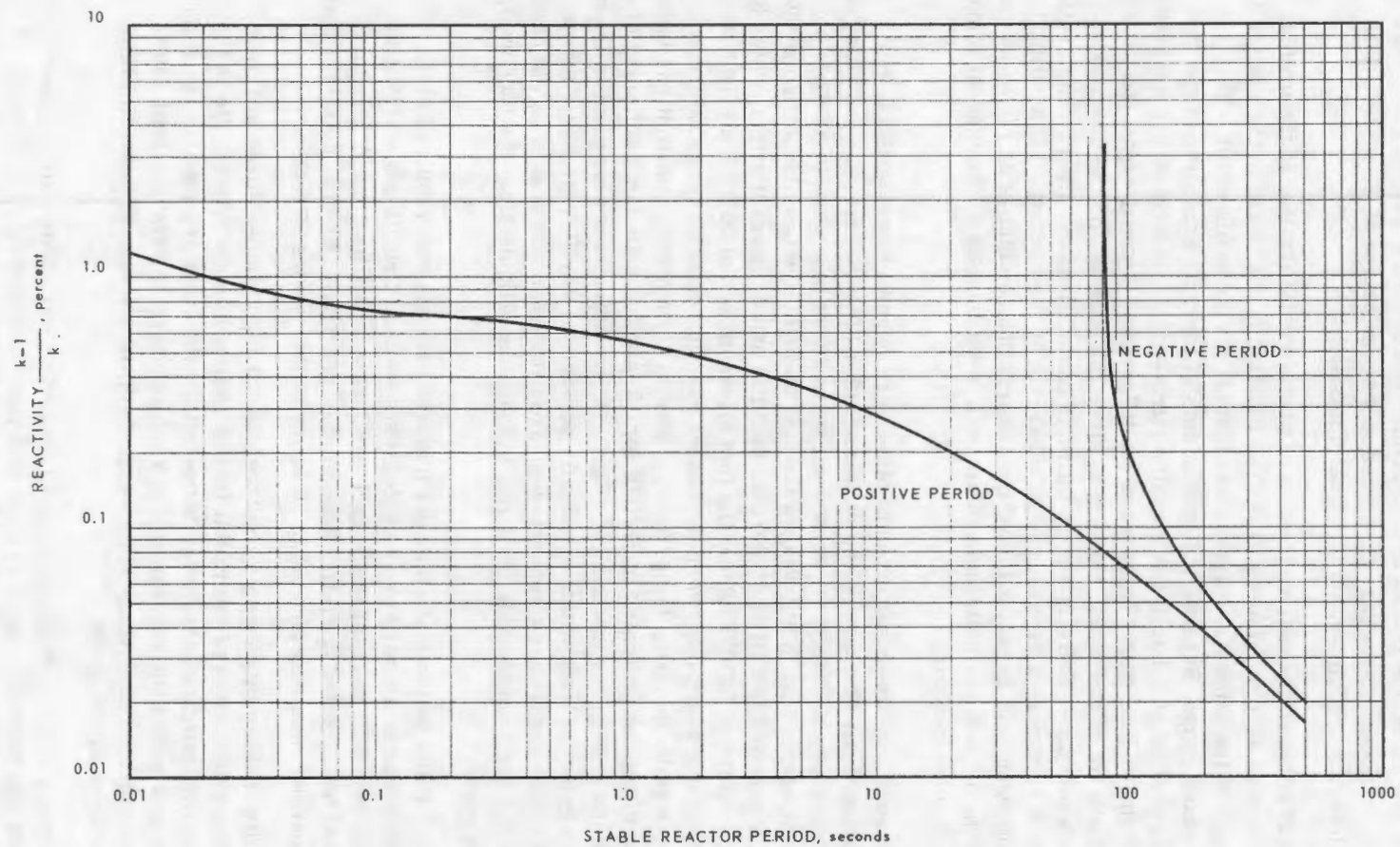


Fig. 2.21 - Stable reactor period versus reactivity for the D140E1 reactor at 68°F

SECRET
UNCLASSIFIED

~~SECRET~~

15 percent Y_2O_3 has been added. The over-all diameter of the fuel element across flats is 0.249 inch, the diameter of the bore is 0.167 inch, and the coating thickness is 0.003 inch. The tube and coating are formed simultaneously by an extrusion process. After extrusion, the tubes are heated to approximately 1100°F for removal of moisture and organic binder materials and are then fired at a temperature of about 2900°F to achieve final sintering to high density and final dimensions.

The function of yttria in the fuel element is to prevent volatilization of the urania from the fuel element at high temperatures. The function of the yttria in the coating is to prevent change of the zirconia crystal form that otherwise would occur within a certain temperature range. Because the coefficients of thermal expansion of the stabilized-zirconia coating and that of the beryllia-yttria-urania underbody are essentially the same (differing by less than 1%), there is no differential thermal expansion to cause the coating to flake off of the tubes. Moreover, since the coating and the underbody are extruded at the same time, there is a very intimate contact between the two materials; and this also acts to assure a high degree of adherence to the coating. The coating has proved very adherent, and in only a few of the several thousand tubes so far produced and tested has there been any noticeable flaking off, even in tests at the highest temperatures expected in the reactor.

The fuel elements have been subjected to other very careful investigations. For example, the phase equilibria among the various oxides (urania, zirconia, beryllia, and yttria) in the fuel element have been worked out in an effort to ascertain whether any low-melting components that might weaken the fuel element are possible. The lowest-melting eutectic possible is that of 17 percent beryllia and 83 percent yttria, which has a liquidus temperature of 2870°F. Since the fuel elements run at 2530°F (at the hottest), there is a comfortable margin between the lowest possible eutectic temperature and the maximum possible operating temperature. Moreover, experimentally it has been observed that the tubes can be heated to 3800°F for 15 minutes with some softening of the material being the only gross mechanical effect. Other indications also point to the conclusion that the eutectic, although theoretically possible at 2870°F, probably forms slowly even at somewhat higher temperatures, and even when formed, does not cause disintegration of the tube material, but tends to exude as a liquid from the tube wall, which remains sound.

The retention of fuel by the fuel elements likewise exceeds that required in the reactor by substantial margins. For example, tests made at 2600°F showed that in 1000 hours, less than 0.03 percent of the fuel was lost by volatilization. A loss up to 10 percent could be tolerated from the standpoint of reactivity. Even at 3000°F a loss of only 3 to 5 percent was experienced in 10 hours in this series of tests.

The possibility that the tubes would bond together at high temperatures and over long periods under the action of the radial forces imposed on the tube bundle in the reactor has been investigated. At forces between the tubes that are roughly twice the maximum expected within the reactor and at a temperature of 2675°F (about 150° above the maximum operating temperature expected), no sticking of tubes to each other occurred in even 500 hours.

The effectiveness of the zirconia coating in protecting beryllium oxide against water-vapor corrosion has been measured in tests that have extended up to 1000 hours at temperatures of 2500°F in air having a dew point of 25°F. In these tests the roughening of the surfaces of the tubes due to corrosion (this effect is the first one noticeable as a result of the corrosion process) produced an increase in the friction factor of less than 1 percent. An increase of 10 percent or more could easily be tolerated. Other tests in

~~SECRET~~

which the weight loss of beryllium oxide coated with zirconia was observed also have been made, and these prove that the zirconia coating has a high degree of protective action.

The fuel materials operate at a temperature sufficiently high so that some creep under compressive forces might be expected. As much as 0.5 percent creep at 2200°F, however, would be acceptable. A large number of measurements have been made at various temperatures. At 2200°F the creep is immeasurably small in 1000 hours (less than 0.1 percent). At 2500°F the creep in 1000 hours also is not measurable. At 2675°F, the largest creep rate measured is about 0.7 percent in 1000 hours. Evidently there is a very adequate creep margin.

The question of whether nuclear burnup will adversely affect the strength of the fuel material has been investigated. In a test in which the degree of burnup (fissions per unit volume) was roughly twice the maximum expected in the reactor over its entire operating life, the minimum crushing strength of the tubes after the test was not detectably different from that of the tubes before the test.

A substantial amount of the work on the degree of release of fission products in the fuel also has been done. This work establishes that, at temperatures below about 2500° to 2600°F, there is essentially no diffusion of the fission products within the fuel body to the surface, although at higher temperatures diffusion becomes noticeable. Since the maximum operating temperature in the reactor is expected to be 2530°F, the fission products released from the reactor will be those that are ejected into the airstream as a result of direct recoil from the surfaces of the fuel tubes. A considerable number of tests leads to the conclusion that the amount of fission product escape will be considerably less than 0.1 percent of the fission products formed in the fuel. Other studies indicate that escape rates of a few tenths of a percent can be tolerated for the operation of substantial numbers of nuclear aircraft from certain bases. Thus the indication is that the fission product retention in the fuel elements in normal use is satisfactory from the standpoint of ultimate utilization.

A final point of considerable study in fuel elements is related to thermal-stress cracking. It should be pointed out that the occurrence of cracks in the fuel elements does not necessarily render them unfit for use in the reactor. To verify this, tests have been conducted in which bundles of tubes simulating a portion of the reactor have been assembled and have been put through a variety of mechanical and thermal treatments aimed at producing a disintegration of the bundles or dislodging pieces of the tubes, if this could occur under conditions foreseeable in the reactor. It was found that even when the tubes used in such tests had two full-length longitudinal cracks in them, (so that each tube was in two parts), the bundle was sound and remained sound throughout the entire series of tests. However, although of questionable practical importance, the occurrence of cracks due to thermal stress is an indication of the strength of the tubes in service and, for this reason, has been studied extensively in the laboratory. These studies have shown that the critical stress condition for the tubes occurs after they have been heated for a substantial period to a high temperature and have been brought to an essentially zero-stress condition (by virtue of plastic flow) at this high temperature and then cooled. On cooling, tensile stress is developed in the outer fibers of the tube and, if sufficiently high, can produce cracks. It has been found that this condition can be predicted analytically with accuracy and that the stresses calculated to produce cracks are essentially identical with those measured in modulus-of-rupture tests as being necessary to break the tube.

In the reactor the expected stress is a function of position within the core and has been calculated for appropriately conservative loading conditions. If the radial com-

~~CONFIDENTIAL~~
~~SECRET~~

pressive loads were uniformly distributed on the fuel elements, the maximum stress within them would be a 75-psi compressive stress. However, in making stress calculations it has been assumed that the loading can be two-sided as opposed to six-sided and uniform. It has further been assumed that a load multiplier of 3 applies because of possible non-uniform load paths through the core. For inertial loading during flight an additional factor of 4 is used, based on analyses that showed that the tubes near the top of the core will experience 4 times their normal load during the transient inertial loading of the core. Bending of tubes due to non-uniform longitudinal temperature distributions is also considered. The magnitude of the stress and the combination of mechanical and thermal stress varies axially through the core. The maximum calculated stress is 15,000 psi, which is primarily bending stress, and which occurs near the inlet end of the active core. The thermal stress component at this point is only about 2,000 psi. The point of maximum calculated thermal stress is 6 inches downstream from the inlet end of the core. At this point, the thermal stress component is 4,000 psi and the total stress is 8,000 psi. Since the modulus of rupture of the material at the lowest level is approximately 25,000 psi, a considerable margin exists between the stress calculated on the tubes and their strength as measured. It should be noted further that the thermal stress component is small enough so that there is a considerable margin for variation of the power density from that required for the cruise condition.

2.1.1.5 Instrumentation

Objectives

The general purposes of establishing of instrumentation are (1) to provide thermal design verification, (2) to identify changes in reactor performance with operating history, and (3) to provide a broad coverage of localized fuel element surface and air temperature. Specifically, the detailed objectives of the described instrumentation are threefold. First, fuel element temperature and fuel element discharge air temperature distributions should be identified as accurately as possible. Second, core over-all pressure ratio should be determined. Third, operating temperatures of secondary components such as guide tubes, springs, aft retainer, reflector, and others should be monitored.

Of particular importance is the first objective, that of adequately identifying fuel element surface temperatures and air discharge temperature distribution. This section is devoted primarily to a description of the techniques proposed for fulfilling this objective.

The second objective will be attained by a series of pressure probes within the fore and aft plenums. The core pressure loss characteristics as well as flow distribution within the core will be established by developmental testing. These pressure probes will be used for a check of the design input.

Configuration

The thermocouples to measure the reactor fuel element temperatures and the active core discharge air temperatures will be noble metal, coaxial-construction thermocouples with magnesium oxide insulation. The thermocouples will be platinum - platinum-rhodium. The sheath outside diameter is expected to be 0.0625 inch, and the wire diameter, 0.012 inch.

Thermocouples used for measuring fuel temperatures will have leads that enter at the forward periphery of the core and then pass radially between the front face of the forward reflector and the instrumentation cover. Leads will then enter selected unfueled instru-

~~SECRET~~
~~CONFIDENTIAL~~

mentation tubes after passing through the front reflector and transition pieces. The unfueled tubes will be closed downstream from the thermocouples to prevent airflow in the dead tube. Thermocouples used for measuring air temperatures will pass axially along the outer reflector to the rear of the core before turning radially inward. Air discharge temperatures will be measured at selected aft retainer channels.

Secondary Components

It is planned that a total of 364 thermocouples be used for secondary component and exit air temperature measurements. Table 2.14 shows the detailed locations and quantity to be used for each component.

Radial and Circumferential Locations - Active Core

Thermocouple locations for fuel temperature measurements are shown in Figure 2.22. Three thermocouples are to be inserted in each instrumentation tube located on the radial planes marked "A." Within the active core there are six such planes, each with ten instrumentation tubes, that thus provide a total of 180 thermocouples. Two thermocouples are to be inserted in each instrumented tube located on the radial planes marked "B." There are also six of these planes, and each has six tubes so that 72 more thermocouples can be accommodated. Additional thermocouples will be used at points marked "a" on Figure 2.22 for a total of 12 and at points marked "b" for a total of 24 thermocouples. The grand total of fuel temperature measurements is therefore 288. Figure 2.22 shows additional details of the method to be used for locating thermocouples radially and circumferentially. Note for instance that in successive radial planes marked "A" in a clockwise fashion the instrumentation tubes are located at successively larger radii. At least one thermocouple will be at some circumferential location in every annular zone of different fuel loading. This technique for distributing thermocouples within the reactor core eliminates having many instrumentation tubes in any given sector.

Longitudinal Locations - Active Core

Each instrumentation tube within the active core along the "A" and "B" radial planes shown in Figure 2.22 carries one thermocouple for measuring the surface temperature at the longitudinal location $x/l = 0.80$. Thus, there will be 96 measurements at this location. Also there will be 96 measurements of surface temperature at the longitudinal location $x/l = 0.40$. The remaining thermocouples located on radial planes marked "A," that is, one per tube or a total of 60, will be used for measuring surface temperatures at various longitudinal locations so that other points in the longitudinal temperature profile of a given tube may be measured.

Measurement of active core air temperatures will be made at selected aft retainer discharge channels after some mixing of air from individual tubes has occurred. These measurement locations will be such that air from those channels having surface temperature measurements will contribute to the mixed air temperature measurement. Thus there will be 96 such thermocouples. Additional air temperature measurements will be made at each point marked "c" in Figure 2.22 with a total of 12 thermocouples. The total number of thermocouples measuring air temperature is 108.

Summary

A summary of thermocouple locations and also the quantity of thermocouples measuring fuel temperatures within the active core and measuring core discharge air temperature is shown in Table 2.15.

Of the 24,881 channels at the predicted longitudinal location of maximum surface temperature ($x/l = 0.80$), there will be 96 separate measurements of different surface

~~CONFIDENTIAL~~
SECRET

TABLE 2. 14
SECONDARY COMPONENT SURFACE AND AIR THERMOCOUPLES

Component	Thermocouple Location ^a	Number of Thermocouples	
		Surface	Air
Forward beryllium reflector	Forward face, on 0° radius	6	
Tunnel	0.4 $\frac{x}{l}$, 0.8 $\frac{x}{l}$, (0 and 90 degrees each)	4	
	Air Discharge		2
Shaft liner	0, 0.4, 0.8, 1.0 $\frac{x}{l}$ (180 and 270 degrees each)	8	
	Air discharge		2
Island reflector	See Figure 2. 23, radial planes "A," 0.4 and 0.8 $\frac{x}{l}$	12	
Outer reflector	See Figure 2. 23, radial planes "A" and "B", 34 tubes, 0.4 and 0.8 $\frac{x}{l}$	68	
	Air discharge		34
Hex arches	At insulation and hexagonal arch boundary	32	
Poison rod guide tubes	4 locations on 2 units	8	
	Air discharge, 24 units		24
Outer reflector tubes, outer row	Air discharge opposite even-numbered alternate pads		24
Pads	Odd-numbered, alternate pads, center	24	
Springs	Alternate axial rows at 0° and 180° (2 per spring at pad bearing locations)	16	
	At 0.8 $\frac{x}{l}$ alternate springs at center	12	
	Air discharge; 30-degree intervals around reactor		12
Aft retainer	12 radial locations each for forward plate and aft plate at 0 and 90 degrees	48	
	Air discharge before mixing		8
Rear transition pieces	10 at midpoint, 10 at aft end; 330 degrees	20	
	Total thermocouples: Component surface	258	
	Air		106
	Combined surface and air	364	

^aAngular locations refer to reactor circumferential locations with 0 degrees at the top, measuring clockwise and looking in the direction of airflow.

SECRET
~~CONFIDENTIAL~~

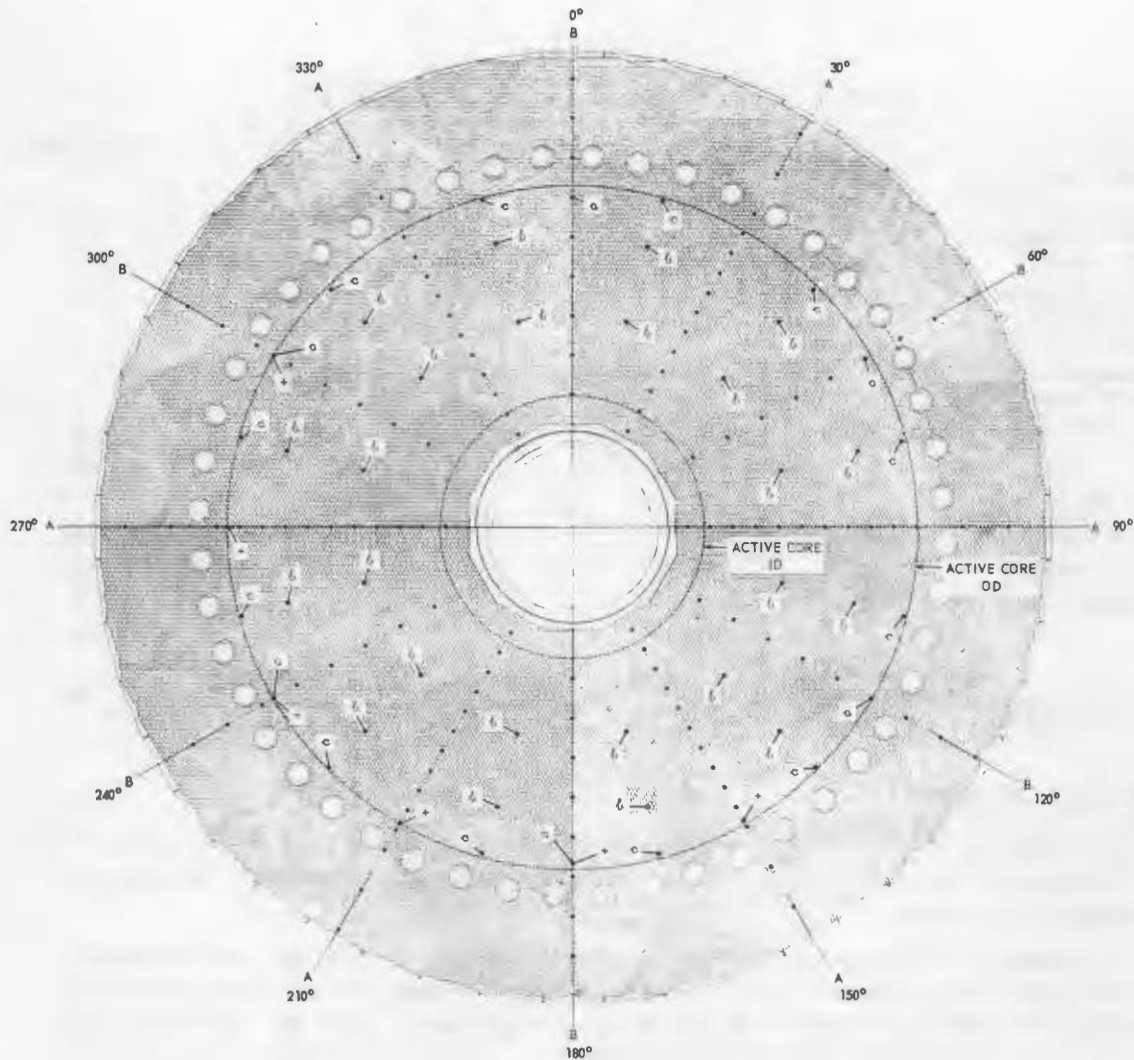


Fig. 2.22 - D140E1 instrumentation thermocouple locations

temperatures. Every zone having a different fuel loading will have a thermocouple at some circumferential location. Of the 1310 transition pieces delivering air to the aft retainer, there will be a mixed air temperature measurement at the discharge from 108 of the transition pieces. The total of all active core and secondary component thermocouples is 760.

It is believed that instrumentation described here will provide adequate monitoring of reactor temperatures to obtain necessary control indications, design verification, and measurements of changing performance during the life of the reactor.

2.1.2 ENGINES

Turbomachinery for the D140E1 assembly consists of a compressor, turbine, chemical fuel combustor, exhaust duct, exhaust nozzle, accessory drives, and various accessory and control systems.

SECRET

TABLE 2. 15

ACTIVE CORE FUEL AND AIR DISCHARGE THERMOCOUPLES

Circumferential Locations ^a	Number of Groups	Number of Tubes Per Group	Number of Thermocouples Per Tube	Axial Location of Thermocouples	Total Thermocouples
Fuel Thermocouples					
Radial planes "A" 30, 90, 150, 210, 270, 330 degrees	6	10	3	0.4 π /1, 0.8 π /1 plus 1 additional	180
Radial planes "B" 0, 60, 120, 180, 240, 300 degrees	6	6	2	0.4 π /1, 0.8 π /1	72
Radial planes "B" Locations marked "a"	6	1 (outermost)	2	0.8 π /1	12
Locations marked "b"	12	2	1	0.4 π /1	24
TOTAL FUEL THERMOCOUPLES					288
Air Thermocouples					
Radial planes "A"	6	10	1	Core discharge	60
Radial planes "B"	6	6	1	Core discharge	36
Locations marked "C"	12	1	1	Core discharge	12
TOTAL AIR THERMOCOUPLES					108
TOTAL AIR AND FUEL THERMOCOUPLES					396

^aSee Figure 2. 23.

2. 1. 2. 1 Compressor

The 16-stage rotor is the rotating member of the compressor assembly that forces air through the compressor. It provides the inner wall of the compressor air passage and a route for cooling air.

The stator assembly consists of the front and rear casings, stator vanes, shrouds, lever arms, and actuation rings. The casings form a cylindrical shell that serves as an outer wall for the compressor air passage and provides support for the compressor front frame, 16 stages of stator vanes and their linkages, the outlet guide vanes, air-extracting hardware, and accessory gearboxes. The first two stages of the compressor stators are shrouded. The inlet guide vanes and stator vanes of stages 1 through 10 can be scheduled to provide optimum performance over the operating limits of the power plant. The stage-16 vanes will close completely to act as a shutoff valve.

The front frame assembly consists of the front frame, inlet guide vanes, No. 1 bearing sump and No. 1 bearing, and air and oil seals. It provides structural rigidity for the compressor stator and supports the No. 1 bearing, gearbox equipment (including starter), bellmouth extension, and bulletnose hardware.

The rear frame provides support and service passage for the No. 2 bearing sump (the No. 2 bearing carries the total thrust loads of the main rotor system as well as its portion of radial loads) and provides forward power plant support, reacting horizontal, vertical, and side power plant loads. The rear frame also ducts compressor discharge air into the forward shield area and provides auxiliary air bleed on the port side.

2. 1. 2. 2 Turbine

The front frame provides support and service passage for the No. 3 bearing sump (shaft radial loads only) and supports the rear trunnion for the power plant (side and vertical loads only). Part of the front frame serves as a section of the rear shield. The turbine front frame also provides air passage and all mounting provisions for the combustor and

SECRET

~~CONFIDENTIAL~~
~~SECRET~~

provides flow passages for speed bleed, aftercooling, and turbine cooling. Other functions of the turbine front frame include provisions for turbine-stator mounting, axial anchor mounting of the side shield, and ground-handling pads for the rear portion of the power plant.

The rotor extracts power from the kinetic energy of the heated primary air that flows over it and transmits the extracted power through its shaft to the compressor and associated accessories.

The turbine shaft passes through the center of the reactor and is connected to the compressor-rotor rear stub shaft and the turbine-rotor first-stage disk. Shaft length, diameter, and section properties have been established so that the critical speed of the shaft is above the required military-operation engine speed of 5000 rpm.

The stator accelerates airflow into the turbine buckets, directs the airflow through the nozzle diaphragms to provide proper flow angles for effective energy extraction, and connects the turbine front and rear frames. A trailing-edge bleed is provided in the first stage to improve cooling. Internal cooling is accomplished by means of air ducted from the speed-control bleed annulus.

The rear frame provides a diffusing air passage for exhaust gas from the turbine, supports and provides service passage to the No. 4 bearing sump, supports the exhaust duct (including tailpipe), and provides structural rigidity for the turbine casing.

2. 1. 2. 3 Combustor

The series chemical combustor enables chemical checkout of the engines prior to nuclear running, chemical startup, and test operations over a wide range of nuclear power. The exact design of the combustor has not been determined. Design effort at present is based upon an internal fuel-injection flame holder with a blockage area of approximately 60 percent installed in the area just aft of the turbine front-frame struts. The annular burner will have approximately 50 fuel nozzles to ensure uniform injection of fuel. The burner will consist of the flame-holder dome plus heat-radiation-resistant liners; downstream mixers probably will be added to aid combustion.

2. 1. 2. 4 Exhaust Duct

The exhaust duct section provides for passage of exhaust gases to the jet nozzle and supports the jet-nozzle assembly. The sections consists of two cylinders of Inconel W joined by a bolted flange. The ducts are essentially casings stiffened externally for rigidity. The jet nozzle, as presently designed, is a convergent finger nozzle. The function of the jet nozzle is the control of engine speed and thrust.

2. 1. 2. 5 Accessory Drives

The function of the accessory drives is to supply mechanical power for various engine and aircraft accessories. Power extraction for engine-driven accessories is accomplished through the compressor front frame. An inlet gearbox, located in the front-frame hub, transmits main shaft power through a radial drive shaft to the transfer gearbox, which is mounted on the compressor front-frame outer casing. A horizontal drive shaft transmits power from the transfer gearbox to the rear gearbox, which is mounted on the compressor stator casing.

2.1.3 SHIELD

The reactor shield for the D140E1 test assembly is a flight-type shield based on the divided-shield concept, in which shielding is located around both the reactor and the crew compartment in such a way that the total weight of shielding is minimized and the

~~CONFIDENTIAL~~
~~SECRET~~

CONFIDENTIAL
~~SECRET~~

activation and radiation damage of power plant and aircraft components is held within tolerable limits. The shield assembly, shown in Figure 2.23, is located between the compressor rear frame and the turbine front frame and consists of a radial shield and front and rear shields. Primary air is used to dissipate nuclear heat in the front and rear shields, and air from an auxiliary supply is used to cool the radial shield for ground testing. In the flight system the radial shield will be cooled with ram air. The shield attenuates the neutron and gamma dose levels around the power plant to the values shown in Figures 2.24 and 2.25.

Radial Shield

The radial (side) shield, shown in Figure 2.26, consists of nearly identical top and bottom sections made up of full-length segments and side cheeks, which in the flight system are contained in the airplane structure and in the test assembly are mounted in the test structure. The segments and cheeks consist of LiH cast in stainless steel cans. The air that cools each of the shield elements enters at the front end of the element, dumps into an inlet plenum, flows through tubes dispersed throughout the element cross section, and then dumps out around the turbine casing.

The inertial loads of the segments in the top and bottom sections are carried by the cans, which act as thin-skinned semimonocoque structures around the shielding-material castings. The segment cans of each section are connected to form a complete structure, and both sections are attached to the power plant at the forward flanges of the pressure vessel and at the aft trunnion ring on the turbine front frame. Vertical and side loads are reacted at the forward attachments. Fore, aft, and side loads are reacted at the vertical centerline of the aft attachment points, and vertical loads are reacted at the horizontal aft attachment points.

For removal each half-section of the shield is freed by disengaging four pins. The aft attachment of the power plant to the airframe pierces the upper half of the radial shield. The aft section of the upper half is therefore split from the forward section and may be slid back to allow installation or removal of the upper half of the shield assembly.

Rear Shield

The rear shield, shown in Figure 2.27, consists of an outer annular portion, which is attached to the reactor core, and an inner island, which is attached to the turbine front frame and to the structural wall of the combustor section.

The outer annulus consists of a ring of shielding material surrounded and supported by a structural shell. The outside surface of the shell is a cylinder, which is flanged to the core support cylinder. The inside surface of the shell forms the wall of the primary air duct and is thermally insulated by pads attached intermittently by fasteners that provide for differential expansions between the duct wall and the insulation pads. Each insulation pad consists of (1) a cover sheet that is exposed to the hot primary airstream and is cooled by air flowing through a corrugated liner attached to the inner surface, and (2) alumina-silica insulation between the liner and the duct wall to provide an additional thermal barrier. The cooling air is introduced into each pad through the duct wall and, after cooling the cover sheet, is dumped into the primary airstream. This duct wall also transmits the loads from the core aft retainer plates to the outside cylindrical shell.

The shielding material in the outer annulus consists of blocks of borated beryllium. The blocks are restrained from touching the structural shell by spacers, and cooling air flows through this void. Cooling air introduced into the front of the annular shield is the same

~~SECRET~~

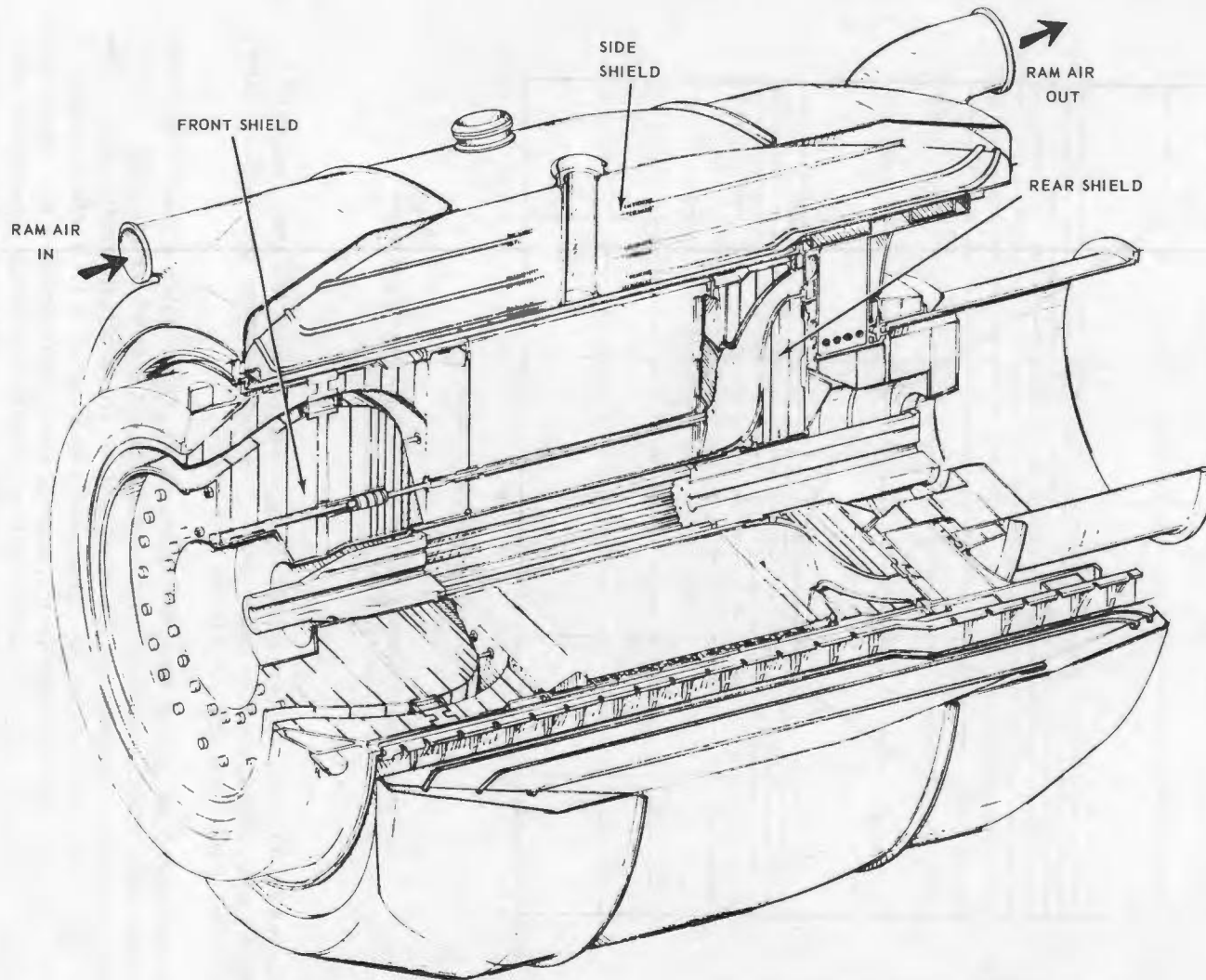


Fig. 2.23 - D140E1 reactor-shield assembly

~~SECRET~~
CONFIDENTIAL

~~SECRET~~
CONFIDENTIAL

CONFIDENTIAL
SECRET

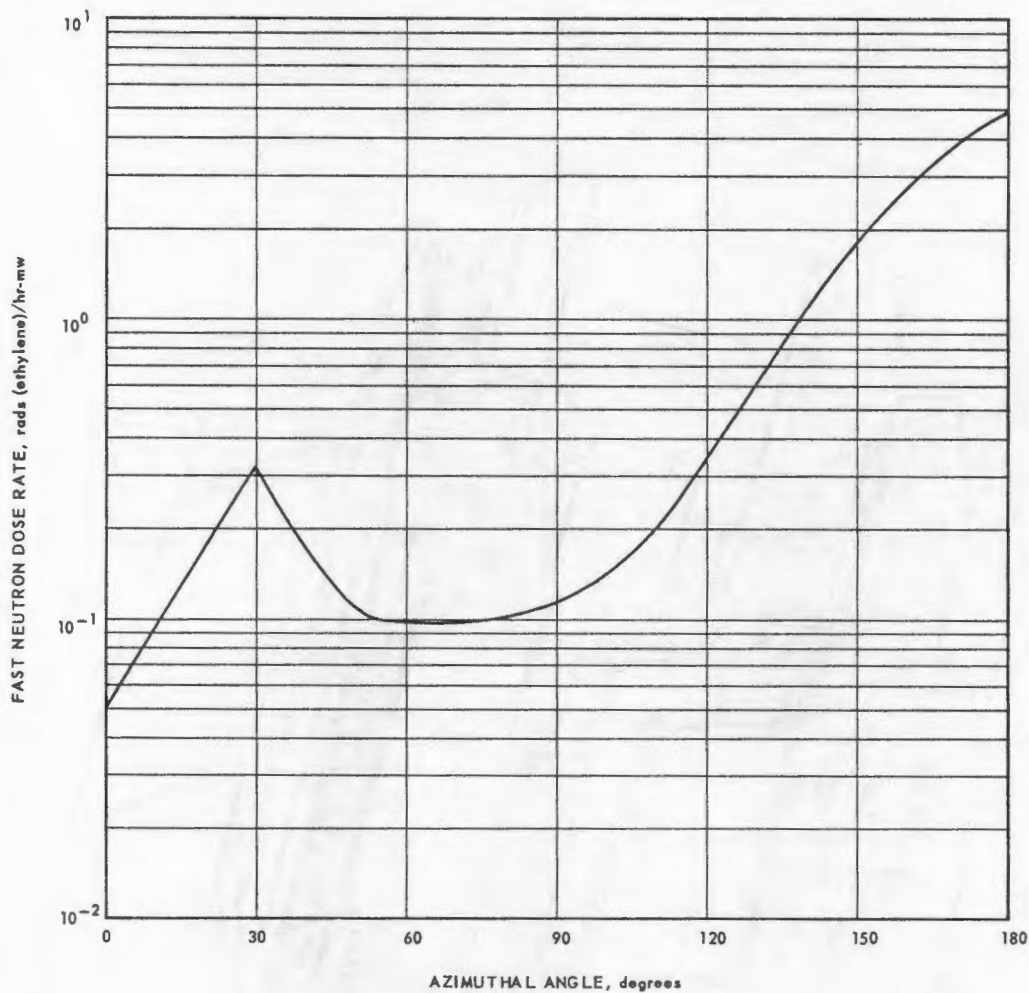


Fig. 2.24 - Objective fast neutron dose rates per megawatt of reactor power 50 feet from D140E1 reactor midpoint

air that was used to cool the core radial springs. After cooling the shield material by passing through internal parallel paths, this air is used to further cool the insulation pads and then passes through holes in the duct walls.

The inner island consists of several subassemblies. One annular subassembly called the forward inner island is attached to the front side of the front turbine frame; another annular subassembly is attached to the aft side of the front turbine frame as part of the nozzle support cone. A third annular subassembly is attached to the combustor structural wall behind the front turbine frame. Each of these subassemblies is designed to be removable during power plant disassembly. Permanently attached subassemblies consisting of blocks of borated beryllium are located in the spaces between the struts of the turbine front frame. In addition, the forward inner island contains borated 304 stainless steel as gamma shielding for the front turbine bearing. This subassembly has an insulated duct wall like that used in the outer-wall annulus described above.

Cooling air for the forward inner island and for the forward insulation liner is supplied from the front shield through the annulus between the shaft tunnel and the core liner.

SECRET

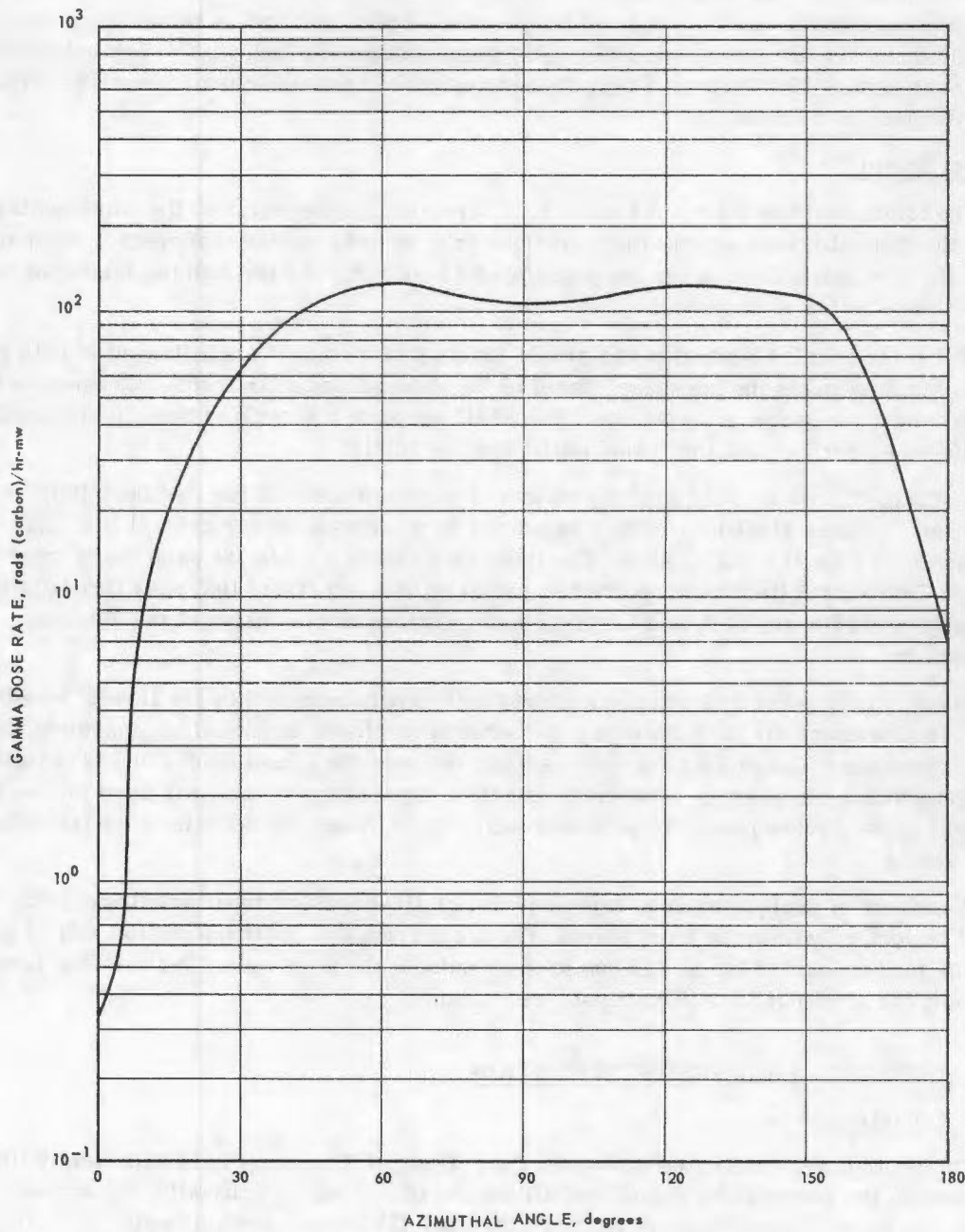


Fig. 2.25 - Objective gamma dose rates per megawatt of reactor power 50 feet from D140E1 reactor midpoint

After circulating through the forward inner island, the air is used to cool the insulation of the combustor duct wall. The subassemblies between the struts are cooled by air flowing from the annulus between the shaft and shaft tunnel to the annulus between the rear shield and the pressure vessel. The aft inner-island subassemblies are cooled by air flowing through the turbine front frame struts from the annulus between the rear shield and pressure shell. A number of instrumentation sensors will be located within the rear shield. The leads will be gathered and passed through one of the struts forming the turbine front frame.

Front Shield

The front shield is shown in Figure 2.28. The annular gap between the outer section and the central island directs the primary-cycle air between the compressor discharge and the core inlet. Access for the passage of 48 control rods through the island portion into the reflector is provided.

The outer annular portion of the shield consists of a conical shell flanged at both ends. This shell connects the pressure vessel to the compressor rear frame and contains the internal air pressure of the system. The shell supports the borated beryllium shield blocks on its inner surface and the island portion of the shield.

The island portion of the shield consists of sectored disks of borated beryllium and borated stainless steel located and supported by a large-diameter central liner that provides access for the engine shaft. The liner also reacts significant axial loads from the core. The central liner is supported by radial beams and struts that pass through the island, cross the air duct, and are attached to fittings on the inside of the annular assembly.

Nuclear heat generated within the shield material is removed by the flow of bleed air from the primary air duct through gaps between the disks. In the island assembly, air is bled from the primary duct outward radially between the shield blocks and is collected in the annular air passage between the shield and pressure vessel. Air used to cool the shield is used subsequently to provide cooling for various components downstream from the shield.

A number of nuclear heating-rate sensors, static-pressure taps, and thermocouples will be located within the front shield. The leads from this instrumentation will be gathered at the forward end of the shield and brought outside the power plant between the flanges joining the shield and the compressor rear frame.

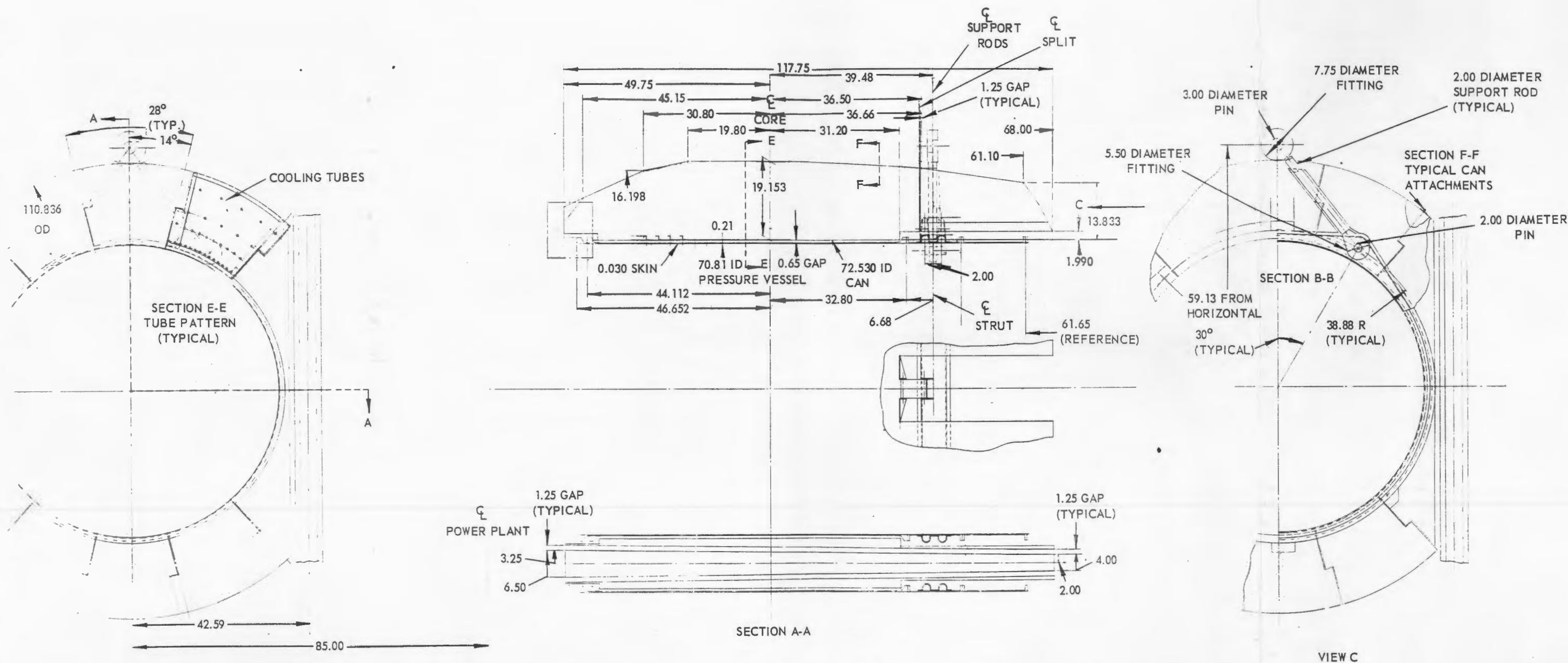
2.1.4 CONTROLS AND INSTRUMENTATION

2.1.4.1 Introduction

The control system for the Advanced Core Test (ACT) assembly is sufficiently flexible to control the power plant throughout all phases of testing. Specifically, the system permits: (1) manual and automatic reactor startups; (2) manual and automatic reactor power control from 150 watts or lower to 150 megawatts; (3) control of turbine discharge temperature either by automatic modulation of nuclear power or manual programming of chemical fuel flow or modulation of nuclear and chemical power in combination; (4) regulation of engine speed from idle to 5000 rpm; (5) manual positioning of the engine exhaust nozzle; (6) automatic positioning of the compressor stators as a function of engine speed and inlet temperature; (7) transfer of power between nuclear and chemical heat sources; and (8) manual starting of the engine on either chemical or nuclear power.

DECLASSIFIED

DECLASSIFIED



NOTE: DIMENSIONS IN INCHES

Fig. 2.26 - D140E1 radial (side) shield

DECLASSIFIED

DECLASSIFIED

CONFIDENTIAL

AL

~~SECRET~~

CONFIDENTIAL
DECLASSIFIED

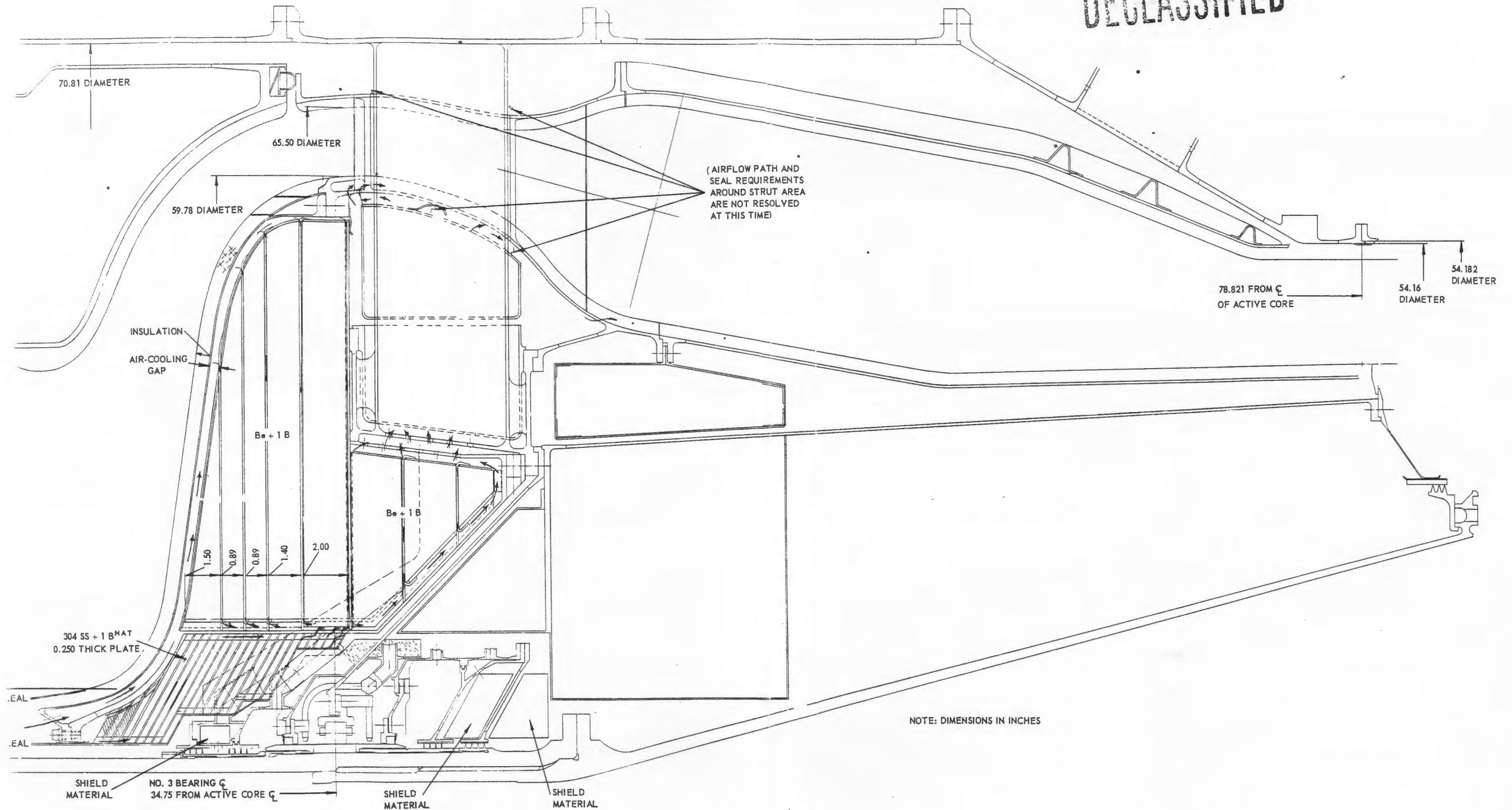


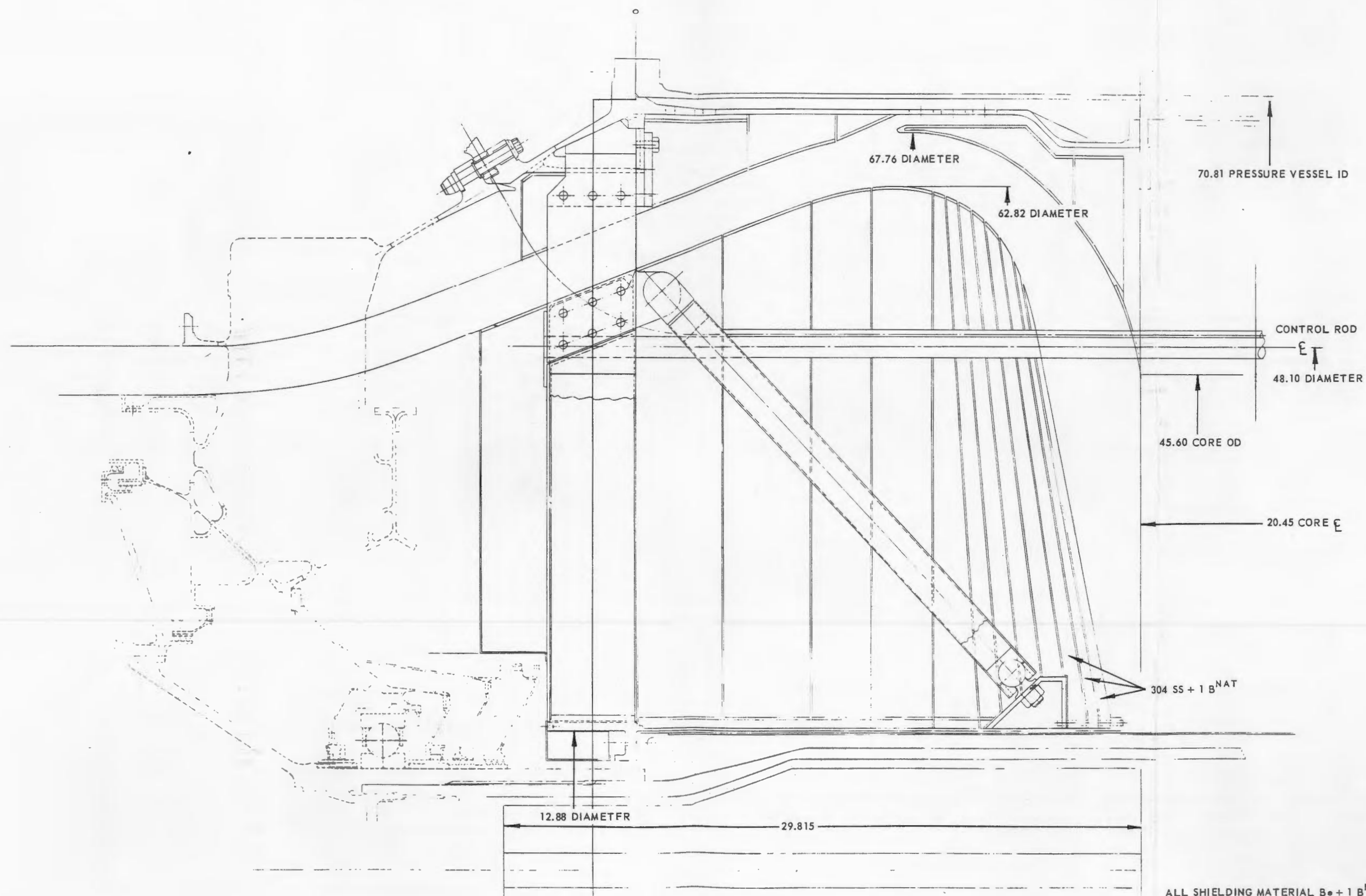
Fig. 2.27 - D140E1 rear shield

~~SECRET~~

CONFIDENTIAL
DECLASSIFIED

DECLASSIFIED

~~SECRET~~
DECLASSIFIED



ALL SHIELDING MATERIAL 304 SS + 1 B^{NAT} UNLESS NOTED

Note: Dimensions in inches

Fig. 2.28 - D140E1 front shield

DECLASSIFIED

~~SECRET~~

CONFIDENTIAL

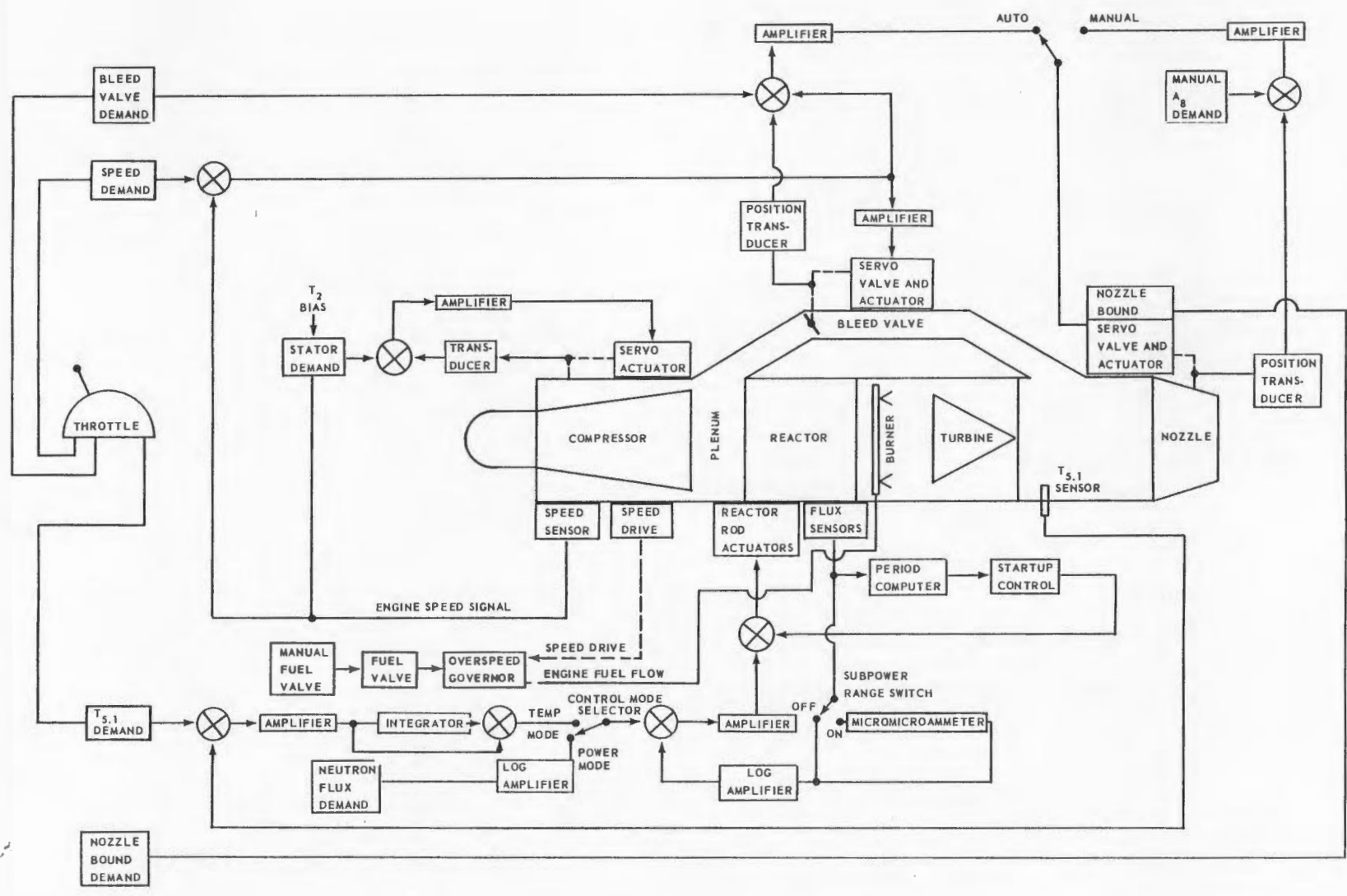


Fig. 2.29 - Block diagram of D140E1 assembly control

CONFIDENTIAL

The ACT assembly control system as shown in Figure 2.29 is composed of a number of separate servosystems, each of which regulates an individual engine parameter to establish the operating conditions of the assembly while performance is maintained within safe acceptable limits. The regulated assembly parameters (controlled variables) are:

1. Engine rotor speed (N) controlled by regulating turbine-bypass bleed area (W_{BC}) and jet nozzle area (A_B).
2. Turbine discharge temperature ($T_{5,1}$) controlled by regulating reactor power (ϕ) and/or combustor fuel flow (W_f).
3. Reactor startup period (τ) controlled by regulating neutron flux.
4. Compressor stator blade angle (β) controlled as a function of corrected engine speed.
5. Turbine-bypass bleed area (A_B) reset by jet nozzle area.
6. Engine fuel flow (W_f) controlled by fuel valve position.

Positive control is achieved by employing stable closed-loop servosystems to accurately and responsively regulate the controlled variables mentioned above. The four main control systems required are (1) the engine-speed control system (includes controls for the bleed valve and jet nozzle area), (2) the reactor control system (startup and power range), (3) the manual fuel control system, and (4) the compressor-stator control system.

The operating condition of the test assembly is governed from a thrust selector shown in Figure 2.30, which programs a combination of input demands to the individual servosystems that influence assembly control parameters. Mounted on the control console is

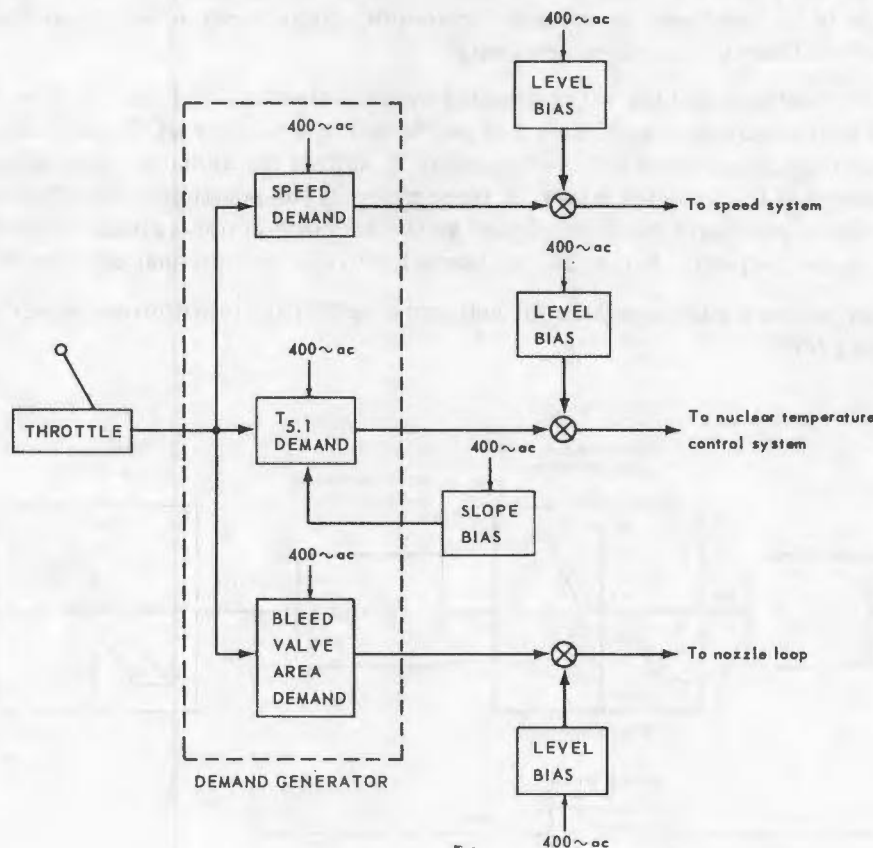


Fig. 2.30 - Thrust selector for ACT assembly

CONFIDENTIAL
SECRET

a throttle lever, the position of which affects the orientation of the cams inside the thrust selector and thus the engine operating point. Individual throttle biases, adjustable from the control console, are incorporated into the engine speed, turbine discharge temperature, and bleed-valve-area reset demands to aid in establishing proper steady-state demand schedules and to establish special off-schedule operating modes required for testing the reactor and the over-all assembly.

The test assembly can be controlled by a single operator from the control console. In addition, other operators are required during the test to operate the accessory systems and monitor supervisory instrumentation. Enough control switching and instrumentation is employed to permit chemical, nuclear, or chemical-nuclear operation without the aid of auxiliary control equipment. The console therefore has nuclear operational flight requirements integrated into its design.

2. 1. 4. 2 Reactor Control Rod Actuation System

The actuation system refers to the control rod actuators, their associated position loops, and the actuator selectors.

Position loops will be utilized to insure that the rods are properly synchronized when the actuators are on automatic control. The actuator controls are utilized to perform functions such as selecting actuators for manual or automatic control and isolating actuators.

Figure 2. 31 shows a block diagram of a position loop in the control rod actuation system. Elements in the loop are the actuator drive unit, control rod actuator, and position sensor. There will be eight independent loops.

The actuator controls include eight actuator mode selectors and an actuator action switch. There is one actuator mode selector per actuator with Servo, Off, and Manual positions. The Servo position allows the position loop to control the actuator. The Off position cuts off the power to the actuator, and it is inoperative at the position attained prior to the action. The Manual position transfers control to the actuator action switch. From one to eight actuators can be put on Servo, Off, or Manual, or various combinations can be obtained.

The actuator action switch operates all actuators on Manual to withdraw, insert, or remain stationary (off).

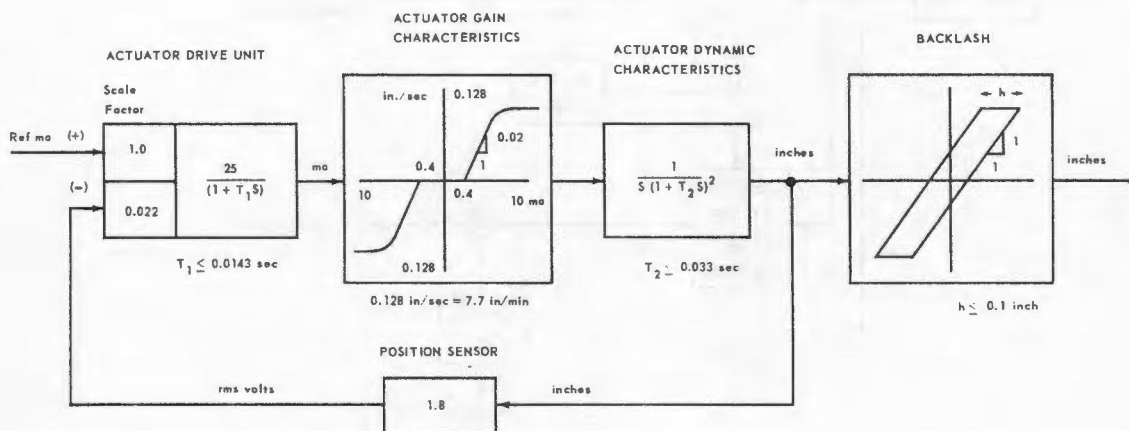


Fig. 2.31 - Control rod position loop

SECRET
CONFIDENTIAL

Position-loop test controls will be provided in such a way that an actuator can be operated over its full range of travel. This is necessary in order to make linearity and gain adjustments, and also as an aid in trouble shooting.

The control rod mechanical actuation system consists of a chain and sprocket system buried in the front shield and driven by a powerhead assembly through a transfer gearbox and radial shafts as shown on Figures 2. 32 A and 2. 32 B.

The powerhead assembly consists of a shaft driven by a pneumatic motor that in turn is controlled by an electric servovalve to provide the shimming function. The shim speed is 0 to 7.7 inches per minute. Scramming is provided by clock-type springs wound up and latched by means of an electromechanical clutch. If at any time during the 24-inch stroke, a scram signal is received, the rods would be fully inserted at a rate of 5 inches in the first 300 milliseconds. The powerhead is stopped at both ends of travel by a set of limit switches.

Shimming and scramming power is transmitted through a drive gear to the transfer box assembly that takes the power from a single powerhead assembly and distributes it to six individual chain-control-rod drives by means of the radial shafts.

The chain-control-rod drive is located in the front shield and consists of two sprockets connected by a continuous 0.25-inch pitch, high-temperature stainless-steel chain. The poison rod is connected to this chain.

Position feedback is provided by an induction potentiometer mounted on the transfer box. This potentiometer provides both position indication and feedback for the entire group of six actuators.

Startup System

The startup system will consist of three separate subsystems of source-range instrumentation operating in parallel. The function of each subsystem will be to generate log-count-rate and reactor-period signals to be displayed on the operating console. The display of calibrated log count rate and reactor period from any two of the three subsystems will be the minimum requirement for performing a reactor startup.

The reactor period signal will also be used to cause reactor scram when any two of the three period trip signals are in violation of the established period limits.

One of the instrumentation subsystems will be employed as a feedback channel for a period-regulating servomechanism. The reactor period generated will be compared with a fixed demand voltage, and, when in the servo operating mode, the control rod actuators will vary reactivity until the reactor period signal satisfies the demand.

Each instrumentation subsystem will consist of three equipment channels with each channel differing from the other only in sensitivity of the neutron sensor (Figure 2. 33). The range of each channel will be about five decades of neutron flux in such a way that nine decades can be spanned by operating each channel consecutively as the reactor startup is performed (Figure 2. 34). The count rate signals are used to accomplish reliable automatic transfer between channels of differing sensitivity. The low-count-rate signal of the next-most-sensitive channel will initiate transfer to that channel. A reactor scram will result if the high count level is attained without the simultaneous existence of a low-count signal on the succeeding channel.

The startup system will be relieved of control at 1.5 percent of maximum flux on command of the power-range-control ion chamber. If the transfer is not initiated by the power-range control, reactor scram will result from the ensuing high-count-rate signal.

~~CONFIDENTIAL~~
~~SECRET~~

Power-Range System

The power-range system refers to the neutron-flux and temperature automatic control loops, the associated reference input elements, the control mode selector, and various test and calibration controls.

An automatic neutron-flux control loop will be provided for low-level power holding, for automatically transferring from the startup to the power range, for power-range operation at low airflows where the temperature control is ineffective, and as a possible backup for the temperature loop. Power-range operation officially begins with operation of a relay in the control ion chamber circuit at approximately 2 mw (1.5 percent of full power). This relay transfers control of the actuators from the startup to the power-range system and performs other logic and switching functions. Refer to Figure 2.35 for the block diagram of the loop.

A sub-power-range control system that utilizes the components of the normal power-range system but has a sensitive amplifier (micro-microammeter) accepting the ion chamber input will be provided. This operation extends the power range down 10 decades from full power. The purpose of sub-power-range automatic control is to provide low-level power-holding capabilities.

The turbine discharge temperature ($T_{5,1}$) control will be the primary power-range control. The flux control will be used as a minor loop in the temperature control for stabilization purposes. The temperature control demand, the schedule for which will be generated from the throttle (and a manual bias), is a function of the engine cycle. Refer to Figure 2.36 for the block diagram of the temperature control.

Various selector switches will be used to obtain the desired operating mode for the control. The control mode selector will be used to select the power or temperature servo mode so that the operator can change servo modes conveniently. This selector also has an Off position that prevents the power and temperature servos from controlling the position loops. A sub-power-range switch will be provided to put the micro-microammeter into the feedback of the flux loop. A decade selector switch will also be provided to change the sensitivity of the micro-microammeter by factors of 10.

Safety System

The safety system is designed to protect the reactor core against damage by actuating alarms or scrambling the control rods when established operating or safety limits are exceeded. No provision is made for protection against sabotage, and no extra precautions are taken with respect to natural disaster such as an earthquake. In addition to protection against component failure, the design concept includes the prevention of improper operation where such operation would lead to dangerous conditions.

In the first power plant intended for ground test operation the system is designed so that components fail safe, i. e., fail in such a manner that the result of failure is a safety action. As a result of this philosophy, the operational reliability (ability to operate continuously) is decreased but the safety reliability (ability to protect the reactor) is increased. There are no instances where the failure of a single control component will cause reactor damage.

Two levels or degrees of severity of safety action are provided, alarm and scram. The alarm system indicates to the operator that something is abnormal, whereas scram results in complete, rapid shutdown of the power plant. No intermediate safety levels are provided.

~~SECRET~~
~~CONFIDENTIAL~~

DECLASSIFIED

~~SECRET~~

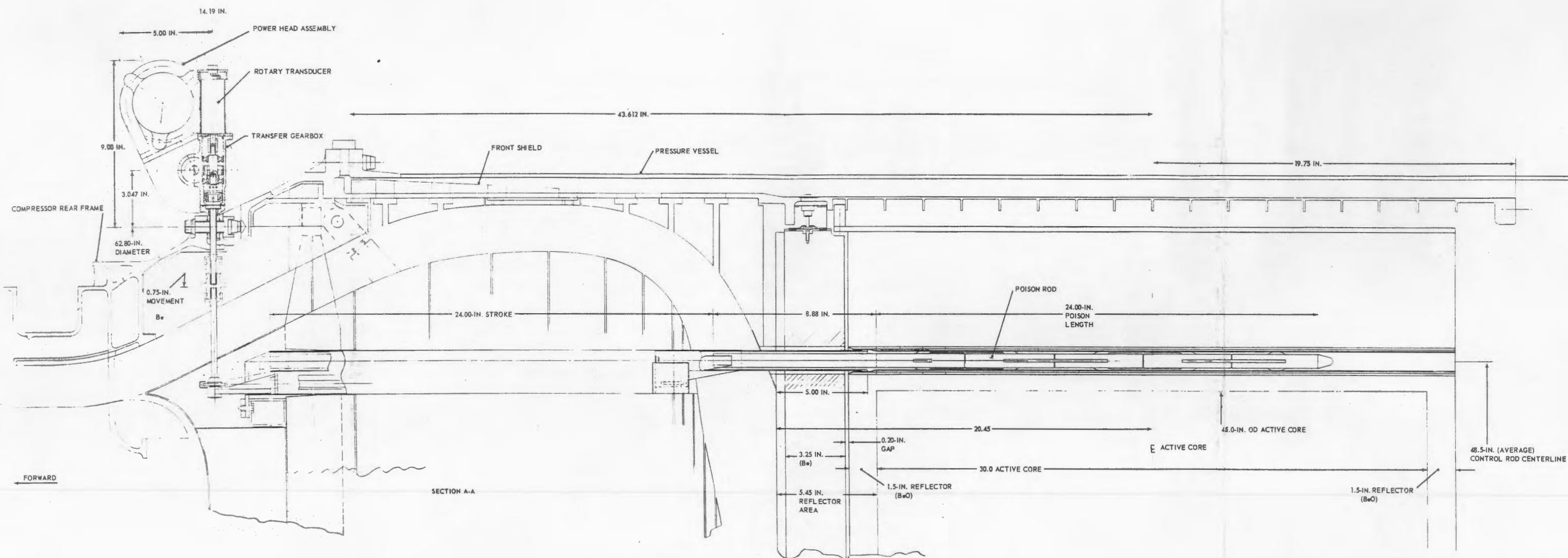


Fig. 2.32A - Control rod mechanical arrangement

DECLASSIFIED

~~SECRET~~

~~SECRET~~

DECLASSIFIED

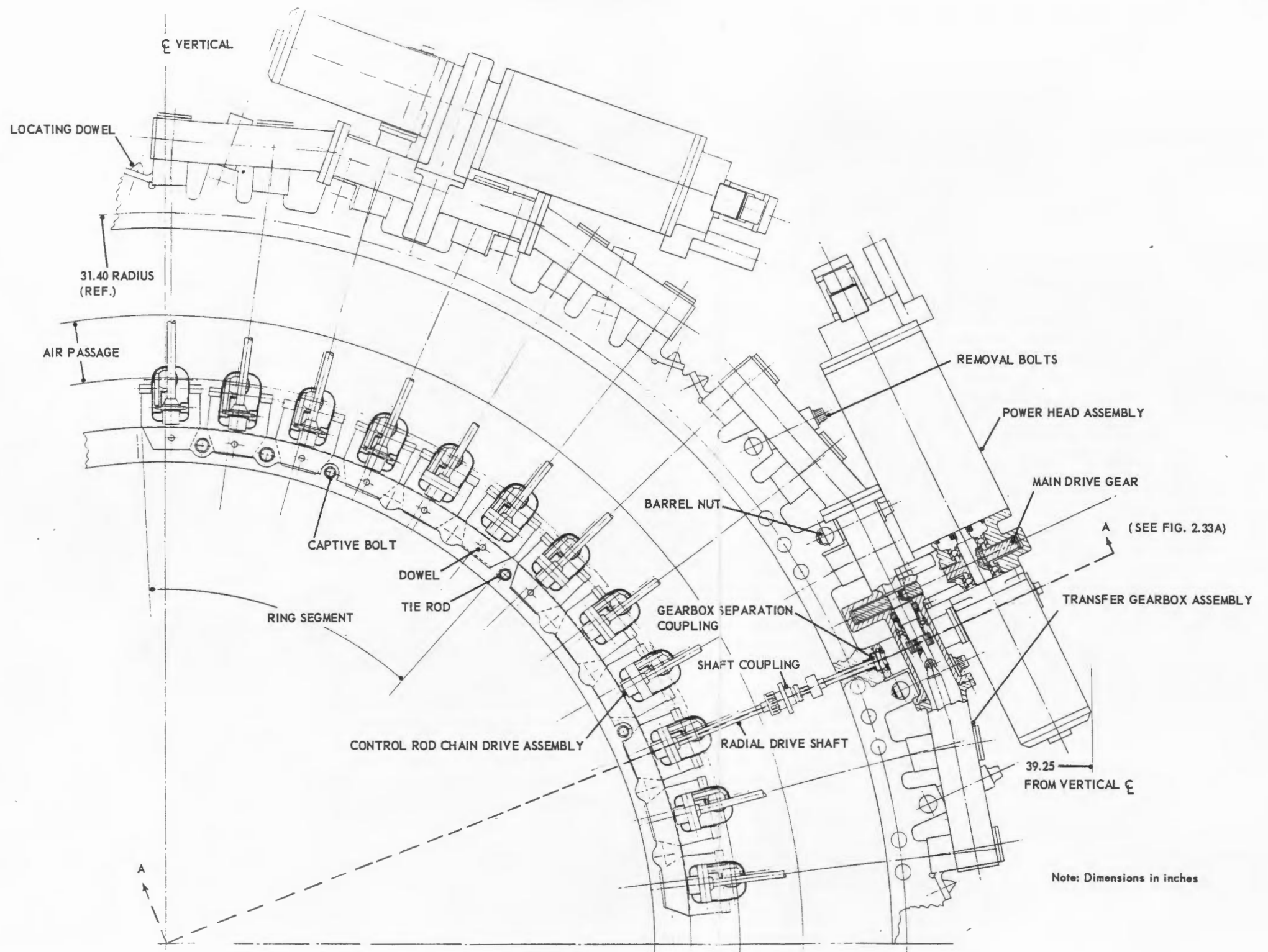


Fig. 2.32B - Control rod mechanical arrangement

~~SECRET~~

DECLASSIFIED

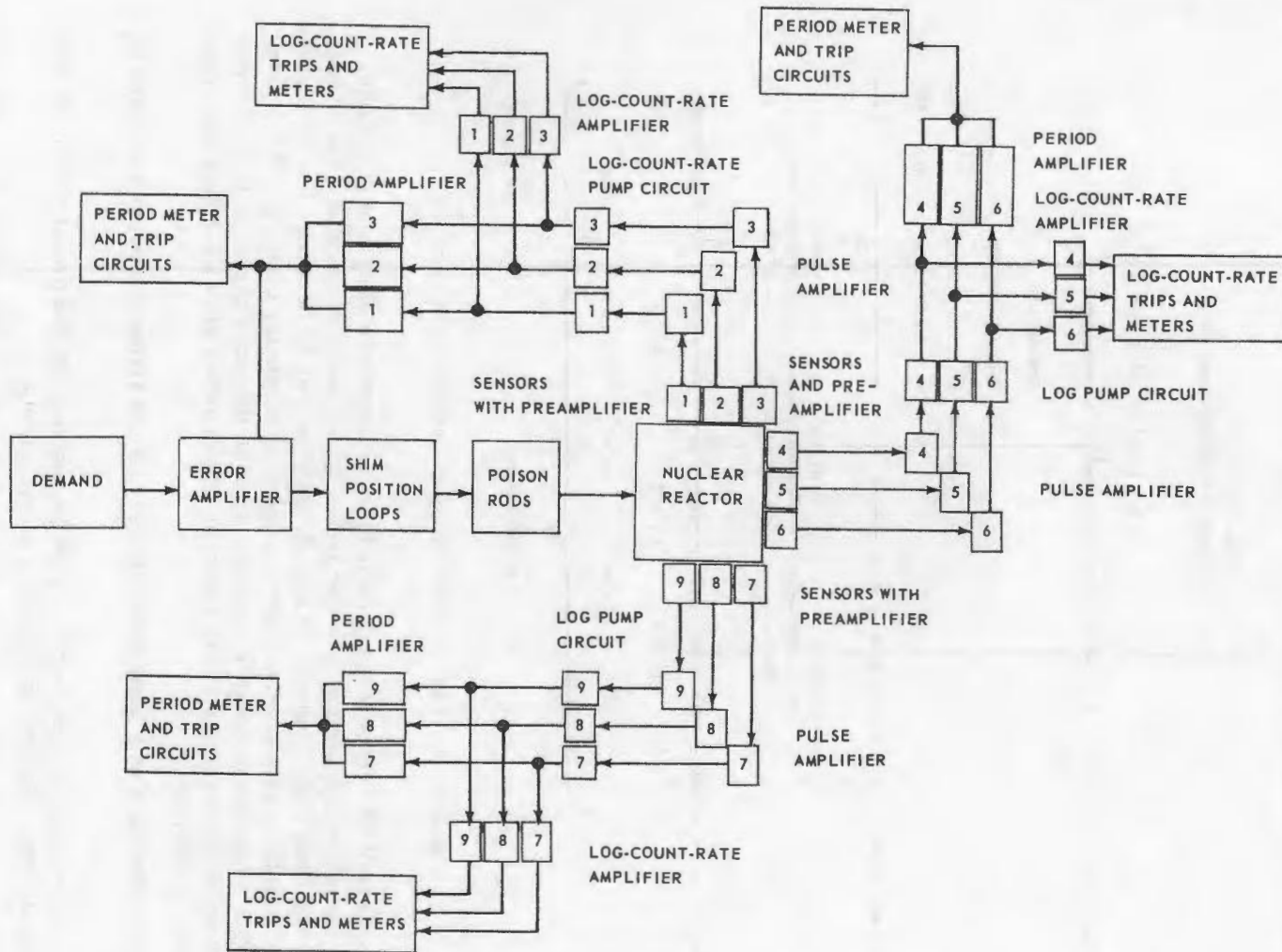


Fig. 2.33 - ACT reactor startup control

~~CONFIDENTIAL~~
~~SECRET~~

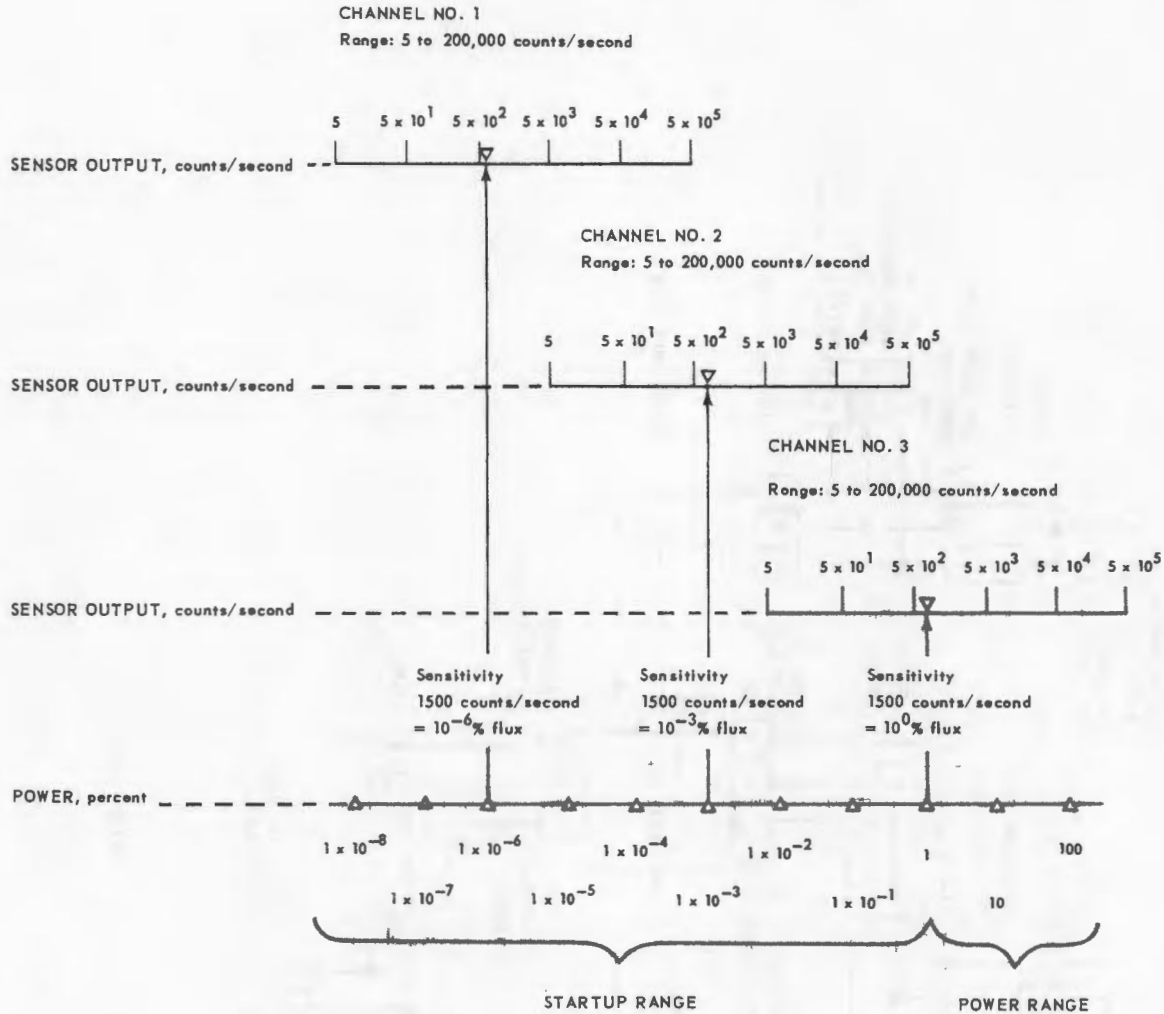


Fig. 2.34--Range and sensitivity of a single instrumentation subsystem

Three channels of fuel element temperature instrumentation will protect the reactor core. Each channel will consist of five thermocouples operating in parallel. The couples will be selected from high-temperature core areas predicted by heat transfer calculations. They will be interchanged with other thermocouples as necessary during testing to monitor actual high-temperature areas of the core. Each of the three channels of five couples will act independently to initiate safety alarm or scram action when their average temperature exceeds a safety limit.

The safety parameters with their associated scram and alarm trip points are listed in Table 2.16.

Alarms - Alarms are provided when certain parameters exceed preset levels and when certain critical power supplies deviate from preset bounds.

The alarm response is the sounding of an audible alarm and the lighting of an individual indicating light to indicate the nature of the alarm. The alarm lights will be located in an annunciator panel or in meters indicating the sensed parameter. An alarm Reset pushbutton will be used to silence the audible alarm and reset the audible device for operation by new alarms, but not for operation by suppression of an existing alarm. An operated light

~~CONFIDENTIAL~~
~~SECRET~~

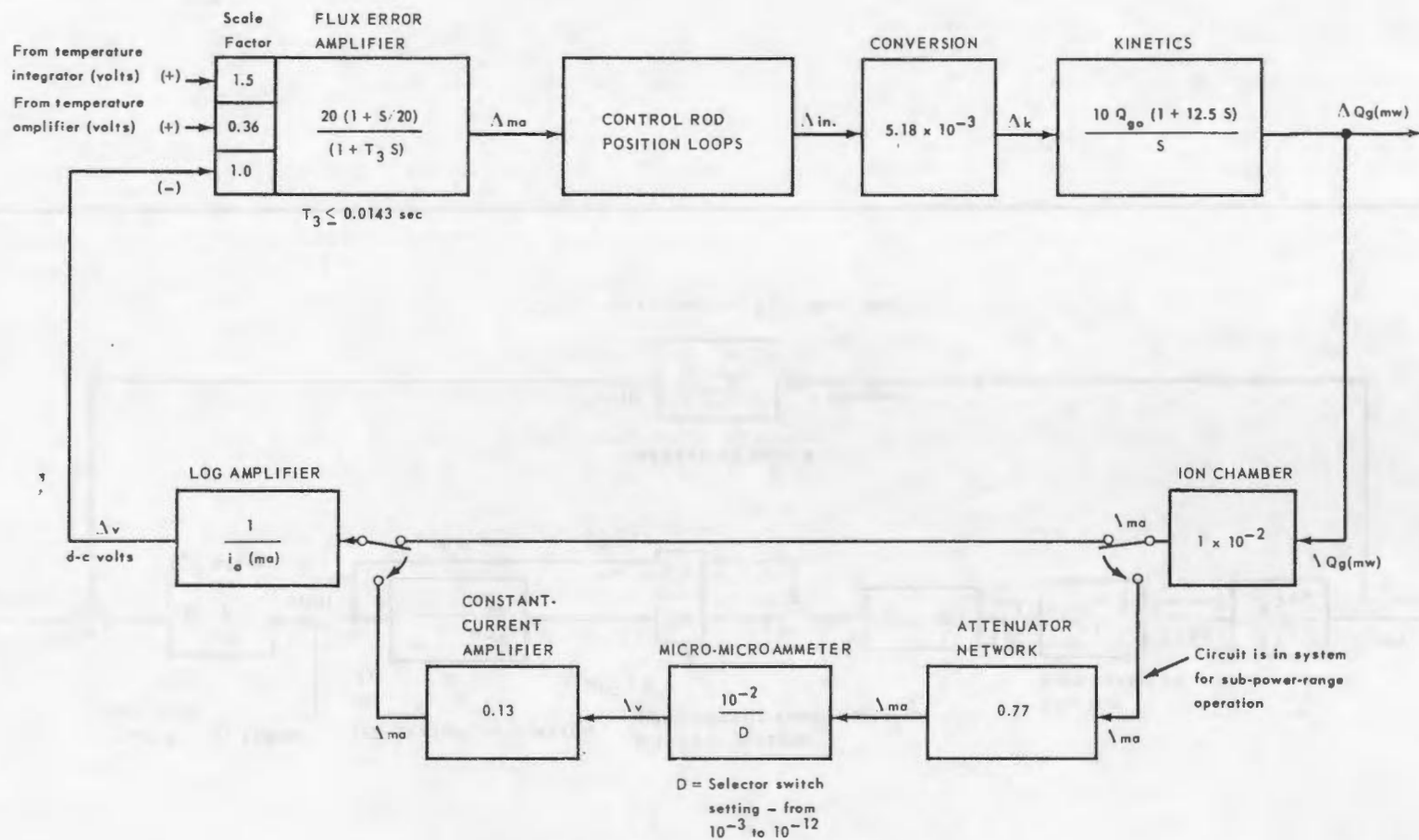


Fig. 2.35 - Flux loop block diagram

TOP SECRET

TOP SECRET

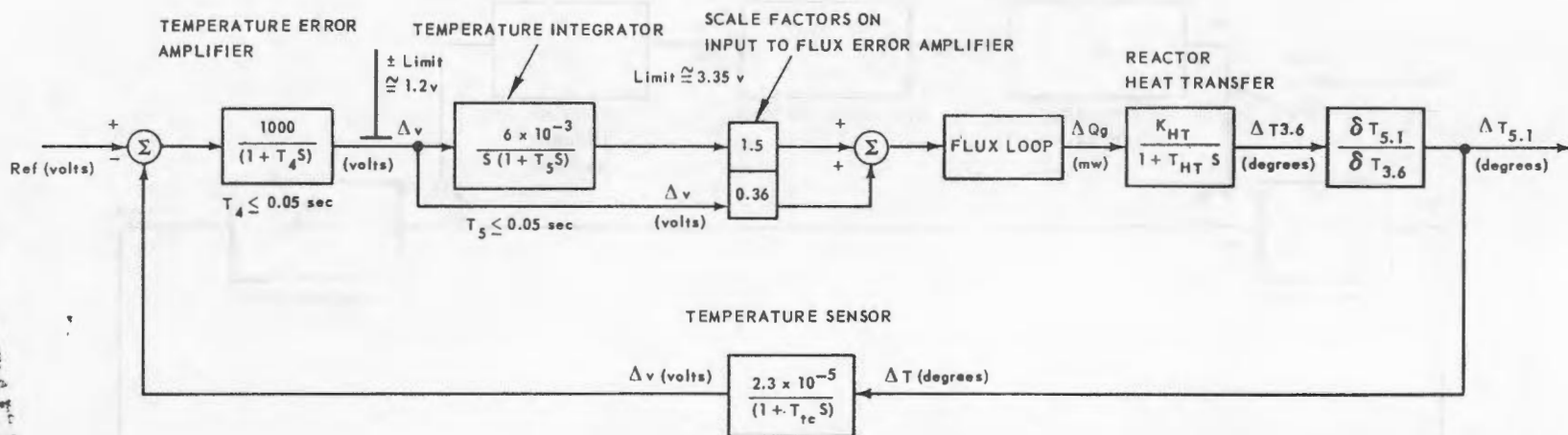


Fig. 2.36 - Temperature loop block diagram

CONFIDENTIAL
SECRET

TABLE 2.16
SAFETY RESPONSES

Parameter	Scram Trip	Alarm Trip
Fuel element temperature	(3) 700° - 2800°F	(3) 50° - 100°F below scram
Air temperature (T _{5, 1})	(3) 700° - 1500°F	(3) 50°F below scram
Power level (high power)	(2) 20 - 200 mw	None
Power level (low power)	(2) 3 - 6 mw (if armed)	None
Switching monitor	(10) Any channel open	None
Period (startup range only)	(3) 5 sec, 2 out of 3 coincidence (if armed)	(3) 10 sec, any channel (if armed)
Engine speed	(1) 105% N	None
Temperature mode, low power	Both low-power trips unoperated	None
Facility neutron-level monitor	0. 0020 - 200 mw	None
Exhaust gas monitor		Increased to 10 times
Low actuator pressure	70 - 90%	None
Power demand	Positioned above 2 mw, 2-mw transfer relay unoperated (if armed)	None
400-cycle voltage	± 10%	± 5%
400-cycle frequency	± 10%	None
28-v d-c bus	- 6 v	None
1500-v d-c bus	- 300 v	None
± 200-v d-c bus (startup only)	20-v decrease (if armed)	None
2 80-v d-c bus (startup only)	-30 (if armed)	None
60-cycle voltage	-10% (μμ ammeter operation only)	None
Operation discretion	At will	None
Emergency engine shutdown	At will	None
Test sets	Connector uncovered	None
Key switch	Unoperated	None
Shim gangs	None	(8) Any unlatched
Equipment continuity	None	Any interlock open

will not be extinguished until the individual alarm clears, at which time it will be self-clearing without use of the alarm reset. When an individual alarm clears, it will automatically reset the audible alarm for subsequent operation of that particular alarm. This system permits the operator to silence the audible alarm in the event that a particular alarm persists for a period of time, yet keeps the individual light on as a reminder that the alarm still exists and automatically darkens the console when the alarm clears.

Alarms are provided on reactor period, fuel element temperature, turbine discharge air temperature (same station as temperature control sensors), facility neutron-level monitor, equipment chassis continuity, 400-cps power supply, and a rod gang not latched to its actuator.

Each of three independent subsystems of period instrumentation will generate an alarm for a short period. Any subsystem will cause a short-period alarm, independent of coin-

chance of the other two. The alarm trip level is not adjustable. The three period signals generated by the three subsystems are metered on the operator's console.

Any of three independent turbine discharge air temperature sensing and alarm-scrum trip circuitry can generate an alarm for high air temperature. Each channel will consist of eight thermocouples operating in parallel. The alarm trip is adjustable, and is maintained automatically at a given level below the scram trip level as the scram trip level is adjusted. The three discharge air temperature levels sensed by these three channels are metered on the operator's console.

The 400-cps power-supply voltage and frequency are both monitored by circuitry that generates alarm and scram responses. The reactor control system is sensitive to voltage and frequency deviations of the 400-cps supply from the nominal values. The effect is to decrease the accuracy and change the transient response of the control. The deterioration of performance increases as the magnitude of the power supply deviations increase. The alarm trips will be set to trip at voltage deviations in such a way that, while the control is still safe to operate, its accuracy and dynamic performance have changed to an extent such that the operator should be informed. The 400-cps power supply will not be adjustable during operation, but the operator will be cognizant of the performance deterioration and can make the decision to continue to operate or shut down for repair. Scram trips will be set at power supply voltage and frequency deviation levels such that the control is no longer safe to operate. The alarm and scram trip levels are adjustable.

An alarm is also provided for each actuator to indicate when the control rod gang is not latched to the actuator. If the unlatching occurs during operation, the result will be a reactor power transient; and this alarm feature will identify the reason for the transient.

Scrams - Scram safety provides two basic functions. The first function is to shut the power plant down before damage occurs in the event of failure or malfunction. The second function is to prevent the operator from taking improper actions that might lead to a dangerous operating condition and to restrict the operator to a specific mode of operation in order to provide intelligence to the safety system. Scrams of the first type are called parameter or power supply scrams, since parameters are sensed and power supplies are monitored and if prescribed bounds are exceeded, scram ensues. Scrams of the second type are categorized as operating procedure violations.

The operating procedure violations will not in all cases result in dangerous operation per se, but by requiring the operator to strictly adhere to a given operating procedure in a few instances, it is possible for the safety system to recognize the power level and condition of the automatic control. The parameter scrams can then be automatically programmed to cover various operating conditions.

A specific example of what is meant above is the case of overflux protection during reactor startup. It is imperative that an overflux trip be set very low in the power range during reactor startup, regardless of whether manual or automatic startup is employed, because neither temperature scrams nor high-level flux scrams will protect the reactor if a reactor runaway occurs. At the same time, when the power range is reached after a normal startup, the low-level trip must obviously be released before normal power-range operation can ensue. In order to be certain that the low-level trip is in force during a startup, it is activated by the operator's power demand dial being set at the minimum demand, which is tentatively set at 2 megawatts. To insure that the demand is set at minimum (and for other reasons discussed later), it is required that the demand be set at minimum until the power range is reached, otherwise the reactor is automatically scrambled. The power-range control normally stops the automatic startup and levels power at the level set on the power demand dial. It would nominally make little difference whether the opera-

tor set the demand at 2 or 3 megawatts; but in order to provide intelligence to the safety system, the demand is required to be in the 2-mw position before the control is released from scram and startup can be initiated.

The usual manual Scram pushbutton is provided so that the operator can initiate scram. In addition, the emergency engine-shutdown pushbutton will also cause reactor scram.

A key switch is also placed in the scram bus in such a way that the key must be in place before the continuity of the scram bus is complete.

The scram response consists of rapid insertion of the control rods, lighting an individual scram light on the operator's console to indicate the source of the scram, lighting two master scram lights, and sounding the audible alarm. The individual lights and the master scram lights will lock in when scram occurs. The audible alarm is silenced by the Alarm Reset pushbutton. The individual lights are cleared by the Light Reset pushbutton, provided the reason for the light being on has been removed. The two master scram lights indicate that both the scram relays are functioning. The two scram relays perform identical functions in releasing the scram latches on the shim rod actuators and are redundant to achieve greater reliability. The relays are de-energized when scram occurs and can only be picked up by operating the Scram Reset pushbutton, which simultaneously extinguishes the two master scram lights and any individual lights.

Thus the individual indicating lights are extinguished by the Light Reset, but the control will remain in the scram condition until the Scram Reset is operated. The fact that the control is still in a scram condition after the individual lights have been extinguished is indicated by the two master scram lights, which are cleared only by releasing the control from scram. Operating the Scram Reset before operating the Light Reset will clear all lights and release the control from scram. The two master scram lights, being independent of the Light Reset, will always indicate the condition of the control as far as scram is concerned.

Power plant integrity is maintained by preventing certain parameters from exceeding prescribed limits. The parameters directly sensed and used to initiate scram if a prescribed level is exceeded are fuel element temperature, turbine discharge air temperature (same station as temperature control sensors), reactor flux level, and engine speed. Reactor period is computed and used as a safety parameter when the power demand is at the 2-mw position. When these parameters are held within prescribed limits, the reactor is in a safe operating condition. The prescribed limits vary as a function of the operating condition. The prescribed limits vary as a function of the operating mode and the status of the reactor.

The safety directly associated with the startup range consists of reactor period safety and the switching monitor. As briefly mentioned in the section covering alarms, three independent sets of period instrumentation compute reactor period, using fission chambers for sensors. Two-out-of-three coincidence is used; i. e., it requires two of the three sets to agree before scram is initiated for short period. In the event of a complete channel failure, an appropriate switch located on the equipment chassis may be thrown to a scram position. This places this set in the scram condition, and then either of the remaining operating channels will cause scram for short period. Assurance that the fission chambers overlap and that the startup period computing circuitry is functional from the fission chambers through the count rate computers is provided by a switching monitor for each set. Low and high count-rate trips are provided for each chamber and its associated circuitry. The high and low count-rate-trip contacts are combined in a logic network in the scram bus known as the switching monitor. The effect of the switching monitor is to require that a less sensitive chamber be providing a usable signal (low count) before the more sensi-

~~CONFIDENTIAL~~
~~SECRET~~

tive chamber preceding it becomes saturated (high count); and that the control ion chamber produce a current to operate the 2-mw relay (transferring rod control from the startup control to power-range control) before the least sensitive fission chamber indicates 3 - 5 megawatts of power. Increasing the power demand above 2 mw causes the period safety, alarm and scram, to become ineffective; i. e. , period safety is not provided in the power range after it has been safely reached. However, the period meters will continue to indicate period throughout the power range.

Scram safety on the other parameters, engine speed, fuel and air temperatures, and power level based on ion chambers as sensors, is in effect in the startup range (below 2 mw). The fuel element temperature scram level will be adjusted to a low level during startup range operation by operation of a High-Low switch on the operator's console.

Excessive engine speed, as sensed by a mechanical speed switch geared to the engine rotor, will cause scram at any time. This trip is not adjustable.

Any of six independent sets of temperature-sensing and alarm-trip circuitry will cause scram at any time if the trip levels are exceeded. The six sensed temperatures are metered on the operator's console. The alarm-scram levels of each set are adjustable, the adjustment being made at the equipment racks. A single adjustment, per channel, adjusts both alarm and trip levels with 50 degrees maintained between alarm and scram trip points. Three sets are used for fuel element temperature and three for turbine discharge temperature. The thermocouple instrumentation will be as previously described. In addition to the above adjustments, the scram trip level of the fuel element temperature system is automatically set at 700^oF when the High-Low switch on the operator's console is thrown to the Low position.

Two independent sets of ion chambers and scram trip circuitry are used for flux level protection. A third ion chamber is used in the power-range control system and is referred to as the control ion chamber. All three ion chamber signals are metered on the operator's console. Two scram trips are provided in each safety set; one nominally set at 5 mw and the other adjustable from 20 to 200 mw. Both high-level trips are adjusted simultaneously by manipulation of a potentiometer on the operator's console. The control ion chamber signal is used in a trip circuit to operate a transfer relay to transfer the control of the control rods from the startup control to the power-range control. The transfer relay operates with an ion chamber current representing slightly less than 2 mw, 2 mw being the minimum setting obtainable on the power demand, and has come to be known as the "2-mw" relay. This relay thus furnishes intelligence to the control system and also to the safety system.

The operation of the high-level power trips is obvious; the operator sets them just above the power level at which he expects to operate. The function of the 5-mw trips is explained below.

It has been determined that a flux level trip set low in the power range is necessary to protect the reactor in the event of a classical startup accident (control rods are withdrawn at maximum rate, reactor becomes critical at low level, period safety fails, and power-range control cannot level power). A high-level flux trip, which potentially may be set as high as 200 mw, may not save the reactor from damage because of time delays associated with presently available components. The scram trip level on flux is automatically set at 5 mw whenever the reactor power is in the startup range, and raised to whatever level the high-level trips are set at when the reactor is in the power range after a normal startup is accomplished.

~~SECRET~~
~~CONFIDENTIAL~~

Scram protection for loss of ion chamber feedback, discussed later in this section, is also provided.

Scram protection is provided from an independent neutron flux detector mounted in the FET and not interconnected with the control system other than through the scram bus. The system is known as the facility neutron-flux monitor.

A system that will detect any unexpected increase in the release of radioactivity from the power plant will be tied into the alarm system. Provisions will be made for incorporating it in the scram system if it is later deemed necessary. The system will probably be a delayed neutron detector or a gamma activity monitor.

The control system and the safety system depend upon certain critical power supplies for proper operation. Failure of some of these power supplies will cause an immediate excursion of power, while failure of other supplies will render the safety system ineffective. When reasonably possible the critical power supplies are protected by scram. In certain cases protection is supplied by redundancy because the measures needed to monitor the supply are deemed less reliable than the supply itself.

Automatic control and safety both depend upon proper operation of the fission chambers. If the voltage drops below the level required for proper sensor operation, scram will be initiated by a low-voltage relay.

The ± 200 -volt d-c reference supplies associated with each set of startup range equipment are also protected by low-voltage relays, since low voltage will cause abnormal control-system operation and also affect the safety system.

The scram protection for both the fission chamber voltage supplies and the d-c reference supplies is automatically eliminated during power-range operation. This is accomplished by shunting the contacts of the low-voltage relays in the scram bus with contacts of the 2-mw relay.

The power supply protection described in this section is effective at all times.

The protection provided for the 400-cps supply has been discussed earlier in this report. Deviations in voltage or frequency sufficient to cause unsafe operation of the control system or the safety system will cause voltage or frequency trip circuits to operate and initiate scram.

Both the power-range control system and the safety system depend on proper operation of the ion chambers. Assurance of proper ion chamber voltage supply is provided by redundancy and a low-voltage relay. Two power supplies are provided, operating through diodes into a high-voltage bus that supplies the chambers. Should either supply fail, the diode will prevent reverse current flow through the defective supply, while the remaining supply will carry the full load. The bus is protected by a low-voltage relay so that reduction of high voltage, because of loss of both supplies or grounding of the bus, will cause scram.

Low-voltage protection is provided for the 28-volt d-c supply to insure proper relay operation.

For sub-power-range operation a low-voltage relay is used to provide scram in the event of loss of the 60-cps power used for the micro-microammeter.

Reduction of the control-rod-actuator power supplies below a certain pressure level will cause unsafe control operation. The pressure level of the actuator power is monitored as close to the actuator as possible, and scram is initiated if the pressure drops below a critical value. This feature represents an attempt to prevent maloperation before

~~CONFIDENTIAL~~
~~SECRET~~

it occurs, since the safety system is independent of the actuator power and should protect the reactor in event of parameter violation.

The power-range control system and the scram trip circuits for fuel and air temperature and power level depend upon proper operation of d-c reference power supplies. These power supplies are very precisely regulated constant-current devices. Unfortunately, to monitor such a supply and detect unacceptable deviations requires an equally well-regulated reference and precise sensing devices. An alternative method of providing protection is chosen in this situation, the use of several reference supplies. The failure of one d-c reference will cause at most the failure of the control system or the failure of one each of the power level and air temperature safety channels.

There are a limited number of operating procedures that the operator must follow. If these procedures are not strictly followed, the result will be a scram.

These operating procedures are intended either to prevent the operator from performing certain actions that have potentially hazardous results or to provide intelligence to the safety system.

The procedures that must be followed to avoid scram are as follows:

1. The power demand must be maintained at its minimum setting until the control ion chamber indicates 2 mw of power and the 2-mw relay operates, regardless of the operating mode.
2. The control mode selector must not be placed in the "temperature" position until one of the safety ion chambers indicates 5 mw of power, at which time a corresponding 5-mw relay operates.
3. When the reactor is being operated manually, the operator must increase the power demand above 2 mw before raising power above the 5-mw level.

These features prevent the operator from doing the following:

1. Performing an automatic startup and having the power-range-control power level at a high value in the power range, which would otherwise happen if the power demand were inadvertently set at a high level.
2. Performing an automatic startup and having the power-range control assume control in the temperature mode. This is undesirable because the power-range control will attempt to satisfy the temperature demand. If the temperature demand is considerably different from the temperature existing during a startup, a severe transient with possible parameter violation will result.

These features provide intelligence to the safety system that allows it to distinguish between the operator causing power to increase above 2 mw and a runaway causing power to increase above 2 mw. This intelligence is used to activate a scram trip at 5 mw for start-up operation and to raise the level to that chosen by the operator after the power range has been safely reached.

A safety feature that results from the interlocking of operator-manipulated controls and the power-level trips is the assurance that the control ion chamber is functional. Scram occurs if the control ion chamber signal is lost at any time after the power level reaches 2 mw. If the power demand is set at minimum when this occurs, scram will occur either when the power level reaches 5 mw on the safety ion chambers or 3 to 5 mw on the high-range fission chambers or when short period is detected, whichever event occurs first. If the power demand is not set at minimum, scram will occur immediately. The above actions result because of the release of the 2-mw relay when the control ion chamber current fails.

~~SECRET~~
~~CONFIDENTIAL~~

Safety Bypass Panel - The operating experience gained from HTRE No. 3 has indicated an apparent need for the capability of operating a power plant without all of the safety features included in the basic safety system. Presumably the need for such operation will exist with this test assembly. A typical example that indicates why such operation may be desirable is to consider the failure of one fission chamber. The safety system as designed will not permit startup unless all chambers are functional because of the switching monitor associated with each startup channel. A trip to the hot shop, which would entail considerable delay, would possibly be necessary to replace the fission chamber. Rather than accept the delay, the decision might be made to operate with only two channels of startup instrumentation, and the switching monitor in question would be bypassed.

A safety bypass panel is provided so that any pair of contacts in the scram bus can be bypassed by the operation of a toggle switch. This is considered preferable to the alternative method of altering the wiring of the scram bus. Each bypass switch will be associated with an indicating light to indicate which scram features are bypassed. The primary need occurs during checkout.

Sub-Power-Range Operation - The power-range control will be used during the preliminary testing phase to regulate power for several decades below the 2-megawatt level. A single switch on the operator's console will permit the power-range control to function below 2 megawatts and simultaneously cause slight changes to the safety system.

Operation of the Sub-Power-Range switch will cause the following changes to the safety system and operating procedure.

1. The period safety will be effective at all times.
2. The 5-megawatt power level trips will be effective at all times.
3. The scram trip on the 60-cps power supply feeding the micro-microammeter will be effective.
4. Operation of the automatic startup system will be prevented.
5. The operator will be able to manipulate the power demand at any time.

It is intended that the operator will manually increase power to the desired level and then use the automatic control to regulate power. Automatic startup using the power-range control should not be attempted. This mode of operation will be restricted by operating instructions.

Reactor Control and Safety Instrumentation

Temperature Sensors - The air temperature sensors for the D140E1 ACT for control and safety will be located behind the turbine at station T_{5, 1}.

There are 16 probes equally spaced around the circumference at station T_{5, 1}. Each probe has two thermocouples, which are electrically and mechanically independent.

The thermoelements are to be Chromel-Alumel. This material has been used successfully in the turbojet engine industry for a number of years. It can be designed for fast response in gas temperatures up to 1650°F.

On the ACT assembly the 16 probes are to be equally spaced around the circumference of the bleed-speed-manifold spool.

The 32 thermocouples will be grouped into eight groups of four thermocouples in parallel in each group. These groups will then be connected into sets for control, safety, and indication.

~~CONFIDENTIAL~~
~~SECRET~~

The probe will be of the swaged construction. It will be one continuous piece from the hot junction to the first junction box. The probe has an outside diameter of 0.310 inch with a 0.040-inch-thick Inconel jacket, MgO insulation, and 0.040-inch-thick Chromel-Alumel thermoelements. The portion of the probe to be immersed in the gas stream will have a 0.5-inch reinforcing jacket over two-thirds of its length for structural stability.

The fuel element temperature sensors for the D140E1 will have noble metal thermoelements and a noble metal sheath with MgO insulation. The hot junction will be enclosed within the sheath.

Nuclear Sensors - The control nuclear sensors will consist of two types, i. e., fission chambers and uncompensated ionization chambers. There will be three fission chamber clusters consisting of three separate chambers per cluster and three uncompensated ionization chambers.

The fission chamber cluster consists of three chambers so sized and spaced that their operating ranges will overlap by two decades. The chamber gains will be as follows:

- chamber No. 1, 1500 ± 450 counts per second per 10^{-6} percent nuclear fission power.
- chamber No. 2, 1500 ± 450 counts per second per 10^{-3} percent nuclear fission power.
- chamber No. 3, 1500 ± 450 counts per second per 1 percent nuclear fission power.

The main structural materials of the chambers will be stainless steel, and the sensitive areas will be coated with enriched uranium.

The uncompensated ionization chamber consists of concentric electrodes and an outer case. The structural materials will be stainless steel with the sensitive area being coated with boron-10. The gain of the sensor will be 1×10^{-2} milliamperes per megawatt of heat power output.

The chambers will be designed to operate at a temperature of 900°F. They will be located in sensor wells in the side shield.

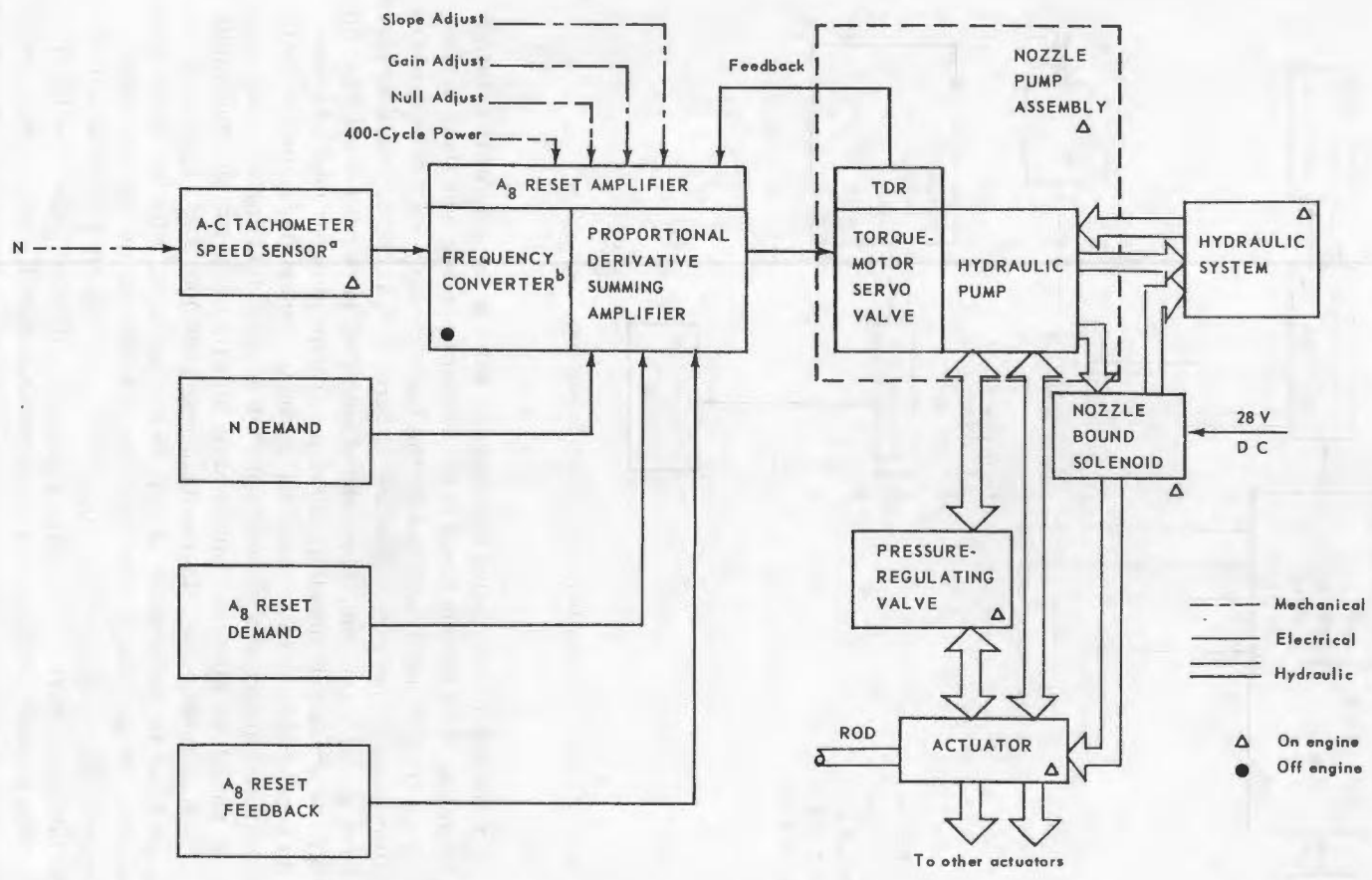
Engine Controls

Engine Speed Control - The speed-control system regulates engine speed by the simultaneous modulation of two engine-control parameters, exhaust or jet nozzle area (A_g) and the turbine bypass bleed area (A_B). The jet nozzle accomplishes this by variation of turbine back pressure (P_5), which increases when jet nozzle area decreases. Nozzle speed control, however, is only effective at high engine speeds when A_g modulation can produce sufficient variation of P_5 to accomplish effective speed control. The turbine bypass bleed valve modulates turbine work by diverting a portion of the main gas stream from the compressor plenum around the turbine and back into the tailpipe. This method of speed control is equally effective throughout all values of the speed range.

The engine speed control is shown in Figure 2.29. It is a straightforward electrohydraulic system. Two control loops are required to properly modulate the jet nozzle and turbine bypass bleed valves shown in Figures 2.37 and 2.38, respectively. The control receives engine-speed and bleed-valve-area demand signals from the thrust selector as a function of throttle angle and/or throttle bias position. The speed demand signal determines the engine operating speed, and the bleed-valve-area demand signal adjusts the engine cycle for peak performance and acceleration potential. The speed demand signal feeds both the nozzle and bleed-control-loop amplifiers. The speed-loop amplifier accepts the demand signal and compares it with a speed feedback signal proportional to actual engine speed to generate an actuating-error signal to the bleed-valve actuation system. A compensating speed-derivative signal is also compared in this amplifier, which effectively shapes the actuating error signal in a way that dampens and stabilizes the speed response of the system.

~~SECRET~~
~~CONFIDENTIAL~~

SECRET
REF ID: A68541



^aSignal from bleed or stator sensor.
^bPackaged with N-bleed and stator amplifier.

Fig. 2.37 - Jet nozzle area (A_0) reset loop for ACT and later test assemblies

SECRET
REF ID: A68541

CONFIDENTIAL
SECRET

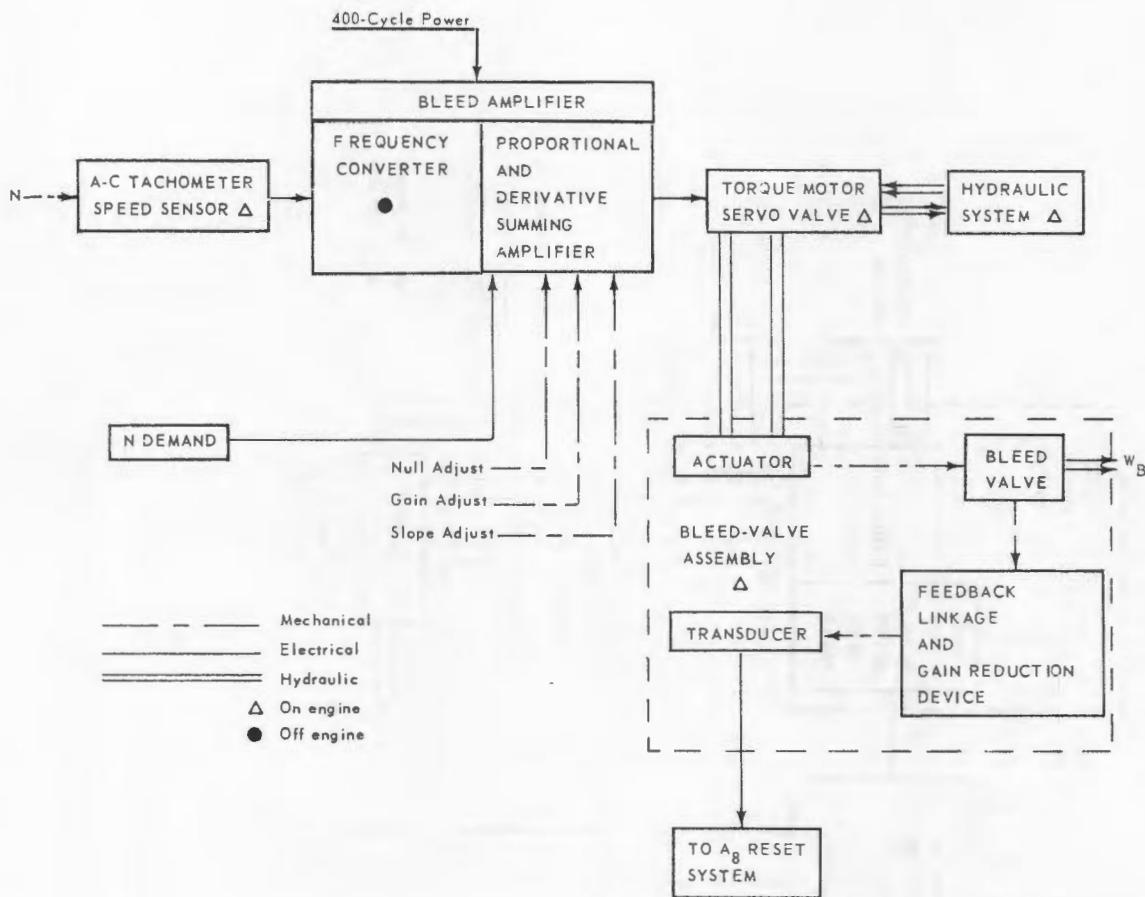


Fig. 2.38 - Bleed loop for ACT and later test assemblies

The presence of an actuating error signal displaces a wand in the servovalve torque motor, which ports hydraulic fluid to four bleed valve actuators and causes them to move until either the actuating error signal disappears or the valve reaches its mechanical travel limits. The actuators always move in a direction to force actual engine speed to agree with that demanded from the throttle; and, since the bleed valve is in motion until the difference between actual and demanded speeds is zero, a zero speed error control is obtained. In addition, an average bleed-valve-position signal is transmitted from the four bleed valve actuator positions and compared with speed demand, actual engine speed feedback, speed derivative, and bleed valve position demand signals in the nozzle loop amplifier. The bleed valve loop is substantially faster than the nozzle loop and will quickly achieve an engine speed equal to the demand. It will do so, however, with the bleed valve biased off normal position. Proper bleed valve position is called for by the scheduled bleed-valve-area demand input to the nozzle loop, which eventually by jet nozzle action establishes or resets the bleed valve to the desired position with no change of engine speed from that demanded. Nozzle loop operation can easily be explained if one assumes speed is at the steady-state demand value with the bleed valve not at the position of best performance. If this is true, the speed demand, speed feedback, and speed derivative signals, compared in the nozzle amplifier, sum to zero. The only two signals remaining that can be compared in the nozzle amplifiers to produce an actuating error voltage to the nozzle loop are the bleed area demand and bleed valve position signals. If such a signal exists, the nozzle actuation system, a typical high-load electrohydraulic actuation system, will

SECRET

move the nozzle to force a change of engine speed. The bleed loop, being faster than the nozzle loop, will change bleed valve position to maintain speed exactly at the demanded value. The nozzle will move until it reaches its mechanical bound or until bleed valve position reaches the demanded value, i. e., the condition of zero error voltage.

To reduce the amount of bleed required to safely limit overspeed in the event of the nozzle failing open, a nozzle bound will be provided to limit mechanically the area of the jet nozzle to a value less than full open (1400 square inches). Additional safety is incorporated into the design and mechanization of the system by the use of six nozzle actuators, four turbine bypass bleed valves and actuators, and redundancy in the generation of speed feedback signals, the details of which are yet unresolved. The speed sensors are permanent-magnet-type tachometers requiring no electrical excitation and thought to be extremely reliable because of their simplicity and ruggedness. All actuators are hydraulic; all electrical computing elements are magnetic amplifiers; and all position and demand transducers are of the a-c variable-reluctance type.

A closed-loop jet-nozzle position control is also provided and is intended for test purposes only whenever manual nozzle positioning is required. It is independent of the automatic nozzle control system to the greatest degree possible in order to provide redundancy. Transfer from automatic nozzle control to manual jet nozzle control by operation of a switch on the control console will be accomplished when the null meter is indicating a zero-error condition so that no transients will occur. Operation of the switch transfers a manual nozzle-position-demand error signal, generated in the manual nozzle amplifier by comparison of actual to demanded position signals, to the nozzle actuation system. The error signal causes the nozzle actuation system to move the nozzle toward the demanded position, the signal going to zero when the actual and demanded positions agree. The nozzle position feedback signal at the input to the manual amplifier is a d-c signal from a variable-reluctance position transducer mounted on the nozzle.

Manual Fuel Control System - The manual fuel control is shown in Figure 2. 39. The operator will be able to manually demand a fuel flow that in conjunction with other engine conditions will determine items such as engine speed, engine temperature, and thrust.

In operation, fuel is received from the facility supply and is boosted to the required pressure by the engine main fuel pump. The fuel flow filter cleans the fuel and passes it onto the main fuel valve. The fuel flow from this valve is determined by the position of an internal metering valve. The metering valve is positioned by a servomotor driven by the manual fuel amplifier whenever there is an error between demanded and actual position. The bypass element in the main fuel valve regulates the pressure drop across the metering valve; therefore, the net flow to the engine is a function of metering valve area or position. A primary pressurization valve assures that adequate differential pressure is maintained across the bypass element for proper servo action. In case of engine overspeed, sufficient fuel will be bypassed back to the main fuel pump to reduce speed to a safe value. Under normal conditions the full fuel flow would go to the seven small slots of the dual-cone fuel nozzle on each burner can. When the required fuel flow is great enough, the secondary pressurization valve will allow fuel flow to the large slots of the dual-cone nozzle.

The block diagram shows a solenoid drain valve, which is provided to prevent accumulation of fuel from leakage or false starts. An air purge line is also shown. Whether this is necessary has not been determined.

Stator Control System - The stator control, Figure 2. 40, is an electrohydraulic position control system. The variable stator blades of the compressor are linked together and tied to the two stator actuators. The required stator position is scheduled as a func-

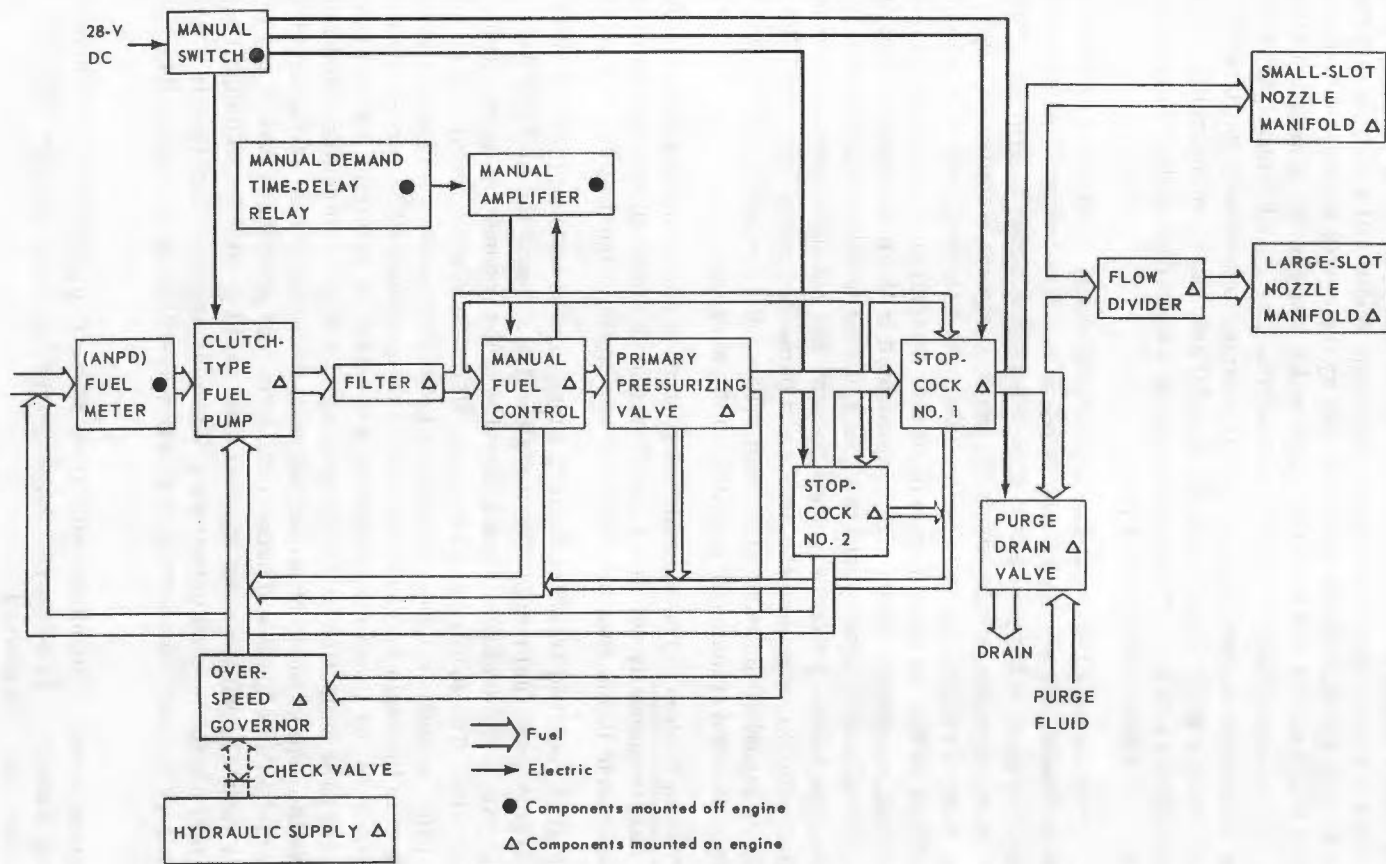


Fig. 2.39 - Manual fuel system for ACT assembly

SECRET

CONFIDENTIAL
SECRET

SECRET
UNCLASSIFIED

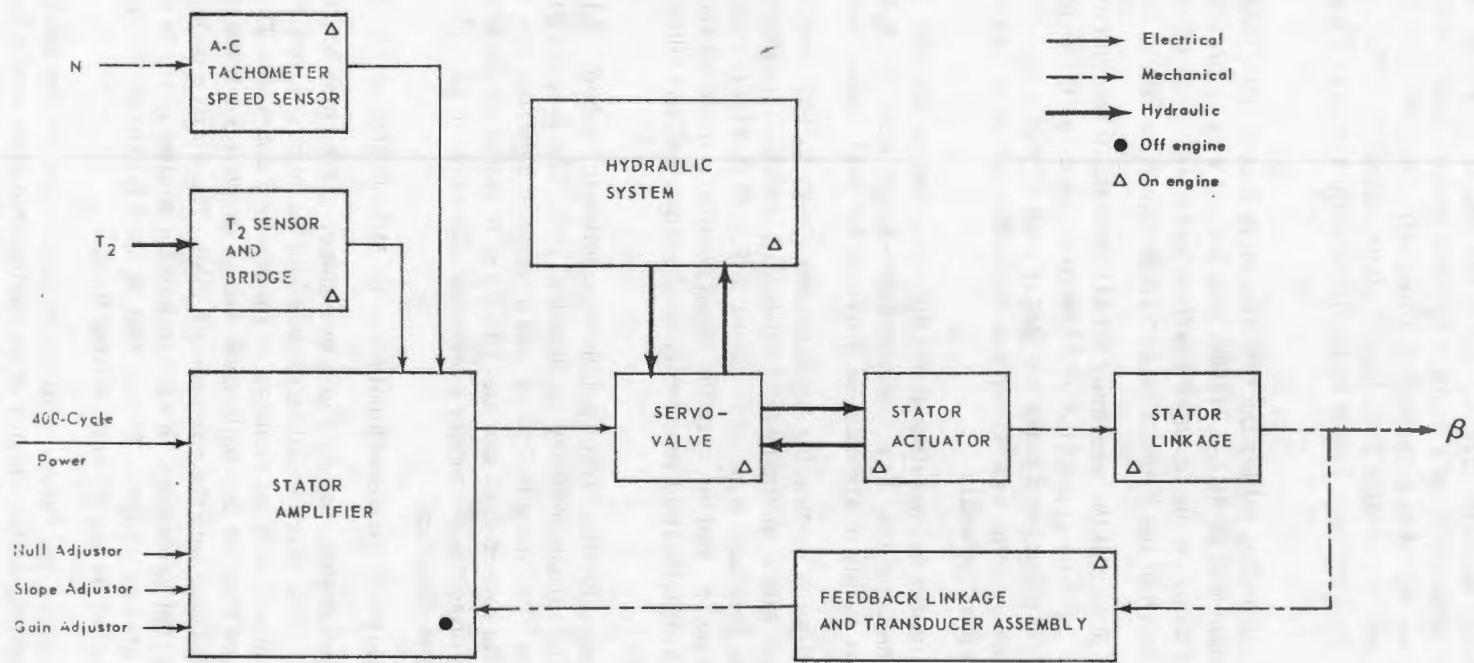


Fig. 2.40 - Stator system for X211 assembly

SECRET
UNCLASSIFIED

CONFIDENTIAL
SECRET

tion of corrected speed. A speed signal from a tachometer is converted to a direct current and combined with a T_2 temperature signal from a temperature-sensitive resistive bridge in the corrected-speed generator magnetic circuit. The corrected-speed signal is compared with the stator position feedback from a position transducer attached to a stator vane. When an error exists, the signal is amplified in a magnetic amplifier and used to control the hydraulic flow from a servovalve into the two stator actuators. The stator control is supplied hydraulic fluid by the common hydraulic system shown in Figure 2.41.

Accessory Systems

Lubrication System - The lubricating oil for the test assembly comes from tanks located in the test facility. The lubricant will be MIL-L-7808C lube oil and will be pumped by elements of the main lube supply pump on the transfer gearbox and a scavenge pump on the rear gearbox. A schematic sketch of the lubrication system is shown in Figure 2.42.

Provisions are made in the design of the assembly for (1) draining of the lubrication system quickly and easily in a horizontal position or 15 degrees nose up, (2) an oil filter at the scavenge outlet to prevent passage of particles larger than 46 microns, (3) venting of the pumps through a common system, and (4) air pressurization external to carbon seals to minimize oil leakage past the seals.

The lubrication system is limited to operation above 500 rpm. Below 500 rpm insufficient lube oil is provided to the bearings. For continuous low-speed motoring operations (500 to 3000 rpm), an external supply of air must be provided for seal pressurization.

Hydraulic System - The hydraulic system for the turbomachinery will be used in the actuation of the variable stator vanes, primary exhaust nozzle, and the bleed speed control valve. A schematic of the hydraulic system is shown in Figure 2.41. The variable-stator pump, primary nozzle pump, and the variable bleed pump are mounted and driven from the rear gearbox. The hydraulic fluid reservoir, heat exchanger, and filter will be mounted on the accessory tray.

Fuel System - The fuel system for the turbomachinery supplies the scheduled fuel requirements for operation of the turbomachinery on chemical fuel. The fuel system schematic is shown in Figure 2.39. The main fuel pump and overspeed governor are mounted on the front gearbox. The main fuel control and fuel filter are mounted on the accessory tray. The fuel nozzle incorporates the secondary pressurization valve to provide the proper atomization of fuel to the combustors.

Fuel to be used in the operation of turbomachinery will be MIL-F-5624 Grade JP 4 fuel.

Starter System - The starter system consists of a two-stage, air-turbine starter unit and an inlet-air control valve. The starter unit is mounted on the inlet gearbox within the engine bulletnose. The control valve is mounted on the power plant dolly. The air is piped to the starter through the front of the bulletnose and is discharged through the forward outer part of the bulletnose into the compressor inlet. The starter includes an oil reservoir, oil pump, and heat exchanger. It also includes a cooling pump to circulate the cooling fluid through the heat exchanger. The oil that is used for the power-plant constant-speed drive is also used as the starter cooling fluid.

The starter control provides for two torque settings, a low torque for the initial part of the start cycle and for motoring on the starter after engine shutdown, and a high torque for that part of the start cycle after engine firing. The torque settings are selected manually by the operator. On the low-torque setting, the starter will motor the engine at approximately 1100 rpm with 700°F inlet air. During engine coastdown, the starter may be set to automatically re-engage on the low-torque setting at an engine speed of 2450 rpm, or it may be manually re-engaged at any speed under 2450 rpm. During the

SECRET

CONFIDENTIAL

SECRET
DECLASSIFIED

SECRET
DECLASSIFIED

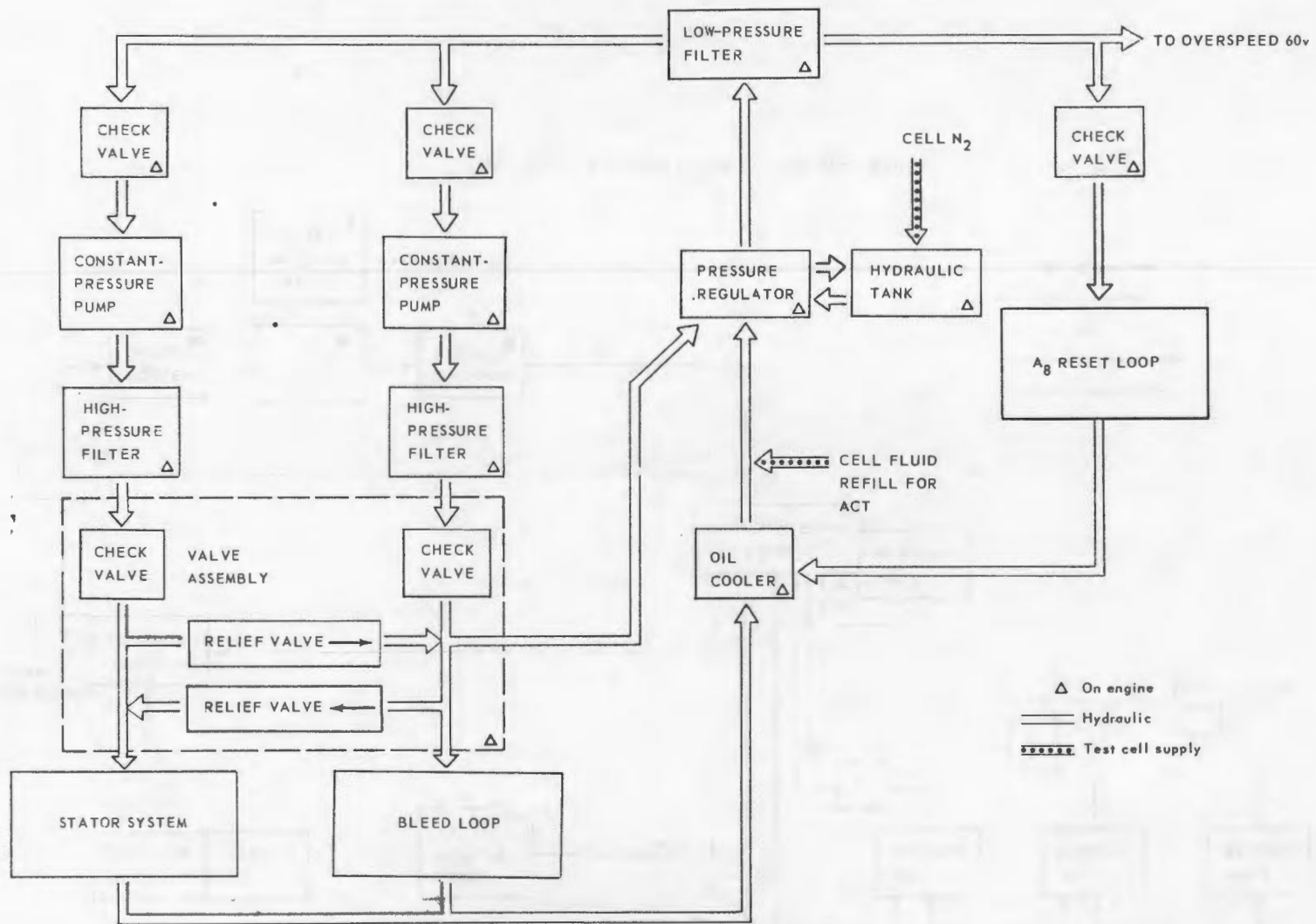


Fig. 2.41 - Hydraulic system for ACT assembly

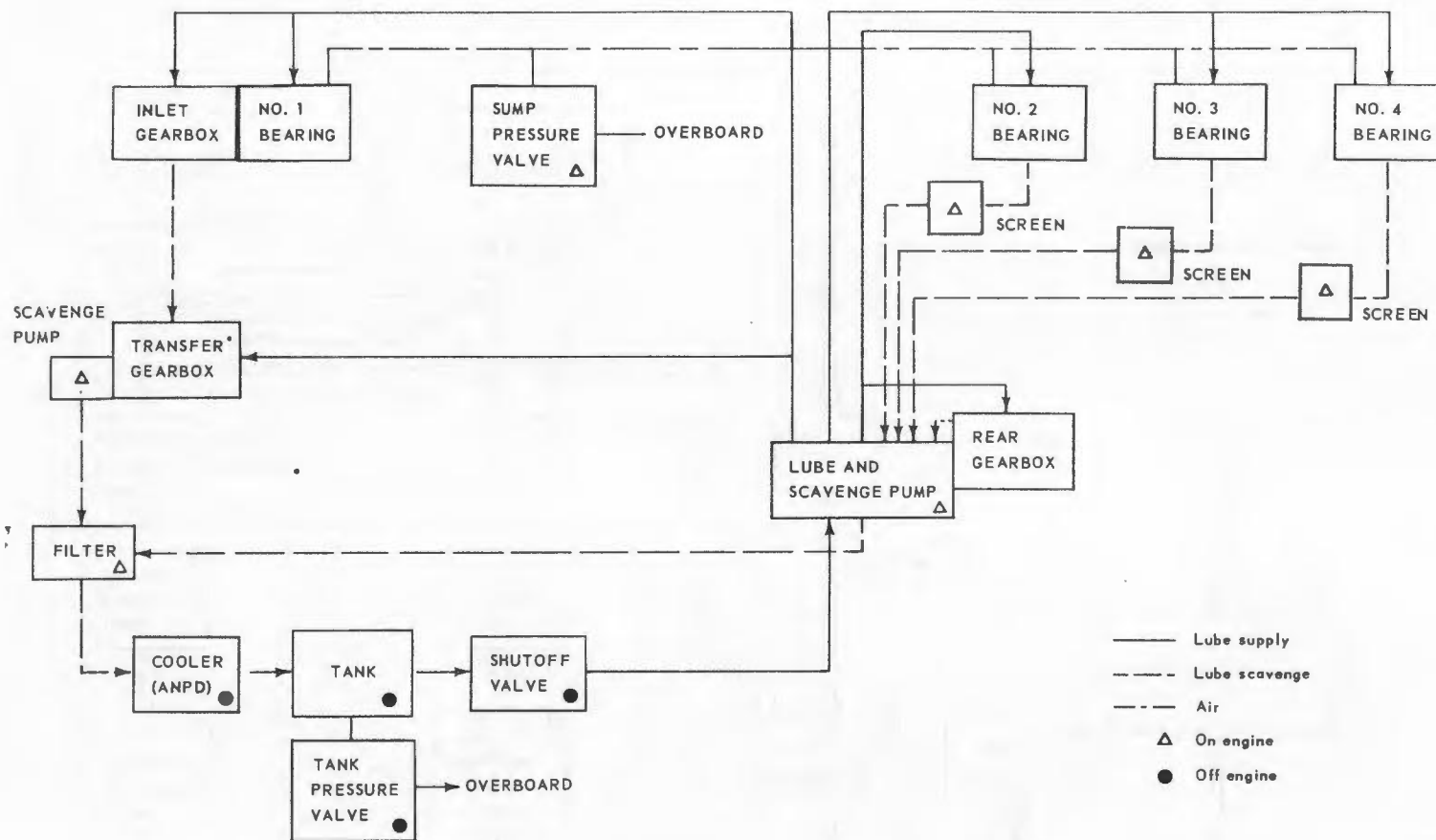


Fig. 2.42 - Lubrication system for ACT assembly

start cycle the starter will automatically disengage and shut itself down when the engine speed reaches 3500 rpm.

The inlet-air control valve serves as a shutoff valve for the starter as well as a pressure regulator to provide 35 psig for the low-torque setting and 65 psig for the high-torque setting.

Electric Power

Electric power for operation of controls during startup is supplied by facility supplies. At idle speeds and above, the power may be supplied by either the facility supply or a system driven by the ACT assembly.

The facility power supply consists of a motor-generator set that supplies 400-cycle power and a motor-generator set that supplies direct current. Power for the motors of both sets is supplied by primary facility power.

The assembly-driven system consists of a 400-cycle alternator driven by a pad on the rear engine gearcase through a hydraulic constant-speed drive. This drive takes the variable output speed of the gearbox shaft and provides a constant-speed output to the alternator. Alternating current from this system is converted to direct current through use of transformer rectifiers.

The test assembly is started with facility power because the ACT system does not regulate frequency adequately much below idle engine speed. When idle speed is reached, operation may be continued on facility power or transfer may be made to the ACT test assembly supply. If the latter is desired, the systems are paralleled electrically and then unparalleled to prevent any interruption in power to the system.

2.1.5 AUXILIARY EQUIPMENT

Transport Vehicle and Support Structure

The transport vehicle is a special flatcar, which is mounted on four railroad trucks and travels on four rails. It is propelled by a shielded locomotive and is used to transport the test assembly and its support structure between facilities. The support structure is a four-legged frame that supports the power plant and some auxiliary equipment during test and transportation on the transport vehicle. Instrument, power, and fluid lines on the structure are connected to the test facility through the coupling plug attached to the aft end of the structure.

Aftercooling

Initial aftercooling air for the reactor is provided by either of two systems, which operate in parallel. One, the shield and aftercooling system, is connected to the aftercooling part of the test assembly through a quick-acting valve. The other system provides aftercooling air by turning on the starter and motoring the engine compressor. During engine operation the first system supplies cooling air to the shield but is blocked off from the reactor by the quick-acting valve. After the engine is shut down and coasts down to 2400 rpm, the starter begins operating and provides aftercooling air by motoring the compressor. If the starter fails to begin operating, the engine will continue to coast down and the shield and aftercooling system will cut in through the quick-acting valve when the engine compressor discharge pressure drops below the system pressure.

The shield-cooling and aftercooling system is shown in Figure 2.43. Air will be supplied by a facility air supply and ducted to a point located on the left side and aft of the support structure. Automatic quick-disconnect couplings will be provided to couple the ducting

~~CONFIDENTIAL~~
~~SECRET~~

mounted on the facility to the ducting mounted on the support structure. The ducting mounted on the support structure is routed to the ducting on the power plant and connected at the aft end for aftercooling flow and at the forward end for shield-cooling flow. Manipulator-operated quick-disconnect couplings will be provided to couple the ducting mounted on the support structure to the ducting mounted on the power plant.

During the time the power plant is being transported from the FET to the hot shop, cooling air will be supplied to the reactor core from a pair of blowers mounted on the support structure. These blowers are connected in parallel so that in the event of failure of one of the blowers, the other blower can keep the system operating. The ducting from the discharge of these blowers will tie into the ducting mounted on the support structure and will follow the same route as the initial aftercooling airflow.

When the in-transit aftercooling system is required to supply air, the initial system will have been in operation for some time already, thereby materially reducing the flow requirements. Before the initial system is shut down, the in-transit system is put in operation and checked out. The initial system is then shut down; and as the pressure decays below that of the in-transit blower discharge pressure, a check valve in the in-transit blower discharge line automatically opens and allows air to flow through the structure and power plant ducting and then through the internal passages to and through the core.

The flow and pressure requirements for the shield and aftercooling system and the in-transit aftercooling system are:

Initial aftercooling system

Flow - 25 lb/sec

Pressure - 20 psia

In-transit aftercooling system

Flow - 10 lb/sec

Pressure - 15.5 psia

2.1.6 EFFLUENT-CLEANING EQUIPMENT

An effluent-cleaning system will be designed to permit extensive, uninterrupted, endurance testing of advanced power plants at the FET. It will be located adjacent to the northeast side of the existing test cell in the FET facility.

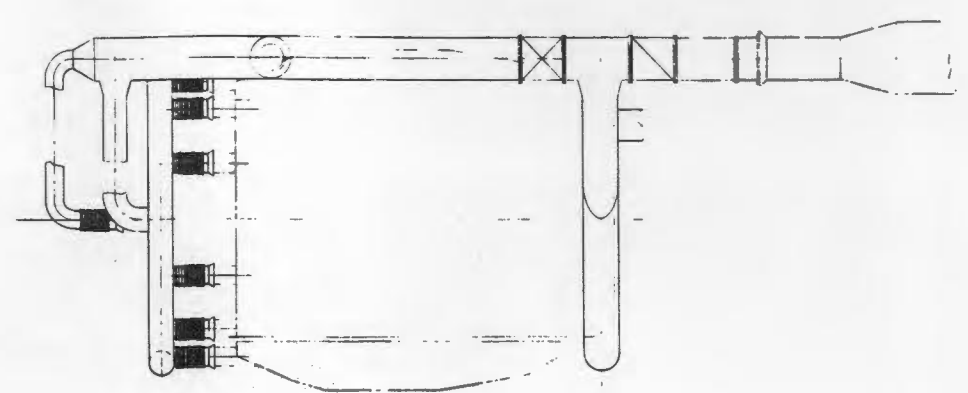
A significant feature of this effluent-cleaning system is the utilization of an electrostatic precipitator to remove fission product contaminants from the power plant exhaust stream. It is planned to inject into the gas stream a particulate material that will collect the fission product contaminants and in turn be collected on the precipitator plates. This particulate, with associated contaminants, would be discharged to hoppers and subsequently to a contaminated-waste disposal system.

For the effluent-cleaning system a special duct called an augmenter will be designed to receive the primary exhaust jet from the engine. It will induce a minimum quantity of secondary airflow, thus providing free discharge from the engine. This design will permit normal engine operation and accurate thrust measurements. The flow of ambient secondary air will also permit the augmenter to be constructed entirely of carbon steel. The augmenter duct will be approximately 8 feet in diameter and 40 feet long. The transition from the augmenter duct to the main duct will be approximately 36 feet long. Cooling-water spray rings will be located to provide desired cooling and to provide effective mixing of the primary and secondary gas streams and the injected additive.

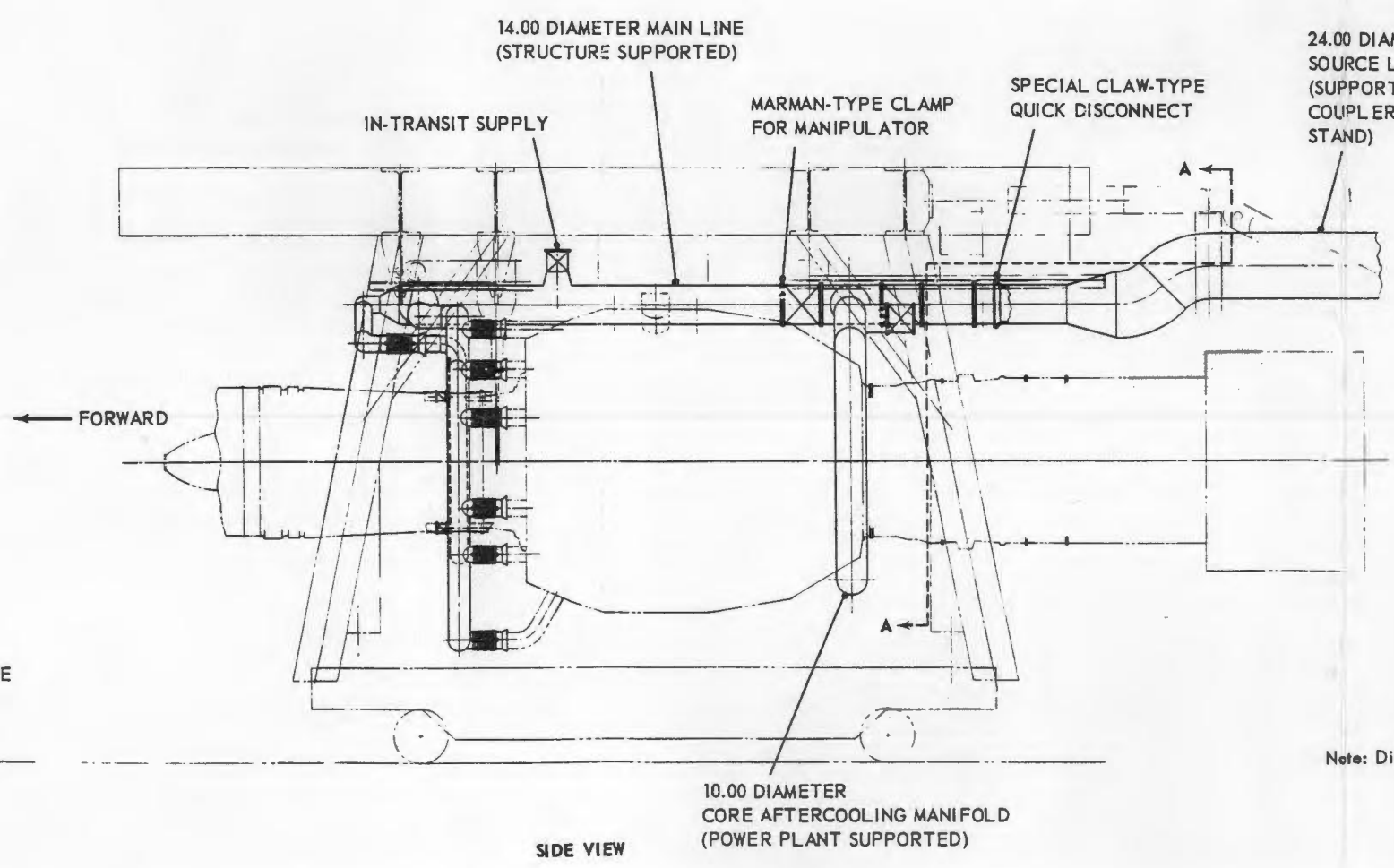
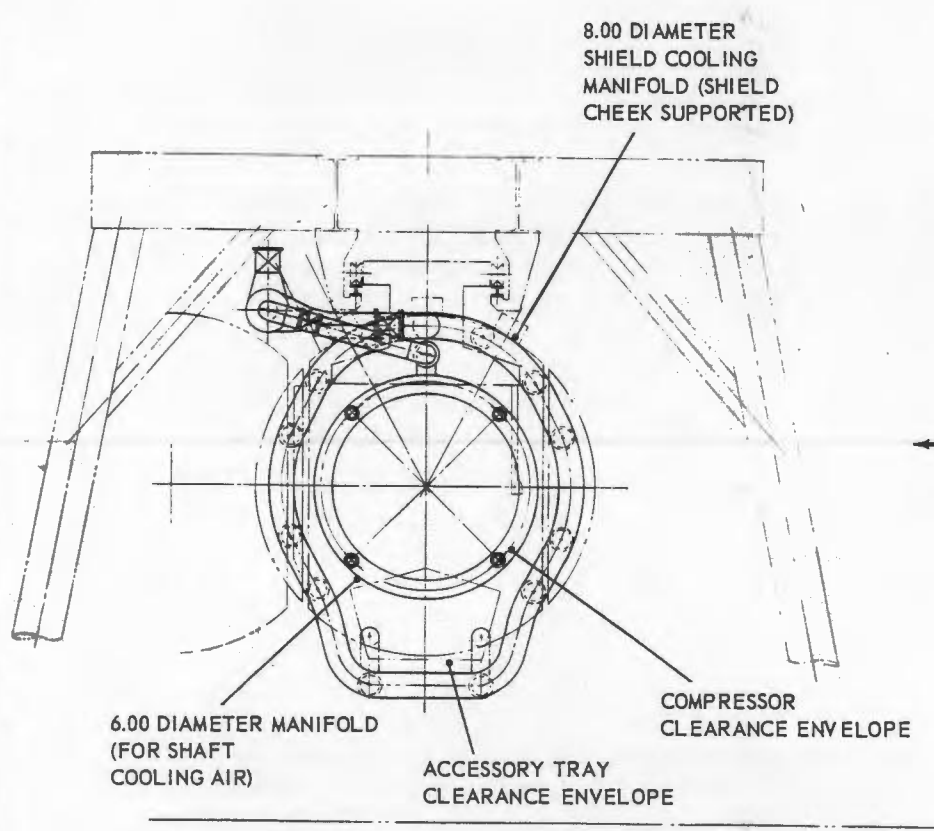
~~SECRET~~
~~CONFIDENTIAL~~

~~CONFIDENTIAL~~

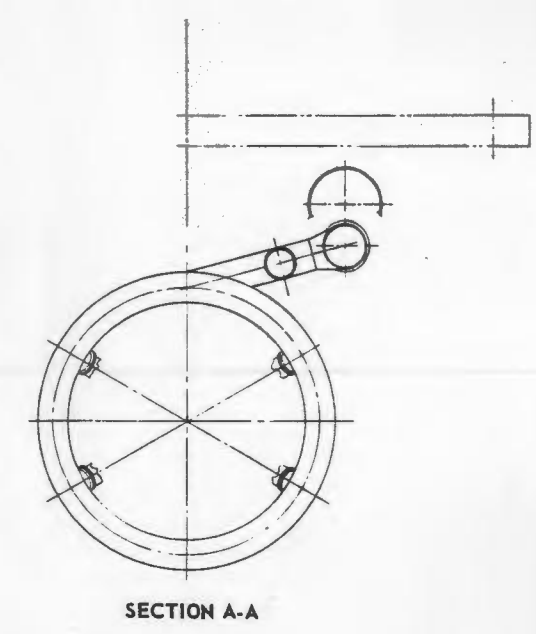
~~SECRET~~



PLAN VIEW



SIDE VIEW



Note: Dimensions in inches

Fig. 2.43 - Shield cooling and aftercooling system for full-power assembly

~~CONFIDENTIAL~~

~~SECRET~~

~~SECRET~~
CONFIDENTIAL

The main duct, approximately 18 feet in diameter and 70 feet long, will connect the augments transition to the precipitator inlet plenum, which will be a chamber across the inlet face of the precipitator to distribute the gas flow through the precipitator. Adjustable louvers will be provided for equal flow distribution.

The electrostatic precipitator will be of the wire-and-plate-electrode type, specially designed to remove efficiently the type of additive injected into the gas stream. It will consist of six sections and will provide a maximum design flow rate of approximately 1,100,000 cubic feet per minute at a face velocity of 300 feet per minute and a gas temperature of 300°F. The precipitator structure will be approximately 60 feet high, 150 feet wide, and 40 feet deep. Each section will have suitable hoppers to receive the material removed from the plates. Provisions will be made in the precipitator shell to accommodate the future installation of additional plate sections in case higher collection efficiencies should be desired.

The flow from the precipitator will enter multiple-exit plenum sections, each having a separate duct leading to one common exhaust stack. The exhaust stack will be a carbon-steel structure approximately 18 feet in diameter and 100 to 150 feet high to ensure a minimum effective stack height to provide protection against local contamination on the ground.

The additive processing and injection equipment will be located in an underground addition to the basement level of the existing FET control and equipment building. Storage of additive material for 100 hours of operation will be outside and adjacent to this addition. The additive processing and injection equipment will be used to prepare the additive in the desired form and concentration for injection into the augments duct. The form and concentration of additive will be selected from data obtained from IET side loop experimental tests currently in progress. The additive that shows the greatest effectiveness in removing radioactivity from the exhaust stream will be selected.

A contaminated-waste disposal system will be provided to handle the radioactive wastes removed from the precipitator plates. These wastes will be collected in hoppers located beneath each precipitator section, and the waste from rapping and spray-cleaning operations will be conveyed through underground piping to a shielded storage tank. This storage tank will have a capacity for 1000 hours of precipitator operation and will be located above ground approximately 350 feet from the FET test cell. This storage tank will be surrounded by an earth berm, sized to provide both radiation shielding and a basin with a volume at least equal to that of the tank. An isolation fence will surround the tank area.

Several auxiliary features will be provided to complete the system: utility services such as cooling water and electrical power; suitable process instrumentation and control equipment for the precipitator proper, as well as all auxiliary equipment in the system; and sampling and monitoring equipment throughout the system.

2.2 ASSEMBLY PROCEDURE

The initial full-power assembly will utilize, if they are available, the primary fixtures and handling equipment that will be used during subsequent remote disassembly; however, the complete operation can be performed manually, making the use of most secondary equipment unnecessary.

In all cases the reactor core will be assembled in the Low Power Test facility. The assembly will be performed step-wise using critical experiment techniques and monitor-

~~SECRET~~
CONFIDENTIAL

ing multiplications, in order to preclude accidental criticality. The assembled core package is then delivered to the hot shop for insertion into the test assembly.

The pressure shell will be installed in the upending fixture with the reactor mounting flange upward. Lowered into the shell by means of a sling are the assembled reactor, front shield, and control rod and drive unit. This unit will be built up in the hot shop after the core is returned from the zero-power test and the temporary front shield and control system are replaced by the operating components. This unit is complete with instrumentation and can be bench-checked for wiring continuity and control rod response. If necessary, the source rod used in the critical experiment can be replaced for power test at that time.

After the core package is inserted and the compressor assembly, consisting of the rotor and stator and front and rear frames, is mounted, the assembly is upended and the turbine rotor, stator, and front and rear frame unit, including the rear shield, are attached to the aft flange of the pressure shell. The assembly is then returned to the horizontal position, and the tailpipe and accessory package, which is designed so that testing of functions and connections can be performed before mating to the power plant, are added. At this time the power plant will be moved to the side-shield handling stand where the side shield and intermediate support frame will be mounted and final electric and hydraulic connections completed.

The ACT assembly will then be inserted into the support structure where final service connections will be made. At that time checkout of all electric connections and, by either motoring the power plant with the starter or supplying external pressure, checkout of the hydraulic loops for continuity and leakage should be accomplished.

2.3 DISASSEMBLY PROCEDURE

The after-shutdown gamma dose level around the D140E1 ACT assembly varies from a low of 3 to 5 roentgens per hour in front, to between 2000 and 3000 roentgens per hour from midpoint to tailcone at a distance of from 5 to 10 feet from the surface of the power plant. These figures are based on a full-power run of the reactor for periods of 100 hours and up. Consequently, except for the compressor area, work performed on the power plant from a major disassembly to minor maintenance must be done remotely or under heavy shielding.

Upon receipt of the power plant in the hot shop, the in-transit aftercooling must be discontinued and the shop aftercooling begun. The power plant will then be unlatched and rolled back in the test frame where the 100-ton crane may pick up the lifting bail and transfer the power plant to the side-shield removal fixture.

In the side-shield removal fixture, the side shields and power plant support yoke are unfastened and removed. In order to reach all the fastenings, a 15-degree tilt has been incorporated into this fixture. At this point, 80 percent of the bolts in the front and rear pressure vessel flanges, which support the compressor and turbine assemblies, must be removed to allow the flanges to fit into the lifting girdle.

An optional step in the procedure to this point is the removal of the starter and accessory tray from the compressor. The starter can be removed at any point in the procedure prior to removing the compressor. The accessory tray can be removed or can be left with the compressor on the basis of work to be done. Piping and wiring must be removed

prior to the side-shield disassembly. To make it possible to reach all bolts in the pressure-vessel flanges, the power plant must be removed from the hot shop on a flatcar and turned on the turntable.

The lifting girdle is then applied, and the power plant is lifted to the rotary erecting fixture on one of the hot shop turntables. The crane then lifts the aft end of the power plant to a vertical position, and the tailcone is unbolted and removed. A strongback is then bolted to the turbine rear frame and shaft to hold the shaft in radial and axial alignment during subsequent operations.

The assembly is then turned end for end with the compressor pointing upward, and the main-shaft unbolting tool is applied. The compressor rear flange bolts are removed, and the component-removal fixture lowered and attached to the compressor pick-up points. The main compressor-turbine coupling shaft nut is then turned while the compressor is slowly lifted. After the internal nut has cleared its threads, the component-removal fixture will be lifted with the compressor and set onto the compressor stand where the compressor will be left for transfer to manual maintenance areas.

The component-removal fixture is then fitted to the front shield adapter, and the assembly is lowered to contact the forward flange of the transition section between the compressor rear flange and the pressure-vessel front flange. The remaining pressure vessel front flange bolts are removed, and the transition assembly between the reactor and the front shield is picked up and removed. This assembly is then set into fixturing where the reactor may be unbolted from the front shield and the components separated.

The handling of the control rod actuators has not been finalized yet, but the actuators and rods probably will remain assembled until the front shield and core are separated. The rods will be removed one group at a time and replaced with transport rods that will stay with the reactor. Currently, if a control rod or actuator is to be changed, the compressor must be removed to provide access. The method will be finalized later. The nuclear sensors are attached to and will remain with the side shields during a general disassembly.

Since no maintenance procedures are planned for the front shield and reactor, fixturing will be provided for separation operations only. The reactor tubes will be released from the pressure shell and grouped into bundles of suitable size for transport and storage.

After the reactor and front shield have been removed from the pressure vessel, an adaptor is bolted to the front flange for stiffening and counterbalancing, and the assembly is inverted with the turbine on top. The remainder of the bolts holding the turbine are removed, and the component-removal fixture with the necessary adaptors is applied to the turbine. The assembly is then removed, and the turbine is separated and carried to a decontamination area.

Reassembly of the power plant will be in reverse order to the disassembly, and the same equipment will be used. There will be no reassembly of a used reactor or of the end shields when they are separated into their smallest components. Aftercooling therefore probably will not be a part of the assembly procedure, since either a fresh reactor will be used or the cooling time on a used reactor may have been long enough to require only intermittent cooling, if any, during the assembly.

~~CONFIDENTIAL~~
~~SECRET~~
~~CONFIDENTIAL~~

3. TEST REQUIREMENTS

3.1 LOW-POWER OPERATIONS AT LPT

Low-power operations at the Low Power Test facility (LPT) will consist of a critical-experiment test program performed with the ACT test assembly reactor. The purpose of these operations is to determine the nuclear characteristics of the D140E1 reactor prior to operation of the full ACT assembly.

Cold critical tests will be performed to evaluate excess reactivity in the reactor and to calibrate the control rods. Detailed three-dimensional power mapping will be accomplished for various rod insertion depths by means of wire or tape activation methods. The reactor core will be poisoned preferentially to simulate the spatial effects of fuel burnup and the predicted reactivity worth of xenon, fuel depletion, and long-term fission products. The control rod bank will be moved to compensate for these effects.

Hot critical tests (maximum temperature of 1000°F) will be performed to evaluate the changes in power distribution at the core-reflector interface and the changes in temperature and to study the effects of temperature on reactivity. Heating of the reactor will be accomplished by blowing hot air from an external source through the reactor.

The nature of the foregoing test program requires that the reactor be made critical and shut down many times. The power requirements however, are not to exceed 100 watts.

3.2 COLD-SYSTEM CHECKOUT

Prior to power operation, a checkout procedure will be carried out to insure that all power plant mechanical, electrical, and airflow systems are functioning properly.

Phase I

The first portion of the testing will consist of a complete wiring check. The continuity of signal flow will be established through each minor control loop. Continuity and proper termination will be established for all cables and leads from the electrical component racks and the operator's console to the dolly coupling plug. Similarly, each signal and power lead from the power plant to the dolly coupling plug will be checked for continuity and proper termination. The power plant will not be connected to the control during Phase I, Phase II, or Phase III.

Phase II

The second portion of the testing will establish proper control component calibration. Correct power supply and demand voltages will be established. Amplifiers, safety trips, console meters, and demand dials will be calibrated according to established procedures.

Phase III

The third testing phase will establish proper reactor control operation using an analog simulation of the reactor characteristics.

~~CONFIDENTIAL~~
~~SECRET~~
~~CONFIDENTIAL~~

The proper closed-loop gain and time constant will be established for the position loop and flux loop. Adequate response of the temperature control to step-function inputs will be established.

Steady-state power-holding ability will be measured at a number of operating points using both flux and temperature control. Proper computation of steady-state count rate and reactor period by the startup control will be confirmed.

Phase IV

Final pre-operational testing will establish signal continuity and proper signal polarities throughout the control when connected to the actual power plant. Each poison rod actuator will be observed to insert, withdraw, cock, latch, and scram on manual command from the operator's console. The existence of proper high voltage at each nuclear sensor will be confirmed. Manual operation of the reactor control in accordance with accepted operating procedures will precede automatic control throughout all operating ranges. The engine will be motored by the starter to establish hydraulic pressure for the speed and stator controls and to establish fuel pump pressure. The fuel control system will be checked through the use of the calibrating fuel loop. The position of the stators at the checkout speed will be compared with its schedule, and the functioning of the nozzle and bleed loops will be verified by controlled movement of their respective actuators.

Airflow Checkout

Cold-flow tests will be carried out to determine the distribution of shield cooling flow between the segments of the side shield and to check out the action of the various valves in the shield and aftercooling system.

3.3 CHEMICAL OPERATION AT FET

Prior to nuclear operation, the ACT will be operated by means of its chemical interburner. The purpose of this operation is to insure that the turbomachinery is in good working condition following shipment to Idaho and to obtain flow-distribution data.

The assembly will undergo a normal chemical startup after which the power will be slowly increased by change in the fuel control valve setting until an engine speed of 100 percent rpm is achieved. After testing at this speed, shutdown in accordance with normal shutdown procedure will occur. During chemical operation, data will be taken to determine the flow distribution between the primary flow circuit and the secondary front- and rear-shield cooling-flow circuits.

3.4 LOW-POWER NUCLEAR OPERATION AT FET

Upon completion of the chemical run-up test and prior to self-sustained nuclear power operation of the ACT, a series of low-power nuclear runs will be made with the engine starter used to motor the compressor as an air supply. The purpose of this operation is to obtain thermal and nuclear shield information before high-power operation of the power plant.

Pressure, airflow, and temperature distributions within the end shields will be determined by operating at power levels up to 10 mw. Instrumentation permanently fixed in the end shields will be monitored as necessary to provide input for the data-reduction program by which aerothermal distributions will be determined.

The temperature distribution within the radial shield will be established by operation at approximately 10 mw. This will require several runs with adjustment of cooling-tube orifices between runs.

The main purpose of the shield nuclear measurements during the low-power testing is to verify nuclear heating levels at critical locations in the shield. In addition, external dose-rate and spectra measurements are planned for correlation with predictions to check the validity of methods used for nuclear analysis of the shield.

Calorimetric sensors will be used to measure nuclear heating. These sensors will be permanently located at approximately 10 to 15 positions in both the front and rear shields. These are the only internal nuclear measurements anticipated within the end shields because of the inaccessibility of these regions when the power plant is fully assembled.

Calorimetric as well as dose-rate and spectra measurements will be taken in instrument wells in the side shield or in a separate side shield segment that can be replaced by a normal segment for high-power operation. These measurements will include calorimeters, neutron and gamma dosimeters, and threshold and activation foils and wires.

Nuclear emulsions for determining foil neutron spectra and a gamma ray spectrometer will be used in making external measurements.

Power levels up to 5 mw will be required for the calorimetric measurements. All other nuclear measurements require power levels only up to 1 kilowatt. In general, the tests will be performed in the order of the test power requirements, with those requiring lowest power being performed first.

3.5 FULL-POWER-RANGE OPERATIONS AT FET

Upon completion of the low-power test program, the ACT assembly will be operated over its full power range. Although this test program has not yet been planned in detail, it will include endurance runs, accelerations, decelerations, chemical to nuclear and nuclear to chemical power transfers, startups, shutdowns, and scrams. An attempt will be made to demonstrate the 1000-hour life capability of the test assembly either directly or by equivalence to operating times demonstrated at different operating conditions.

~~CONFIDENTIAL~~
~~SECRET~~
~~UNCLASSIFIED~~

[Faint, illegible text]

SECRET

[Faint, illegible text]

~~CONFIDENTIAL~~
~~SECRET~~
~~UNCLASSIFIED~~

4. OPERATING PROCEDURES

4.1 CHECKOUT

The power plant and its control will be checked out according to the approved operating procedures before each days operations. The checkout procedure followed will depend on the type of operation to be accomplished. For example, a chemical run will not require checkout of the reactor control system. The checkout will be accomplished immediately prior to operation.

In the event that repairs or modifications are made that affect the control or accessory systems, checkout of these items will be repeated.

4.2 OPERATION

The operating procedure presented is typical but will be varied in details depending on specific test requirements.

4.2.1 OPERATION ON CHEMICAL POWER ONLY

A prestart of the chemical system is accomplished by motoring the engine with the starter and introducing minimum fuel flow without ignition to establish that fuel flow exists. The fuel introduced is removed by engine airflow and the fuel drain system. After the engine coasts down, a chemical start may be initiated.

Starting is accomplished by motoring to firing speed with the starter, setting the throttle at idle position, setting speed control on either manual or automatic, turning on ignition, and introducing light-off fuel flow. Speed is brought to idle by manually demanding an increase in fuel flow. The starter turns off automatically when the speed reaches between 3000 and 3300 rpm.

Operation between idle and military speed will be accomplished by manual manipulation of fuel flow, speed bias, bleed bias, and the nozzle-area demands. To prevent damage from engine overspeed, an overspeed governor is used to bypass fuel. The responsibility of avoiding compressor stall lies with the operator since no means is provided for automatic stall detection or automatic prevention. Acceleration times are limited by the chemical fuel system, and, therefore, operator caution is relied upon to keep the engine out of stall conditions.

In case of an engine malfunction, the discretion of the operator will determine whether operation is continued or the power plant shut down. Normal shutdown will require that fuel flow and speed be set to idle and the nozzle fixed open until the engine stabilizes. Fuel is stopcocked and the engine permitted to coast down.

~~CONFIDENTIAL~~
~~SECRET~~

4.2.2 REACTOR STARTUP

Reactor startup (increase of reactor power from source level to approximately 1.5 percent full power) may be effected with cooling air supplied by the aftercooling system, by the engine compressor motored by the starter, or by the engine compressor during all-chemical operation at idle speed or above.

After pre-operational checkout has been completed, the key switch that allows the startup system to be operated may be turned on. If the safety annunciator is clear, the safety actuators may be cocked and latched. The period demand is then set on the desired value between -30 and +7 seconds, and the mode selector is turned to period. The period servo will then manipulate the control rods to maintain the demanded period until the flux level reaches 1.5 percent full power. At that point control is automatically transferred to the power-range control, which holds power at 1.5 percent of full power until its demand is changed by the operator.

4.2.3 TRANSFER FROM CHEMICAL TO NUCLEAR POWER

The transfer of power from the interburners to the reactor will be accomplished at high operating speeds. Initially a manual transfer procedure will be used. The nozzle will be set on manual and fixed in an open position. A maximum and minimum transfer speed will be selected. With the engine operating at minimum transfer speed and the reactor on flux control, reactor power is increased until maximum transfer speed is reached. Fuel flow then is reduced to bring speed back to the minimum transfer level. This procedure will be repeated until the interburners blow out and fuel is stopcocked.

Later in the program a preliminary operational procedure will be developed to minimize thrust transients. This will consist of setting a speed with the bleed-nozzle-reset speed loop and switching the reactor immediately to T_{5.1} temperature control. The operator will then reduce fuel flow slowly and allow the automatic reactor temperature control to increase power and the speed control to minimize engine perturbations.

4.2.4 ALL-NUCLEAR OPERATION

Provisions for integrated power operation are provided by a throttle that supplies reactor temperature and speed and bleed control demands. A bias is provided on each of the demands for manual operation. Manual operation, therefore, will consist of locking the throttle into place and then adjusting the bias required to achieve a desired operating point. Throttle operation is provided to demonstrate the transient-performance capability of the ACT assembly on nuclear power. The bias signals will be turned to zero, and the throttle moved to achieve a desired operating point. The assembly may be operated steady state and transiently between sub-idle and military power when the automatic speed control is used. Steady-state operation is possible only between 80 to 85 percent and 100 percent speed when the fixed-area jet nozzle is used and the bleed system is biased out.

4.2.5 TRANSFER FROM NUCLEAR TO CHEMICAL POWER

Transfer of power from nuclear to chemical will initially be accomplished by placing the engine on open manual nozzle, the reactor on power control, and the speed at the minimum transfer level. Enough fuel is added to the interburners for light-off and then gradually increased until speed is at the maximum transfer level. Reactor power is then retarded until the speed is reduced to the minimum level. Alternate increases in fuel flow and decreases in reactor power that maintain speed in the specified limits will be used until reactor power is reduced to 1.5 percent. The reactor can then be shut down by scrambling.

~~SECRET~~
~~CONFIDENTIAL~~

A procedure that would minimize thrust variations during transfer would include bringing the engine to transfer speed by use of the speed-control and reactor-temperature control loops; lighting off the interburner, and allowing the transient to settle. The reactor temperature control would be used to automatically reduce reactor power level. Fuel flow would be slowly increased to insure that the engine speed is maintained constant by the speed control. When reactor flux is reduced to a low level, a switch to power control would be made and the power would be brought to 1.5 percent. The reactor would be shut down by scrambling.

4.2.6 NUCLEAR START

An engine startup using nuclear power only will be demonstrated. The engine will be rotated on the low-torque position of the starter with the throttle set at idle. The reactor is started by the previously outlined procedures and transferred to flux control. The starter then is switched to the high-torque position and reactor flux increased until idle operation is reached. The speed control will be used to hold the engine at idle speed.

4.2.7 POWER PLANT SHUTDOWN

To shut down the engine when operating on nuclear power, speed is first reduced to idle with the nozzle wide open and the power plant is allowed to stabilize. The reactor is then scrambled, and the power plant shuts down.

~~CONFIDENTIAL~~
~~SECRET~~

5. RELEASE MECHANISM FOR RADIOACTIVE MATERIALS

5.1 NORMAL OPERATIONS

The description of the path of a fission fragment through a dispersion-type fuel element becomes complicated when recoil, decay properties, chemical state, and various diffusion modes are considered. Fission product release studies on many types of fuel elements involve a failure mechanism, such as pinhole formation in a can or cladding. These studies do not involve detailed explanation of the mechanism because failure is usually arbitrary and the release is negligible under normal operating conditions. In contrast, the ACT fuel element as it now exists operates with a continuous but controllable release. Therefore to achieve proper control, it is necessary to understand more details of the mechanism of release, the parameters affecting release, and the magnitude of release. The remainder of the section will describe the mechanisms of release that have been identified with the BeO-Y₂O₃-UO₂ fuel element. A more detailed discussion of fission product mechanism will be reported in the ACT Materials Report to be issued shortly.

5.1.1 RECOIL

In any fuel element where the fuel is within a few microns of the surface, the fission fragments will have sufficient energy to escape by recoil. Recoil, therefore, depends upon the fractional amount of fuel that is located within the recoil range of the surface. For example, if the fuel element is a slab 40 mils thick and the recoil range is about 0.4 mil, the instantaneous fraction of fission fragments escaping is

$$J_R = 2(1/4) \frac{0.4}{40} = 0.5 \text{ percent}$$

or 0.25 percent for each side of the slab. The factor 1/4 determines the fission products that are borne within the recoil range and are going in the right direction to escape. When the ACT fuel element shape, a hexagonal tube with an inner bore diameter of about 0.170 inch is considered, the recoil escape fraction is less because many of the fission fragments recoil into the opposite wall. Monte Carlo calculations indicate that for tubes with diameters of 0.170 inch the escape fraction should be about 0.03 to 0.04 percent. Since the outside surfaces of the fuel element are in intimate contact, there is very little chance of an air capture of the fission fragments.

The release fraction determined experimentally from bare tubes closely agrees with the Monte Carlo calculation. The instantaneous release for these different isotopes has been found to be: 0.05 percent Sr⁸⁹, 0.03 percent I¹³¹, and 0.02 percent Ba¹⁴⁰. The Sr⁸⁹ is believed to be highest because of the slightly greater recoil range of the lighter-weight fragments. Close agreement has also been obtained for release from a slab as described in the previous equation.

~~CONFIDENTIAL~~
~~SECRET~~

CONFIDENTIAL
SECRET

If recoil is the main mechanism of release of fission products from the fuel, the rate of release should be independent of temperature or fission product inventory. Many tests show that independence of temperature or fission product inventory is characteristic of the ACT fuel elements up to 2500° to 2600°F. Above this range, temperature and inventory dependence are noted.

5. 1. 2 DIFFUSION

When temperatures are sufficiently high, diffusional release should begin to predominate over recoil release. The release now becomes dependent upon temperature and upon inventory, which increases with time. In calculations with a slab model, a diffusion coefficient greater than 10^{-13} cm²/sec is necessary before the contribution of release due to diffusion exceeds that due to recoil. In in-pile tests this situation appears to be reached somewhere between 2500° and 2750°F.

Because of the longitudinal temperature gradient that exists in irradiation test assemblies, the exact temperature dependence is difficult to determine since only a portion of the tube is at the higher temperature. In tests performed at a maximum temperature of 2750°F the release is observed to be a factor of 2 to 5 above the recoil level.

5. 1. 3 WATER-VAPOR CORROSION

If water vapor comes into contact with a bare surface of the fuel element at a high temperature, the BeO in the fuel element will volatilize. Corrosion exposes fuel particles dispersed within the matrix and releases the accumulated inventory of fission products stored in the BeO. Thus, as corrosion proceeds, the release fraction increases as more of the fuel fraction is exposed. If the corrosion rate is constant, the release fraction will increase proportionally with time.

The effect of corrosion on release has been verified experimentally. When increases due to corrosion are not severe, good agreement is obtained with the ACT fuel element model. Some deviations are noted when corrosion is deeper, particularly during long time tests. Over longer time periods, it appears that relationships between corrosion and fission product release become complex.

5. 1. 4 EFFECT OF COATING ON MECHANISM

When coatings are applied to fueled bodies, the transport processes are altered. Direct recoil into the airstream is no longer present because the recoil flux is absorbed by the coating. The amount of release depends on the transport properties of the fission products within the coating. If the coating is porous, a large fraction of the recoil flux can escape. At temperatures above ACT operating conditions, fuel migration and interactions between coating and matrix are possible. The ACT fuel system has a co-extruded layer of ZrO₂ on the inside surface of the tube. Since ZrO₂ and UO₂ form solid solutions, some fuel is found in the coating after sintering. In addition to the contribution from the diffusion mechanism previously described, these factors can influence the amount of fission product release.

The ZrO₂ coating eliminates the corrosion of BeO and thereby eliminates the effects of corrosion on fission product release. The coating as currently applied does not appear to retain a significant quantity of fission products that recoil into it. Based on recoil calculations, approximately 0.17 percent of the fission products recoil directly into the coating. For ZrO₂-coated tubes, the amount of release measured from in-pile tests is about 0.08 percent for I¹³¹ and indicates that about 60 percent of the iodine is retained. The amount of release of strontium and barium isotopes is somewhat lower than iodine. It is believed that the isotopes that are borne as short-lived rare-gas precursors are most mobile as

SECRET

CONFIDENTIAL

rare gases. Only a short holdup period in the coating is required to allow the rare gases to decay into nonvolatile, ZrO₂-soluble strontium and barium compounds. Consequently the isotopes in these chains show a release lower than that of iodine.

5. 1. 5 CONCLUSIONS

In the above paragraphs the mechanism of fission product release from ceramic fuel has been discussed in a general manner. The relative contribution of the three mechanisms outlined - namely, recoil, diffusion, and corrosion - depend on the conditions to which the fuel element is subjected, particularly the temperatures and the amount of flow that might be passing uncoated surfaces. In section 2 the core temperature patterns were discussed in some detail. In that section the relative volume of the core operating at different temperatures was discussed and quantitatively presented. It is important to re-emphasize in this discussion that, since the core volume operates over a wide range of temperatures for any steady-state operating point, quotation of fission product release cannot be based only on the maximum temperature of the core. Fraction of core volume at each temperature must be considered in arriving at the final result. However, in the case of the ACT operation the maximum temperature in the core at any point is predicted to be 2500°F. As pointed out in the previous discussion, at this temperature and below, fission product release appears to be independent of temperature and is governed by recoil mechanism. Corrosion does not appear to be a factor because of restricted access to the uncoated surface of the tubes and because most of the core operates at temperatures at which water-vapor corrosion is very slow.

It may therefore be concluded that the fission product release from the ACT is characteristics of the recoil mechanism only. Using this assumption the data below give the best values of the release fractions for the various fission products expected during steady-state operations of the reactor at its design point. These release values are biased toward the high side of the available data, and in addition, represent the values that would be expected at the core discharge. In other words, no credit is taken for possible reduction due to plate-out of fission products in ducting or on engine parts. Therefore the following release rates are believed to be appropriately conservative.

I131	8 x 10 ⁻⁴
I133	3 x 10 ⁻⁴
I134	3 x 10 ⁻⁴
I135	8 x 10 ⁻⁵
Te132 - I132	(8 x 10 ⁻⁴)
Sr89	5 x 10 ⁻⁴
Ba140	8 x 10 ⁻⁵
Gross Activity	(5 x 10 ⁻⁴)

5. 1. 6 COMPARISON OF LABORATORY RELEASE MEASUREMENTS WITH IN-PILE MEASUREMENTS

Recent experiments at ORNL on the ACT fuel element have indicated that the release measured from furnace-heating specimens that had previously been irradiated is much higher than the release from in-pile tests. The high release rates observed during laboratory heating have been found to occur primarily while transient heating and cooling of the specimens takes place. Bursts of activity are released on initial heating and at various temperatures on cooling to room temperature. Bursts of a similar type are observed in transient conditions during an in-pile test, but the release magnitude is not nearly so

CONFIDENTIAL
~~SECRET~~

large as that indicated by laboratory heating. Differences in the release magnitude between in-pile heating and laboratory heating have been reported by others*† working with compacts of UO_2 .

The different release behavior may be caused by the greater amount of internal surface, such as pores or microcracks, that is formed within a grain during laboratory heating and acts as a drain for fission products stored in the interior of the grain. If internal surfaces are ignored and the mobile species is assumed to diffuse to the grain boundary surface, the calculated diffusion coefficients that result are too high. The internal surfaces formed during laboratory heating result from pore condensation and internal stresses that are caused by pore condensation or by differential expansion of anisotropic crystals. It is believed that in laboratory heating, internal surfaces can be annealed only by heating to sintering temperatures. Sintering temperatures and diffusion temperatures are so closely related that, before sintering is completed, a considerable amount of diffusion that effectively drains the crystal has occurred.

During in-pile heating, when the flux density is sufficiently high, the thermal spikes from the fission fragments can anneal the internal surfaces in a very short time. Calculations made with a thermal spike width of 150\AA determined at Hanford‡ show that any internal surface smaller than 150\AA would be reannealed within a few minutes when fission rates are greater than 10^{11} fissions per second per gram of fuel particle. Thus any internal surface created by heating and cooling is reannealed in such a short time that its effectiveness in draining the fission products from the interior is greatly diminished. This results in a lower diffusional release from in-pile tests. If the diffusional release is low enough, only the recoil contribution will be measured.

The foregoing discussion provides a mechanistic explanation of the fact that in some cases a larger release of fission products apparently can be attained by out-of-pile heating of a previously irradiated tube than was obtained during its irradiation in-pile at the same temperature. Further work on this behavior is under way.

5.2 OPERATIONAL ACCIDENTS

5.2.1 STARTUP RUNAWAY

5.2.1.1 Analysis of Runaways

A startup runaway, occurring during or soon after a nuclear startup, is caused by the addition of reactivity to the system. It is more dangerous than excursions at operating power because it starts at a low power level and for any conceivable rate of increase in reactivity the reactor period can become very small before the physical changes can be detected. For analysis the following conditions pertaining to an ACT startup runaway are assumed. The reactor is just critical ($k_{\text{eff}} = 1.00$) at a power level of 1.0 watt. The blowers are turned on and delivering cooling air at a rate of 25 pounds per second to the system. A controls malfunction occurs, and the shim rods start to withdraw, causing the rate of reactivity increase to be 6.0×10^{-2} percent Δk per second.

*"Gas-Cooled Reactor Project Semiannual Progress Report," ORNL-2767, June 30, 1959.

†W. B. Lewis, "Return of Escaped Fission Product Gases to UO_2 ," DM58 (AECL 964), January 21, 1960.

‡"Fuels Development Operation," Quarterly Progress Report, HW 62085, April 1959.

~~SECRET~~
CONFIDENTIAL

With this set of conditions two startup runaways were analyzed in detail. The first, designated A, was assumed to have no temperature coefficient of reactivity. The second, designated B, was assumed to have the negative temperature coefficient of reactivity that was calculated to apply during an ACT runaway.

Although it is expected that the reactor temperature coefficient of reactivity will be negative and of a significant magnitude, both cases have been analyzed and are reported inasmuch as at this time the capability to predict conclusively temperature coefficients for ceramic reactors has not been experimentally verified. It will be shown that the temperature coefficient, if it exists as predicted, has two effects on the runaway. It will allow the runaway to be stopped by a fuel element temperature scram without any tubes being melted; and if the runaway is not stopped by any of the scram trips, it will extend the time required to reach a violent accident by a factor of about seven.

5.2.1.2 Runaways Terminated by Reactor Scram Trips

Table 5.1 shows the ACT controls specifications that were assumed in the ACT runaway calculations. The power and temperature data in the runaways were generated on the basis of these specifications. Table 5.1 and the plots of power and temperature given in "5.2.1.4 Results of ACT Runaway Analysis" indicate the very important fact that in either runaway A or B three independent controls failures must occur before a runaway will result in any hazardous condition or in damage to the reactor.

The three failures are:

1. A control failure or the operator's pulling rods to initiate the runaway.
2. Failure of period trip (5 seconds) in the startup range.
3. Failure of the 5-megawatt low-power scram trip and failure of the variable high-power scram trip (200 megawatts).

TABLE 5.1
ASSUMED ACT CONTROLS SPECIFICATIONS

System type	Shim-scram
Number of rods	48; 8 gangs of 6 each
Insertion length	
Minimum scram	5 in.
Maximum shim	24 in.
Reactivity worth	
Minimum scram	2% $\Delta k/k$
Total bank worth	9% $\Delta k/k$
Time constants	
Scram initiation	140 milliseconds
Scram insertion	300 milliseconds
Shim insertion or withdrawal (24 in.)	2-1/2 minutes
Scram trips	
Turbine discharge	1400° F
Fuel element	2750° F
Period	5 seconds in startup range
Power	Variable, 200 mw assumed
Power (startup)	5 mw if power demand < 1.5%
Engine	106 to 110% rpm

~~CONFIDENTIAL~~
~~SECRET~~

For the purpose of this discussion, the 5-megawatt low-power scram trip and the variable high-power scram trip are considered one failure because they have certain components in common.

In the case of runaway B, if all of these failures occurred, the reactor could still be scrammed on fuel element temperature, but maximum-average fuel element temperatures might reach 3000° F. Table 5.2 shows the time sequence and energy and temperature information for these scrams.

The assumptions and methods of the nuclear and thermal analysis leading to the results are given in the appendix.

5.2.1.3 Unchecked Runaways

If it is assumed that all ACT scram trips failed, the resulting unchecked runaway would continue until enough energy had been added to the system to generate forces capable of dispersion of the reactor and termination of the excursion. The nuclear model and the calculations that describe the physical events resulting from an unchecked runaway are given in the appendix. The model assumes that the reactor melts and a disk-shaped section at the longitudinal midplane vaporizes and exerts the pressure necessary to separate the reactor components and terminate the excursion.

Figures 5.1 and 5.2 show the power, temperature, and excess reactivity curves for cases A and B through core separation.

TABLE 5.2
RESULTS OF ACT RUNAWAY ANALYSIS

		Case A	Case B
Scram Trip	time, sec	5.5	5.5
5-sec period	energy, mw-sec	negligible	negligible
	peak temperature reached, °F	70	70
	time, sec	12.1	12.1
5-mw power	energy, mw-sec	3.6	3.6
	peak temperature reached, °F	74	74
	time, sec	12.5	12.6
200-mw power	energy, mw-sec	286	161
	peak temperature reached, °F	330	260
	time, sec	12.8	44 → 47
^a 2750°F temperature	energy, mw-sec	not sufficient to stop runaway A meltdown	3120 → 3540
	peak temperature reached, °F		2850 → 3050° F
	time, sec		86
No scram	energy, mw-sec	2.8 × 10 ⁴	2.8 × 10 ⁴
	peak temperature reached, °F	meltdown	meltdown
	time, sec	12.8	86

^aRun only for case B with 0- and 3-second thermocouple lag times.

~~CONFIDENTIAL~~
~~SECRET~~

CONFIDENTIAL

~~CONFIDENTIAL~~

CONFIDENTIAL

~~CONFIDENTIAL~~

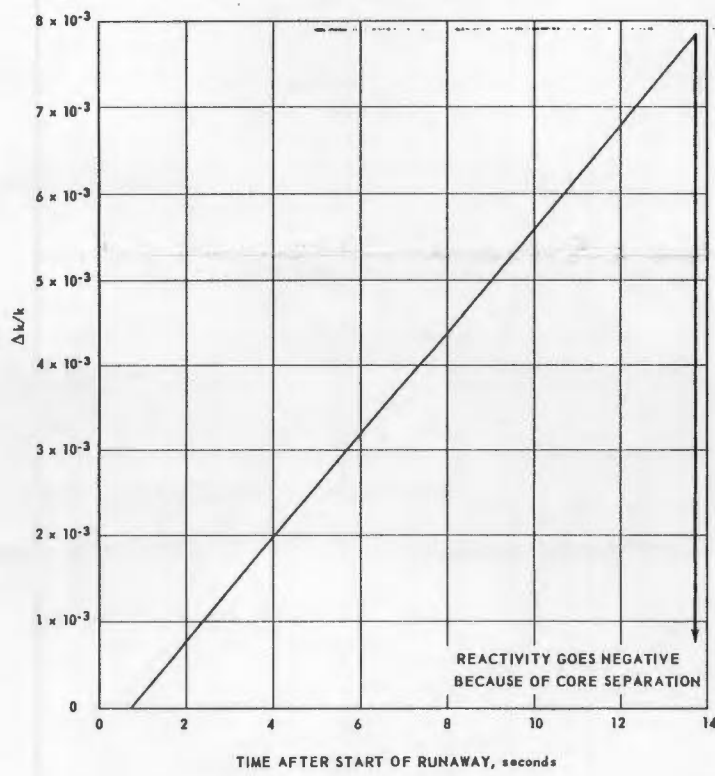
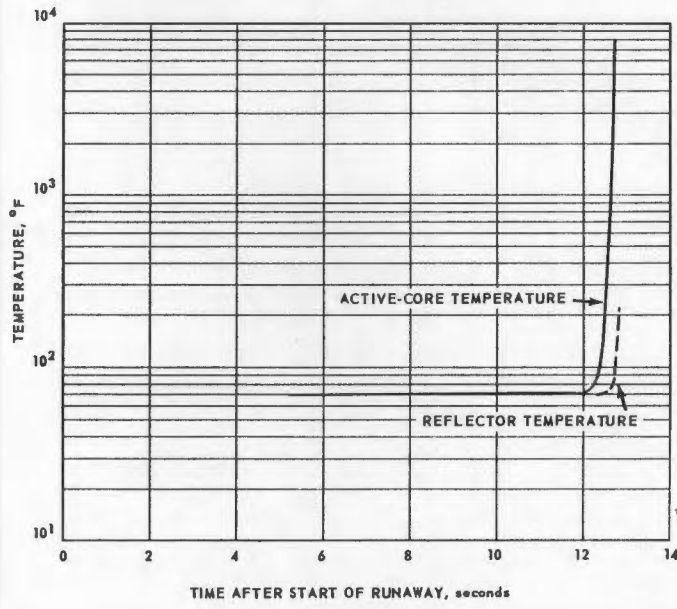
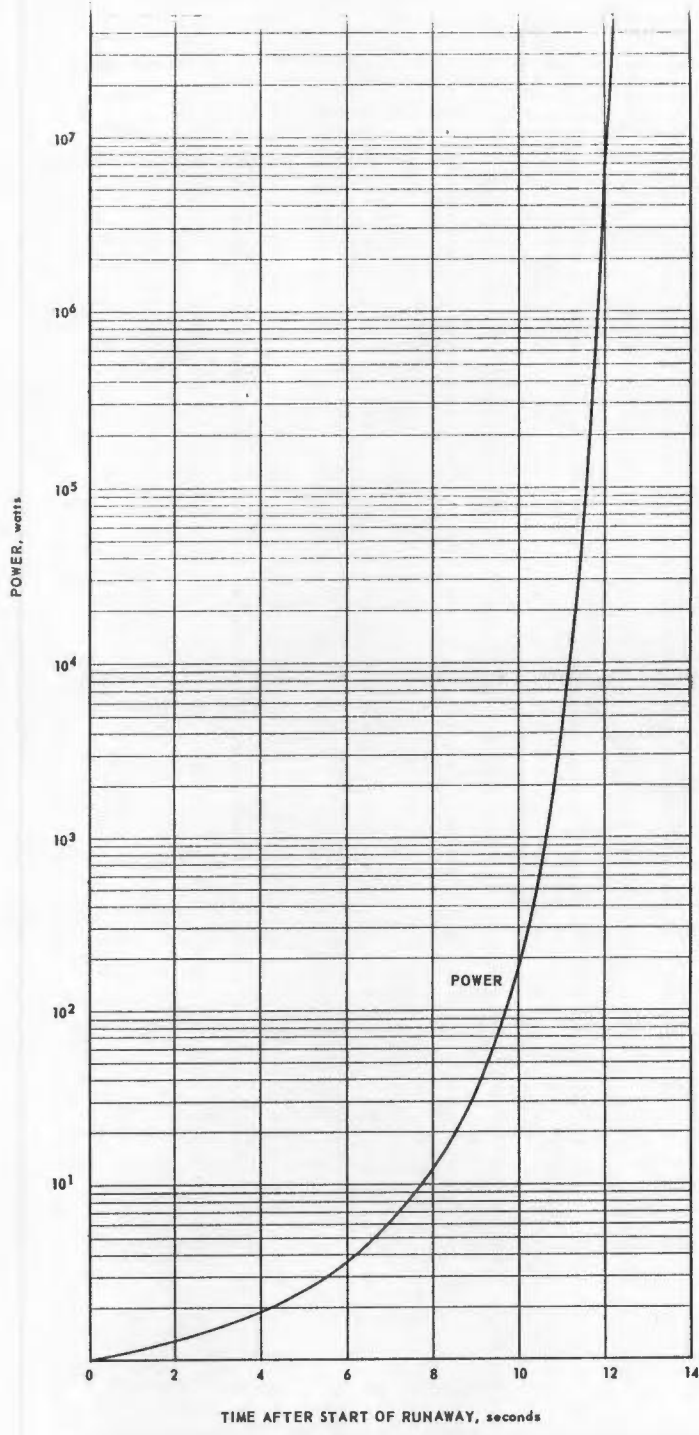
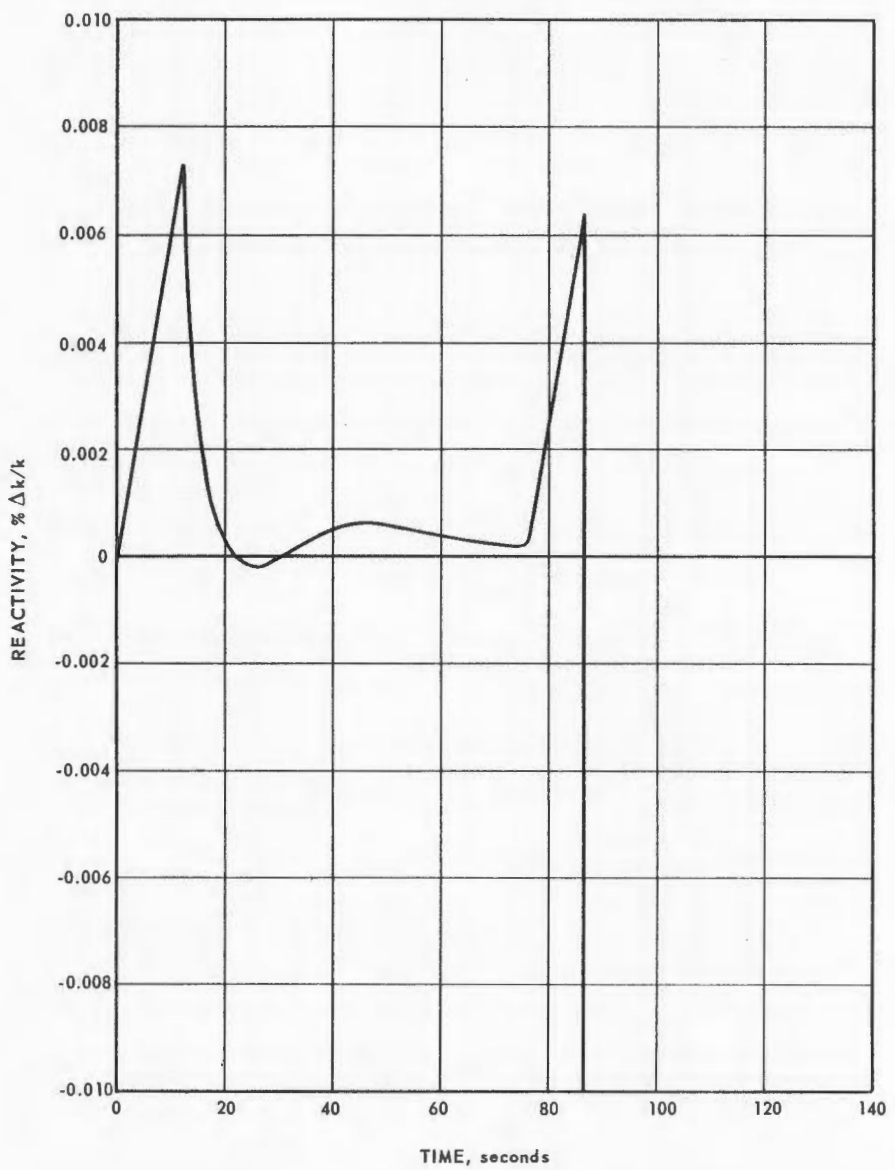
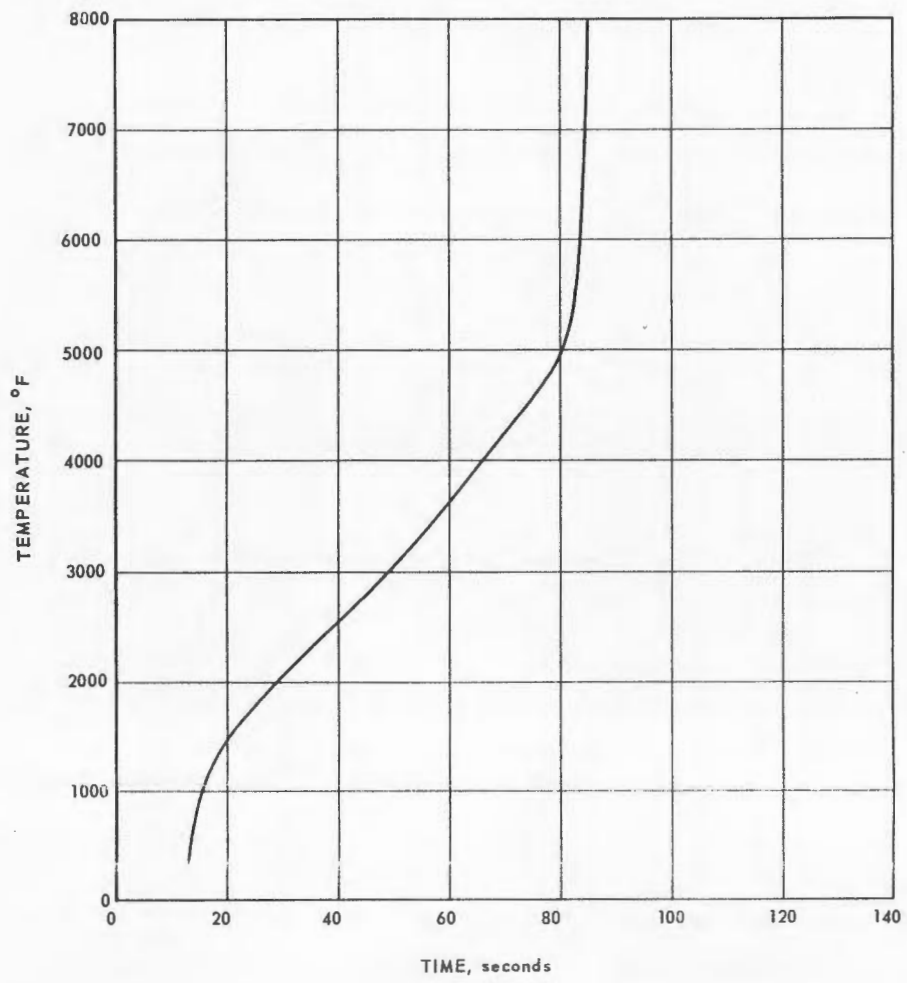
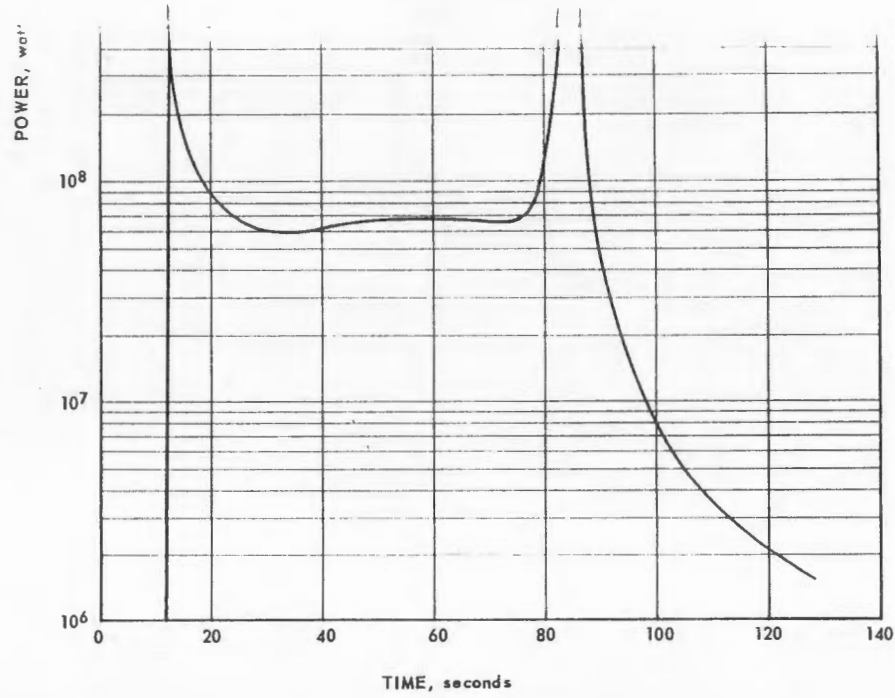


Fig. 5.1—Power, temperature, and reactivity versus time for runaway A, with no temperature coefficient

~~CONFIDENTIAL~~
DECLASSIFIED

CONFIDENTIAL
DECLASSIFIED



DECLASSIFIED

CONFIDENTIAL
DECLASSIFIED

Fig. 5.2—Power, temperature, and reactivity versus time for runaway B, with negative temperature coefficient

In runaway B with the negative temperature coefficient of reactivity the net effect of the control-rod-induced increase in rate of reactivity and the temperature-coefficient-induced decrease in rate of reactivity becomes important.

Figure 5.2 shows the net effect of this combination. It is seen that the temperature-coefficient effect for a time overrides the rod-withdrawal effect, but that eventually the withdrawal effect becomes predominant. It was assumed that the temperature coefficient applied to the melting point (4500° F). The rod locations have a bearing on the final results of these effects. The rods are located in the radial reflector and consequently are somewhat insulated from the active core. This means that because of the temperature differences between the core and the radial reflector, the rods must still be assumed to be withdrawing even after high core temperatures have been reached. The reflector temperature lags the active core temperature considerably, as explained in section "2. 1. 1. 3 Nuclear Design," this is the primary reason for the negative temperature coefficient throughout the runaway.

5. 2. 1. 4 Results of ACT Runaway Analysis

Additional results of analyses of ACT runaways terminated by scrams are shown in Figures 5. 3, 5. 4, and 5. 5. Figure 5. 3 shows active core temperature versus time for

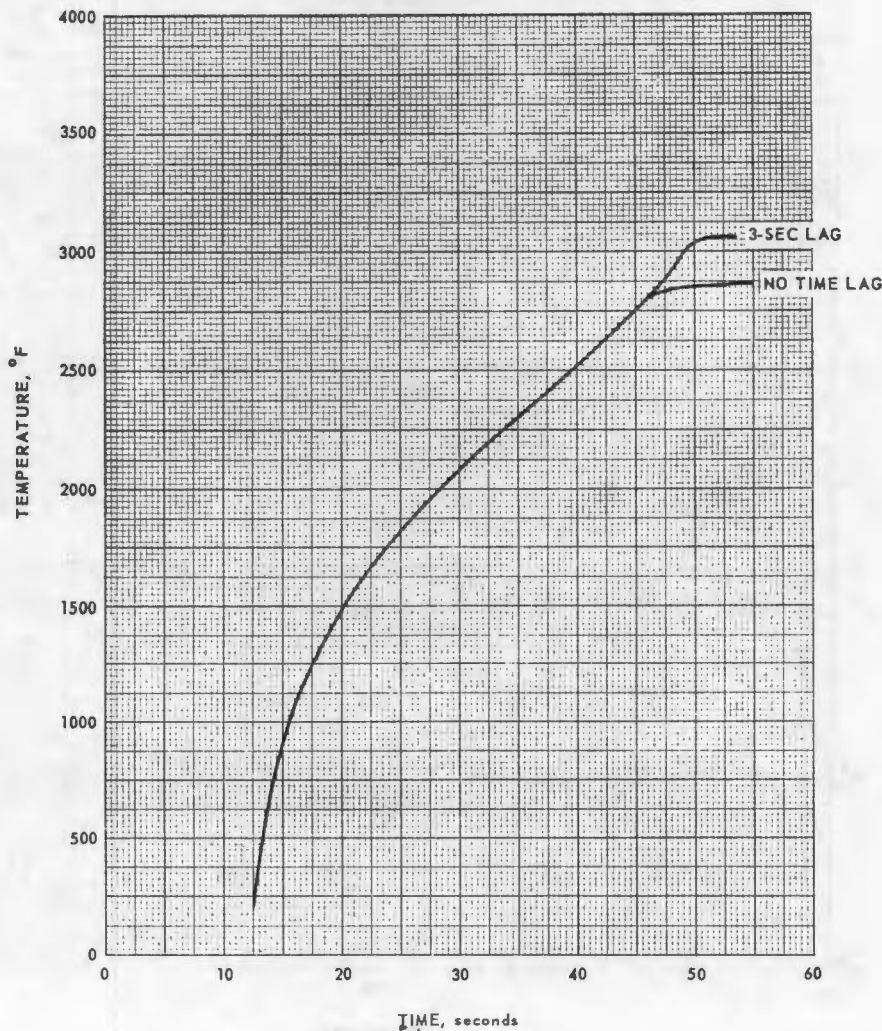


Fig. 5.3 - Temperature versus time for runaway B with temperature scram at 2750°F for two different thermocouple time lags

~~CONFIDENTIAL~~
~~SECRET~~

runaway B terminated by a temperature scram at 2750°F from thermocouples of zero time lag and 3-second time lag. Figure 5.4 shows power as a function of time for runaway B terminated by a 200-megawatt power scram. Figure 5.5 shows active core temperature versus time for both type A and B runaways terminated by a 200-megawatt power scram. No plots are given on transient power excursions terminated by either a period or 5-megawatt scram because the reactor experiences no significant temperature increase for transient excursions terminated by either of these scrams. Figure 5.6 shows when the scram trips outlined in Table 5.2 would be actuated. In each case a 140-millisecond actuator delay elapses before the rod starts in.

In the event of three controls failures and a resulting, unchecked runaway, it is concluded that 4.0 percent of the active core is vaporized and that the rest is melted. The details of the analysis that leads to this conclusion are given in the appendix.

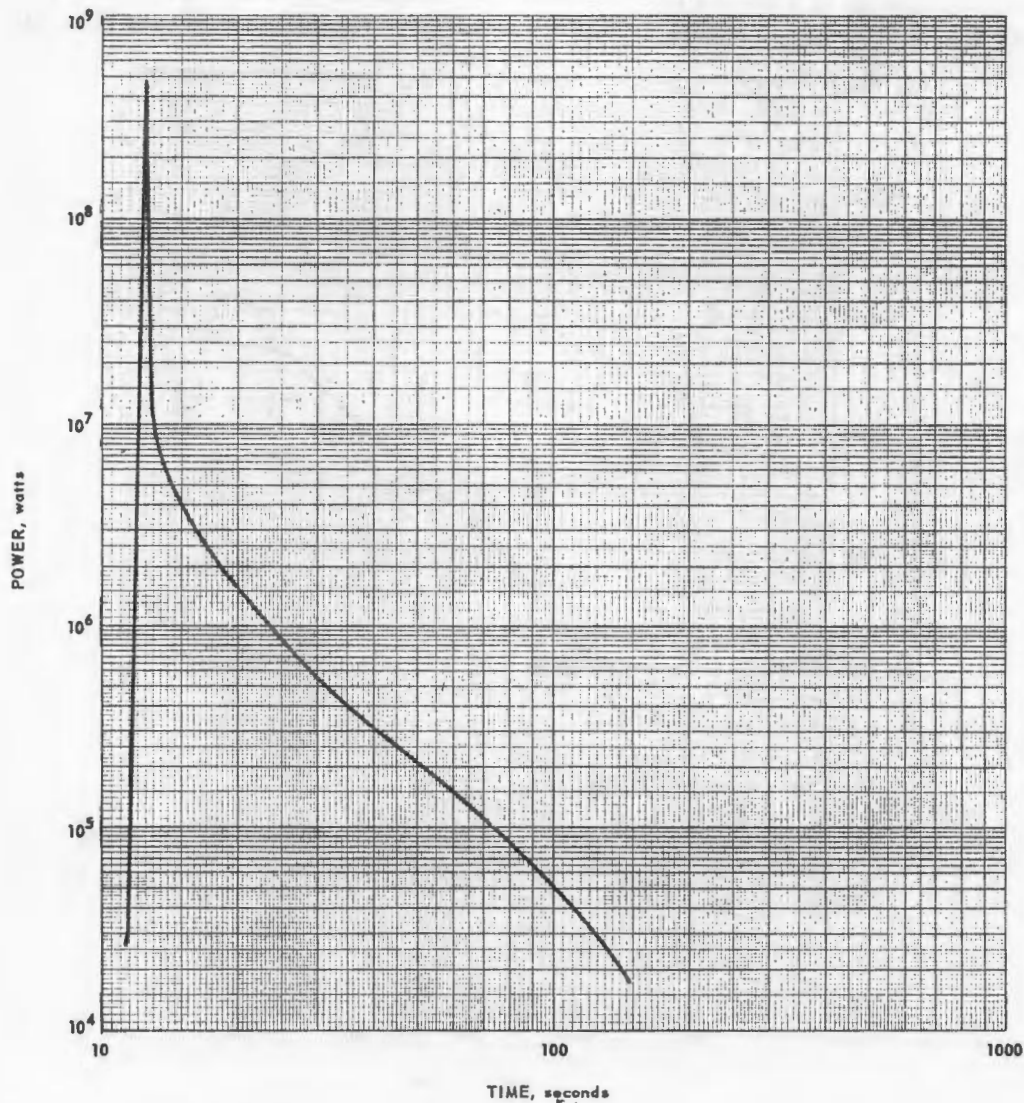


Fig. 5.4 - Power versus time for runaway B terminated by 200-megawatt scram trip

~~CONFIDENTIAL~~
~~SECRET~~

CONFIDENTIAL
~~SECRET~~

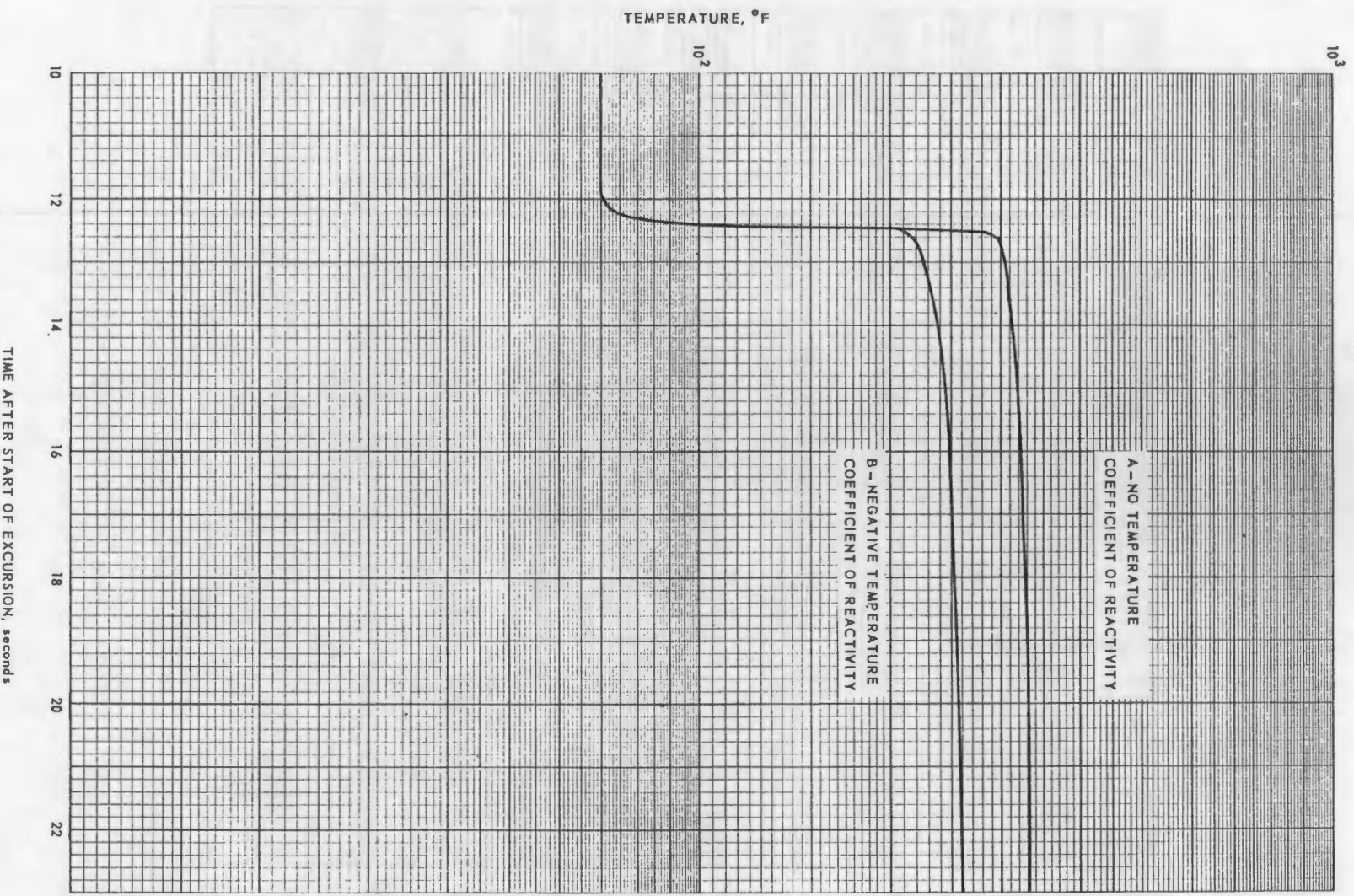


Fig. 5.5 - Temperature versus time for runaways terminated by 200-megawatt scram trip

~~SECRET~~
CONFIDENTIAL

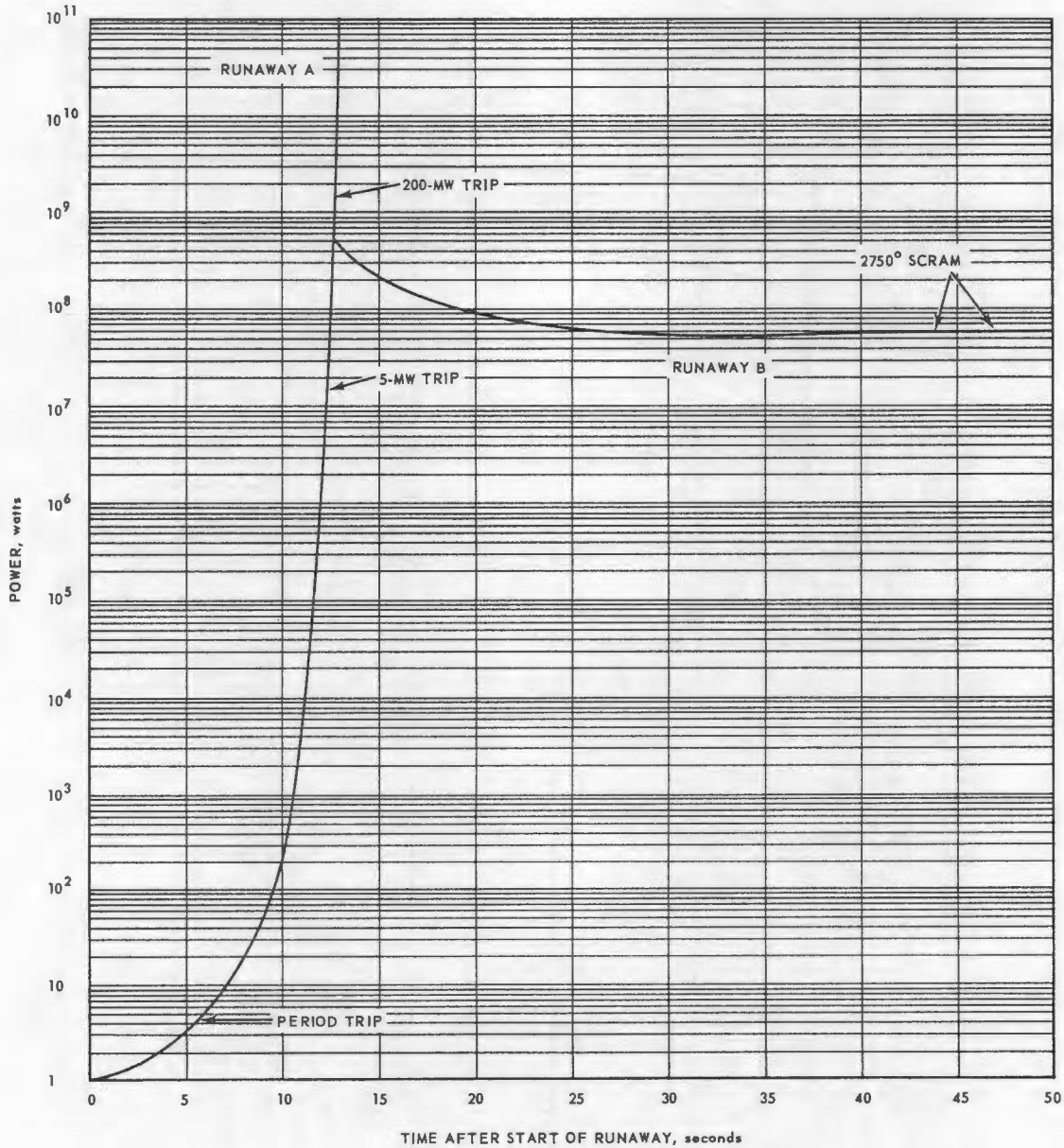


Fig. 5.6 - Runaway power distributions showing scram trip

5. 2. 2 POWER-RANGE FAILURES

5. 2. 2. 1 Control Rod Withdrawal During Steady Operation

If some failure of the ACT controls causes the withdrawal of the shim rods, a transient condition will exist and the reactor power will start to rise from its steady-state value. The withdrawal of various numbers of ACT shim rods was assumed, and the resulting power swings and temperature rises have been calculated.

The controls system as designed has eight frames or gangs of six rods each. The minimum number that can withdraw at any time is six rods.

Figure 5. 7 shows the power transients when one-fourth, one-half, and all rods are withdrawn. Figure 5. 8 shows the temperature transients. In each case the transient was stopped by the 200-mwscram trip. This would be the mechanism of scram in each case because the temperatures do not exceed the 2750°F for which the temperature trip is set.

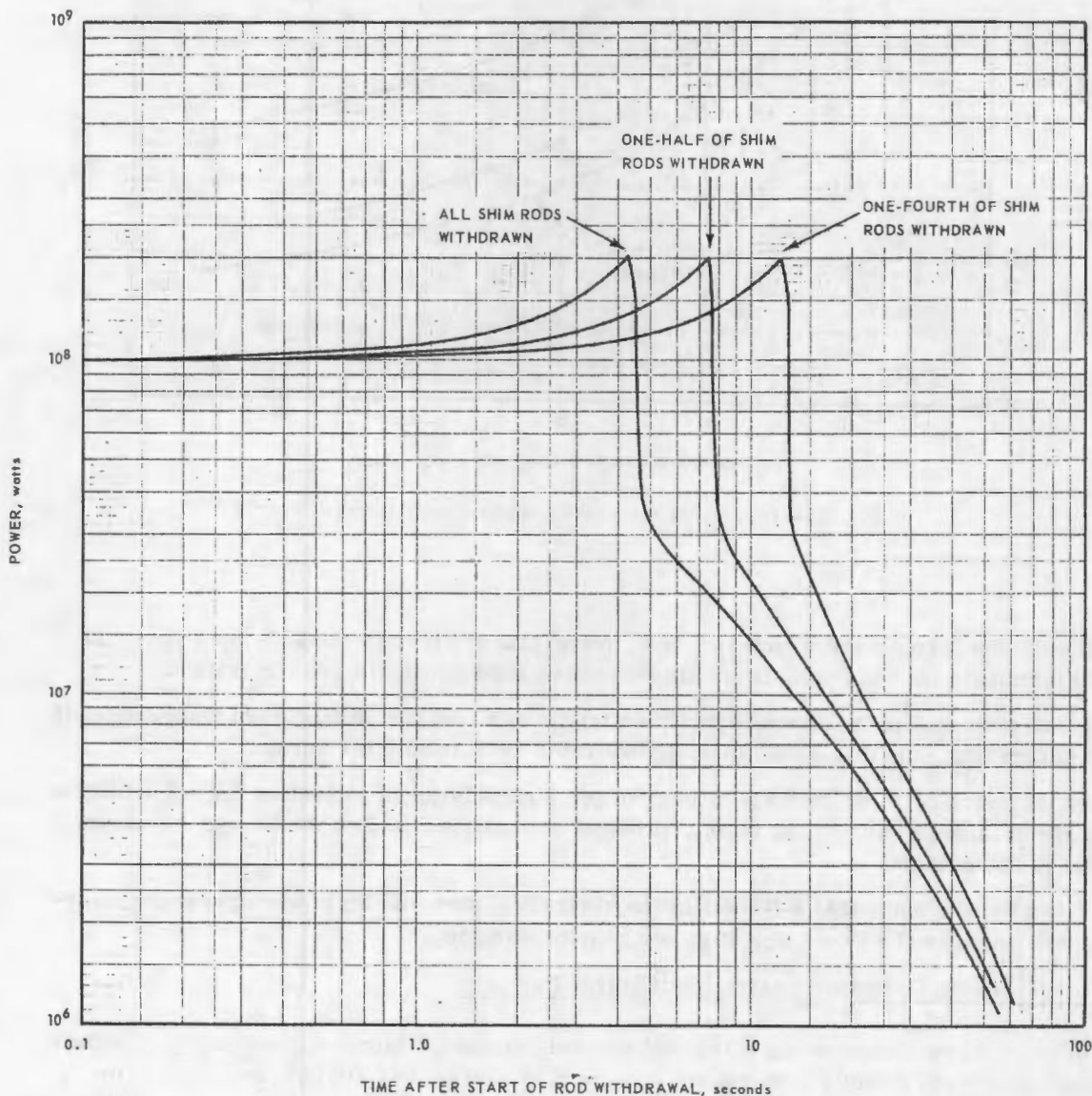


Fig. 5.7 - Power transients terminated by 200-megawatt scram

CONFIDENTIAL
SECRET

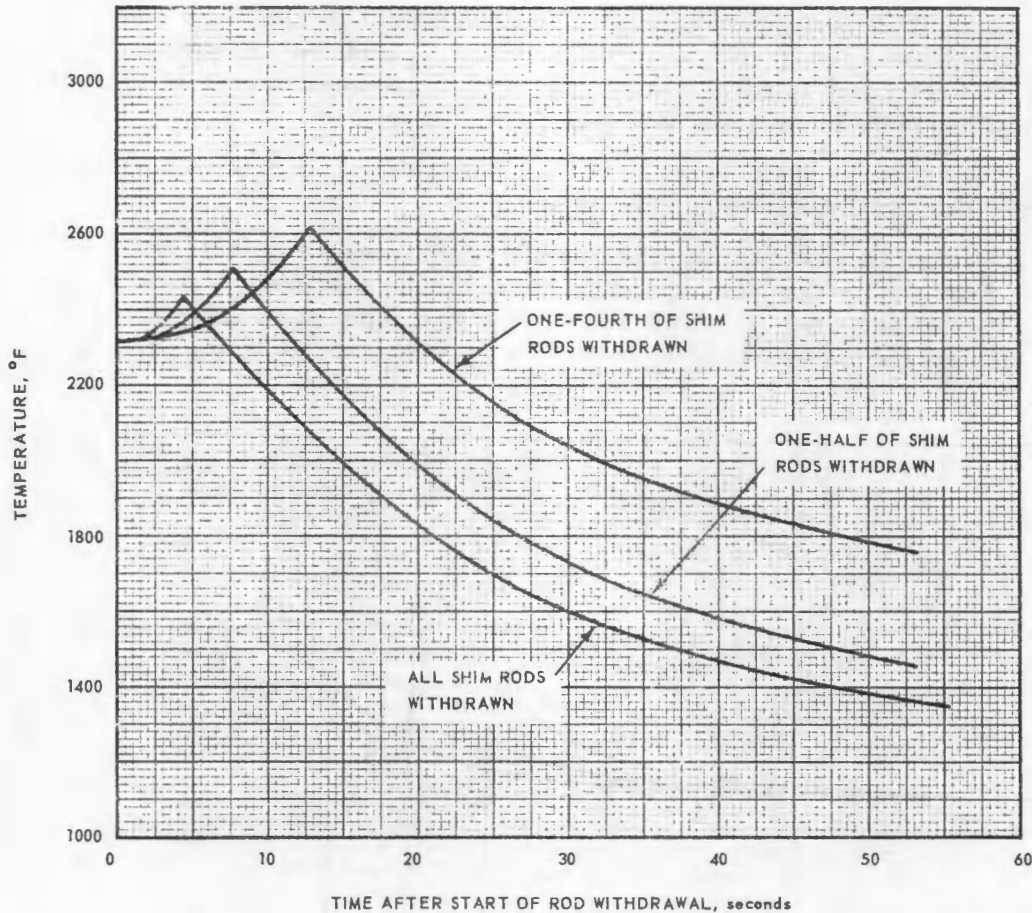


Fig. 5.8 - Temperature transients terminated by 200-megawatt scram

If only one frame were withdrawn, i. e., one-eighth of all rods, the 200-mw trip would still terminate the excursion if any thermocouple time constants are considered.

It was assumed in the analysis that the airflow was constant during each transient until the scram trip, and that coastdown airflow rates were used after scram.

As the more detailed analysis of control component failures in section 5.2.2.2 indicates, the speed increase during the power transient is negligible and so the overspeed scram level is not reached.

It can be concluded that a failure in the controls system during power operations causing rod withdrawal will not result in any reactor damage.

5.2.2.2 Analog Computer Analysis of Control Failures

In order to demonstrate the effects of control parameter failures, the analog computer simulation of the D140E1 power plant was used. Failures that would cause the maximum malfunction to the power plant were assumed. Combination failures and cases when the part of the safety system that normally would protect the power plant following a malfunction also failed were studied.

CONFIDENTIAL
SECRET

Scram and Safety Responses

The following scram responses are normally supplied:

<u>Power Plant Parameter</u>	<u>Level Assumed for this Study</u>
Fuel element temperature (T_{fe})	200°F greater than normal maximum (about 2750°F)
Turbine discharge temperature ($T_{5.1}$)	1400°F
Reactor power level, power range	200 megawatts
Reactor power level, startup range	5 megawatts
Reactor period (startup range only)	5 seconds
Engine rotor speed	105%
Control rod actuator pressure	70% of normal
Various electrical supply voltages and main electrical power	

In addition, a nozzle bound control limits maximum nozzle area to 1500 square inches at high engine speeds.

Nonfailing Scram Circuits

It will be assumed that neither the turbine discharge temperature ($T_{5.1}$) scram nor the fuel element temperature (T_{fe}) scram circuits can fail. Each of these safety circuits uses three complete scram channels, and a signal from any of the six channels will initiate a scram. Three failures will be required to make the $T_{5.1}$ scram or the T_{fe} scram inoperative. Three failures in addition to the initial failure, therefore, will be required to permit an excursion if the $T_{5.1}$ scram or the T_{fe} scram fails to operate, making a total of four failures, which is most improbable.

Speed-Control Failure

The two portions of the speed-control loop, the bleed-valve control and the nozzle control, are independent except for the speed demand signal; therefore, a double failure will be required for both parts of the speed control to fail in a manner that would cause speed to increase.

Thermocouple Time Constants

For this study, the time constants assumed for the $T_{5.1}$ safety-circuit thermocouples are the same as those estimated for the $T_{5.1}$ control-circuit thermocouples.

The fuel element thermocouples are assumed to have no contact with the fuel tubes and are heated by radiation only. Measured radiation properties for thermocouple materials were used to calculate time constants for proposed fuel element thermocouples under study. Choosing from among the more pessimistic results, 5 seconds was used as the fuel-element-thermocouple time constant at the scram-trip temperature.

Double-Failure Philosophy

In all the single-failure studies, normal safety interactions are assumed to occur. For the double-failure analyses, the second failure will be assumed to occur in the control or safety system that first acts to reduce the effect of the single failure. If two or more systems tend to counteract the effect of the failure, failures in both systems will be studied, each in combination with the first failure.

Of all the control failures studied on the analog computer, only two could cause sudden loss of reactor airflow. The double failure in which the jet nozzle failed open and the bleed valve failed closed could cause the rotor to reach 120 percent speed and possibly

~~CONFIDENTIAL~~
SECRET

result in failure of the compressor and/or turbine. This in turn could prevent cooling of the reactor. The simultaneous failures of the T_{5.1} control in the increasing direction and the control bleed open will cause overtemperature of the struts that support the turbine bearing, possibly resulting in failure of the bearing and loss of ability to supply air to the reactor.

For all the single and double T_{5.1} control failures at 100 percent speed, recordings of the analog computer results are included that show the history of various temperatures during the transients. These transients are typical of T_{5.1} control failures at other engine speeds. Traces of two flux-control failures at 100 percent speed are also included for comparison. The flux-control failures, in general, will be over sooner, since flux will increase rapidly up to the flux trip level and scram will occur quickly. As a result, reactor overheating will generally be less for a flux-control failure than for a T_{5.1} control failure.

When engine speed decreases rapidly during transients, T_{5.1} will increase at low engine speeds after initially decreasing. This occurs because the turbine extracts less work from the gas at lower turbine pressure ratios as the turbine decelerates. Careful examination will show that T_{5.1} approaches turbine inlet temperature (T₄) but does not exceed it. Since T₄ is decreasing at low speeds and since the aftercooling blowers provide approximately the same airflow as the compressor at 20 percent speed (1000 rpm), T₄ will continue to decrease when the aftercooling system is operating and T_{5.1} then will decrease also.

The analog computer recording of the gross-speed-control failure, during which engine speed increases to 120 percent, is also included. The assumption necessary to complete the analog transient was that the turbine did not fail although it will during a transient as severe as this. For comparison, the analog trace of the negative-speed-control failure is included to show the rapid increase in turbine exit temperature resulting from this type of failure.

In all the analog recordings of the control failure excursions, a trace of fuel element temperature (T_{fe}) is shown. This temperature is the average-fuel-tube wall temperature in the longitudinal center third of the reactor. Normally this is the hottest third of the reactor, and the peak fuel element temperature will ordinarily be 400° to 500°F higher than the temperature indicated on the traces.

T_{5.1} Control Failures at 100 Percent Speed

T_{5.1} Control Failure Decreasing T_{5.1} - A failure of the T_{5.1} control tending to decrease reactor power will cause a safe power plant coastdown without excessive temperatures. Such a failure might result from a loss of T_{5.1} demand signal. Figure 5.9 shows the recording made during the analog computer run of this failure.

T_{5.1} Control Failure Increasing T_{5.1} - There is a limit on the temperature error amplifier in the temperature control loop, which is designed to be set at an equivalent temperature error of 52°F but may be set as high as 174°F. If the temperature error limit is set as high as 174°F during a failure or if the temperature loop fails beyond this point, the resulting excursion will be indistinguishable from a failure in the reactor flux control loop and, therefore, is not discussed with temperature control failures.

If the temperature error limit is set at an equivalent 52°F and the T_{5.1} control fails in a direction tending to increase reactor power, power will increase from its 100 percent speed value of about 104 megawatts to about 140 megawatts in approximately 3 seconds. At the latter point the temperature error limit saturates, and reactor power increases slowly to about 185 megawatts in an additional 9 seconds. At this point the T_{5.1} safety

SECRET
~~CONFIDENTIAL~~

circuit causes the reactor to scram. No significant engine speed change occurs until scram. Figure 5. 10 is the analog recording of this excursion, and the maximum values are:

T_{5, 1} 1860°R
Reactor power 185 mw
T₄ 2490°R
T₄ exceeds 2370°R for 8 seconds

These temperatures and temperature transients are not severe enough to cause damage leading to a loss in reactor airflow. A failure such as this may occur from loss of thermo-couple feedback in the T_{5, 1} control loop.

T_{5, 1} Control Failure Increasing T_{5, 1} and Speed Control Failure Decreasing Speed - If the second failure occurs in the speed control in a manner decreasing speed, T_{5, 1} increases rapidly because of the lowered reactor airflow and increasing reactor power. This causes a scram in 3-1/2 seconds. Such a failure might be caused by loss of speed demand signal. Figure 5. 11 is the analog recording of the excursion resulting from this failure, and the maximum values are:

T_{5, 1} 1910°R (at 20% speed)
Reactor power 130 mw
T₄ 2315°R

T_{5, 1} Control Failure Increasing T_{5, 1} and Nozzle Control Failure Opening Nozzle - If a second failure occurs in the nozzle control loop and the nozzle opens wide (to the nozzle bound), the reactor flux behaves as if a single failure occurred. The rotor speed increases rapidly to 104 percent, and at this point the bleed control acts to reduce the overspeed. The slight overspeed maintains enough additional airflow to prevent T_{5, 1} from increasing very rapidly, and scram is triggered by fuel element temperature in about 13 seconds. A failure of this nature might result from mechanical failure of the nozzle actuator or link-ages or loss of speed feedback to the nozzle loop. Figure 5. 12 is the recording of this excursion, and the maximum values are:

T_{5, 1} 1840°R
Reactor power 190 mw
T₄ 2575°R
T₄ exceeds 2370°R for 14 seconds.

T_{5, 1} Control Failure Increasing T_{5, 1} and Nozzle Control Failure Closing Nozzle - If a second failure causes the nozzle control to move closed, a rapid reduction in speed to about 90 percent occurs, and the bleed control is unable to overcome this reduction in speed. T_{5, 1} increases rapidly about 100°F and continues to increase as reactor power increases until a T_{5, 1} scram occurs after 9 seconds. Loss of the speed demand signal to the nozzle control loop might cause such a failure. Figure 5. 13 shows the recording from the excursion resulting from this failure, and the maximum values are:

T_{5, 1} 1860°R
Reactor power 188 mw
T₄ 2440°R
T₄ exceeds 2370°R for 6 seconds.

T_{5, 1} Control Failure Increasing T_{5, 1}, and Bleed Control Failure Opening Bleed Valve When a second failure causes the bleed valve to open, a rapid change in engine speed lowers speed to 92 percent and the resulting lowered reactor airflow raises T_{5, 1} about 50°F. T_{5, 1} continues to increase as reactor power increases until a T_{5, 1} scram occurs at 7

CONFIDENTIAL
SECRET

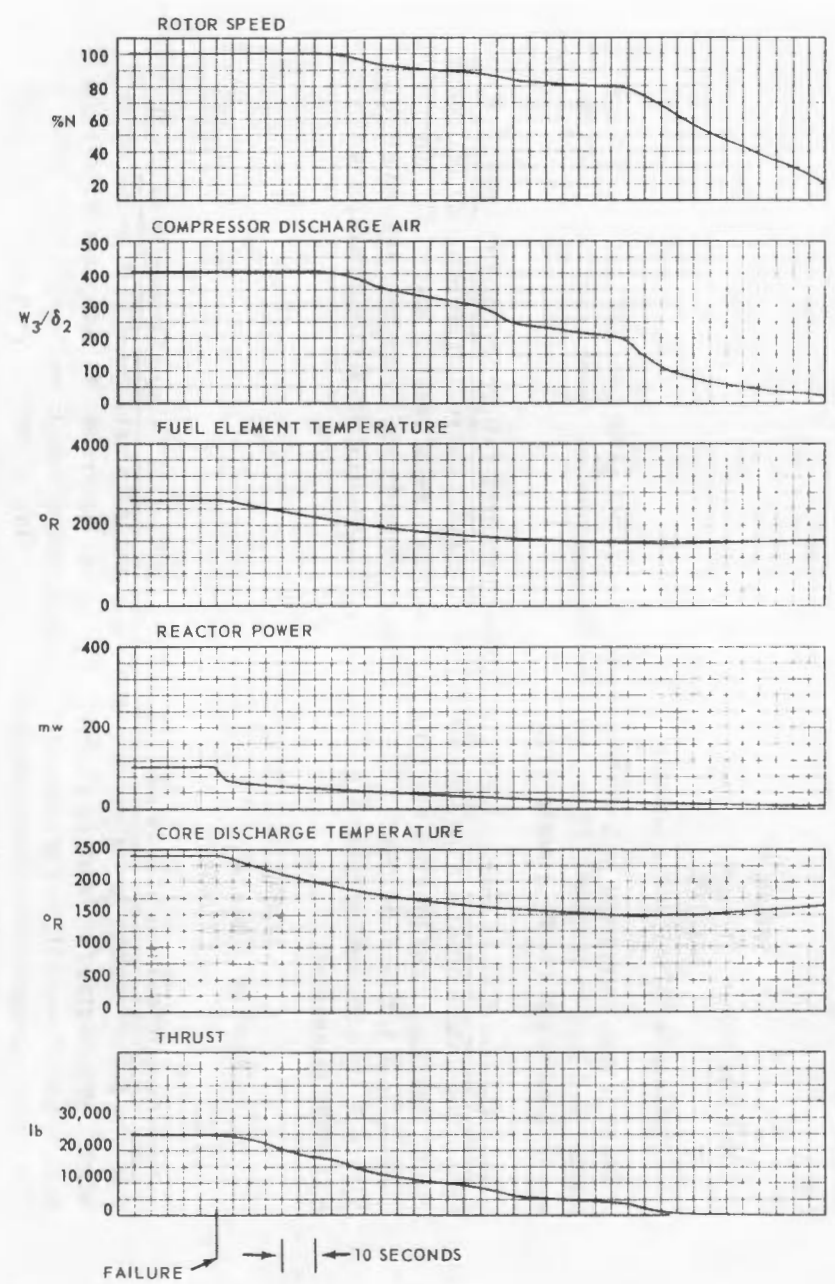
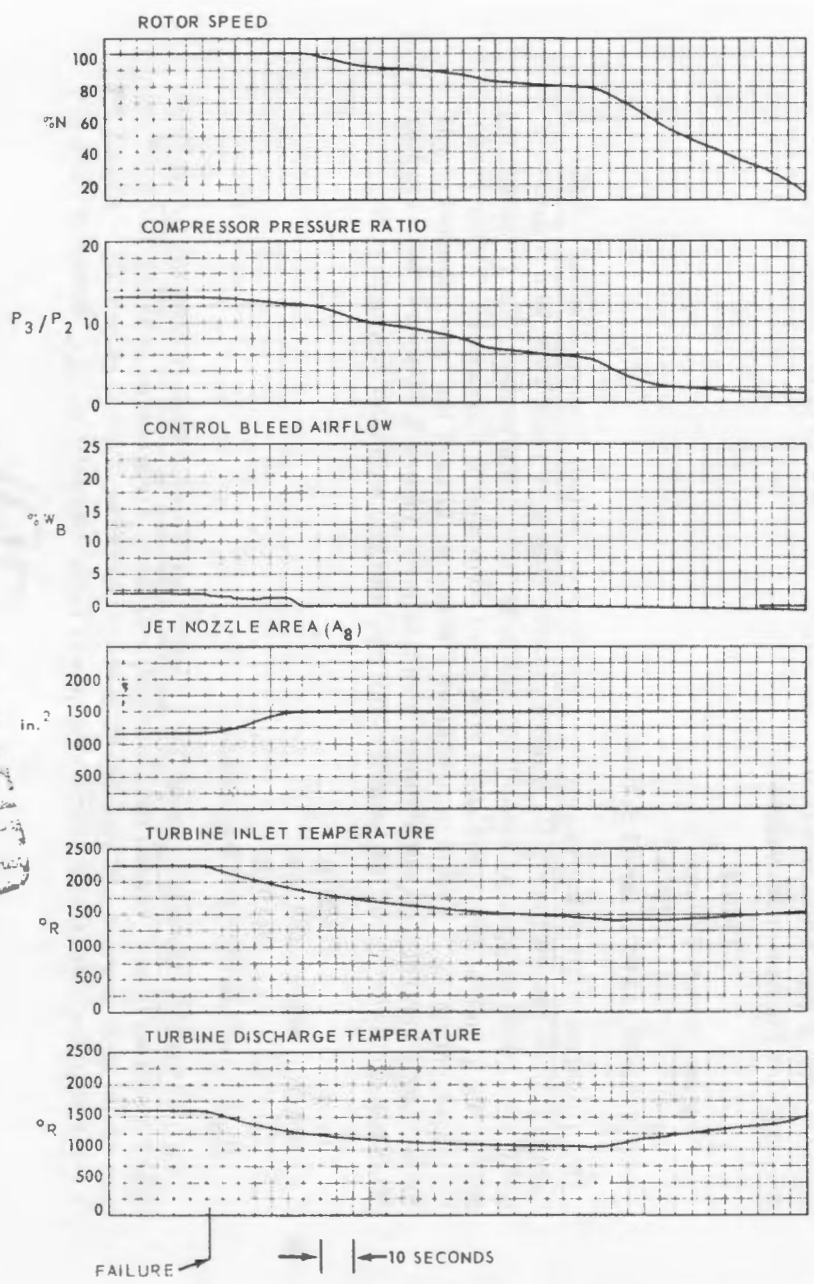


Fig. 5.9 - Single failure: $T_{5,1}$ control failure decreasing $T_{5,1}$

SECRET

SECRETED
DECLASSIFIED

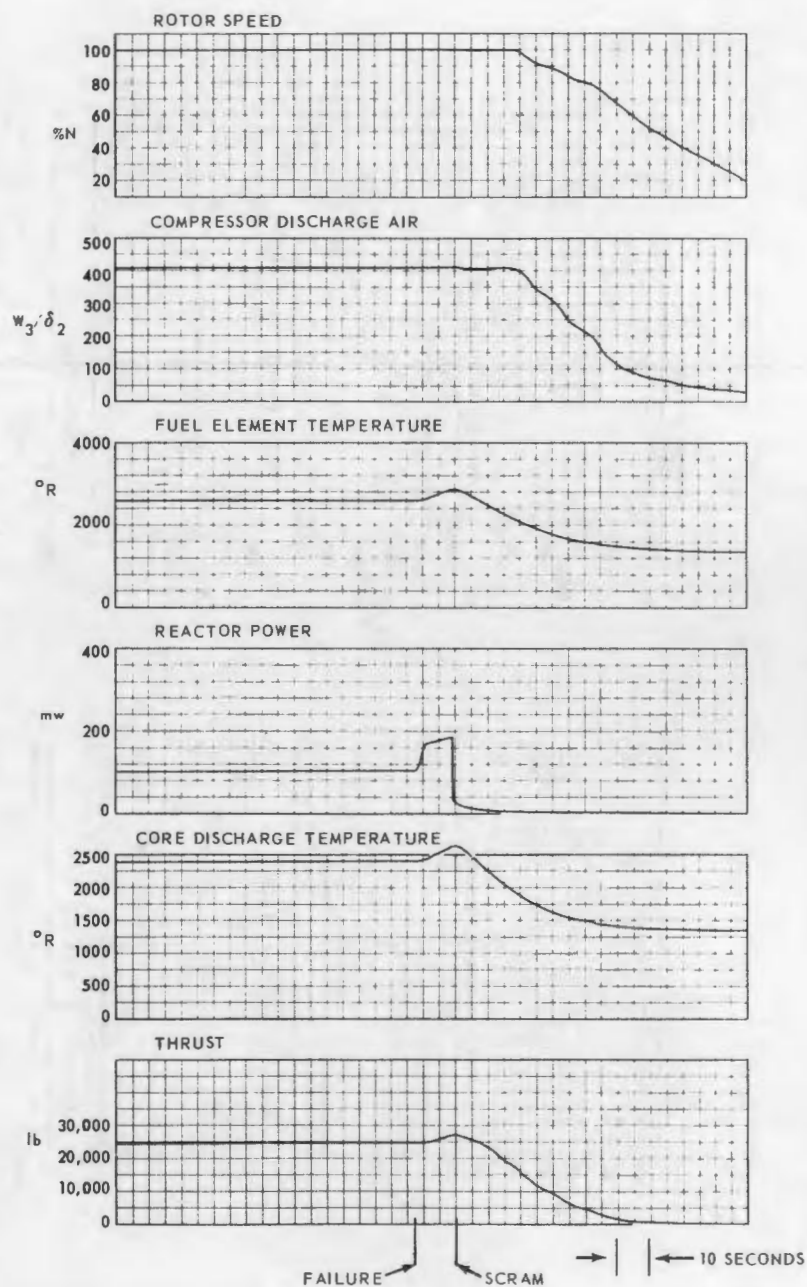
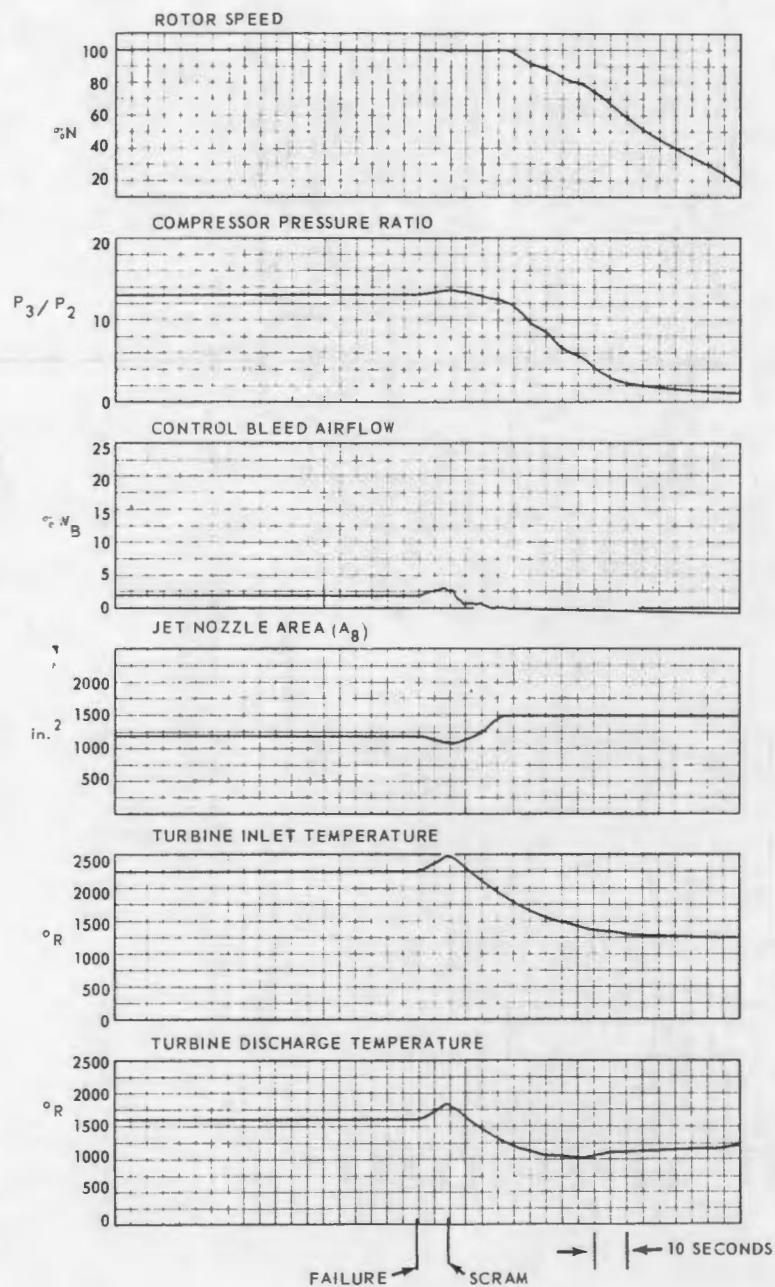


Fig. 5.10 - Single failure: $T_{5,1}$ control failure increasing $T_{5,1}$

UNCLASSIFIED
SECRETED

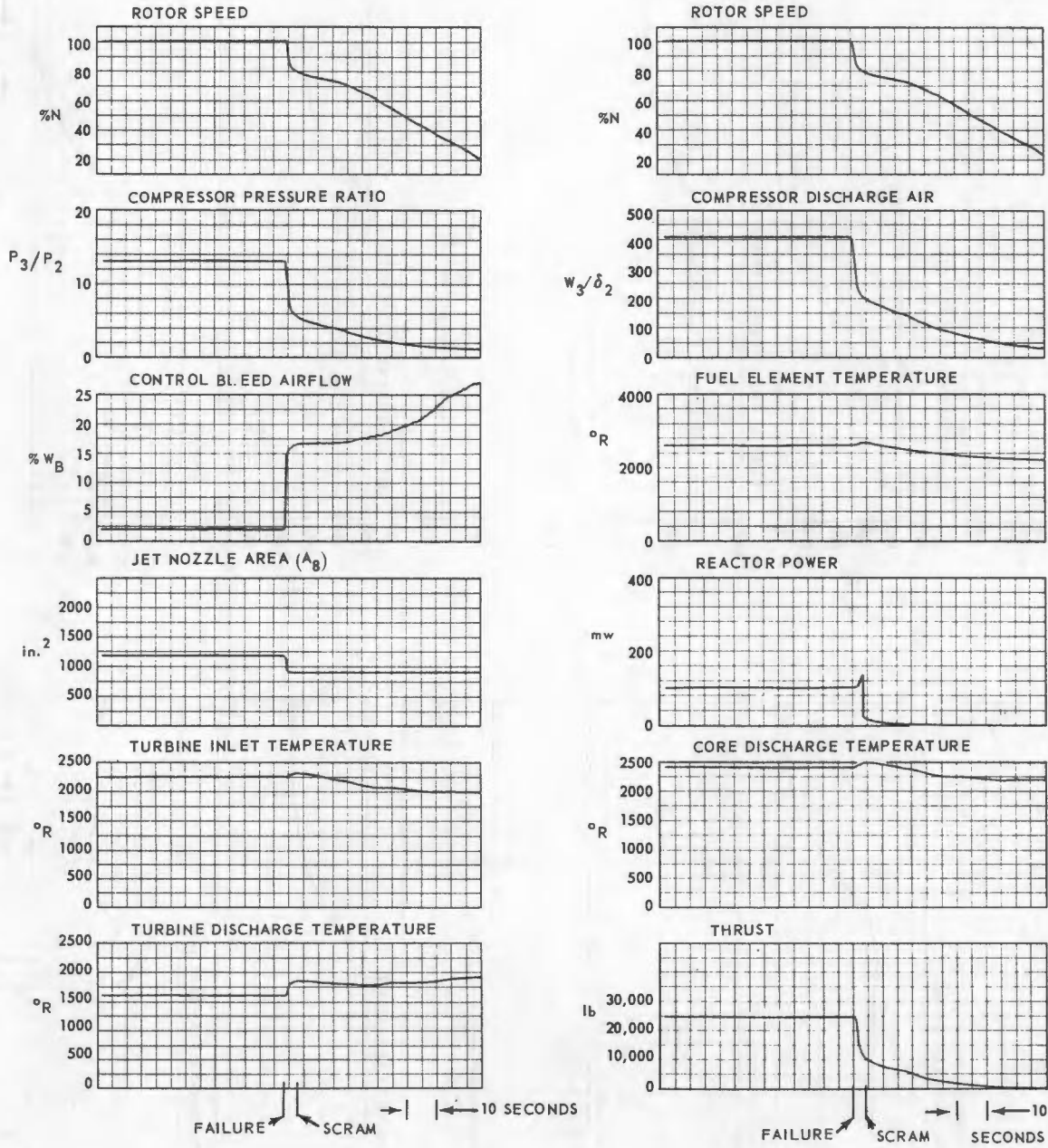


Fig. 5.11 - Double failure: $T_{5.1}$ control failure increasing $T_{5.1}$ and speed
control failure decreasing speed

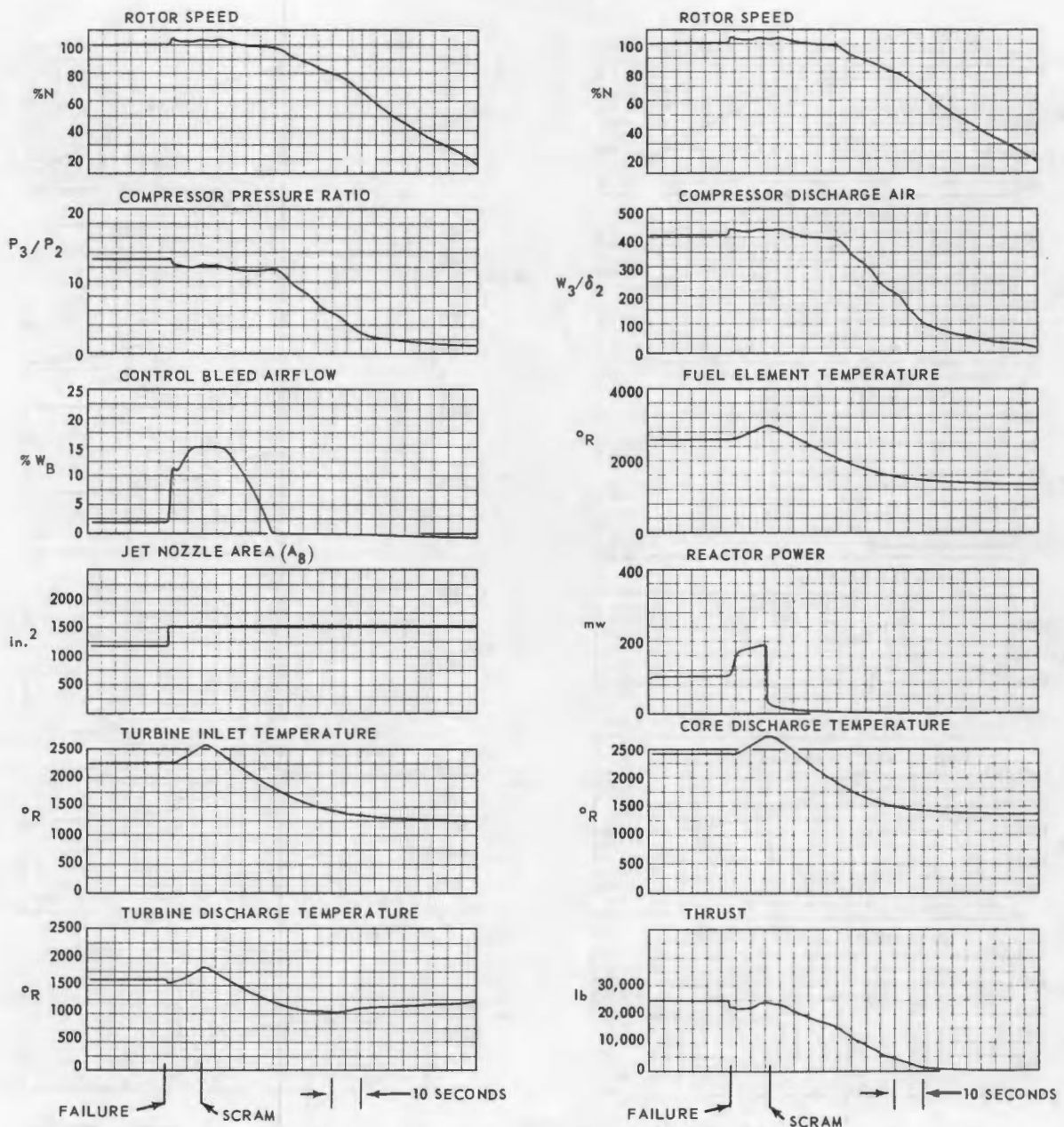


Fig. 5.12—Double failure: $T_{5.1}$ control failure increasing $T_{5.1}$ and nozzle control failure opening nozzle

~~CONFIDENTIAL~~
~~SECRET~~

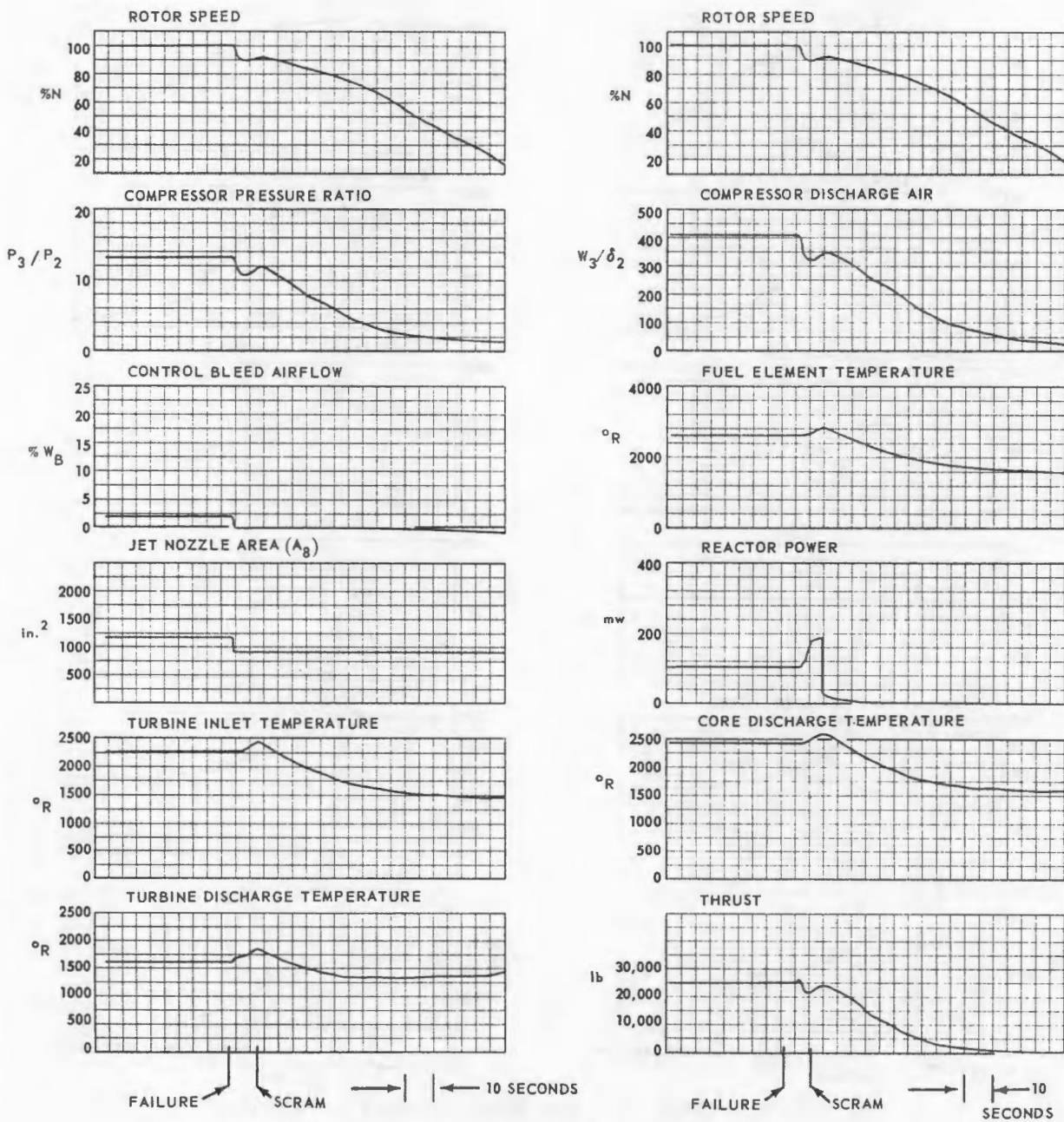


Fig. 5.13—Double failure: $T_{5.1}$ control failure increasing $T_{5.1}$ and nozzle control failure closing nozzle

~~SECRET~~
~~CONFIDENTIAL~~

seconds after the start of the excursion. Loss of speed demand signal to the bleed control loop might cause such a failure. Figure 5.14 shows the analog recording of the excursion, and the maximum values are:

T_{5.1} 1860°R
Reactor power 185 mw
T₄ 2440°R
T₄ exceeds 2370°R for 7 seconds.

T_{5.1} Control Failure Increasing T_{5.1}, and Bleed Control Failure Closing Bleed Valve -
When a second failure causes the bleed valve to close, the maximum speed attained is only 102.5 percent. T_{5.1} increases as reactor power increases until 13 seconds after the two failures when T_{5.1} exceeds the trip level and a scram occurs. A bleed control failure such as this may be caused by loss of speed feedback in the bleed control loop or by a mechanical failure in the actuator controlling the bleed valve. Figure 5.15 is the analog recording made of this excursion, and the maximum values are:

T_{5.1} 1860°R
Reactor power 134 mw
T₄ 2525°R
T₄ exceeds 2370°R for 11 seconds.

Reactor Flux Control Failures at 100 Percent Speed

Flux Control Failure Decreasing Flux - A failure of the reactor flux control loop that tends to decrease reactor power will cause a safe power plant coastdown without excessive temperatures. Such a failure might result from a loss of the flux demand signal within the T_{5.1} control loop or from a loss of flux demand while the power plant is being operated by use of the reactor flux control.

Flux Control Failure Increasing Flux - A failure of the flux control loop tending to increase reactor power will cause the control rods to withdraw and allow power to increase rapidly to 200 megawatts in about 4 seconds. At this power level the reactor flux safety channel will scram the reactor. Because of the automatic speed control engine speed makes no significant change until after the reactor excursion is completed. Figure 5.16 is the analog recording made during this excursion, and the maximum values are:

T_{5.1} 1640°R
Reactor power 200 mw
T₄ 2300°R

Flux Control Failure Increasing Flux and Reactor Flux Safety Channel Failure - If a second failure occurs that makes the flux scram circuit inoperative, the reactor will not scram at 200 megawatts. The reactor power will increase to 385 megawatts in about 7 seconds, and at this point T_{5.1} will have increased enough to scram the reactor. No appreciable change in engine speed occurs until the reactor excursion is ended.

Even though there are two independent flux scram circuits, it is anticipated that the power plant will continue to be operated if one scram circuit should have failed. In this case, the reactor will be operated with only one flux safety channel, which can fail as a single failure.

A reactor flux scram failure will occur if the scram channel indicates a lower power than that existing in the reactor or if the trip circuit fails. Figure 5.17 is the analog recording made of this excursion, and the maximum values are:

T_{5.1} 1860°R
Reactor power 385 mw

~~CONFIDENTIAL~~
~~SECRET~~

T₄ 2525°R
T₄ exceeds 2370°R for 7 seconds.

Flux Control Failure Increasing Flux and Speed Control Failure Decreasing Speed - If a second failure occurs in the speed control and engine speed is decreased, T_{5,1} increases rapidly because of the lowered reactor airflow and the increased reactor power, and causes a scram in 3.5 seconds. Such a failure might be caused by a loss of the speed demand signal to both the nozzle and bleed loops. The maximum values that would occur are:

T_{5,1} 1910°R (at 20% speed)
Reactor power 130 mw
T₄ 2320°R

Flux Control Failure Increasing Flux and Nozzle Control Failure Opening Nozzle - If a second failure occurs in the nozzle control loop and the nozzle opens wide (to the nozzle bound), the reactor flux rises rapidly to 200 megawatts, the reactor scrams, and the engine speed rises to a transient maximum of 104 percent. The bleed control operates to limit the maximum speed overshoot. A failure of this nature might be caused by loss of engine speed feedback to the nozzle control loop or by mechanical failure of the nozzle actuator or linkages. The maximum values that would occur are:

T_{5,1} 1605°R (operating T_{5,1})
Reactor power 200 mw
T₄ 2300°R

Flux Control Failure Increasing Flux and Nozzle Control Failure Closing Nozzle - If a second failure occurs causing the nozzle to close to the minimum area, a rapid reduction in speed to 90 percent occurs. T_{5,1} increases rapidly about 100°F and thereafter increases slowly; the reactor power increases to 200 megawatts in 4.5 seconds and causes a scram. Loss of the speed demand signal to the nozzle control loop will cause such a failure. The maximum values that would occur are:

T_{5,1} 1740°R
Reactor power 200 mw
T₄ 2300°R

Flux Control Failure Increasing Flux and Bleed Control Failure Opening Bleed Valve - When a second failure causes the bleed valve to open, engine speed decreases rapidly to 92 percent and the resultant lowered reactor airflow causes T_{5,1} to increase about 50°F. T_{5,1} increases slowly while reactor power increases to 200 megawatts, and the reactor is scrammed 5 seconds after the start of the excursion. Loss of speed demand signal to the bleed control will cause a failure such as this. The maximum values that would occur are:

T_{5,1} 1750°R
Reactor power 200 mw
T₄ 2350°R

Flux Control Failure Increasing Flux and Bleed Control Failure Closing Bleed Valve - When a second failure causes the bleed valve to close, speed increases slowly to 102 percent. The increased airflow prevents T_{5,1} from increasing significantly, and the scram occurs when reactor power reaches 200 megawatts. Loss of speed feedback in the bleed control loop or mechanical failure in the bleed valve actuator will cause this type of failure. The maximum values that would occur are:

T_{5,1} 1640°R
Reactor power 200 mw
T₄ 2300°R

~~CONFIDENTIAL~~
~~SECRET~~

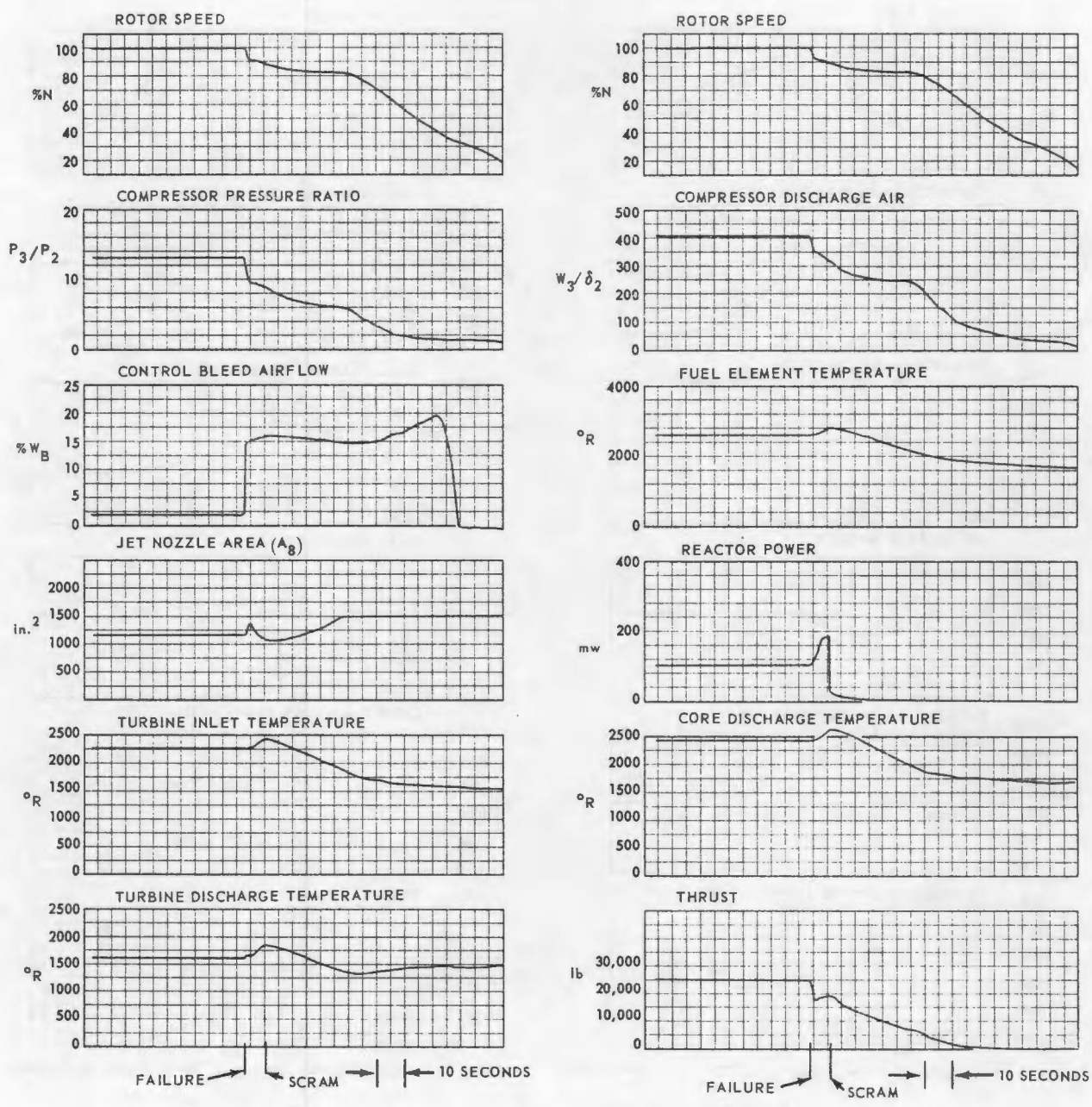


Fig. 5.14 - Double failure: $T_{5.1}$ control failure increasing $T_{5.1}$ and bleed control failure opening bleed valve

~~CONFIDENTIAL~~
~~SECRET~~

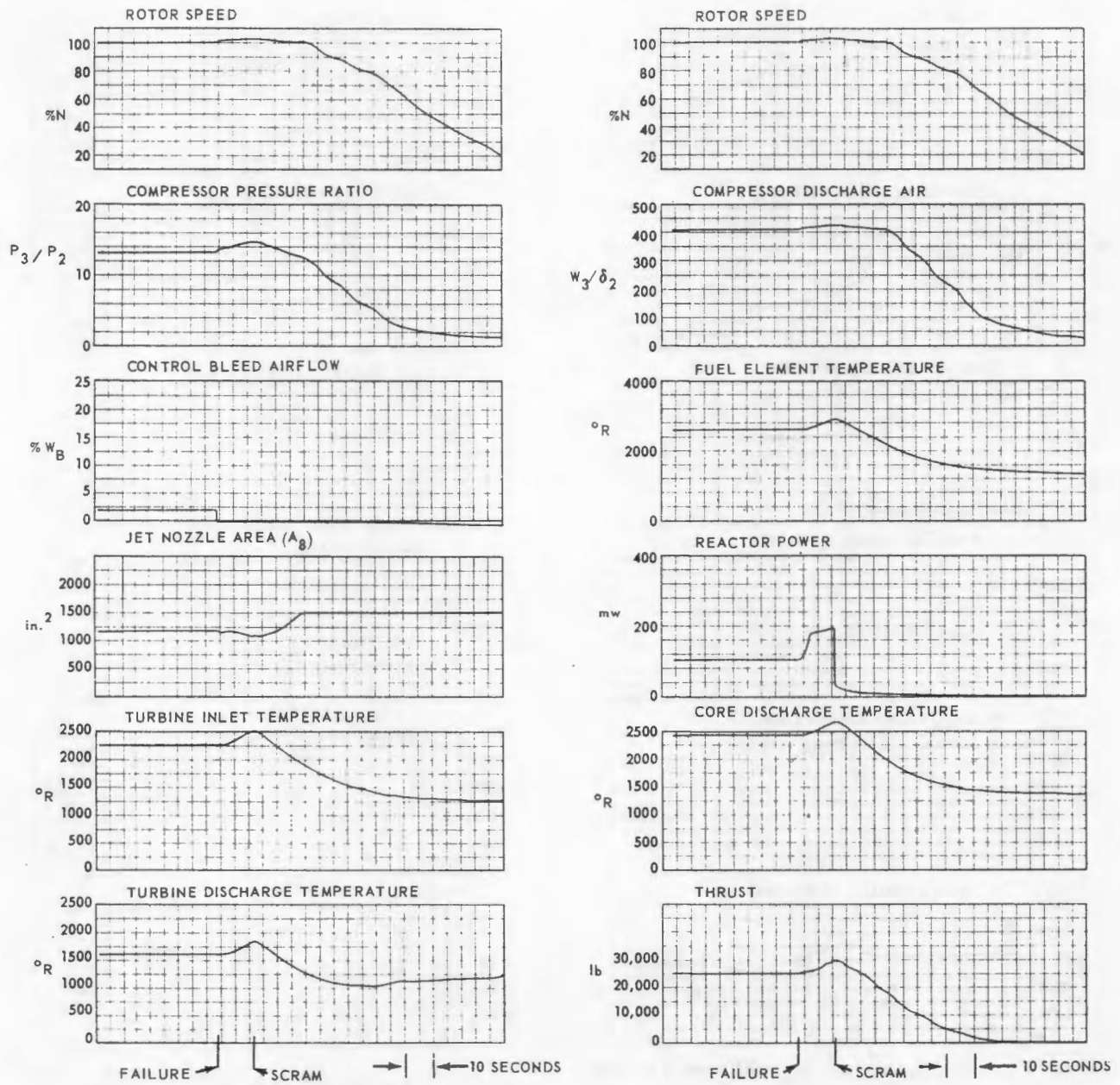


Fig. 5.15 - Double failure: $T_{5.1}$ control failure increasing $T_{5.1}$ and bleed control failure closing bleed valve

~~SECRET~~
~~CONFIDENTIAL~~
~~DECLASSIFIED~~

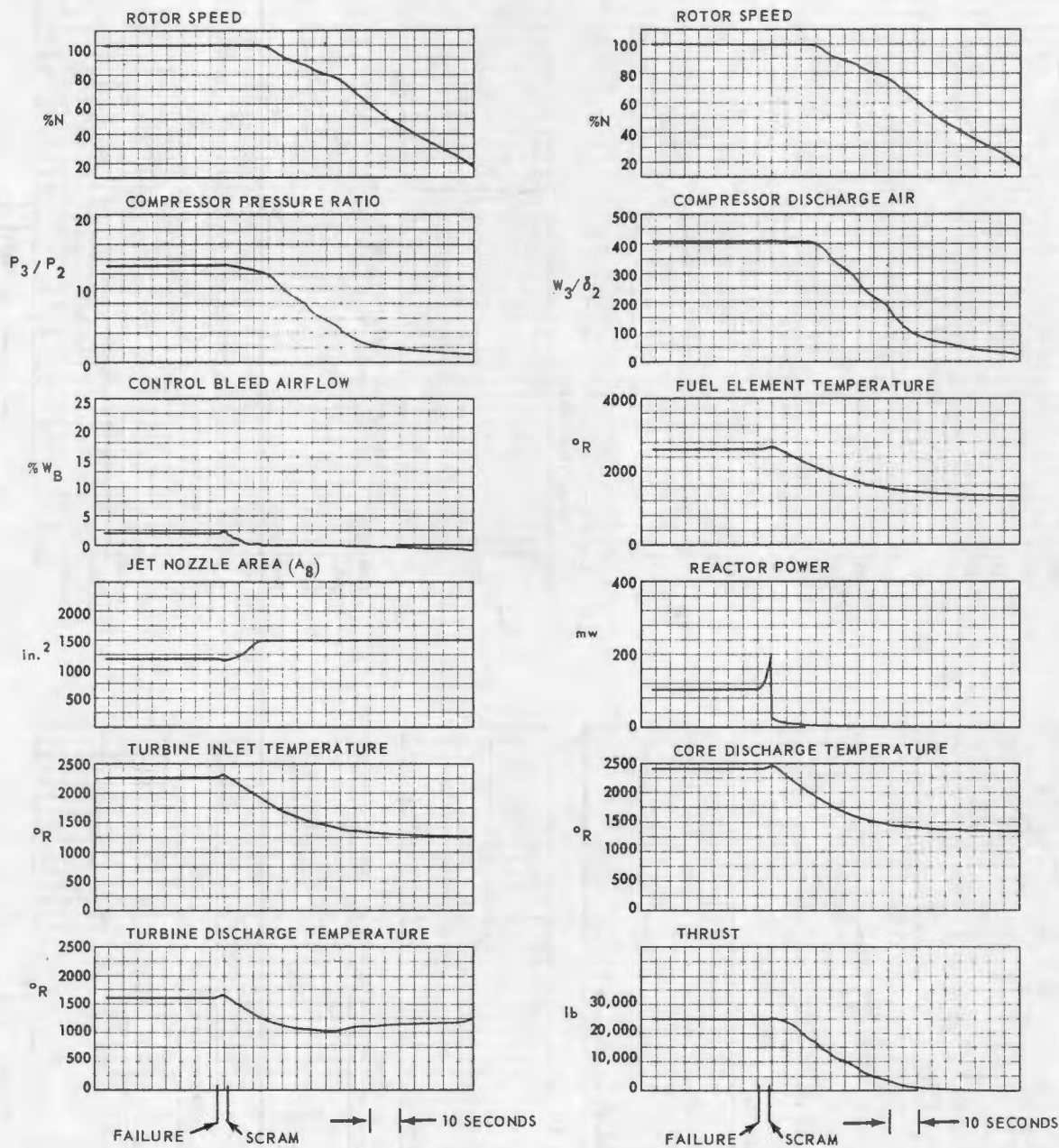


Fig. 5.16 - Single failure: Reactor flux control failure increasing flux

CONFIDENTIAL
SECRET

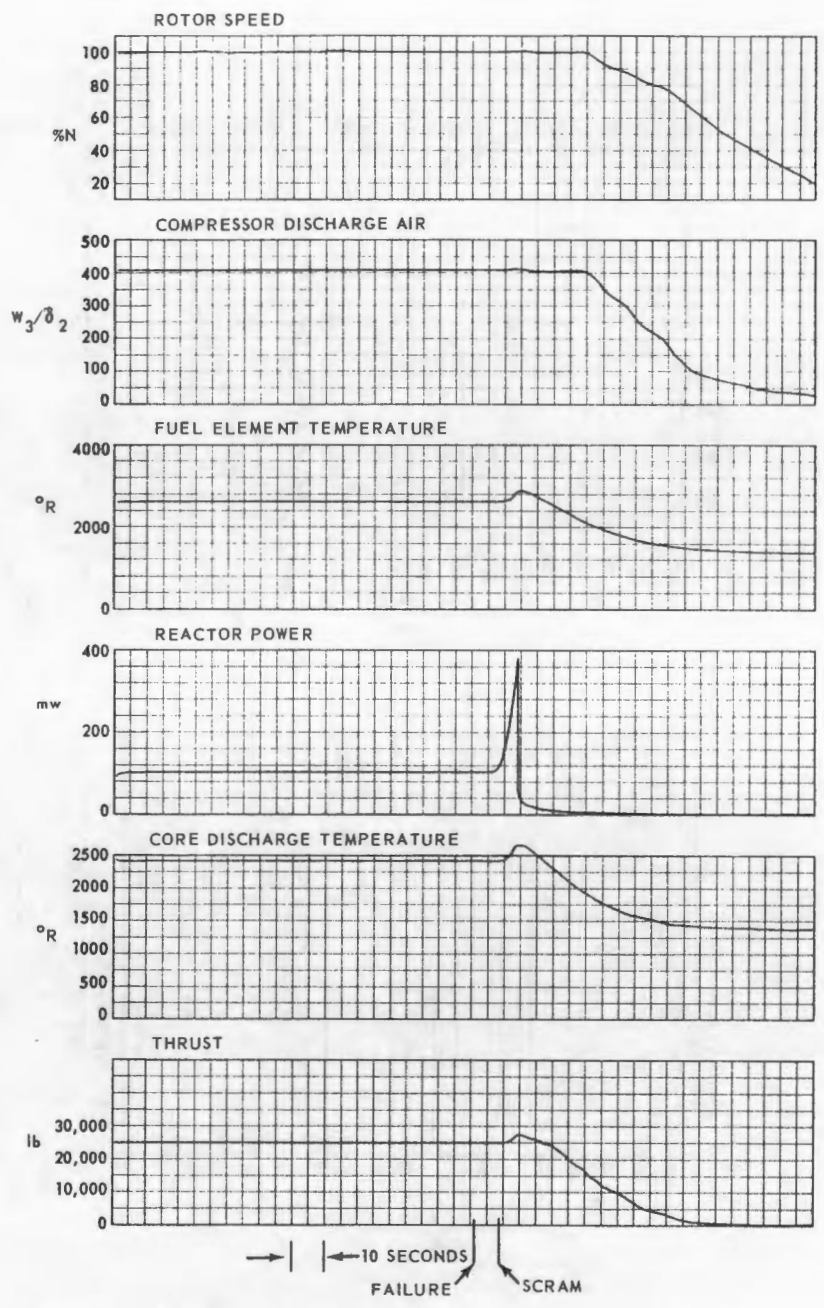
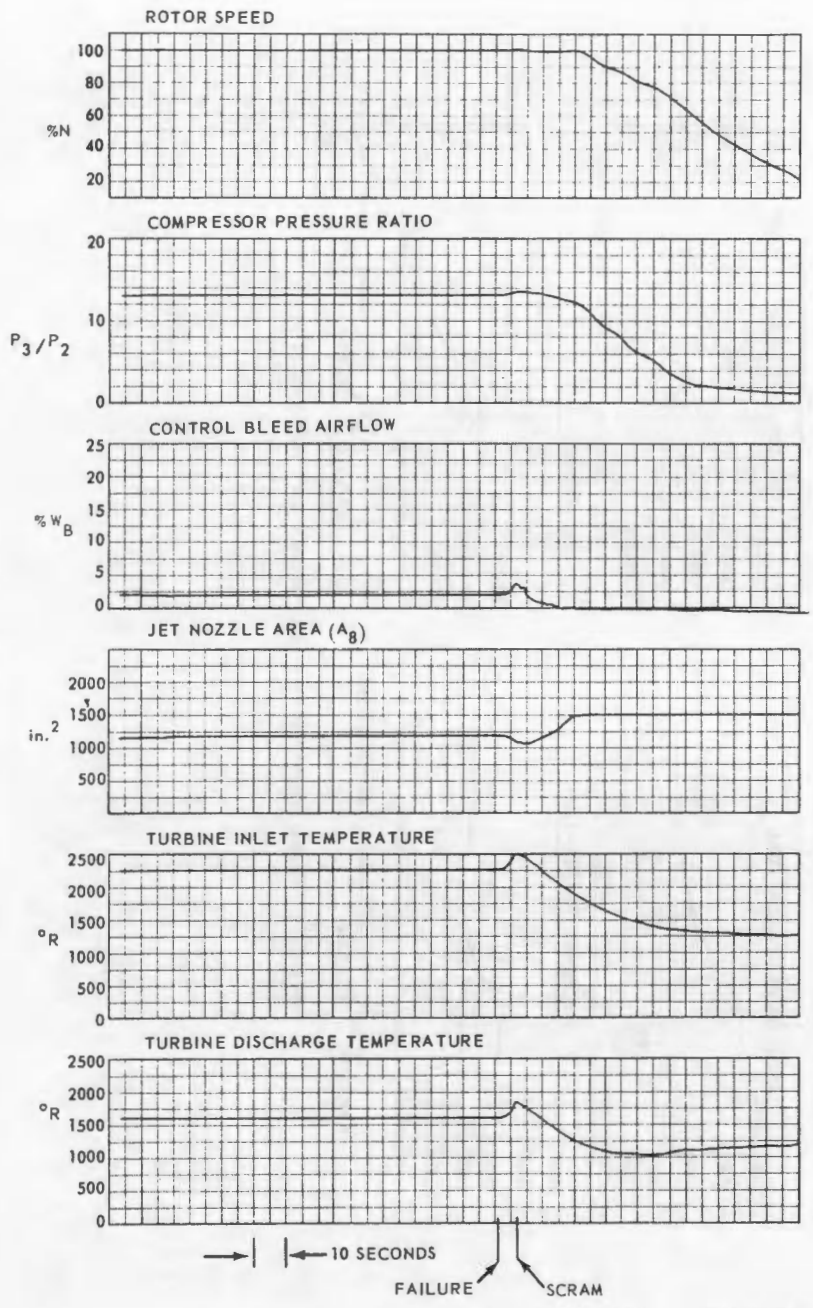


Fig. 5.17 - Double failure: Reactor flux control failure increasing flux and reactor scram circuit failure

CONFIDENTIAL
SECRET

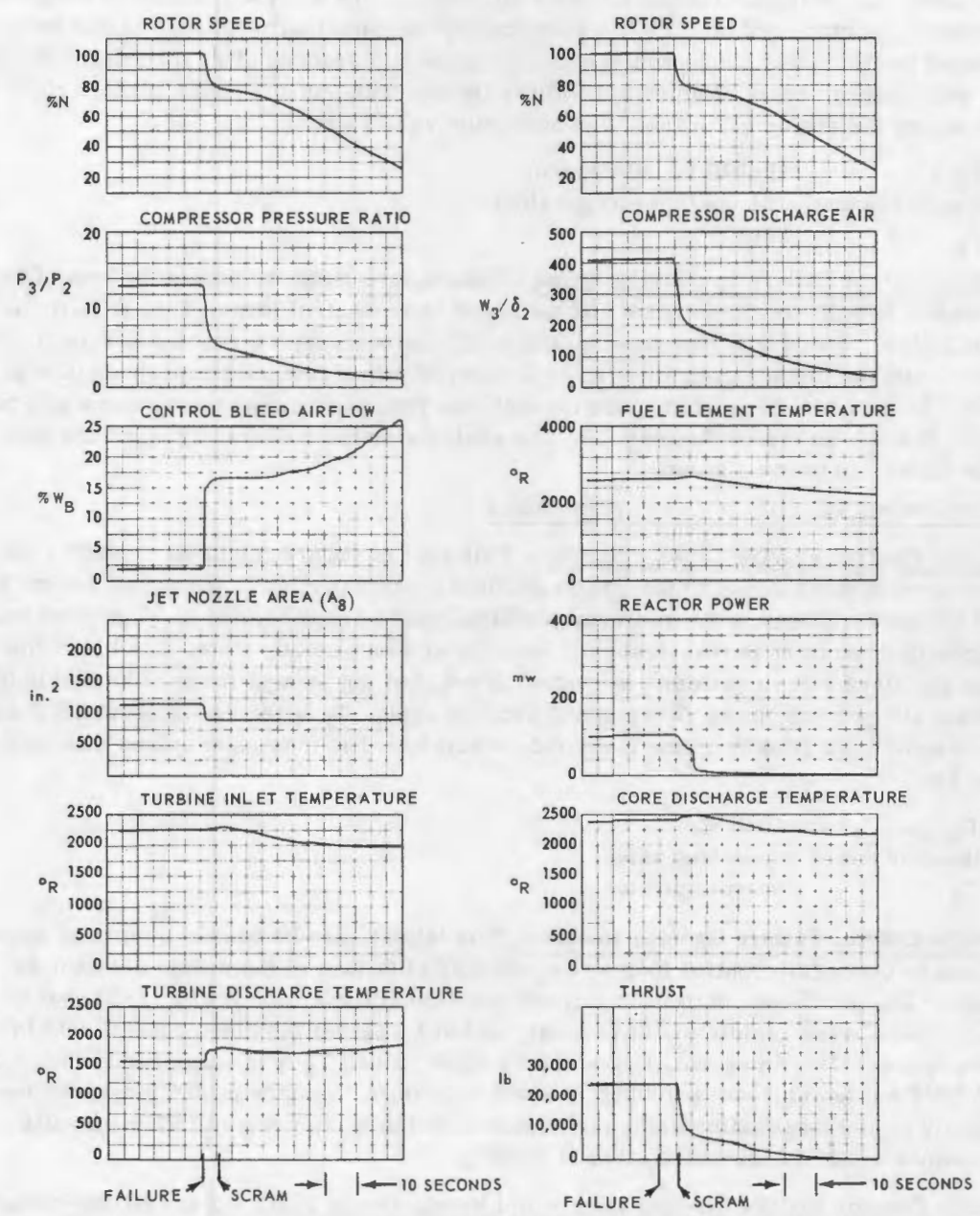


Fig. 5.18 - Single failure: Engine speed control failure decreasing speed

~~UNCLASSIFIED~~
~~SECRET~~

Speed Control Failures at 100 Percent Speed

Speed Control Failure Decreasing Speed - This type of failure might be caused by loss of speed demand signal, which affects both the bleed control loop and the nozzle control loop. Speed will decrease rapidly to below 80 percent, and $T_{5.1}$ will increase because of the reduced reactor airflow. The $T_{5.1}$ control will automatically reduce reactor power somewhat to attempt to hold a constant $T_{5.1}$, but at 5.5 seconds after the failure excess $T_{5.1}$ will cause a scram. Figure 5.18 shows the recording of the power plant variables made during the analog excursion. The maximum values are:

$T_{5.1}$	1900°R (at 20% speed)
Reactor power	104 mw (operating value)
T_4	2285°R

Speed Control Failure Increasing Speed - This failure might be caused by loss of speed feedback to both the nozzle control and the bleed valve control loops. This requires a double failure. Speed will increase rapidly to 120 percent, with a reactor scram at 105 percent, and the turbine probably will be destroyed with a resultant rapid loss of reactor airflow. In the event the turbine does not fail, the resulting temperature traces will be similar to those shown in Figure 5.19. The analog simulator characteristics are inaccurate above 110 percent speed.

Nozzle Control Failures at 100 Percent Speed

Nozzle Control Failure Closing Nozzle - This type of failure might be caused by loss of the speed demand signal to the nozzle position control portion of the speed control loop. After the nozzle closes to its minimum position, speed drops rapidly to 90 percent and then coasts down to 88 percent where it remains at a new steady state. The bleed control closes the bleed valve to attempt to control speed, but not enough range is available to maintain 100 percent speed. When speed drops sharply, $T_{5.1}$ increases about 85°F and then is reduced to 1605°R by the temperature control. The maximum values that would occur are:

$T_{5.1}$	1690°R
Reactor power	operating value
T_4	operating value

Nozzle Control Failure Opening Nozzle - This failure may be caused by loss of speed feedback to the nozzle control loop or by mechanical failure of the nozzle actuator or linkages. The nozzle opens to its maximum position at the nozzle bound, 1500 square inches; speed rises rapidly to 104 percent; and at this point the bleed control acts to reduce speed to 100.4 percent, a new steady-state value. $T_{5.1}$ is temporarily reduced about 70°F but is returned to 1605°R in about 6 seconds. Reactor power increases momentarily to 150 megawatts during the transient and then decreases to 97 megawatts. T_4 assumes a new steady-state value of 2320°R.

Nozzle Control Failure Opening Nozzle and Nozzle Bound Fails - If the nozzle-bounding mechanism and the nozzle control fail at the same time, the nozzle opens to its maximum physical position, 1800 square inches, and the rotor speed increases rapidly to 106.2 percent and trips the scram circuit. No transients occur that are severe enough to cause power plant damage.

Bleed Control Failures at 100 Percent Speed

Bleed Control Failure Opening Bleed Valve - This failure may be caused by loss of speed demand to the bleed control portion of the speed control loop. When the bleed valve opens to its maximum position, the engine speed decreases immediately to 92 percent and then coasts down to a new steady-state value of 84.7 percent. The nozzle control

~~SECRET~~
~~UNCLASSIFIED~~

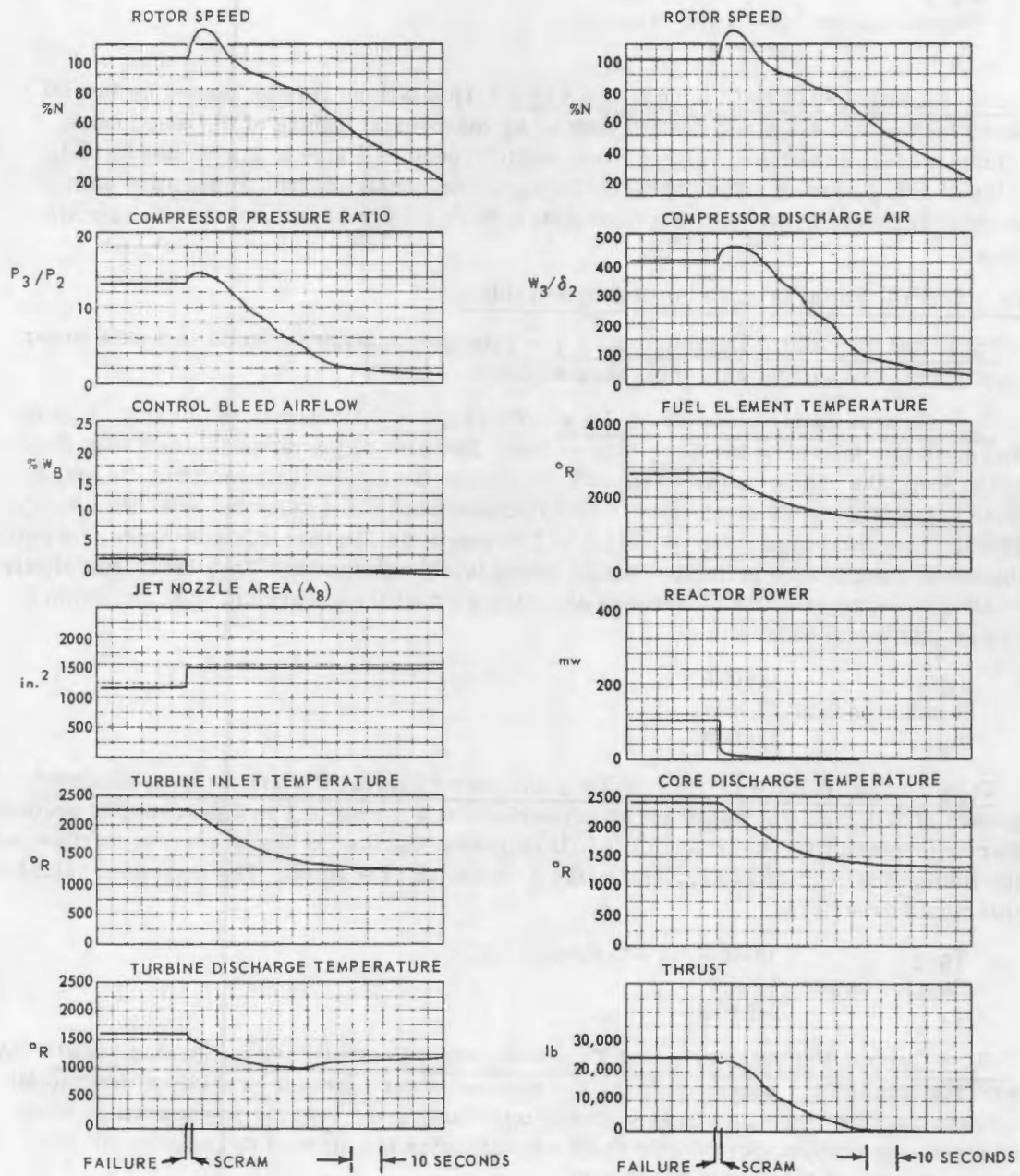


Fig. 5.19 - Double failure: Nozzle control failure opening nozzle and bleed control failure closing bleed valve

~~CONFIDENTIAL~~
~~SECRET~~

action is insufficient to overcome this speed error. $T_{5.1}$ increases about 100°F during this transient but is reduced to 1605°R by the temperature control. The maximum values that would occur are:

$T_{5.1}$	1700°R
Reactor power	operating value
T_4	2275°R

Bleed Control Failure Closing Bleed Valve - This failure may be caused by loss of speed feedback to the bleed control loop or by mechanical failure of the bleed valve actuators. When the bleed valve closes, engine speed will rise to a new steady-state value of 102.4 percent. The characteristics of the nozzle control do not allow this speed error to be overcome. No transients severe enough to damage the power plant occur.

$T_{5.1}$ Control Failures at 70 Percent Speed (Idle)

$T_{5.1}$ Control Failure Decreasing $T_{5.1}$ - This type of failure results in a safe power plant coastdown without excessive temperatures.

$T_{5.1}$ Control Failure Increasing $T_{5.1}$ - This type of failure may result from loss of thermocouple failure in the $T_{5.1}$ control loop. Because of the temperature error limit in the loop, the reactor power will increase, when the failure occurs, from its steady-state value of about 22 megawatts to about 40 megawatts in 4 seconds, and then creep up slowly to its maximum value at scram of 77 megawatts. During this slow power increase, the speed control loop is holding engine speed fairly constant and $T_{5.1}$ increases slowly to 1860°R. Scram occurs 51 seconds after the start of the excursion. The maximum values that would occur are:

$T_{5.1}$	1860°R
Reactor power	77 mw
T_4	2240°R

$T_{5.1}$ Control Failure Increasing $T_{5.1}$ and Speed Control Failure Decreasing Speed - A failure of this type will cause speed to decrease at the rate of 1 to 2 percent per second. During the resulting excursion $T_{5.1}$ will increase, because of the decreasing airflow and the increasing reactor power, and cause a scram in 21 seconds. The maximum values that would occur are:

$T_{5.1}$	1950°R (at 23% speed)
Reactor power	50 mw
T_4	2020°R

$T_{5.1}$ Control Failure Increasing $T_{5.1}$ and Nozzle Control Failure Opening Nozzle - As with the single $T_{5.1}$ control failure, the reactor power increases rapidly at first to 40 megawatts. The rotor then slowly speeds up following the reactor power until an over-speed scram occurs. Scram occurs 95 seconds after the start of the excursion. The maximum values that would occur are:

$T_{5.1}$	1530°R
Reactor power	120 mw
T_4	2280°R
Rotor speed	106.5%

$T_{5.1}$ Control Failure Increasing $T_{5.1}$ and Nozzle Control Failure Closing Nozzle - In this double failure, reactor power behaves much as it does during a single failure. The bleed control tends to hold engine speed, and $T_{5.1}$ increases slowly with reactor power

~~SECRET~~
~~CONFIDENTIAL~~

to the point where a T_{5.1} scram occurs 51 seconds later. The maximum values that would occur are:

T _{5.1}	1860°R
Reactor power	65 mw
T ₄	2240°R

T_{5.1} Control Failures Increasing T_{5.1} and Bleed Control Failure Opening Bleed Valve - Speed decreases at a rate of about 1 percent per second, and the combination of increasing reactor power and decreasing airflow causes T_{5.1} to increase to the scram trip level in 22 seconds. The maximum values that would occur are:

T _{5.1}	2000°R (at 21% speed)
Reactor power	50 mw
T ₄	2060°R (below 25% speed)

T_{5.1} Control Failures Increasing T_{5.1} and Bleed Control Failure Closing Bleed Valve - Speed increases at a moderate rate up to about 83 percent, and at this point the nozzle control becomes effective in holding speed to 80 percent until the minimum nozzle limit is reached. From this point, speed increases slowly as reactor power increases until T_{5.1} reaches the scram trip level 120 seconds after the failures. The maximum values that would occur are:

T _{5.1}	1860°R
Reactor power	138 mw
T ₄	2440°R
Rotor speed	93%
T ₄ exceeds 2370°R for 9 seconds.	

Reactor Flux Control Failures at 70 Percent Speed (Idle)

Flux Control Failure Decreasing Flux - This failure will cause a safe power plant coastdown without excessive temperatures.

Flux Control Failure Increasing Flux - The reactor power will increase rapidly to 200 megawatts in about 8 seconds, causing a flux scram. Engine speed will increase only about 0.5 percent during the excursion. T_{5.1} will increase about 90°F in the early part of the excursion. The maximum values that would occur are:

T _{5.1}	1430°R
Reactor power	200 mw
T ₄	1790°R

Flux Control Failure Increasing Flux and Reactor Flux Safety Channel Failure - If the second failure makes the flux scram channel inoperative, the reactor power will increase to about 800 megawatts in 8-1/2 seconds and T_{5.1} will have increased enough to scram the reactor. Engine speed increases from 70 to 76 percent during this period, and the maximum fuel element temperature is 2600°R. Other maximum values that would occur are:

T _{5.1}	1860°R
Reactor power	~800 mw
T ₄	2330°R

Flux Control Failure Increasing Flux and Speed Control Failure Decreasing Speed - This double failure will result in a drop in engine speed at an initial rate of 1 percent per second.

~~CONFIDENTIAL~~
~~SECRET~~

The decrease in engine speed with an increase in reactor power causes $T_{5.1}$ to increase, and a flux scram occurs in 8 seconds. The maximum values that would occur are:

$T_{5.1}$	1740°R
Reactor power	200 mw
T_4	1875°R (55 to 20% speed)

Flux Control Failure Increasing Flux and Nozzle Control Failure Opening Nozzle - The bleed control maintains speed at 70 percent, and a flux scram occurs in 8 seconds. The maximum values that would occur are:

$T_{5.1}$	1370°R
Reactor power	200 mw
T_4	1725°R

Flux Control Failure Increasing Flux and Nozzle Control Failure Closing Nozzle - The bleed control attempts to hold engine speed, which decreases from 70 to 66 percent, and the resultant increase in reactor power causes the speed to return to 70 percent. A flux scram at 200 megawatts occurs in 8 seconds. The maximum values that would occur are:

$T_{5.1}$	1520°R
Reactor power	200 mw
T_4	1815°R

Flux Control Failure Increasing Flux and Bleed Control Failure Opening Bleed Valve - Engine speed coasts down at the rate of 1 percent per second, and $T_{5.1}$ rises. A flux scram occurs in 8 seconds. The maximum values that would occur are:

$T_{5.1}$	1700°R
Reactor power	200 mw
T_4	1830°R

Flux Control Failure Increasing Flux and Bleed Control Failure Closing Bleed Valve - Engine speed increases from 70 to 83 percent in 6 seconds, and the increasing airflow prevents $T_{5.1}$ from increasing. A flux scram occurs in 8 seconds. The maximum values that would occur are:

$T_{5.1}$	operating value
Reactor power	200 mw
T_4	1730°R

Speed Control Failures at 70 Percent Speed (Idle)

Speed Control Failure Decreasing Speed - The engine will coast down, and the temperature control loop will decrease the reactor power in an attempt to maintain $T_{5.1}$. No scram will occur before 20 percent speed. The maximum values that would occur are:

$T_{5.1}$	1750°R (at 23% speed)
Reactor power	operating value
T_4	1800°R (at 23% speed)

Speed Control Failure Increasing Speed (Double Failure) - Speed will increase rapidly to 95 percent, and reactor power will increase in an attempt to maintain $T_{5.1}$. The increasing reactor power will accelerate the engine slowly until overspeed causes scram 93 seconds later. The maximum values that would occur are:

$T_{5.1}$	1340°R (operating value)
Reactor power	90 mw

~~SECRET~~
~~CONFIDENTIAL~~

T ₄	1900°R
Rotor speed	105.5%

Nozzle Control Failures at 70 Percent Speed

Nozzle Control Failure Closing Nozzle - Speed will decrease at a moderate rate, and the temperature control loop will reduce reactor power in an attempt to maintain T_{5.1}. T_{5.1} will rise slowly to a transient maximum of 1640°R at 20 percent speed. By this time the operator should have caused a scram by starting the aftercooling system to prevent further temperature increase. If the operator fails to scram the reactor, it will scram when power reaches 5 megawatts.

Nozzle Control Failure Opening Nozzle - At 70 percent speed, the effect of the nozzle failure near its wide-open position is small and the bleed control will automatically counteract the effect of this failure. Speed is controlled at 70 percent.

Bleed Control Failures at 70 Percent Speed

Bleed Control Failure Closing Bleed Valve - Engine speed increases rapidly to 83 percent, and the nozzle control closes the nozzle to reduce the speed to 80 percent. Because of the error signal relationships in the nozzle control loop, the engine remains at 80 percent speed as a new steady-state point. The temperature control loop acts to restore T_{5.1} to its operating value of 1340°R.

Bleed Control Failure Opening Bleed Valve - When the bleed valve opens, speed is reduced about 0.5 percent per second. The reduction in airflow causes an increase in T_{5.1}, which the temperature control attempts to reduce by lowering the reactor power. T_{5.1} reaches a maximum value of 1720°F at 24 percent speed.

Reactor Flux Control Failures at 40 Percent Speed (Bottom of Unstable Region)

At 40 percent speed the engine is operating with the starter engaged. The reactor is controlled with the flux control. The speed control is inoperative since the nozzle is wide open and the bleed valve is closed.

Flux Control Failure Decreasing Flux - The engine will coast down slowly to 26.6 percent speed, and at this speed the starter will be providing all the power to turn the engine.

Flux Control Failure Increasing Flux - Reactor power, normally at about 9.5 megawatts, increases to 200 megawatts in about 10 seconds, causing a flux scram. The engine will then coast down to 26.6 percent speed, and at this speed will be turned on the starter only. The maximum values that would occur are:

T _{5.1}	1690°R
Reactor power	200 mw
T ₄	1860°R
Rotor speed	43.5%

Flux Control Failure Increasing Flux and Flux Scram Fails - The reactor power increases to about 1000 megawatts, causing T_{5.1} to increase until it reaches the scram trip level 12 seconds later. Engine speed is increased to about 70 percent by the energy stored in the fuel elements and then coasts back down. Since the starter becomes automatically disengaged during the transient, the engine will coast down to a stop. The maximum values that would occur are:

T _{5.1}	1860°R
Reactor power	~ 1000 mw

~~SECRET~~
DECLASSIFIED

T ₄	2160°R
Rotor speed	72 %
T _{fe}	2320°R

Flux Control Failure Increasing Flux and Nozzle Fails Closed - Reactor power increases to 200 megawatts, and the reactor scrams in 10 seconds. The engine will coast down and operate on the starter after the excursion. The maximum values that would occur are:

T _{5.1}	1440°R
Reactor power	200 mw
T ₄	1615°R

Flux Control Failure Increasing Flux and Bleed Valve Fails Open - The engine speed falls, and the increased reactor power increases T_{5.1} about 150°F. A scram on reactor flux occurs in 9 seconds. The maximum values that would occur are:

T _{5.1}	1520°R
Reactor power	200 mw
T ₄	1650°R

Flux Control Failure Increasing Flux and Starter Fails - Engine speed falls at about 1 percent per second, and T_{5.1} increases until the reactor scrams on flux. The maximum values that would occur are:

T _{5.1}	1540°R (at 20% speed)
Reactor power	200 mw
T ₄	1625°R

Nozzle Fails Closed at 40 Percent Speed

Closing the nozzle at 40 percent speed has virtually no effect on the power plant. Speed is reduced very slowly to 38.5 percent after about 5 minutes, and T_{5.1} is increased about 40°F.

Bleed Valve Fails Open at 40 Percent Speed

Speed decreases slowly to 35.5 percent, then creeps upward, and reaches a new steady-state speed of 37.4 percent about 10 minutes later. During this time T_{5.1} increases slowly from its operating value of 1340° to 1690°R.

Starter Fails at 40 Percent Speed

Speed will decrease at about 1 percent per second. T_{5.1} increases slowly as speed decreases, and by the time the speed reaches 20 percent, T_{5.1} reaches 1480°R, 150°R greater than the operating value. Normally, the operator would scram the reactor by this time; but, if he fails to do so, T_{5.1} will reach the scram trip level before a significant increase in T_{fe} has occurred.

Other Control and Accessory Failures

Period Control Failure (Startup) - The period control is used only in the startup range. If it should fail and cause continuous withdrawal of the control rods at their maximum rate, the shorter reactor period would be sensed by the period safety circuit and cause a reactor scram. If the period safety should also fail, the reactor would scram at a power level of 5 megawatts, effectively preventing damage. The increase in average-channel maximum temperature from this type of incident is about 5.5°F.

Stator Control Failure - It was not possible to investigate failure of the stator control system on the analog computer because of the limited knowledge of compressor response

~~SECRET~~
DECLASSIFIED

to such failures. The predicted behavior is based on the assumption that the response of the X211 will be materially similar to that experienced by LJED with other variable-stator engines. Only extreme failures were considered.

The stator blades are fully open at military speeds. Below 90 percent corrected speed, a failure that tends to open the stator blades will most likely cause the compressor to stall. If the failure occurs near idle speed, cycle collapse is possible. Cycle collapse during chemical operation will overtemperature the combustors and the turbine. If cycle collapse occurs during nuclear operation, the reactor will be scrambled by excessive turbine discharge temperature and the engine will be shut down.

The stator blades are fully closed at idle. Above 75 percent corrected speed, a failure that tends to close the stator blades will probably stall the compressor. If the compressor stalls, a reduction in reactor airflow will result with an almost immediate increase in turbine exit temperature ($T_{5,1}$). The reactor will scram in less than 1 second.

Normally, a failure that results in mechanical failure of the stator control or linkages will cause the stator blades to move open.

Engine Hydraulic System Failure - Failure of the engine hydraulic system will cause a loss of hydraulic power and will result in failures of:

1. The speed control - The nozzle hydraulic control system will fail open, and the nozzle bound subsequently will remain in place. The bleed hydraulic control system will fail, and the bleed valve subsequently will fail closed.
2. The stator control - The stator blades will fail open.

The power plant will respond with a rapid increase in engine speed. At or near 100 percent speed, the stators are already wide open and stall will not occur. The reactor will scram when the engine speed reaches 105 percent. At lower speeds, the stators will move open at an undetermined rate as the rotor speed increases. The stators may or may not stay within a stall-free limit of error, but a stall is likely. A scram on $T_{5,1}$ will result.

Lubrication System - Failure of the lubrication system may cause seizure of the engine rotor or the accessory-drive gearbox bearings. However, the system temperatures and pressures are monitored so that the power plant may be shut down and damage avoided if a malfunction of the system should occur.

Seizure of the gearbox bearings will cause loss of the accessory drive system, including the engine hydraulic power supply, and result in failures of:

1. The fuel control system.
2. The speed control system.
 - a. Nozzle hydraulic control system.
 - b. Bleed hydraulic control system.
3. The stator control system.

Seizure of the engine rotor will cause loss of airflow to the reactor.

Starter Failure - Failure of the starter will make it impossible to start the engine. If a nuclear start is in progress when the starter fails, starter failure may cause combustor overtemperature, turbine overtemperature, fuel element overtemperature, or turbine rear frame overtemperature.

In an analog computer run, the engine was at steady state at 40 percent speed when a starter failure was inserted into the problem. The engine coasted down to 20 percent speed, the effective limit of the simulation, and neither T_{fe} nor $T_{5,1}$ was near its

DECLASSIFIED
SECRET

respective scram level. It is estimated that a scram on T_{5.1} would occur at approximately 10 percent speed. The reactor power level was about 9.5 megawatts during this run. At this power level, the fuel elements probably would not overheat before after-cooling could be supplied.

Facility Electrical Supply Failure - Complete loss of electric power will cause a scram and power plant shutdown. Loss of electric power to any single control component will cause that control component to fail and may also cause an immediate scram if a reference or supply voltage fails.

Facility Pneumatic System Failure - When the engine is operating at low speed, the control rod actuators will be using facility pneumatic air for power. If the facility air supply fails, the actuator manifold air pressure will drop and a reactor scram will result. If this scram fails, the control rods will become sluggish in response and a reactor excursion no worse than after a T_{5.1} control failure or a reactor control failure will occur.

5.2.3 LOCAL OVERHEATING

5.2.3.1 Causes of Overheating

Two core conditions that could result in local overheating and possibly the melting of individual tubes are excessive power and limited airflow to a fuel channel. The match of power and airflow during normal operation has been discussed in the description of reactor design. Since this match is performed very carefully, the possibility is extremely remote that very substantial increases in local temperature would be produced by a mismatch due to excessive nuclear power in any location. The power variations predicted for the life of the reactor are slight; and thus, once initial experimental confirmation of design predictions has been established, further changes in the core to produce excessive power generation are almost inconceivable. The only condition that need be considered therefore is the limitation of airflow, which would presumably be caused by mechanical blocking of tubes resulting from structural failure of the tubes, coating failures, or ingestion of foreign material.

Structural Failure of Tubes

Much care has been taken in reactor design to assure that allowable stresses within the fuel elements will not be exceeded as a result of mechanical conditions. In addition, because the tube bundle is close-packed, stress failures that might occur would probably be limited to cracks that would then not propagate to the point where chunks of fuel element would be dislodged. This probability has been substantiated consistently in a number of in-pile tests and is expected to be further demonstrated in subsequent tests; therefore it does not seem likely that structural failure of the tubes would cause tube blockage.

Coating Failures

Tens of thousands of fuel tubes coated with 3 mils (0.003 inch) of zirconium oxide have been manufactured, and hundreds have undergone nuclear and non-nuclear testing under a broad range of conditions of temperature and temperature cycling. In only a few cases was there any flaking, spalling, or other removal of coating. Therefore it is not likely that coating failure will cause tube blockage. If for any reason coating were removed, water-vapor corrosion might proceed to the point where the flow in a single tube would be inhibited, and the resulting temperature increase would accelerate the corrosion process. However, a substantial amount of testing has not revealed any coating failures of this kind.

DECLASSIFIED
SECRET

Ingestion of Foreign Material

The ingestion of foreign material into the reactor either from outside the engine or from parts broken off power plant components is the most probable cause of tube blocking. In the current reactor design concept 19 fuel tubes open into one manifold at both the inlet and the exit of the reactor. In the design of the inlet face of the reactor, consideration is being given to semicircular guard ribs protruding above the inlet of each manifold to prevent foreign particles whose diameters are greater than the radius of the manifold from entering the core. In addition, the protruding guard ribs would hold large bodies, such as pieces of sheet metal, away from the inlet, so that appreciable amounts of cooling air would leak around the foreign object. Complete blockage of a large number of holes is therefore unlikely. The arrangement of the guard rib in relation to the reactor inlet air channels is shown in Figure 5.20. Figure 2.4 relates the region shown in Figure 5.20 to the entire reactor.

5.2.3.2 Mechanics and Effects of Melting

For this discussion it was assumed that air blockage resulting in local melting does occur. The primary concern was to determine the extent to which any of the local melting regions might grow, i. e., to show whether or not melting is self propagating. Power and temperature distributions, positions of coolant blockage, and the stability of overheated fuel tubes were the important parameters used in determining the extent of melting for clusters with given numbers of blocked tubes. The thermodynamic and physical properties used in the analysis are given in Table 5.3.

The method of analysis employed the THTA-IBM 704 program, * which gives essentially a transient nodal point temperature solution for a desired geometry and set of boundary conditions. In short, the program calculates the surface areas and volumes of the nodes,

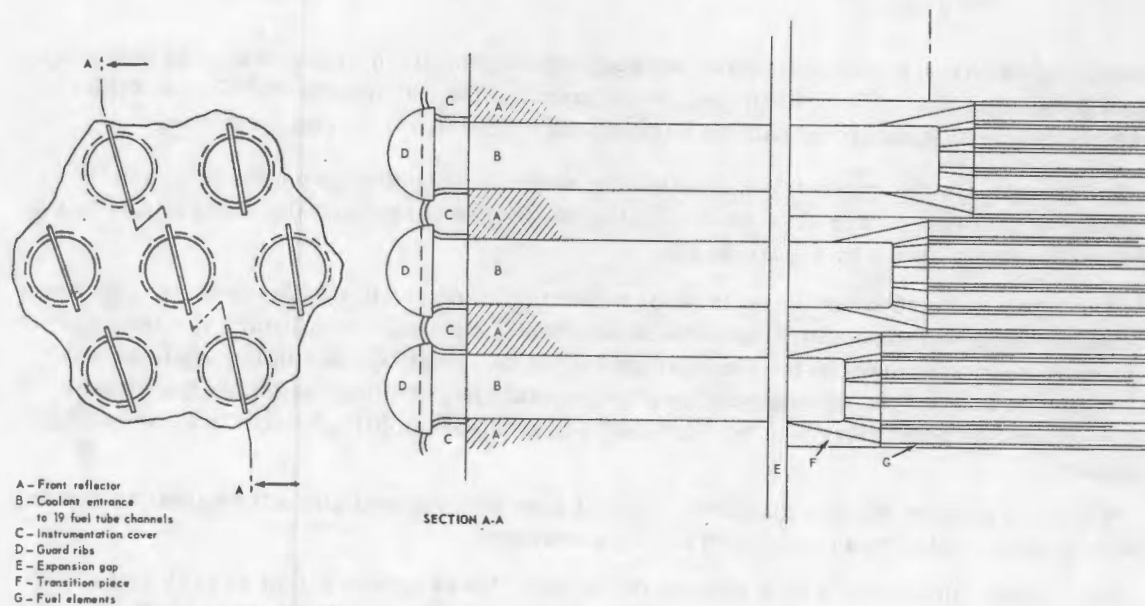


Fig. 5.20 - Guard ribs at reactor inlet

*J. T. Anderson, W. K. Koffel, D. B. Vollenweider, and D. J. Campbell, "User's Manual for the IBM 704 Transient Heat Transfer Program (THT)," General Electric Company, Jet Engine and Flight Propulsion Laboratory Departments, DF58AGT674, September 1, 1958.

~~CONFIDENTIAL~~
SECRET

TABLE 5.3
THERMODYNAMIC AND PHYSICAL PROPERTIES
ASSUMED FOR ANALYSIS

Active Core		
Temperature, °F	Specific Heat, Btu/lb-°F	Thermal Conductivity Btu/ft ³ -°F
0	0.24	110
800	0.377	36
1600	0.454	11.9
2400	0.515	8.1
3600	0.594	6.7
4500	0.64	6.7

Porosity 57%
Fuel Tube Density 3.2 g/cm³

Conditions	
Average reactor power	110 mw ^a
Average power density in fuel element	2.3 × 10 ⁵ Btu/hr-ft ³ -mw
Inlet air temperature	690°F
Airflow	280 lb/sec
Inlet pressure	146.8 psia

^aIn the analysis, a 10% higher power was assumed in the tube clusters investigated.

interpolates physical properties and boundary conditions from given tables, assembles a heat balance in implicit form for each node, and applies the accelerated Gauss-Seidel method to the system of n equations relating the n unknown node temperatures.

In the analysis the geometry consisted of a symmetrical 30-degree pie section of a cluster of fuel tubes. The relationship of the 30-degree sector and the nodal points to the normal tubes is shown in Figure 5.21.

The tubes were assumed to be in perfect thermal contact. If a 0.001-inch air gap were between tubes, a temperature differential of about 20°F would result for the cases analyzed at every tube interface. The heating source distribution used in the analysis was then just 1.1 times the average-channel longitudinal power distribution for the steady-state operating point. Average coolant flow was assumed in all tubes outside the blocked cluster.

For each blocked cluster analyzed, coolant flow was stopped and a transient-temperature analysis followed until equilibrium was reached.

In the tube clusters in which melting did occur, it was assumed that gravity causes the molten material to move to the bottom of the blocked cluster. The mass of the molten material at the bottom of the blocked cluster was assumed to be equal to the mass of all the material within the blocked cluster that had reached the fusion temperature, taken as 4500°F, see *b* in Figure 5.21.

With the molten material redistributed to the bottom of the cluster, a boundary condition of 4500°F was placed on the molten portion. The temperature profiles were then recalculated.

~~SECRET~~
DECLASSIFIED

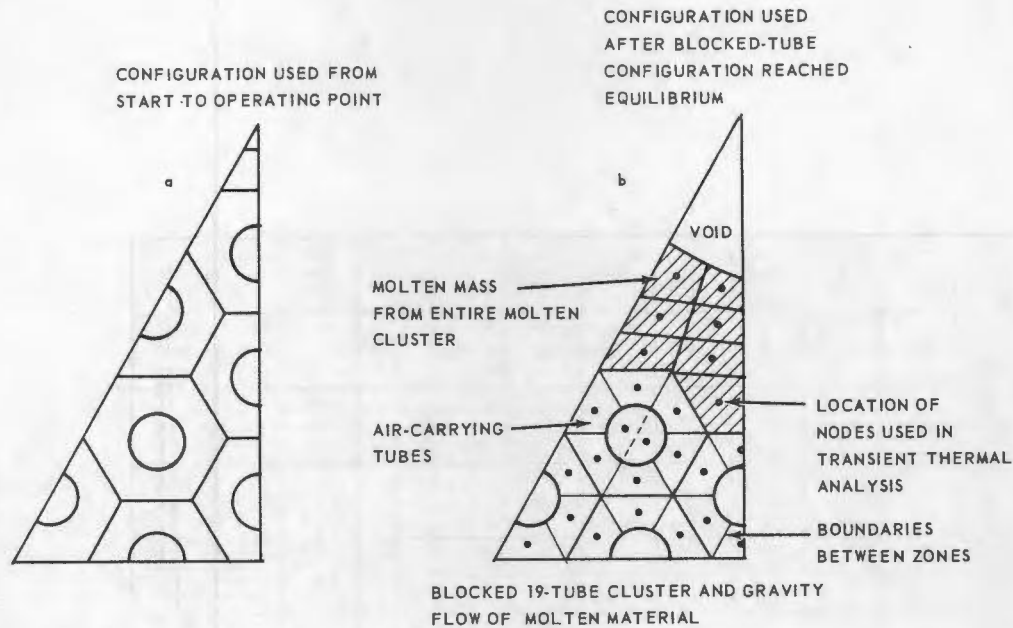


Fig. 5.21 - Geometry used in local-overheating analysis

This procedure was followed for flow blockage to clusters of 7, 19, and 37 fuel tube channels. The radial temperature profiles obtained for the three clusters are shown in Figure 5.22. Melting temperatures were not calculated for the 7-tube cluster, but temperatures of 4500 °F were calculated for the 19- and 37-tube clusters.

In both the 19- and 37-tube clusters the nearest air-carrying tubes in the row directly adjacent to the blocked cluster were at about 3500 °F on the hot side and 3000 °F on the cool side. The nearest tubes refer to those that have two sides adjacent to the molten material. Air-carrying tubes farther away ran at near-normal temperatures. Figures 5.23 and 5.24 show the calculated longitudinal temperature profiles for a 19-tube blocked cluster at average reactor powers of 110 and 55 megawatts. In these figures the length of the melting region within a blocked cluster is that determined without longitudinal displacement of molten fuel. Under actual conditions there will probably be some longitudinal flow of molten mass. As this occurs, the molten material could flow to a cooler region, increase the local heat generation in the cooler region and cause continued melting. This process could continue until the melting had progressed to points near the ends of the active core. There the progression would cease because of the lower power densities.

The stability of the air-carrying tubes adjacent to the melt determines whether the melt can grow radially outward from the blocked cluster. If it is assumed that the flow blockage occurs at the front end of the reactor, an internal or bursting pressure difference of about 12 psi across the wall of the air-carrying tube adjacent to the melt at one-half the length of the active core would result. This pressure difference refers to operation at the 105-megawatt condition. For operation at 50 megawatts the pressure differences are approximately halved.

If the tube wall collapses under a bursting pressure, it is difficult to conceive that this process could lead to blockage of the air-carrying channel. On the other hand, if the blockage occurs at the rear of the reactor, the pressure difference on the air-carrying channel is an external or collapsing pressure of about 12 psi at the half-core length. The

UNCLASSIFIED
SECRET

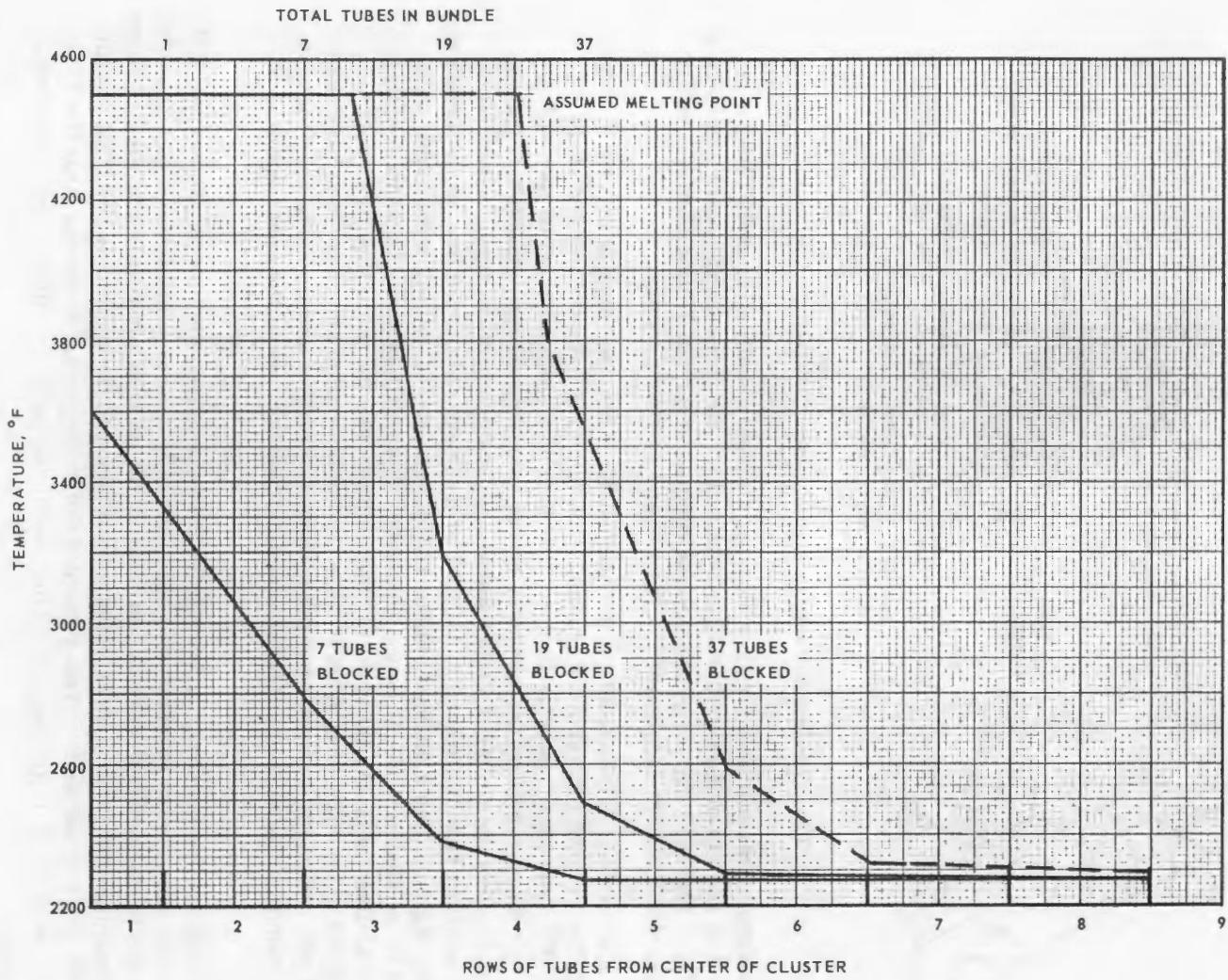


Fig. 5.22 - Temperature distributions across three clusters of blocked tubes

SECRET
CONFIDENTIAL

~~SECRET~~
CONFIDENTIAL

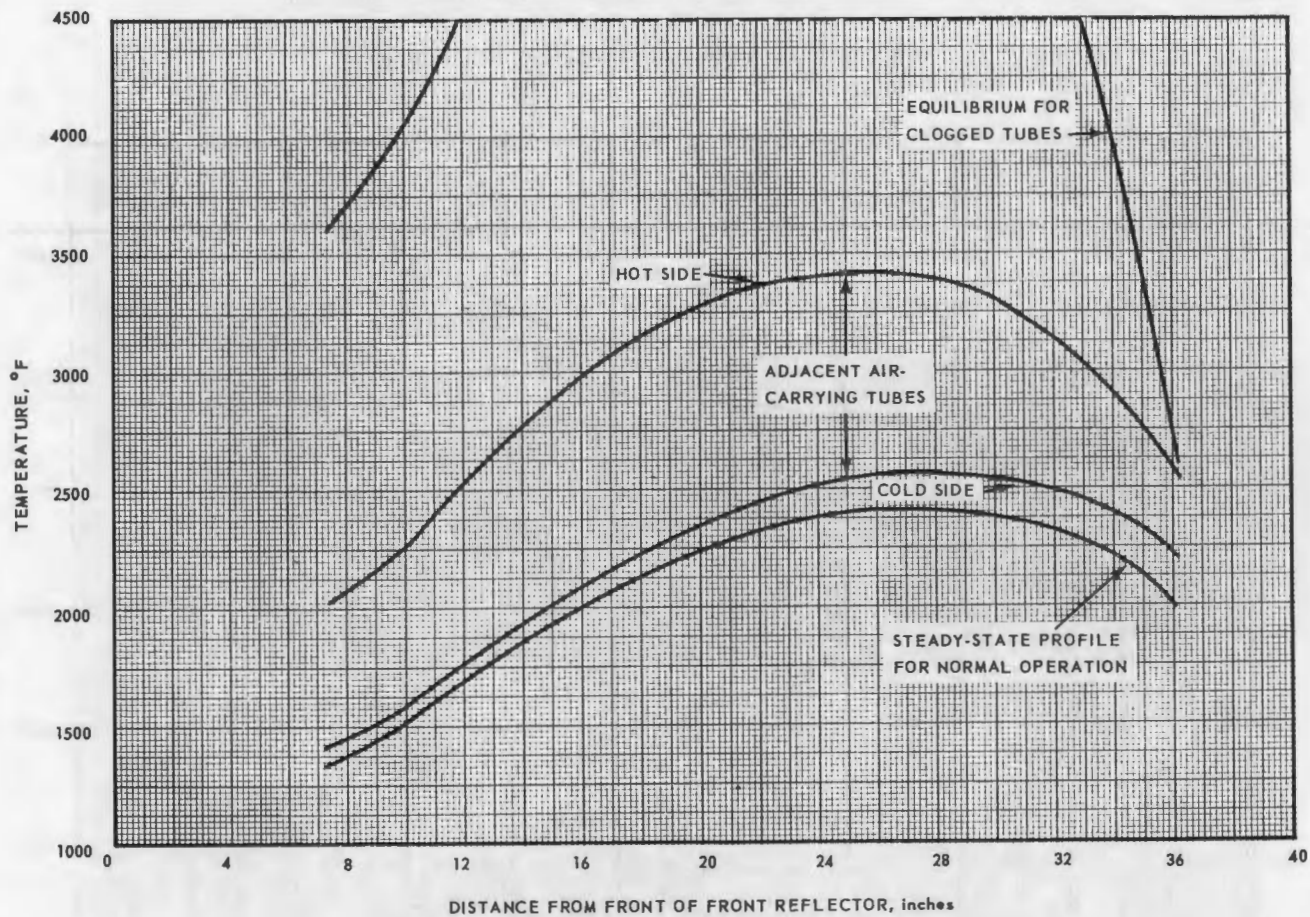


Fig. 5.23—Longitudinal temperature profile for 19 blocked tubes at an average reactor power of 55 megawatts

CONFIDENTIAL
~~SECRET~~

CONFIDENTIAL
SECRET

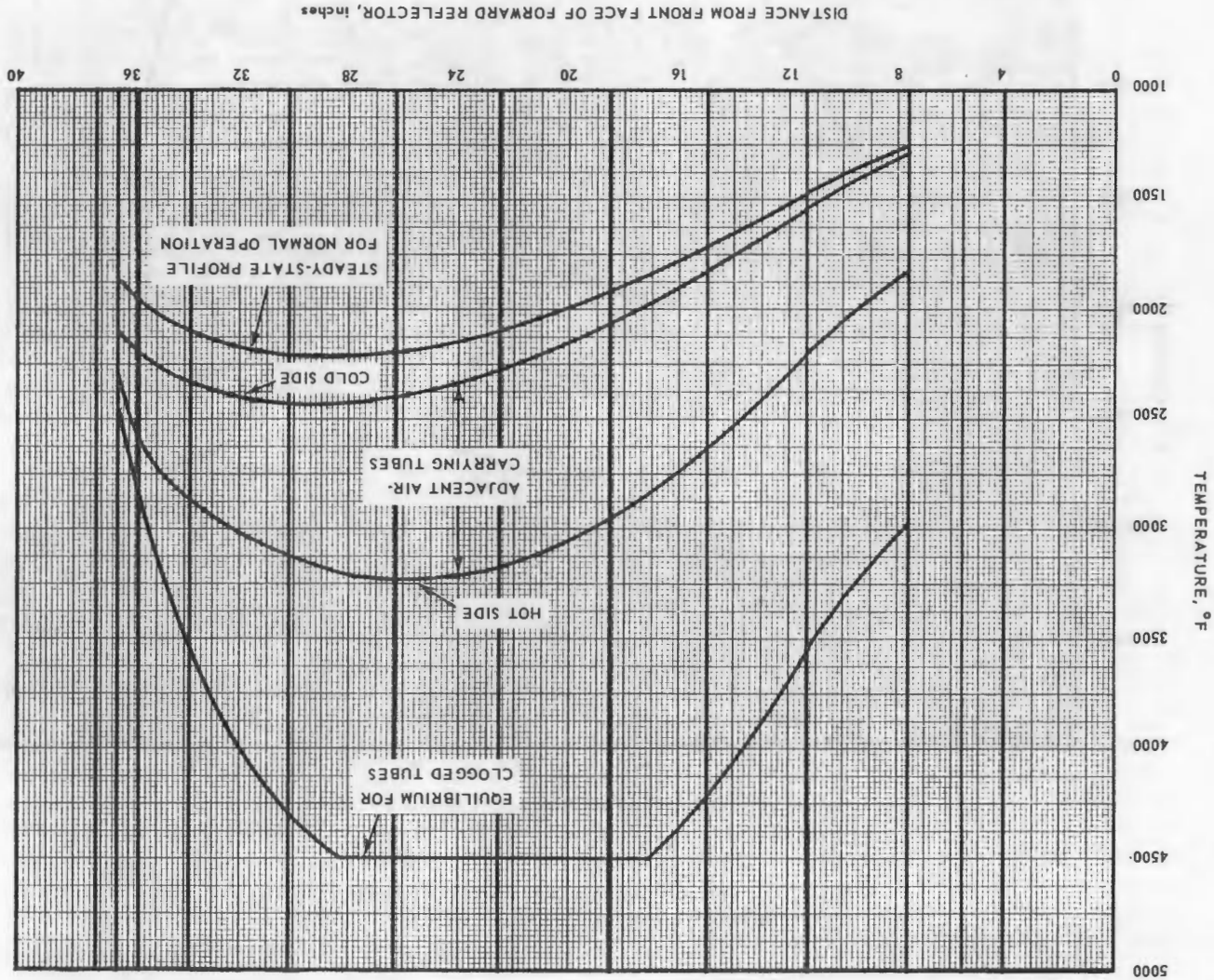


Fig. 5.24—Longitudinal temperature profile for a cluster of 19 blocked tubes at an average reactor power of 55 megawatts

CONFIDENTIAL
SECRET

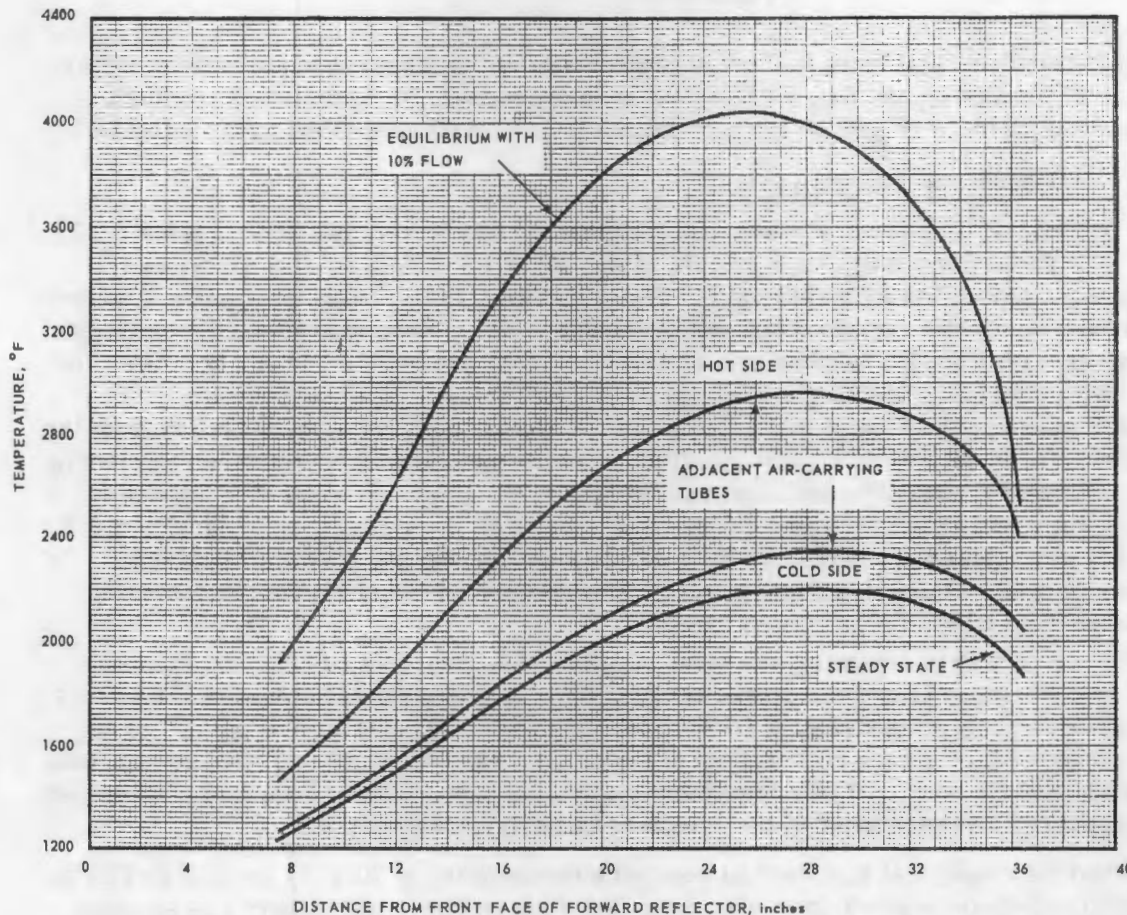


Fig. 5.25—Longitudinal temperature distribution for a cluster of 19 partially blocked tubes at an average reactor power of 55 megawatts and with 10 percent airflow

temperature at which this wall will collapse because of this pressure is the critical factor in determining the radial growth out of the blocked cluster. Results of tests in which fuel tubes with a vacuum of 27 inches of mercury across the tube wall were overheated show that the wall will not collapse until the wall temperature reaches about 4100°F. These tests are described in section 5. 2. 3. 3.

For the 19- and 37-tube clusters the maximum wall temperature of the adjacent air-carrying tubes was about 600°F below this rupture temperature; thus radial growth of the melt is considered impossible.

It was found that once the wall collapses, the molten material, which seems plastic, extrudes longitudinally toward the low pressure ends of the tubes.

It was assumed in arriving at the radial temperature gradients that no longitudinal redistribution occurred. This was a pessimistic assumption since the temperatures of the adjacent air-carrying tubes would be lower because of the reduction in the mass of molten heat-generating material next to them.

If at any time after melting has occurred, a fuel tube at the top of a blocked cluster falls into the molten material at the bottom of the cluster, coolant could then spill into the blocked cluster and cool the molten material. Figure 5.25 shows the results of analysis for a 19-tube cluster that was partially blocked. In this case only 10 percent normal airflow was assumed for the cluster. The tubes did not reach the melting temperature.

~~CONFIDENTIAL~~
~~SECRET~~

It is concluded that there will be no radial growth of melting out of a cluster of either 19 or 37 blocked tubes. Extensions of these analyses must be made before conclusions regarding radial melt growth for very large clusters of blocked tubes can be reached.

5.2.3.3 Mechanical Failure Tests

Core mockup tests have already indicated that the tube bundle is stable. Figure 5.26 shows a picture of a single-tier mockup of the HTRE No. 3A, a reactor arrangement similar to that of the ACT assembly, where a relatively large number of tubes have been removed in several regions of the core. These demonstrations indicate that even though large areas of the core become softened or even melt, the over-all integrity of the core will be maintained. The single-tier mockup shown here was in a static condition. The actual reactor will be subjected to temperature cycles, possibly some vibration from the engine, and in the ultimate flight condition acceleration loads. While it is not possible to simulate these combined conditions without testing the actual core, further laboratory tests under nonstatic conditions are planned in order to demonstrate this stability under severe environmental conditions. In most cases the mechanical condition imposed in these laboratory tests will be deliberately severe because the effects of temperature cycling will be absent.

An experiment to determine the mode of failure of overheated D140E1 fuel elements under a pressure differential has been completed. A seven-tube cluster of fuel elements was subjected to radiant heating from an induction-heated graphite susceptor. The upstream end of the center fuel element of the cluster was connected to a vacuum gage and sealed, and the other end was connected to a system that produced a vacuum of 25 inches of mercury. The remainder of the specimen was exposed to still air.

When the center fuel element had reached a temperature of 4060°F, as indicated by an optical pyrometer sighted down the center fuel element bore, the vacuum was suddenly lost at the upstream-end gage, but the vacuum at the end connected to the vacuum pump was not disturbed. The condition of the specimen is shown in Figure 5.27, which is a side view of the specimen after it was cross-sectioned. Figure 5.28 is an end view of the specimen after the experiment but before the sectioning.

The test tentatively establishes the collapse temperature for these fuel elements under the given pressure differential at about 4000°F. This is lower than the 4500°F BeO melting temperature used for the analysis reported in section 5.2.3.2. However the experiment provides rather good confirmation of the analysis, within reasonable experimental uncertainties.

A series of tests is planned on a three-tier core mockup to prove the core integrity under conditions where regions of the core contain softened or partly melted tubes. Figure 5.29 is a three-tier mockup similar to the ACT core. A group of 19 tubes will be removed initially from the core, simulating a melt condition. If collapse does not occur at this condition, progressively larger groups of tubes will be removed until collapse occurs. To prove stability at other than static conditions, the three-tier mockup will be shocked to a maximum of 4 G's.

The two-tier core mockup, approximately one-half scale, will be used for vibration tests at temperatures to 2000°F. The first series of tests will be again the removal of groups of tubes to set the conditions at which core collapse will occur under vibration.

The next tests with the two-tier mockup will indicate whether or not tubes adjacent to a melting region will collapse into the melt. With the mockup at 2000°F and under vibration, a small cluster of tubes, 7 to 19, will be heated electrically to induce melting. Since most of the tubes around the melting region will soften, it can be determined whether this weakened condition increases the probability of collapse into the melted region.

~~SECRET~~

~~CONFIDENTIAL~~

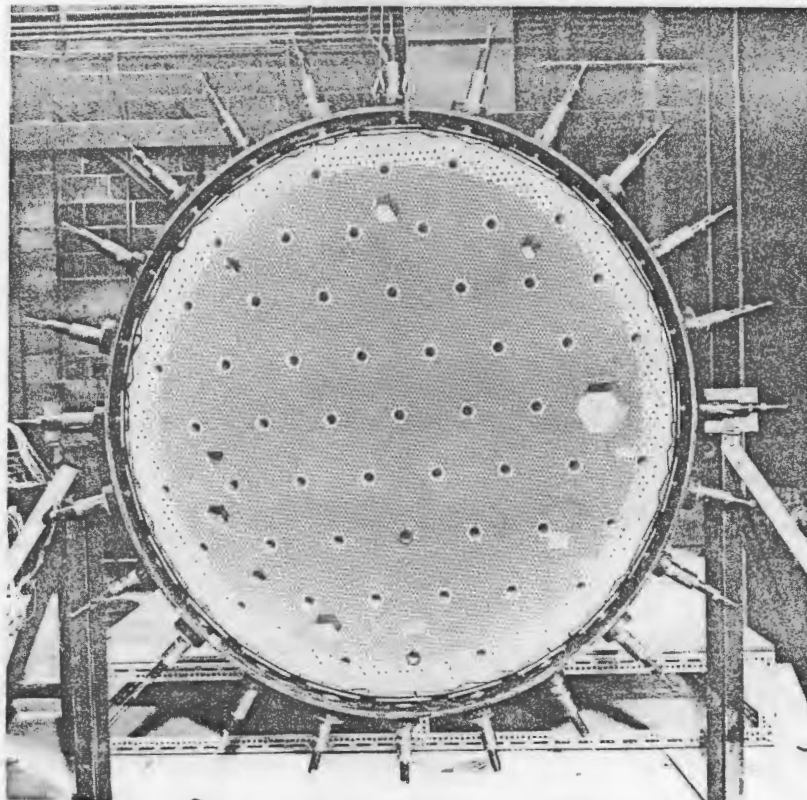


Fig. 5.26 - Single-tier mockup with large numbers of tubes removed to test core integrity



Fig. 5.27 - Longitudinal section of seven-tube specimen used to determine mode of failure of overheated D140E1 fuel elements under a pressure differential

~~SECRET~~
~~CONFIDENTIAL~~

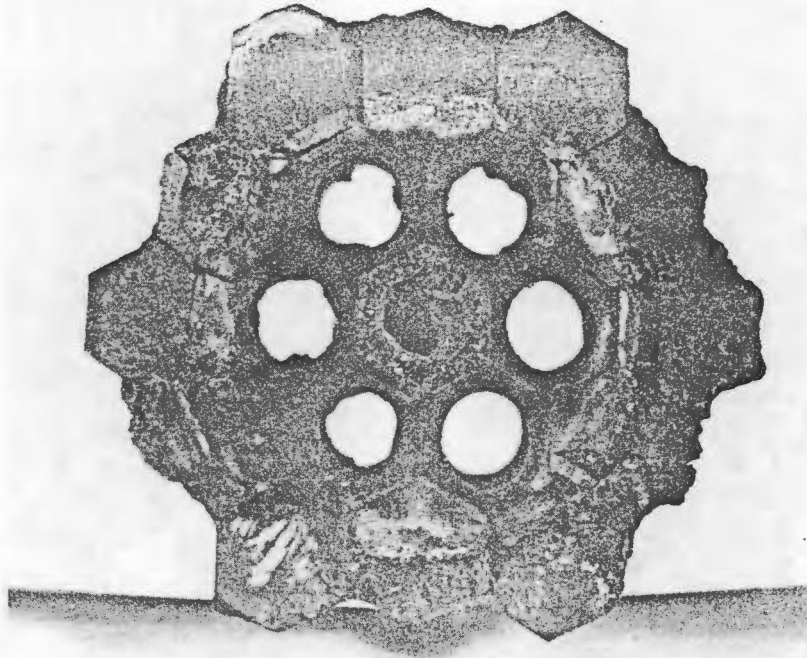


Fig. 5.28 — End view of seven-tube specimen used to determine failure of overheated D140E1 fuel elements under a pressure differential

5.2.3.4 Reactivity and Power Distribution Effects

The reactivity effect of fuel redistribution and the effect of evolution of fission product xenon resulting from a hypothetical localized melting occurrence have been investigated. The discussion of reactivity changes due to fission product evolution (boil-off) in fuel element melting is restricted to changes caused by xenon since it is the principal fission product nuclide from a poisoning standpoint and is also a gas under the conditions of interest. Power increases connected with xenon boil-off in a local melt have also been investigated.

The reactivity effects due to local melting present a hazard only if such effects cannot be adequately controlled, or if the localized melting itself cannot be detected at an appropriate stage. The power increase presents a hazard if it contributes appreciably to the growth of a local melting region.

The power increase associated with xenon boil-off was investigated as follows. The equilibrium xenon concentration was calculated for each region of the active core. The three-energy-group constants were determined for each of the reactor regions, using, as weighting functions, the nineteen-level, one-dimensional neutron flux distributions from a one-dimensional multiregion slowing-down diffusion calculation. The radial power distribution was calculated by one-dimensional three-group diffusion theory, using group constants corresponding to equilibrium xenon. The three-group radial calculation was repeated with group constants for the region adjacent to the radial reflector corresponding to zero xenon concentration. The resulting power increase is 1.3 percent. A slightly larger power change results from a three-group hand calculation for the region, re-

~~SECRET~~
~~CONFIDENTIAL~~

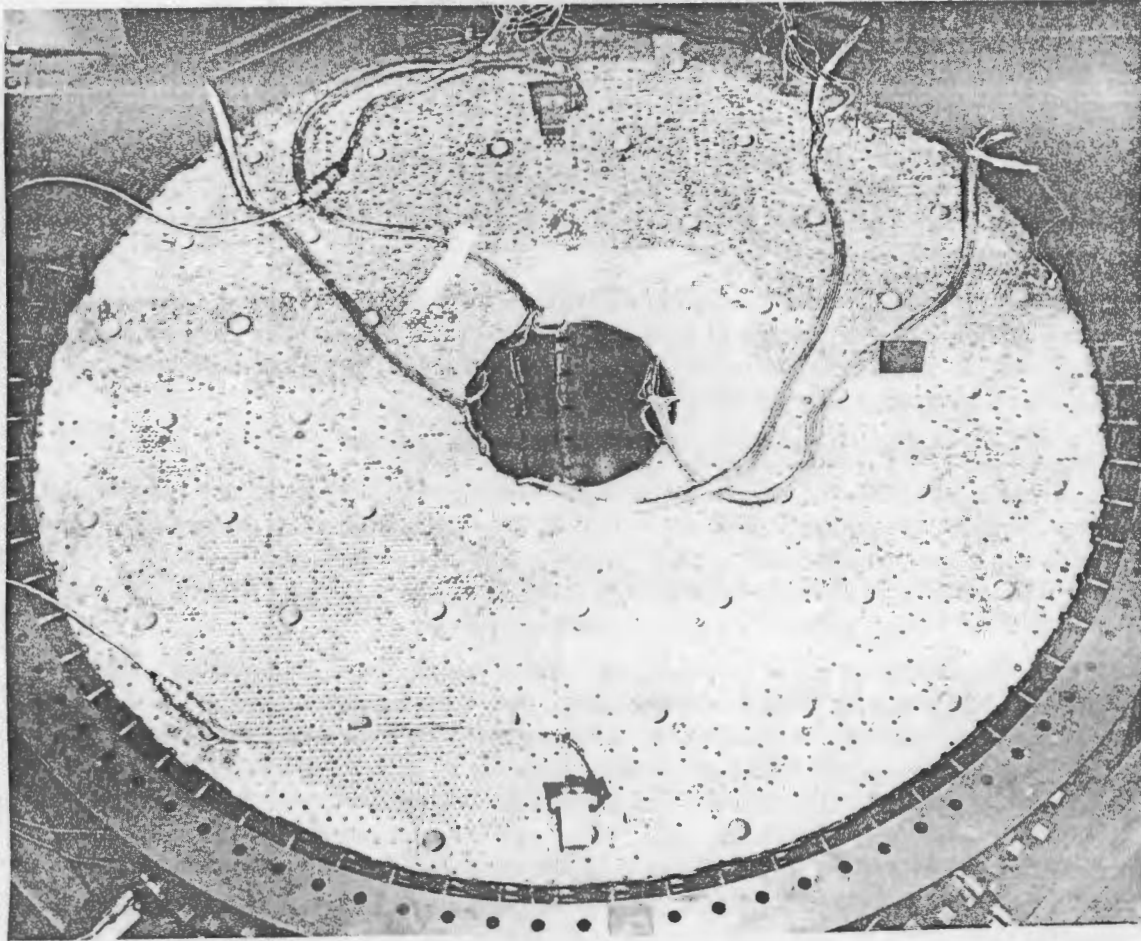


Fig. 5.29 - Three-tier mockup

quiring the group fluxes to adjust so that the nonleakage losses in the region will be equal before and after xenon boil-off.

The data and dimensions in section 5.2.3.2 includes the assumption that the fission power density in the fuel elements with blocked coolant channels is 10 percent above the average. Therefore it is concluded the small increase in power density associated with assumed complete xenon boil-off following melting will not, by itself, lead to further growth of a local melted region.

The principal calculations of the reactivity change resulting from partial melting of the active core have assumed that melting starts over the entire annular intersection of the core midplane, perpendicular to the axis of the active core, and proceeds longitudinally toward both inlet and outlet ends of the active core. The methods and results for these calculations are given in section 8.5.3. The composition of the molten portion of the active core into a near-critical component is a major factor in the characteristics reported in section 8.5.3.

For local melting due to hypothetical coolant blockage to one or more groups of fuel element coolant channels each containing 19 or more fuel element channels, the above-mentioned results may be conservatively applied in a proportional manner with the inclusion of a factor of 1.2 to account for the radial peak importance in the active core as compared to the average.

CONFIDENTIAL
SECRET

It will be assumed here that the minimum-shutdown excess multiplication constant is $-0.02 \Delta k$, as previously postulated for the runaway analysis. The change in multiplication constant for melting the entire active core, and assuming no collapse of side reflectors, is about $+0.174 \Delta k$, as indicated on Figure 8.31. On a proportional basis, the fuel elements forming about 2,400 full-length coolant passages at a radial position having 1.2 times the average importance would have to be melted to exceed the minimum-shutdown excess multiplication constant.

If structural collapse of the reflector is assumed, the data in Figure 8.29 shows that melting 30 percent of the length of about 13 percent of the fuel element passages at a radial position of 1.2 relative importance will produce sufficient positive excess multiplication constant to overcome the $-0.02 \Delta k$ shutdown margin.

5.2.3.5 Critical Experiments With Partial-Melt Configurations

A series of critical experiments is planned to check analytical methods of predicting the reactivity effects of melting. Four experiments are designed to check the effects of local melting and two experiments to apply to gross radial melts typical of total air loss to the core. Redistributions of fuel elements characteristic of very big melts are not planned because of the set-up times required for such experiments.

In the experiments to check local melting effects, the fuel and moderator in 7 and 19 critical-experiment cells will be redistributed. A typical critical-experiment cell is hexagonal (1.75 inch across flats) and is filled with a solid BeO moderator piece in the shape of a half hexagon, and seven hollow BeO tubes. Highly enriched uranium foils are inserted into the cell between the moderator piece and the tubes. These experiments will be done near the longitudinal center of the core, which is where local melting would start. The 7- and 19-cell melts will be done for both the case of no collapse onto the melted fuel and for collapse onto the melted fuel and for collapse of adjacent core and reflector tubes onto the redistributed (melted) material.

The same two effects will be run for about a 44-cell sector extending across the radius of the active core to check the initial effects of melting due to air loss for the whole reactor.

These numbers of cells - i.e., 7, 19, and 44 - are equivalent in amount of material redistributed to 435, 1184, and 2740 melted ACT fuel channels, respectively.

5.2.3.6 Detection and Conclusion

Detection

The LIME experiment provided data on fission product release in fuel element melting that may be compared with steady-state fission product release rates to evaluate the possibility of detection of local melting by monitoring effluent activity.

Inserts, closely representative of the ACT reactor, have been tested under realistic conditions in a series of experiments in the HTRE No. 2 power plant. The two most recent inserts - the L2E-2, with 428 alumina-coated beryllia-yttria-urania tubes, and the L2E-3, with 364 zirconia-coated fueled tubes - were reported in APEX-36.* The average gross stack release rate for both of these inserts was constant at about 12 to 13 ten-minute-old curies per hour at a maximum insert-fuel-tube temperature of about 2520°F . The data for this temperature was used rather than the data for 2620°F since the maximum fuel element temperature for the ACT is 2530°F and the maximum calculated surface temperature is 2330°F . See section "2.1.1.2, Thermal Design."

*"Quarterly Engineering Progress Report." APEX-36. General Electric Aircraft Nuclear Propulsion Department. June 1969.

SECRET
CONFIDENTIAL

A reactor of the ACT size operating at 110 megawatts would have a stack release rate of about 6800 ten-minute-old curies per hour if the release rate is taken to be proportional on a power basis to the rate observed with Insert L2E-2 at 212 kilowatts power in the insert. The power level in the L2E-3 was indicated at 140 kilowatts by heat balance, but this is low compared with critical experiment power mapping. The proportional release rate for a 110-megawatt ACT reactor would be about 9400 ten-minute-old curies per hour on the basis of the L2E-3 rate of 140 kilowatts. The HTRE No. 2 insert conditions are close enough to the ACT conditions that this proportioning of release rates would be substantially the same on a core volume or surface heat transfer basis.

The LIME test involved the intended melting of 126 individual fuel elements in 18 coolant channels blocked at the inlet end. The channels are arranged in concentric hexagonal arrays, with the single central tube being unfueled for instrumentation.

The melting of the blocked tubes took place during constant-power operation of the HTRE No. 2 parent core. The observed peak release rate of gross fission product activity was 37,000 ten-minute-old curies per hour. Although the postoperational examination of the LIME insert may show more or less melting, it is assumed for the present that the peak stack release rate is due to melting the 126 blocked fuel elements. The peak gross stack release rate corresponding to an 18-channel melt is thus 4 to 5 times the expected normal gross release rate.

Conclusions

Following are the conclusions concerning local melting of fuel elements.

1. Blockage of coolant flow is the only significant possible cause of local fuel element melting.
2. Complete blockage of coolant flow to groups of one or seven fuel element channels will not produce temperatures high enough to cause melting or collapse of fuel elements.
3. Complete blockage of coolant flow to a cluster of 19 or more fuel element channels will produce melting temperatures in the blocked fuel elements. The walls of air-carrying fuel elements adjacent to either a 19-channel cluster or a 37-channel cluster will not reach melting or collapse temperatures.
4. The release of fission product poisons such as xenon in a region that has melted because of blockage of airflow does not significantly raise the fission power density in the melted region, and thus would not cause an otherwise stable melt region to grow.
5. Melted regions must grow to between 4 and 10 percent of the active-core volume before there is sufficient increase in reactivity to overcome the minimum-scrum capacity of the control system.
6. The mechanism of fission product release into the exhaust stream will permit detection of the smallest (19-channel) local melt that can occur because of coolant blockage. Nineteen channels correspond to about 0.08 percent of the active core.

5.3 AFTER-SHUTDOWN MELTDOWN

Introduction

The possibility of losing all means of supplying cooling air to the reactor after shutdown from power operation constitutes a hazard. Various failures that may lead to a meltdown of the reactor are discussed. The validity of the assumptions as well as analyses of representative cooling failures are discussed in detail. The aftercooling system has been described in section 2.1.5. Below are several mechanisms that could cause partial

~~CONFIDENTIAL~~
SECRET

or complete loss of aftercooling air. Some indication is given of their likelihood, and they are discussed in order of decreasing severity.

Failure Mechanisms

Ducting Failure - Inlet ducting failure producing a large rupture would prevent the delivery of cooling air to the reactor. Temperatures or pressures that can be realized during ACT operations are well below the limits for which these components have been designed. Since the reactor inlet ducting is an intimate part of the power plant configuration, a violent disruption of the power plant components would have to occur before the reactor inlet ducting would be severely damaged. Turbine failures in general would not produce disruption of airflow, even though the ducts surrounding the turbine were perforated, since the air could still be discharged from the core even though leaks might occur at points upstream of the engine tailpipe, from which the air is discharged into the stack. Turbine failures would have to be violent enough to cause considerable disruption of the power plant before the blower ducts, which are mounted at the rear of the power plant, could be perforated.

Rotor Seizure - In the event of sudden seizure of the compressor rotor, a relatively rapid loss of airflow could occur. However, the aftercooling system air would still flow automatically through the quick-acting valve into the reactor when the compressor discharge pressure drops below the system pressure. Figure 5.30 shows that although the core temperature overshoots in this case, melting temperatures are not reached.

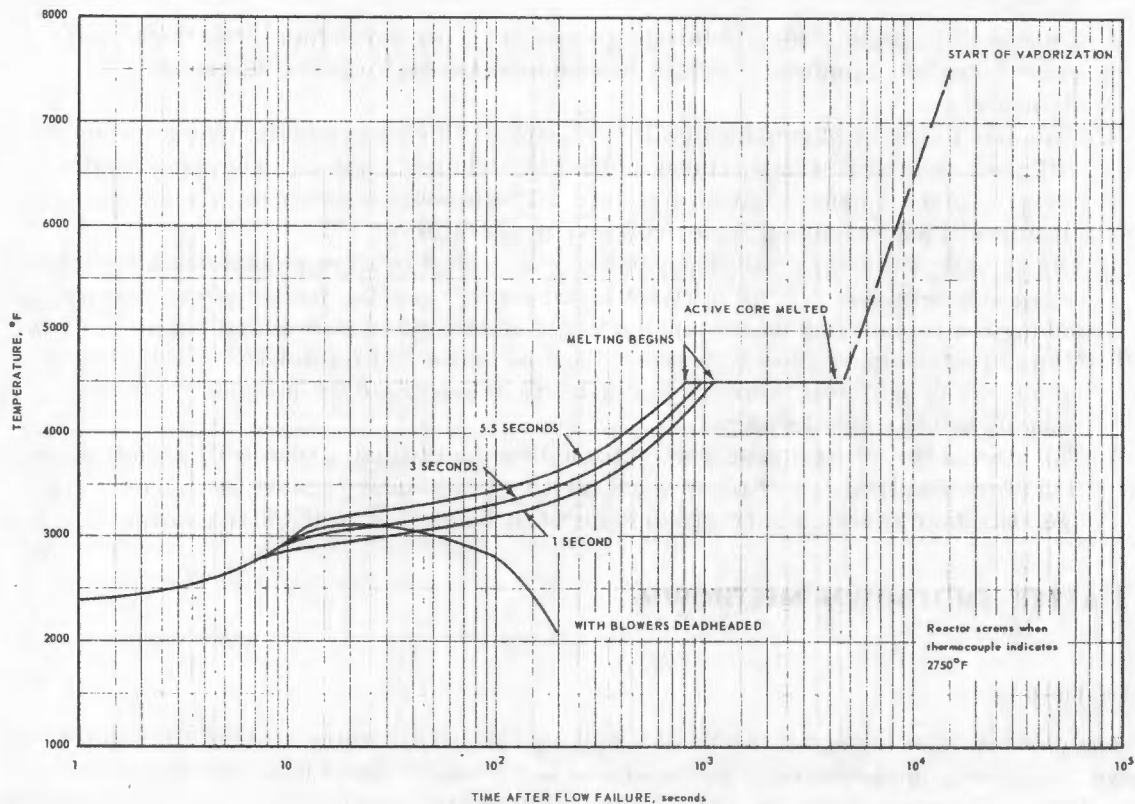


Fig. 5.30 - Average-channel maximum temperature versus time after primary air failure for various thermocouple time lags

SECRET

Air Blockage - The inlet ducting is designed without insulation and corresponding insulation covers. The exit ducting does have insulation and insulation covers, which could conceivably become distorted and inhibit airflow out of the reactor. Complete blocking of substantial fractions of the area might inhibit airflow to the point of producing higher-than-desired temperatures in the core; however, very substantial blockage would be required before the airflow would be reduced to the point of producing melting temperatures.

Blower Loss - As previously mentioned, two independent sources of air have been provided. For normal operations, aftercooling air will be supplied by motoring the compressor with the starter, but in the event of starter failure the aftercooling system cuts in through the quick-acting valve when the compressor discharge pressure drops below the aftercooling system pressure. Since the aftercooling blowers are gasoline driven, they would not be affected by the loss of facility electric power (Standby diesel generators are provided within the facility to supply electric power in the event of main line failure). The loss of all sources of aftercooling air thus seems unlikely. Figure 5.31 shows that, for example, 1 hour after shutdown the afterheat level is low enough that 2.3 hours is required for the core temperature to rise to its melting point. Thus considerable time for corrective action is available in all but very unusual circumstances.

Compressor Stall - Compressor stall leads to only a partial loss of engine airflow. In the event the compressor stalls, the airflow instantly drops to about half the normal value and then continues at the normal rate produced in the coastdown transient. Since actuation of

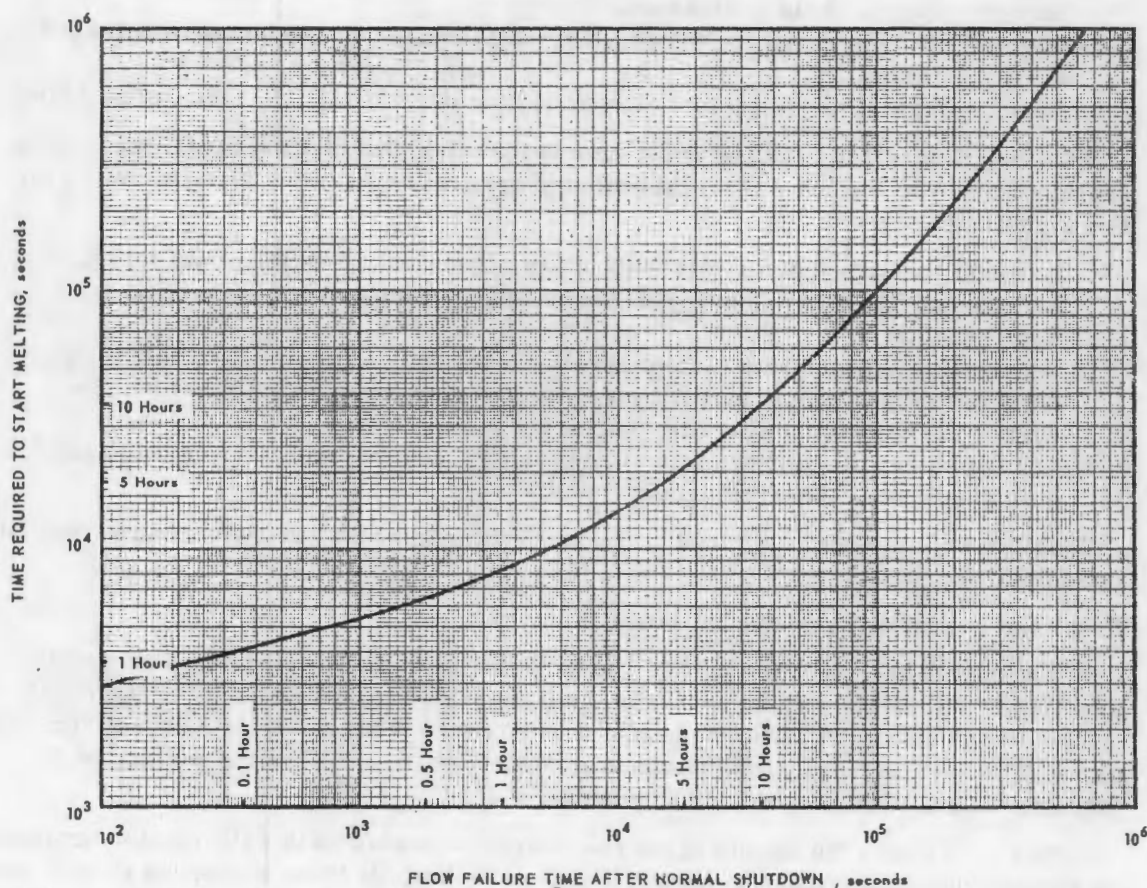


Fig. 5.31 - Time required for melting to start as a function of blower failure time after shutdown

~~CONFIDENTIAL~~
SECRET

engine-shutdown circuits also actuates the scram circuit, it appears that aftercooling the reactor in this event will be routine.

Bleed-Bypass Valve Failure - Four bleed-bypass valves are closed in order to divert aftercooling into the reactor. If one valve failed open, about 25 percent of the blower air would be lost. Since the compressor is also motored in this condition, more than enough air is available.

Discussion of Cases Analyzed

For a given reactor the time interval from coolant loss to start of melting is mainly a function of three parameters: (1) fuel element temperature at time of air loss, (2) time that coolant loss occurs after shutdown, and (3) the operating history preceding the reactor shutdown.

With various combinations of these three parameters, many "typical" failures could be studied, each of which would require a different time to start melting. Since it is not possible to study all of these combinations, in describing an ACT meltdown, one set of reasonable conditions was studied, and then logical variations of these conditions were studied.

The following assumptions define a reference case for the study of reactor melt following ACT shutdown.

1. Long-term operation at 110 megawatts preceding reactor shutdown, i. e., saturated fission product activity at shutdown.
2. Reactor shutdown by normal scram, i. e., the insertion of poison worth at least 2 percent in reactivity.
3. Average-channel maximum fuel element temperature of 2330° F at time of shutdown.

This case is assumed to be the worst case in the sense that melting should occur in the shortest time. With this case as a basis, studies were made with several variations of air-flow conditions assumed.

1. Scram at the instant of air loss without any subsequent aftercooling air supply. A variation of this case assumed that engine coastdown air, but no other supply, was available.
2. Total engine air loss with reactor scram caused by resulting fuel element temperatures for various thermocouple time lags. These cases were examined with and without the assumption that aftercooling air was available.
3. Loss of blower air at times long after shutdown with the reactor assumed to have been previously cooled normally.

These various cases give a range of times over which the melting starts and a range of rates of core melting.

Results of Transient Temperature Analysis

The results of the analysis for case 1 above are shown in Figure 5.32. Two curves are shown, one considering no source of air from engine coastdown and the other with engine coastdown airflow. With no engine coastdown the melting starts at the reactor mid-plane at 1600 seconds, or about 30 minutes. With coastdown the start of melting is delayed until about 3000 seconds, or 50 minutes.

Figure 5.30 shows the results of the calculation that assumed that the reactor scrambled on temperature following instantaneous primary-air loss. In these cases, the reactor does not scram until the thermocouples indicate a maximum fuel element temperature of 2750° F. Three different thermocouple time lags have been assumed - 1, 3, and 5-1/2 seconds. These give a range of the time after scram to start melting from 800 to 1100 seconds, or roughly

SECRET
~~CONFIDENTIAL~~

CONFIDENTIAL
SECRET

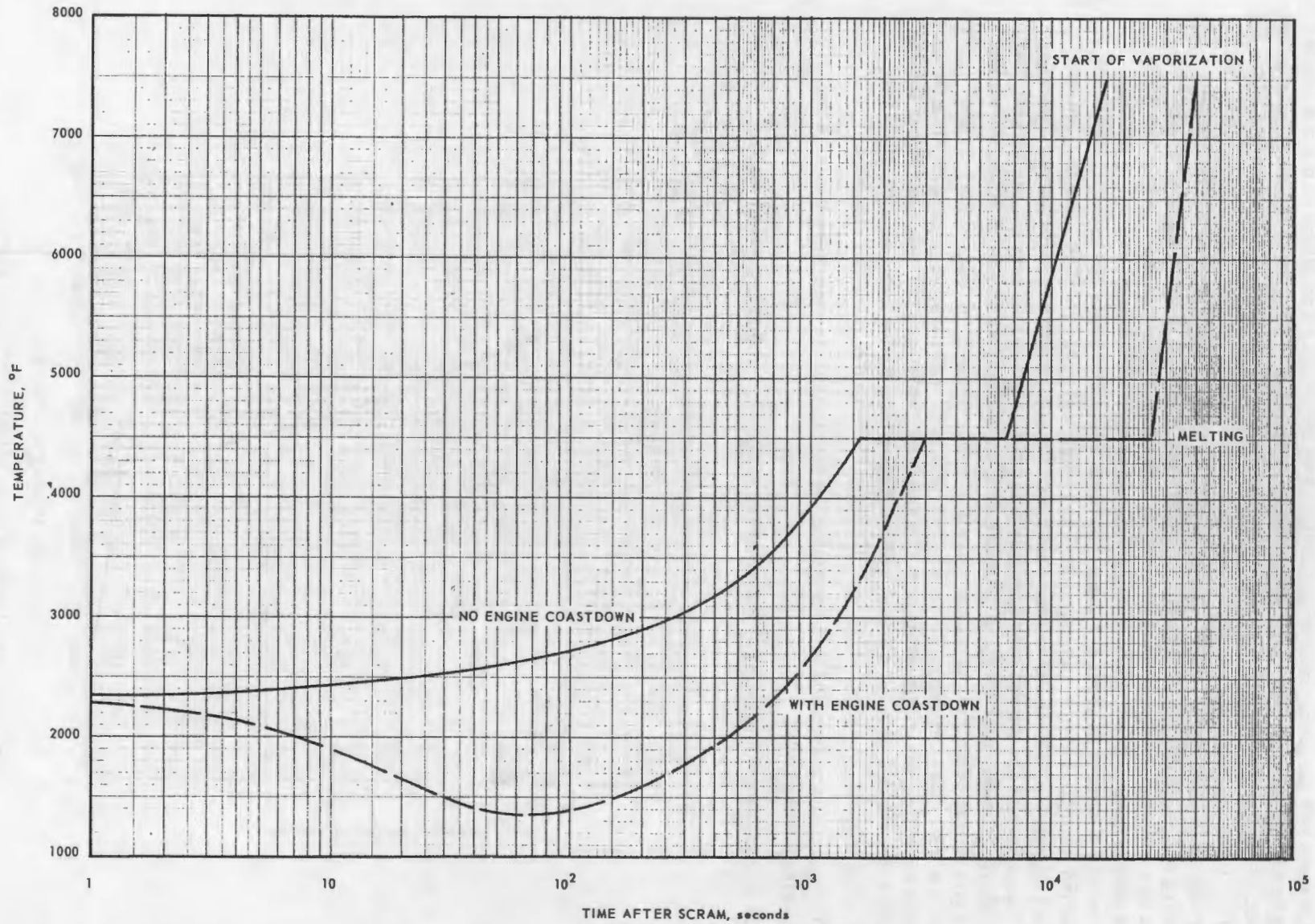


Fig. 5.32 - Active-core temperature versus time after shutdown for aftercoolant failure

CONFIDENTIAL
SECRET

~~CONFIDENTIAL~~
~~SECRET~~

13 to 20 minutes. The bottom curve shows the temperatures attained if the blowers were deadheaded and the check valve opened at the time the reactor scrambled on the 5.5-second thermocouple delay. It was assumed in addition that it takes 10 seconds for the blower to reach maximum output. Although both the assumptions on the time of initiation of airflow and the time for blower output are rather conservative, the results show that melting is prevented. In both the figures described above the curves have been extended to show melting and vaporization. The power level that was assumed in the melting and vaporization was based on fission product power only. However in these cases it is possible that fuel redistribution effect due to melting will cause the reactor to go critical by adding necessary Δk , which is about 3-1/2 percent. (This amount consists of the initial 2 percent inserted when the reactor was scrambled and additional negative effects due to temperature.) Figure 5.33 shows the volume fraction of the core melted versus time for the case in Figure 5.30 of the longest thermocouple delay time. From this curve it can be seen that sometime between about 2650 and 2900 seconds, or between 45 and 50 minutes, the reactor will go critical. This case is picked since it reaches the melting temperature in the shortest time. The time span within which it is argued that the core goes critical is determined by two volume fractions of 0.074 and 0.34, which are the upper and lower limits needed to add 3-1/2 percent Δk to the system. This range comes about as a result of two different melting schemes, which are discussed in section 8.5.3 of the appendix.

The calculations involved in determining the progression of melt were based on the following assumptions:

1. The melting commenced at the midplane of the core and progressed axially.

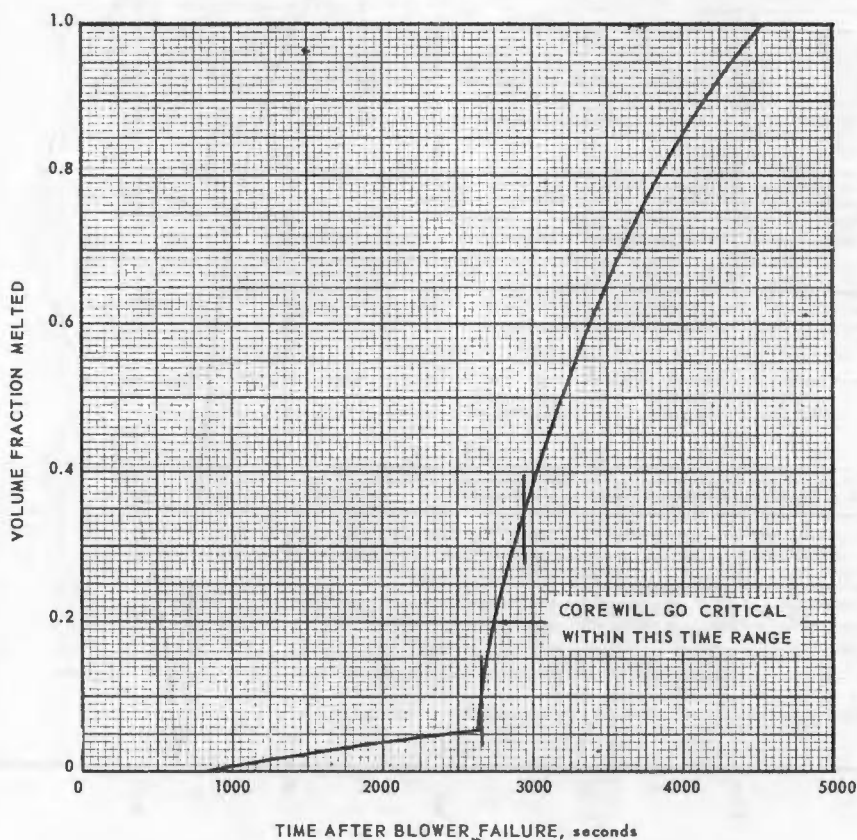


Fig. 5.33—Volume fraction of melted active core versus time after blower failure for a thermocouple lag of 5.5 seconds

~~SECRET~~
~~CONFIDENTIAL~~

2. The power input to the system was based on the after-shutdown power data presented in Figure 5.34.
3. The power distribution in the core was flat radially and simulated a 2:1 cosine axial distribution.
4. The molten material remained intact at the melting point (4500° F), and all heat generated in this portion after fusion was conducted to adjacent, axial solid disks.

The energy input required to melt the postulated 0.05 volume-fraction disk located at the position of maximum heat generation results in raising the temperature of the rest of the core to near-melting temperatures, and subsequent heating of this molten disk results in heat diffusion to adjacent unmolten disks so that core melting proceeds at an increasing rate.

Figure 5.31 shows a graph of the time available before melting will occur as a function of the time after shutdown when blower failure occurs. This corresponds to case 3 above when it is assumed that the core has been cooled normally for the time before blower failure. This curve is given to show the time available for corrective action in this case.

Reactivity Changes Due to Core Melting

If a cooling failure leading to meltdown should occur, three reactivity effects associated with the melting must be considered.

1. Evolution of fission product poisons including xenon
2. Temperature coefficient of reactivity
3. Effect of redistribution of melted fuel

In all cases the reactor has been assumed to have been fully scrammed with the insertion of all available rods. No partial scrams have been considered. The algebraic combination of the reactivity effects discussed above must thus be equal to the 2 percent shutdown margin assumed before the reactor can go critical again.

Evolution of Fission Products - The effect of fission product evolution is neglected in this analysis because the shutdown margin available in control rods was assumed to be that for the cold clean reactor. Therefore if any fission products are present and if they all are boiled off or emitted at high temperatures, this effect of itself will not make the reactor go critical. The second consideration involved in neglecting this mechanism is the fact that fuel redistribution due to melting is a much more complex and more difficult effect to predict. This fuel redistribution can of itself conceivably produce much more reactivity than that contained in the fission products.

Temperature Coefficient of Reactivity - The temperature coefficient of reactivity used for this analysis is shown in Figure 2.14. The calculation of this temperature coefficient is discussed in section "2.1.1.3, Nuclear Design." The result of the reactivity change due to temperature as shown by this curve is to increase by 1.5 percent the reactivity that must be added to make the reactor critical.

Fuel Redistribution - The fuel redistribution effect is the most difficult to predict and overshadows all other effects. For any failure leading to meltdown the time required for fuel redistribution is small compared to the time required for the fuel to melt. From the fission product heating distributions it can be concluded that the core will melt almost uniformly across the radius at the longitudinal center and that then the growth of the melt will be longitudinal toward both ends of the core. Therefore a large portion of the core could be melted before the molten material could escape. Analysis given in section 8.5.3 of the appendix shows that the reactivity effect of fuel redistribution depends strongly on whether the unmelted core collapses on the melted portion and eliminates the hole left by the melted tubes. If collapse occurs, the reactivity effect is positive and proportional to

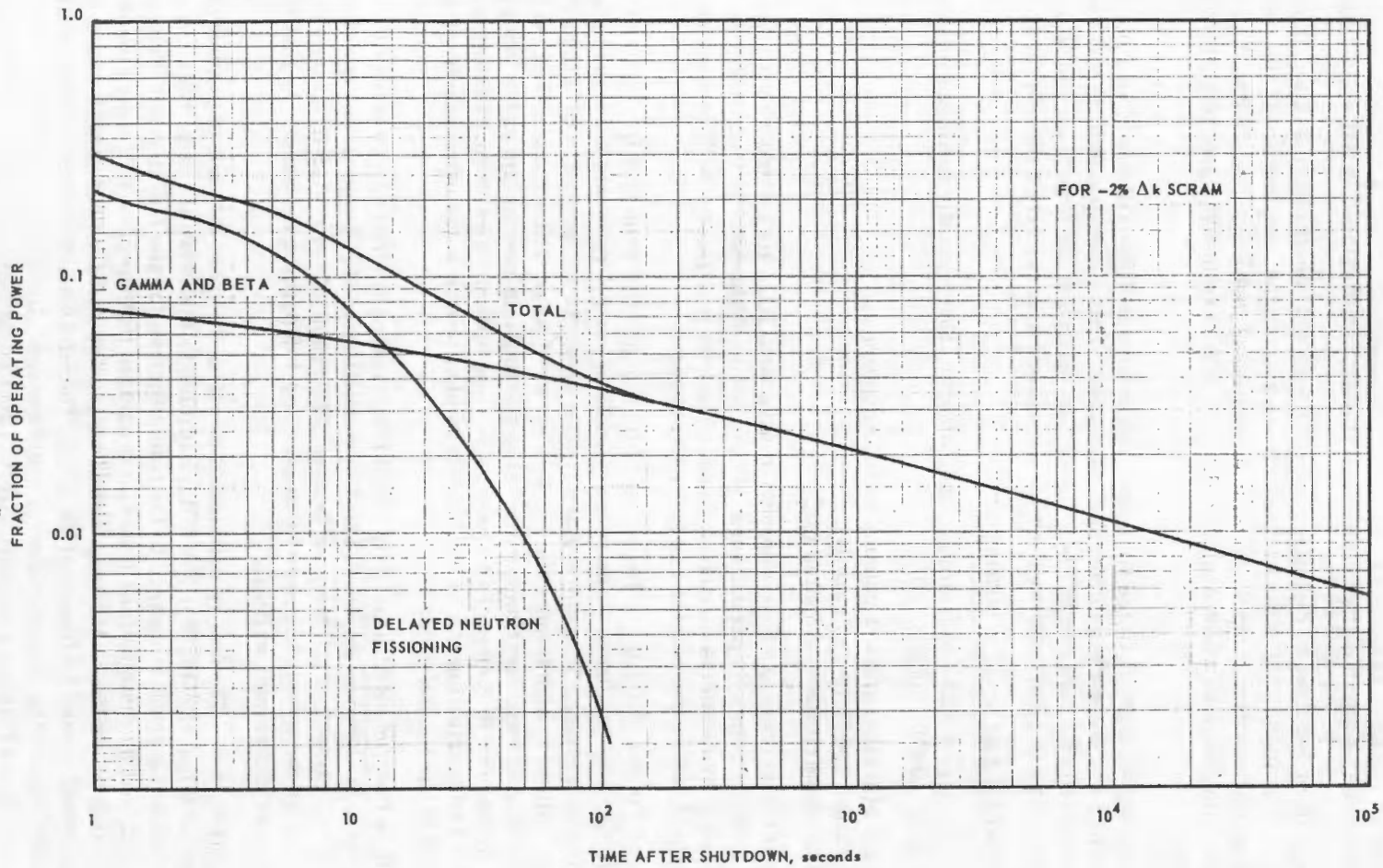


Fig. 5.34 - Power after shutdown

CONFIDENTIAL
SECRET

CONFIDENTIAL
SECRET

the amount of core that is melted. If collapse does not occur, the melting produces small reactivity changes until melting material starts to reach a critical mass. Although mechanical tests indicate that the collapse of unmelted tubes is not likely for smaller melts, it will be assumed here that it does happen in cases of large fractions of melted core. Combining all effects, it has been assumed that the core immediately before melting is subcritical by an amount equal to 3.5 percent as a result of a combination of rod worth and negative temperature reactivity effect. It is assumed to remain subcritical until and if fuel redistribution adds more than 3.5 percent. If this happens, it is assumed that the reactor will experience a runaway very similar to that described in section 5.2.1; and no separate runaway calculations have been made.

Conclusions

The discussion given above indicates the kinds of failures that would be necessary to produce melting of the fuel in the ACT system as a result of loss of aftercooling. It is concluded that it will be possible to provide an aftercooling system with sufficient flexibility that total loss of aftercooling to the core would be unlikely unless a violent disruption of the power plant should occur. The data given also show that in all but very special circumstances, considerable time is available for corrective action should any of the aftercooling systems fail to function properly.

CONFIDENTIAL
SECRET

The following information is being furnished to you for your information only. It is not to be disseminated outside your organization without the express written approval of the source of this information. This information is being furnished to you for your information only. It is not to be disseminated outside your organization without the express written approval of the source of this information.

156
CONFIDENTIAL
SECRET

6. HAZARDS CALCULATIONS

6.1 ASSUMPTIONS

The hazards calculations presented here are based on applications of Sutton's diffusion equations. Conservative values were employed for the diffusion parameters.* The radioactive effluent during normal operations is assumed to be released from a stack 100 feet tall, which will carry cooled and possibly augmented air from one X211 turbojet. Total flow will be about 800,000 cubic feet per minute at 400°F. Effective stack heights are calculated by means of the Bryant-Davidson formula. Reactor power for the major part of normal operations will be 50 megawatts, but there may be some limited operation at 110 mw.

Biological factors for the internal dose calculations are taken from the most recent International Commission on Radiological Protection report.† In the calculation of the dose to thyroids of children who may drink milk from cattle grazing on contaminated vegetation, it has been assumed that the amount of iodine deposited per gram of vegetation is the same for the grasses in arid Idaho as for the grasses that grow in more suitable dairy country. The mass of a child's thyroid was taken to be 1.5 grams. Deposition on vegetation was calculated by the methods suggested by Healy.‡

The three meteorological conditions considered and the associated parameters are given in Table 6.1.

The wind-speed classes and the associated effective wind speeds and stack heights within each meteorological condition are given in Table 6.2.

Release fractions for fission products, air cleaning efficiencies, and reduced release fractions are given in Table 6.3.

Dose calculations based on these assumptions have been made for both the steady-wind cases and for varying-wind-direction cases in which the emission of fission products was assumed to be angularly uniform in any one 22.5-degree sector.

6.2 CALCULATED DOSES FOR NORMAL OPERATIONS

Inhalation thyroid doses per hour of reactor operation for the case in which the air is not cleaned are given in Figures 6.1, 6.2, and 6.3 for the varying winds and in Figures 6.4, 6.5, and 6.6 for steady winds. Results when air cleaning is considered are less by a factor of about 10.

*See Appendix for details of the calculations.

†"Report of ICRP Committee II on Permissible Dose for Internal Radiation (1959) With Bibliography for Biological, Mathematical, and Physical Data," Health Physics, Vol. 3, June 1960.

‡J. W. Healy, "Calculations on Environmental Consequences of Reactor Accidents," HW 54128, December 1957.

~~CONFIDENTIAL~~
~~SECRET~~

Doses to children's thyroids per hour of reactor operation due to the contaminated milk cycle are given for the varying wind cases in Figure 6.7 and for the steady winds in Figure 6.8. Air cleaning would reduce the doses by a factor of 10.

Gamma doses per hour of reactor operation due to material deposited on the ground (fallout) have been calculated for the same meteorological condition; but since the equations do not depend on wind speed ($V_D/u = \text{const}$), no wind-speed variation is included. Results for varying winds are in Figure 6.9 and for the steady winds in Figure 6.10. Doses would be less by a factor of 20 if the air cleaner were used.

Direct gamma dose per hour of reactor operation from airborne fission products for all three weather conditions is given for varying winds in Figures 6.11, 6.12, and 6.13. The steady-wind cases are given in Figures 6.14, 6.15, and 6.16. These are small compared to the inhalation doses. Air cleaning would reduce the doses by a factor of 20.

TABLE 6.1
METEOROLOGICAL PARAMETERS FOR NORMAL OPERATIONS

Condition	n	C_y	C_z	V_D/u	
				Halogens	Particulates
Strong lapse	0.20	0.30	0.30	8.0×10^{-3}	6.0×10^{-4}
Weak lapse	0.25	0.12	0.12	4.6×10^{-3}	3.0×10^{-4}
Weak inversion	0.33	0.06	0.06	3.4×10^{-3}	2.2×10^{-4}

TABLE 6.2
WIND CLASSES

Wind Speed Class, mph	\bar{u} , m/sec	h_e , m
1 - 5	1	230
6 - 15	3	80
16 - 30	8	43
>30	14	37

~~SECRET~~
~~CONFIDENTIAL~~

TABLE 6.3
FISSION PRODUCT RELEASE FRACTIONS

Material	Fraction of Production Rate ^a	Estimated Air Cleaner Efficiency	Fraction of Production Rate from Air Cleaner
I131	8×10^{-4}	0.90	8.0×10^{-5}
I133	3×10^{-4}	0.90	3.0×10^{-5}
I134	3×10^{-4}	0.90	3.0×10^{-4}
I135	8×10^{-5}	0.90	8.0×10^{-6}
T _e 132 - I132	(8×10^{-4})	0.90	(8.0×10^{-5})
Sr89	5×10^{-4}	0.95	2.5×10^{-5}
Ba140	8×10^{-5}	0.95	4.0×10^{-6}
Gross activity	(5×10^{-4})	0.95	2.5×10^{-5}

^aFraction of production rate of fission products released.

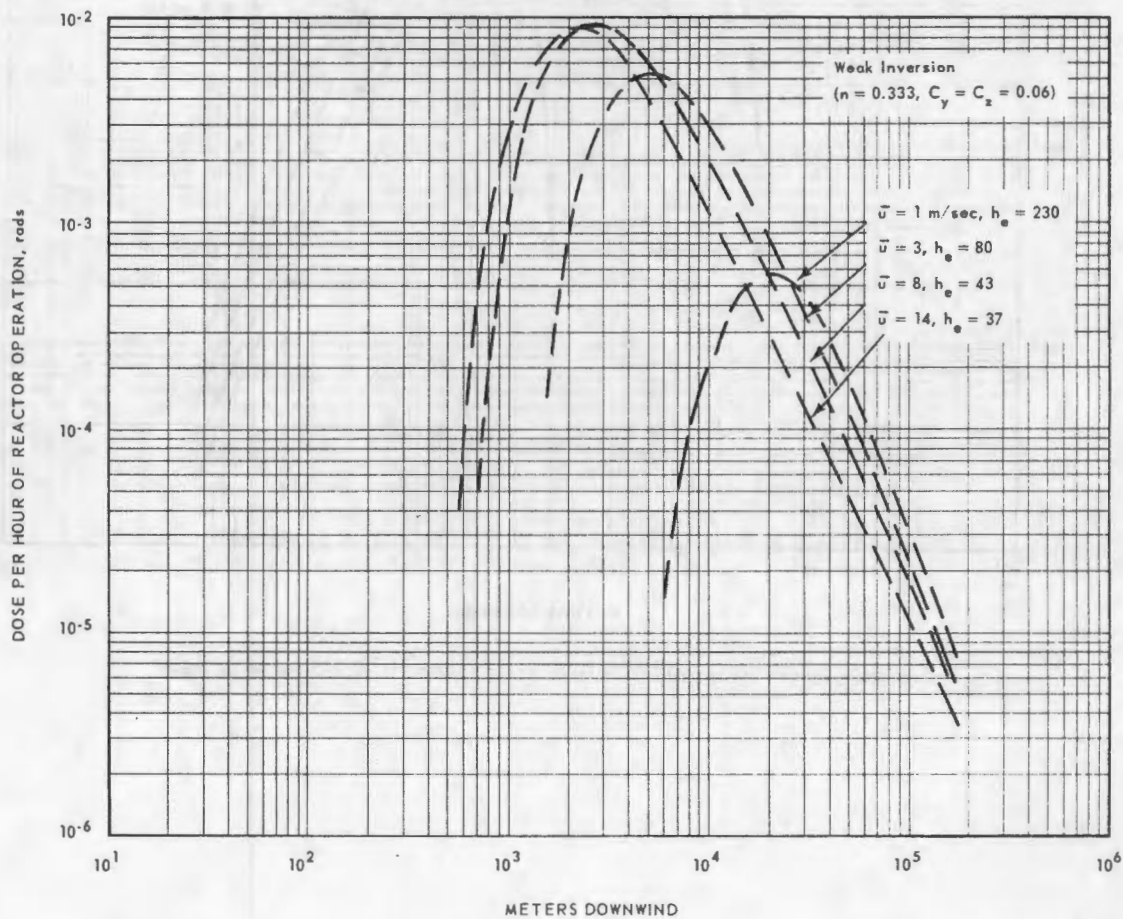


Fig. 6.1—Inhalation thyroid dose in receptor sector $\theta = 0.393$ for weak inversion

~~CONFIDENTIAL~~
~~SECRET~~

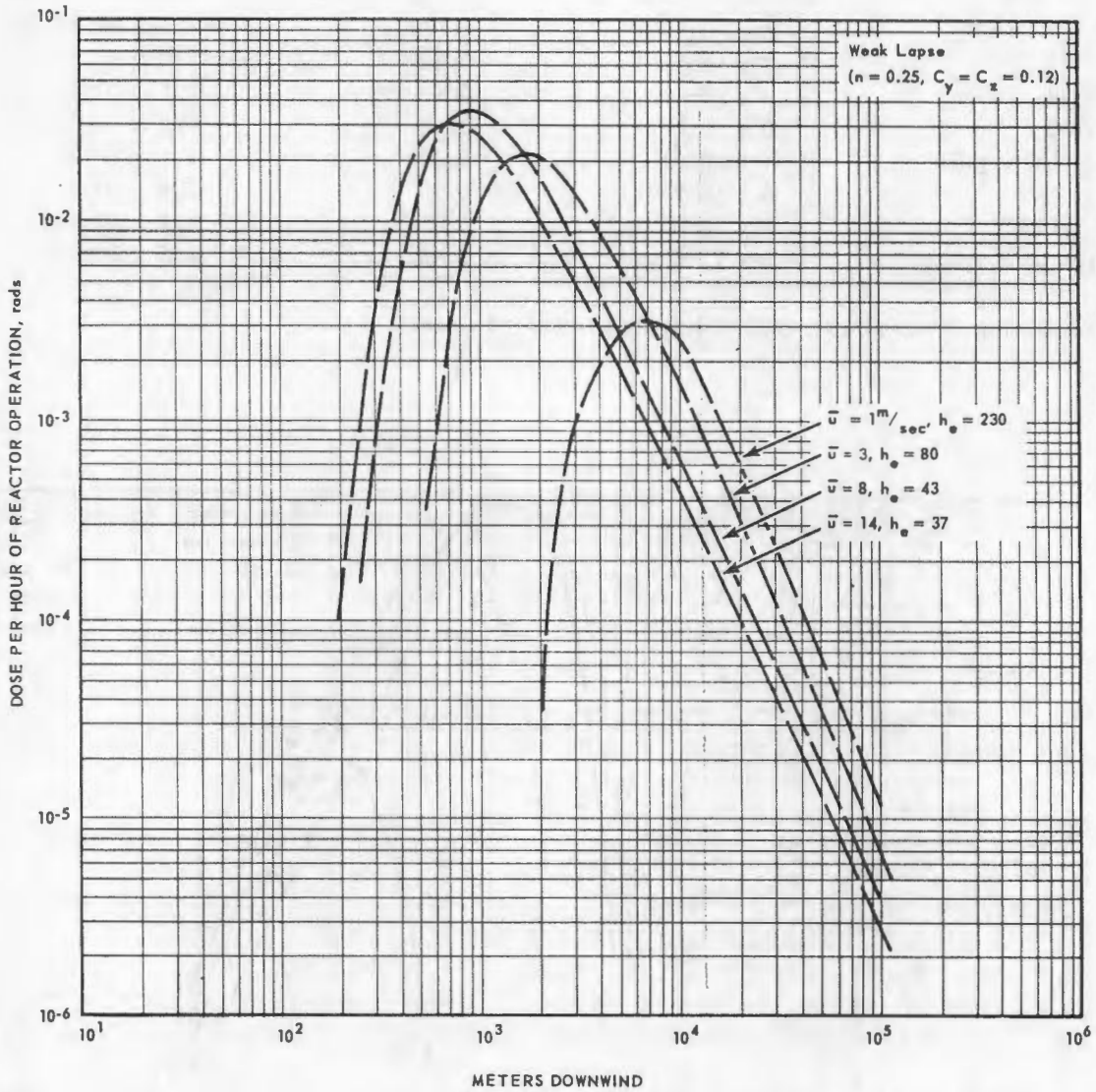


Fig. 6.2—Inhalation thyroid dose in receptor section $\theta = 0.393$ for weak lapse

~~CONFIDENTIAL~~
~~SECRET~~
CONFIDENTIAL

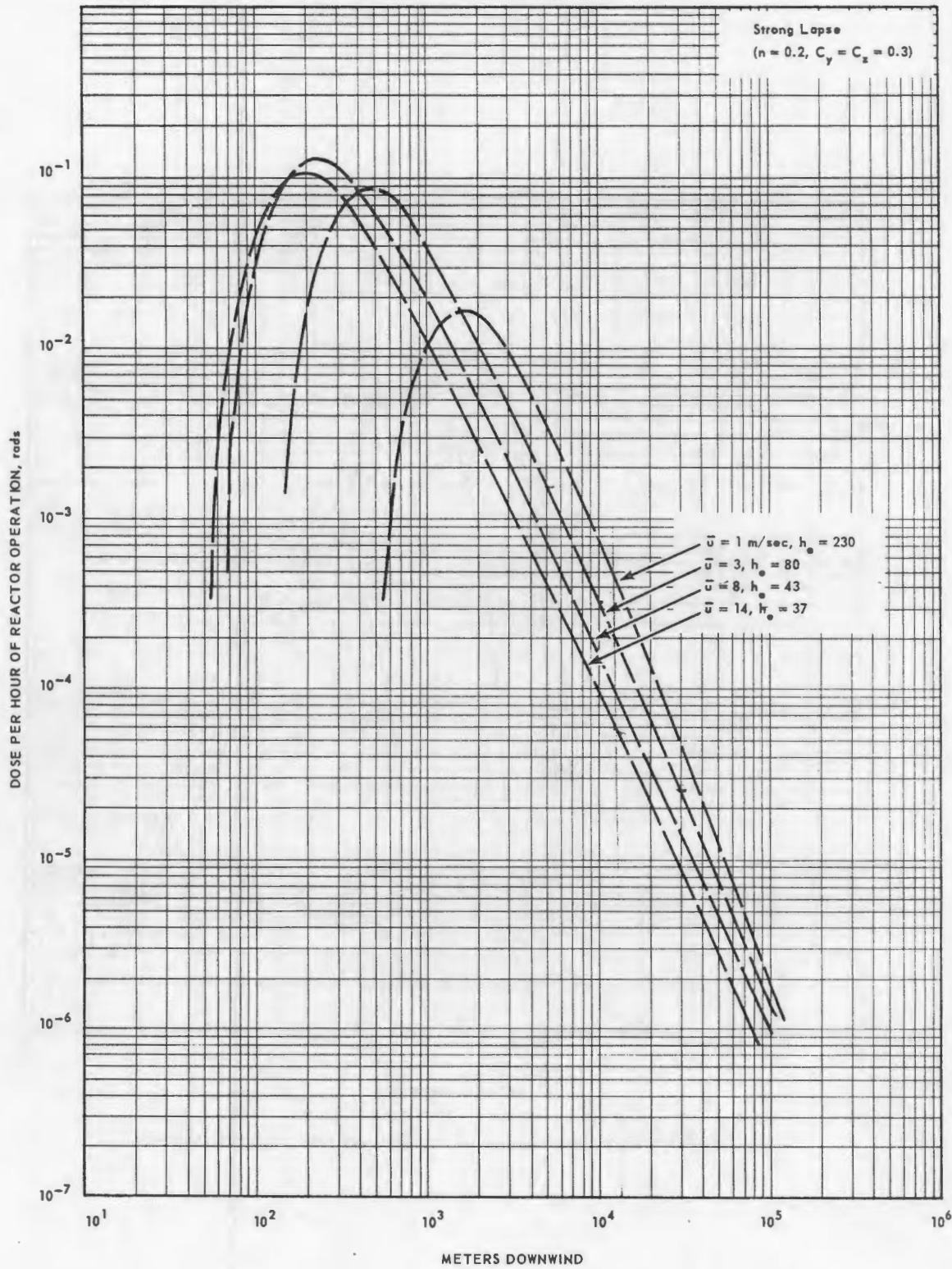


Fig. 6.3 - Inhalation thyroid dose in receptor section $\Theta = 0.393$ for strong lapse

CONFIDENTIAL
SECRET

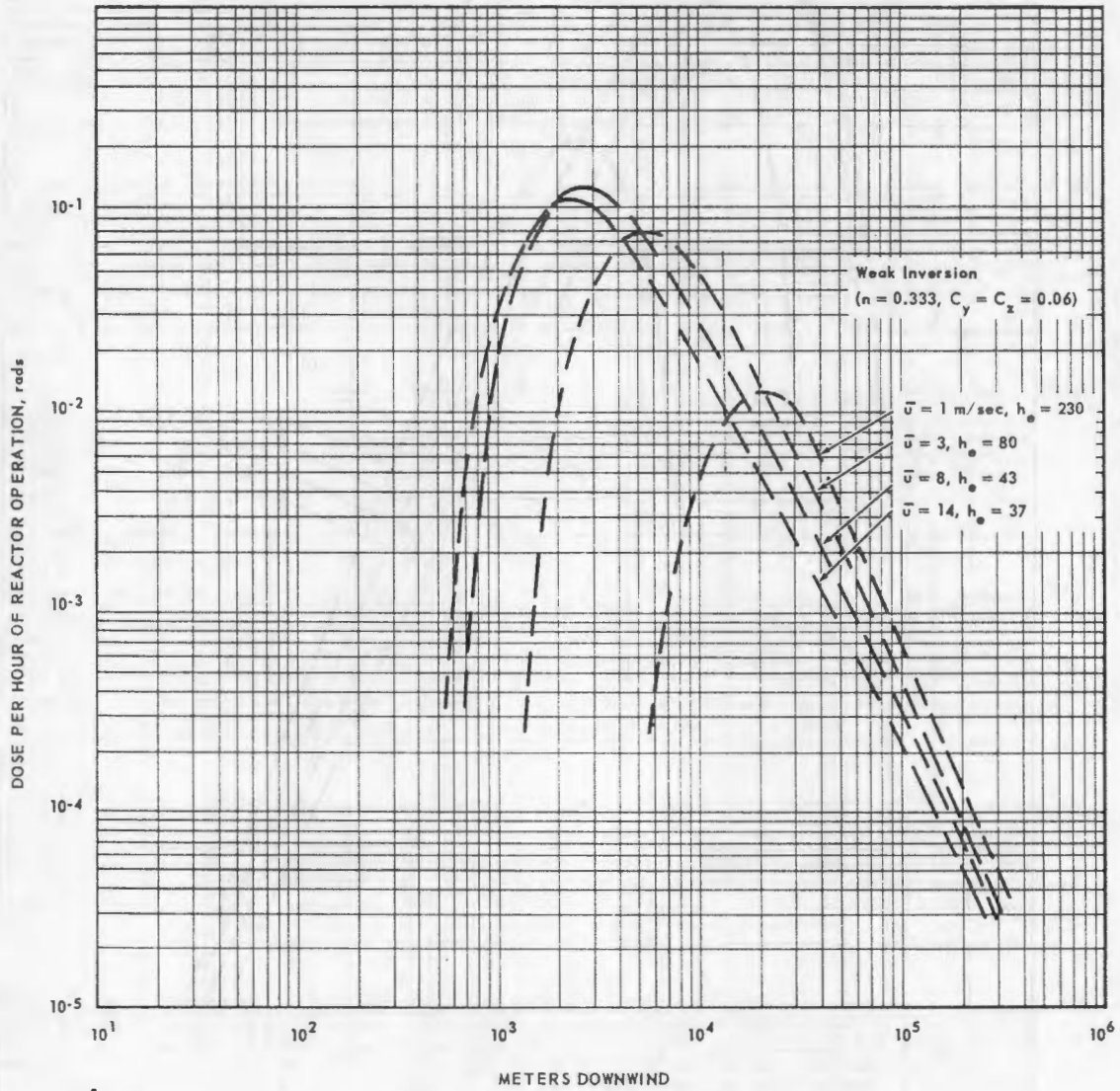


Fig. 6.4 - Inhalation thyroid dose downwind during steady wind and weak inversion

SECRET
CONFIDENTIAL

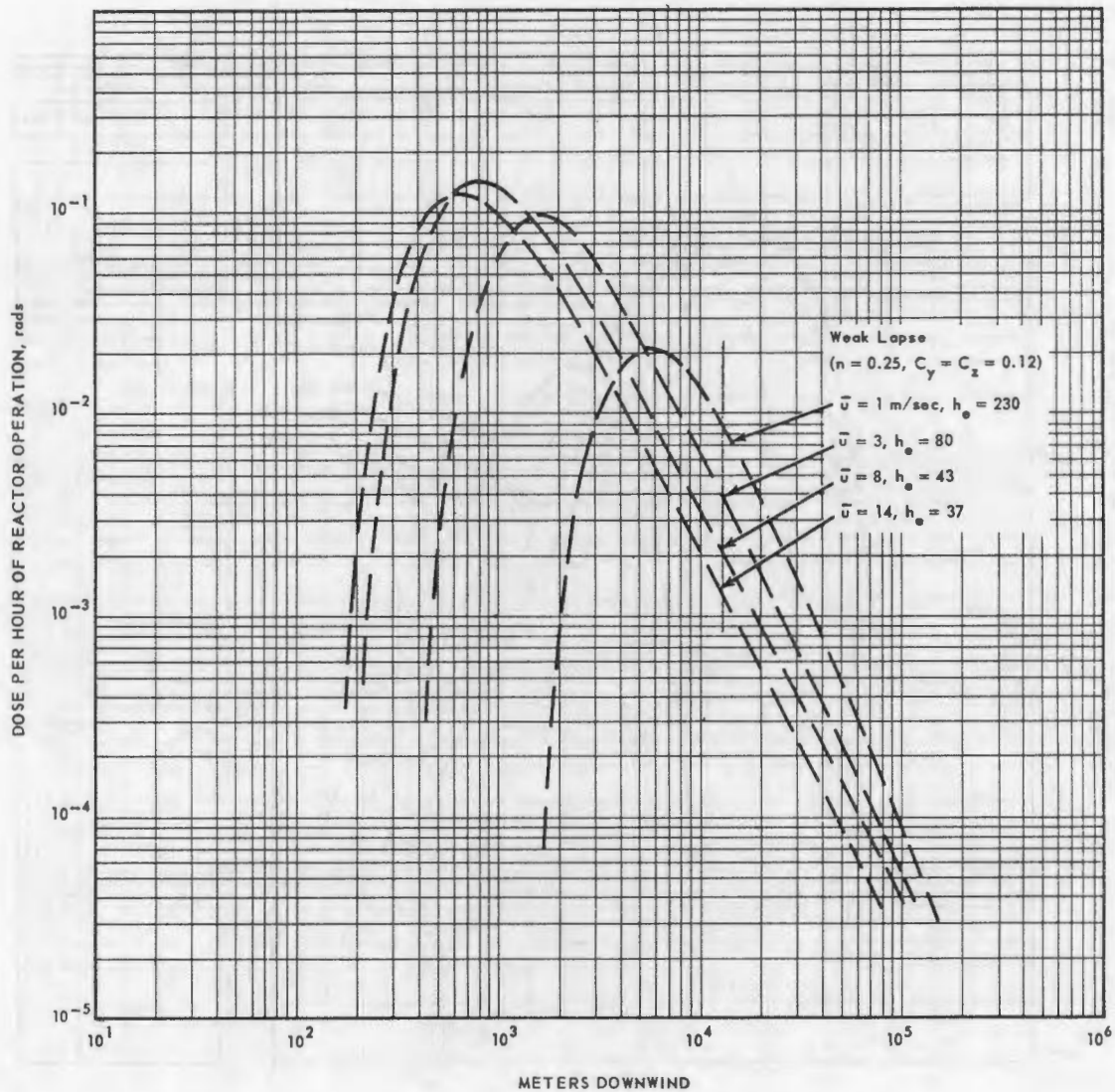


Fig. 6.5—Inhalation thyroid dose downwind during steady wind and weak lapse

CONFIDENTIAL
SECRET

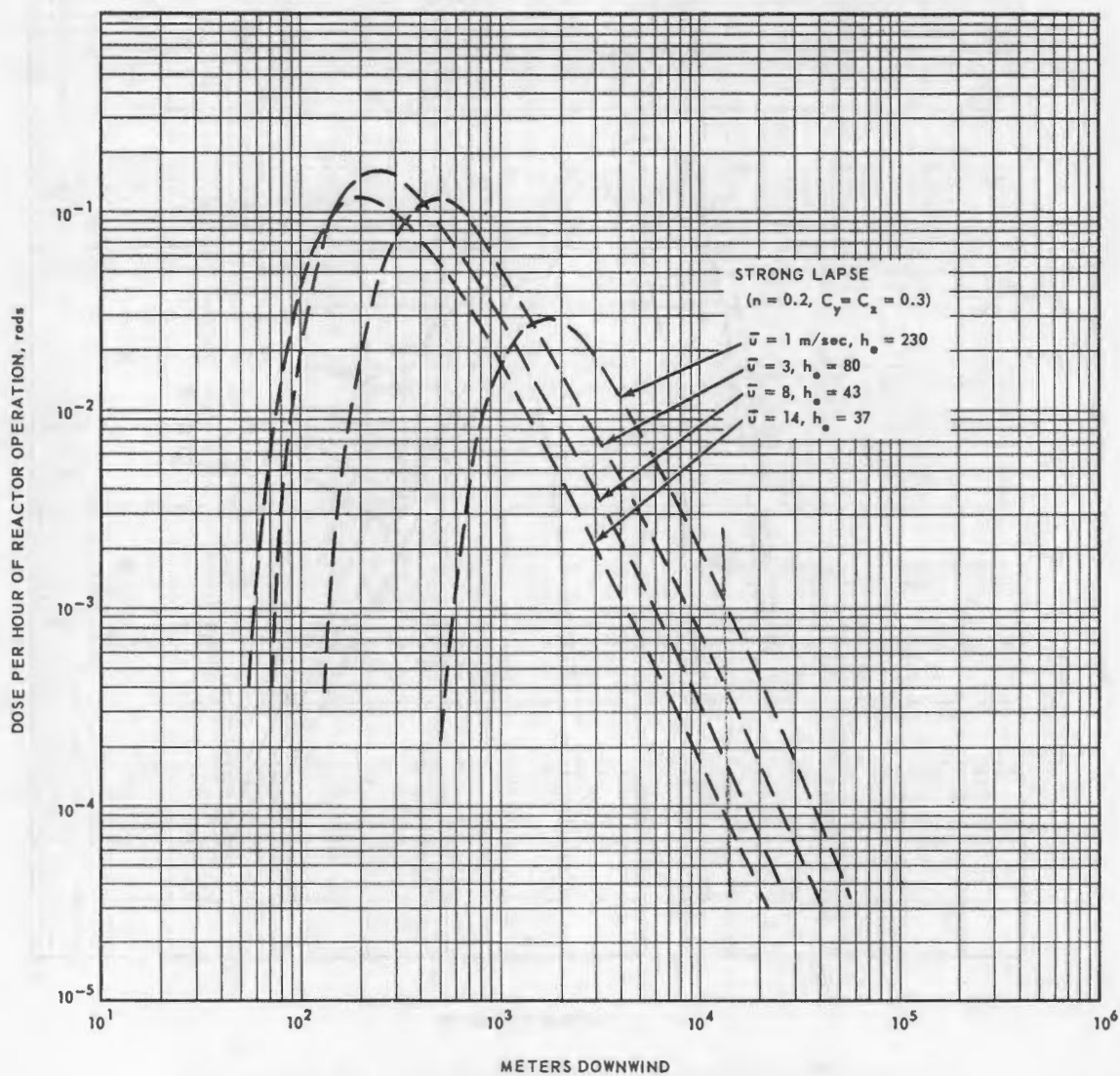


Fig. 6.6—Inhalation thyroid dose downwind during steady wind and strong lapse

SECRET
CONFIDENTIAL

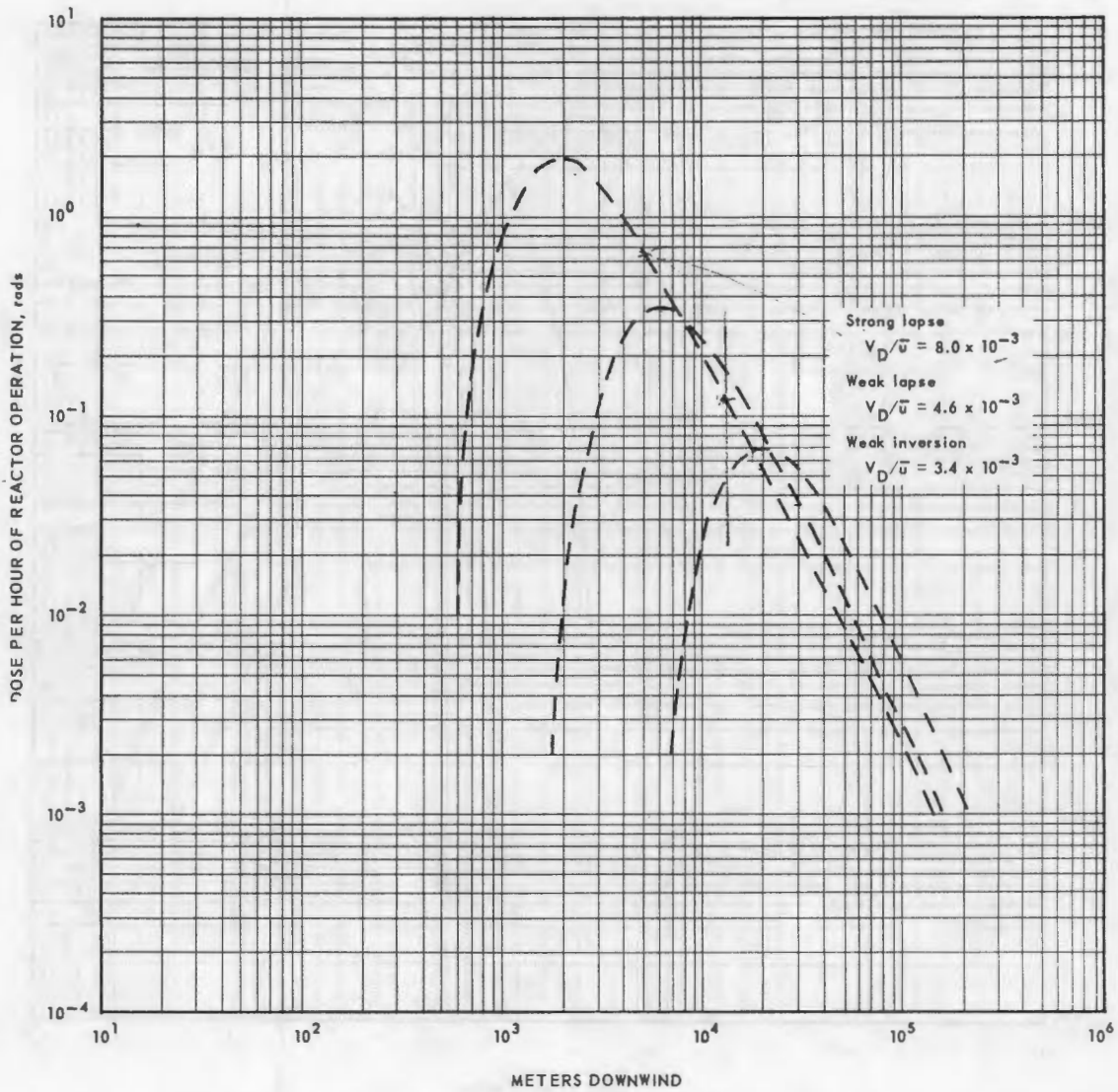


Fig. 6.7 - Child's thyroid dose via milk ingestion in receptor sector $\theta = 0.393$

CONFIDENTIAL
SECRET

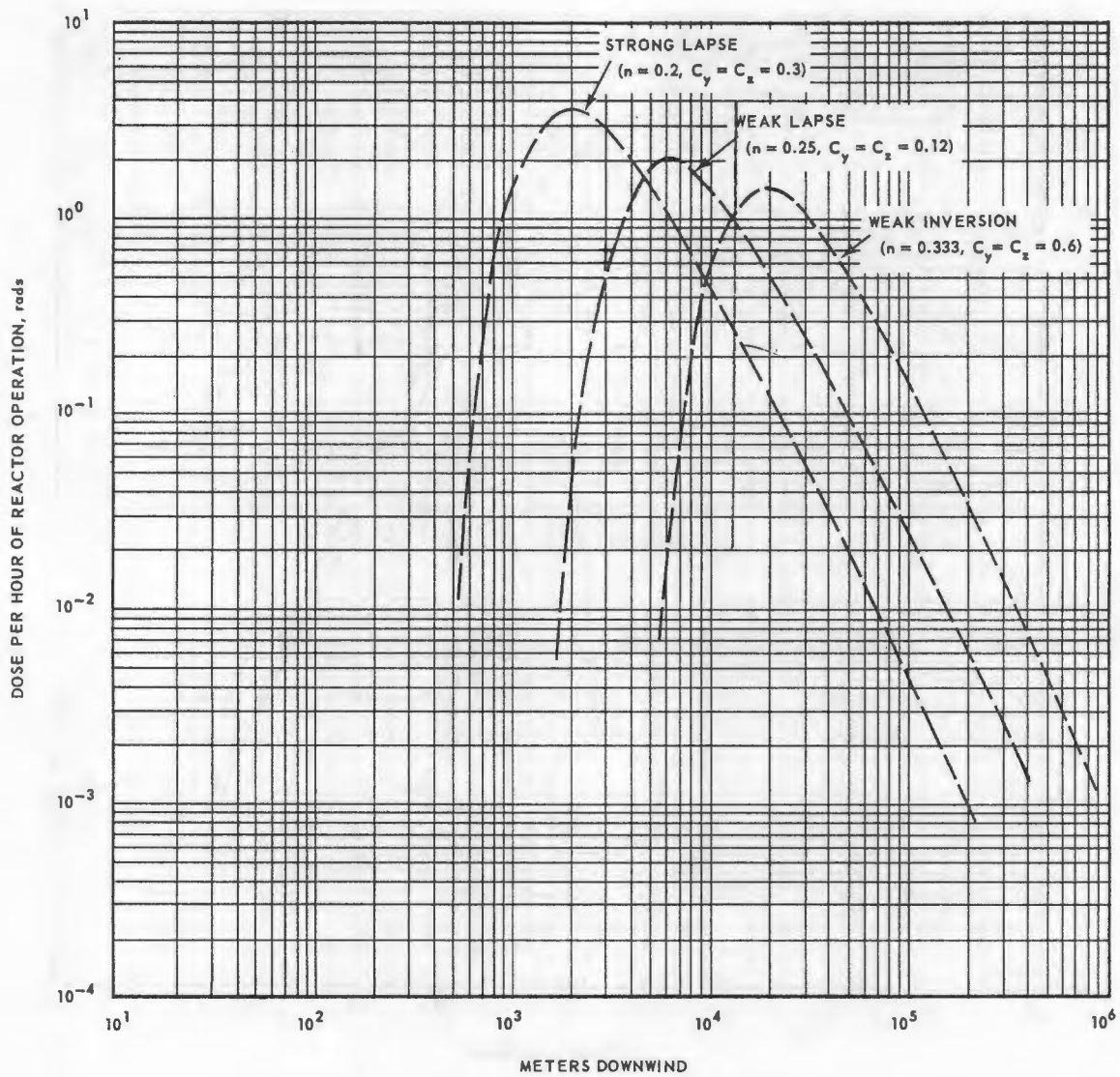


Fig. 6.8 - Child's thyroid dose via milk ingestion downwind from release

SECRET
CONFIDENTIAL

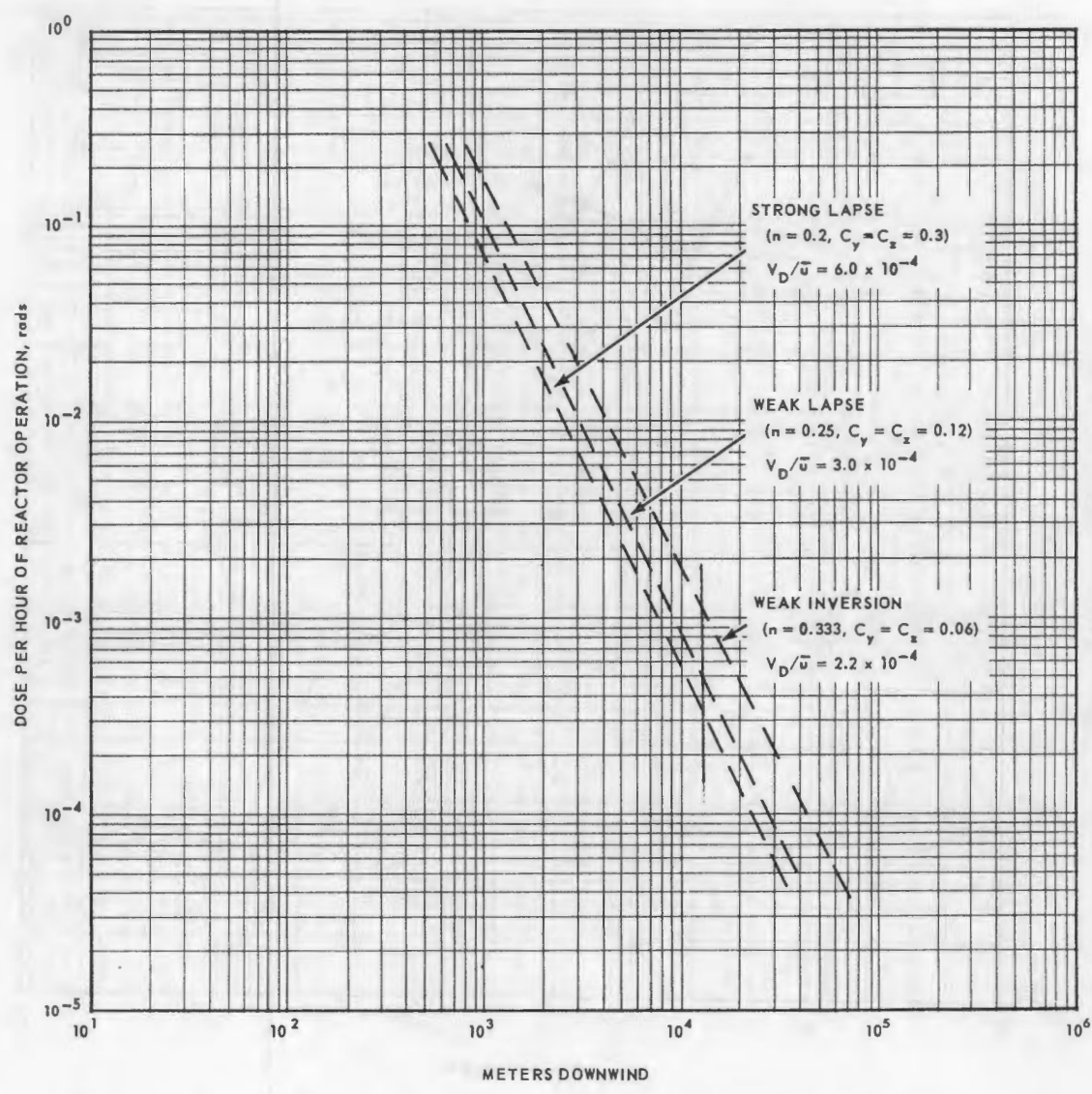


Fig. 6.9 - Fallout gamma dose in receptor sector at 1 meter above ground in $\Theta = 0.393$ sector

~~CONFIDENTIAL~~
~~SECRET~~

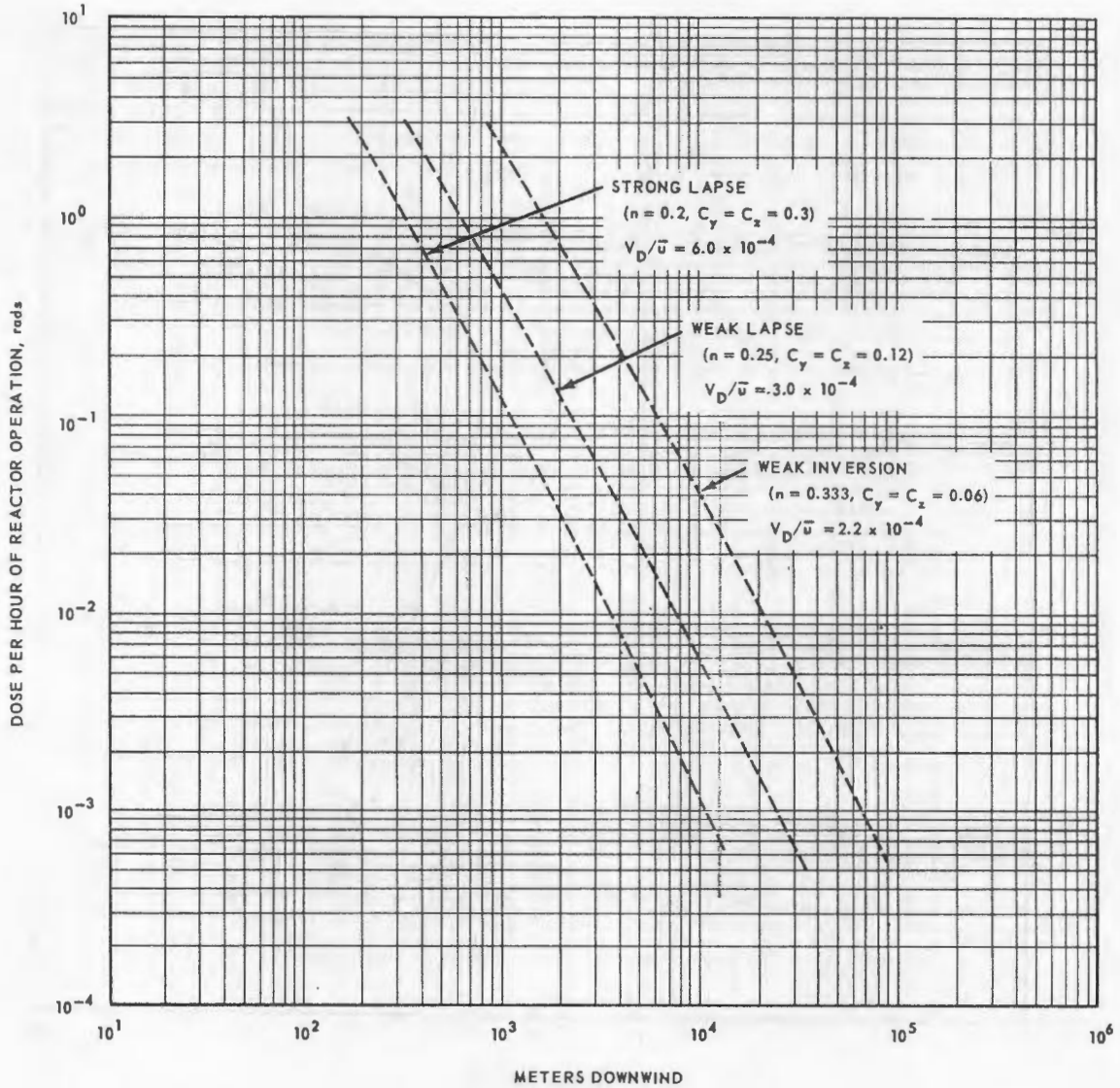


Fig. 6.10 - Fallout gamma dose downwind at 1 meter above ground, steady wind

~~SECRET~~

~~CONFIDENTIAL~~

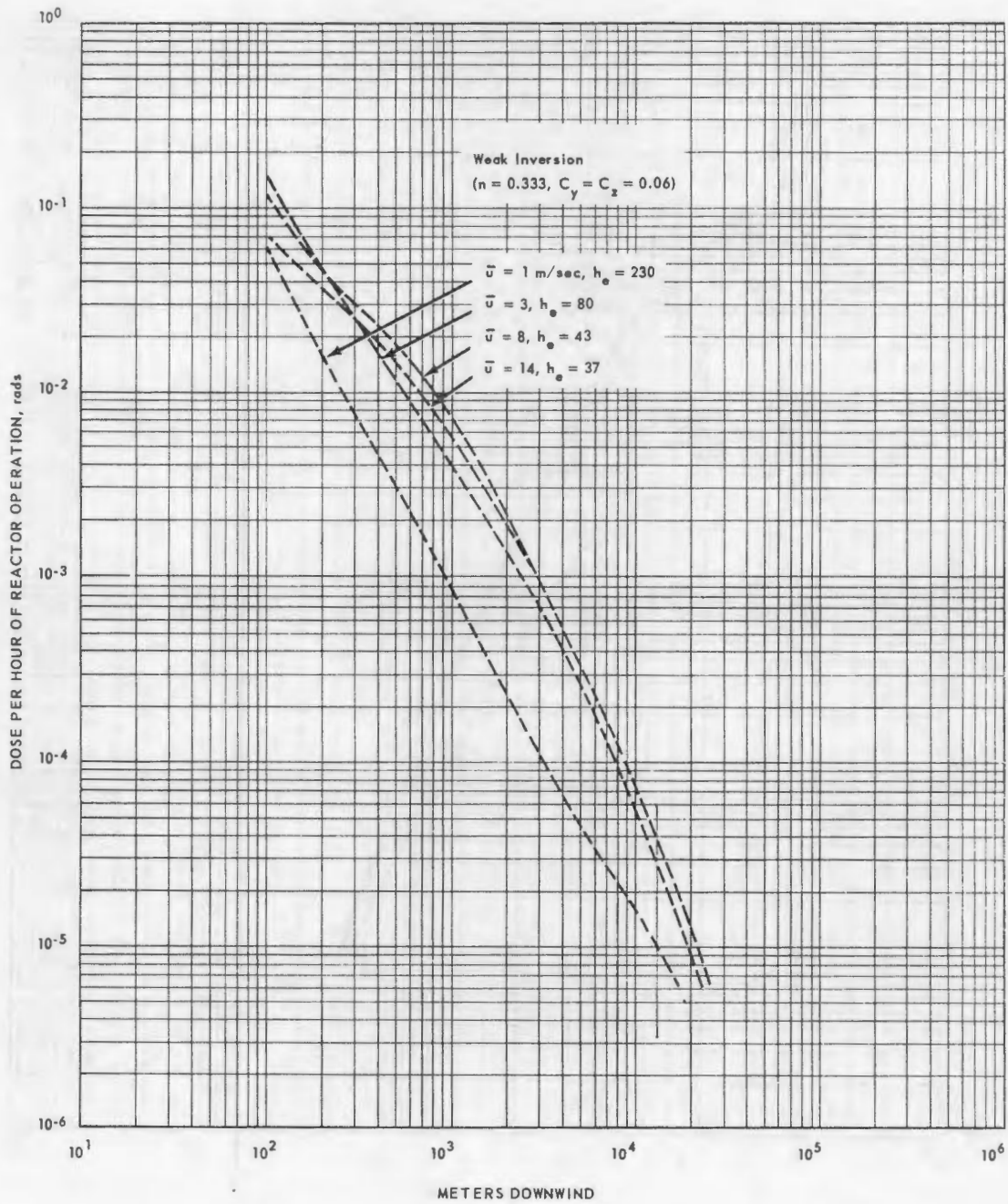


Fig. 6.11 - External dose from continuous release cloud in sector $\theta = 0.393$ for weak inversion

CONFIDENTIAL
SECRET

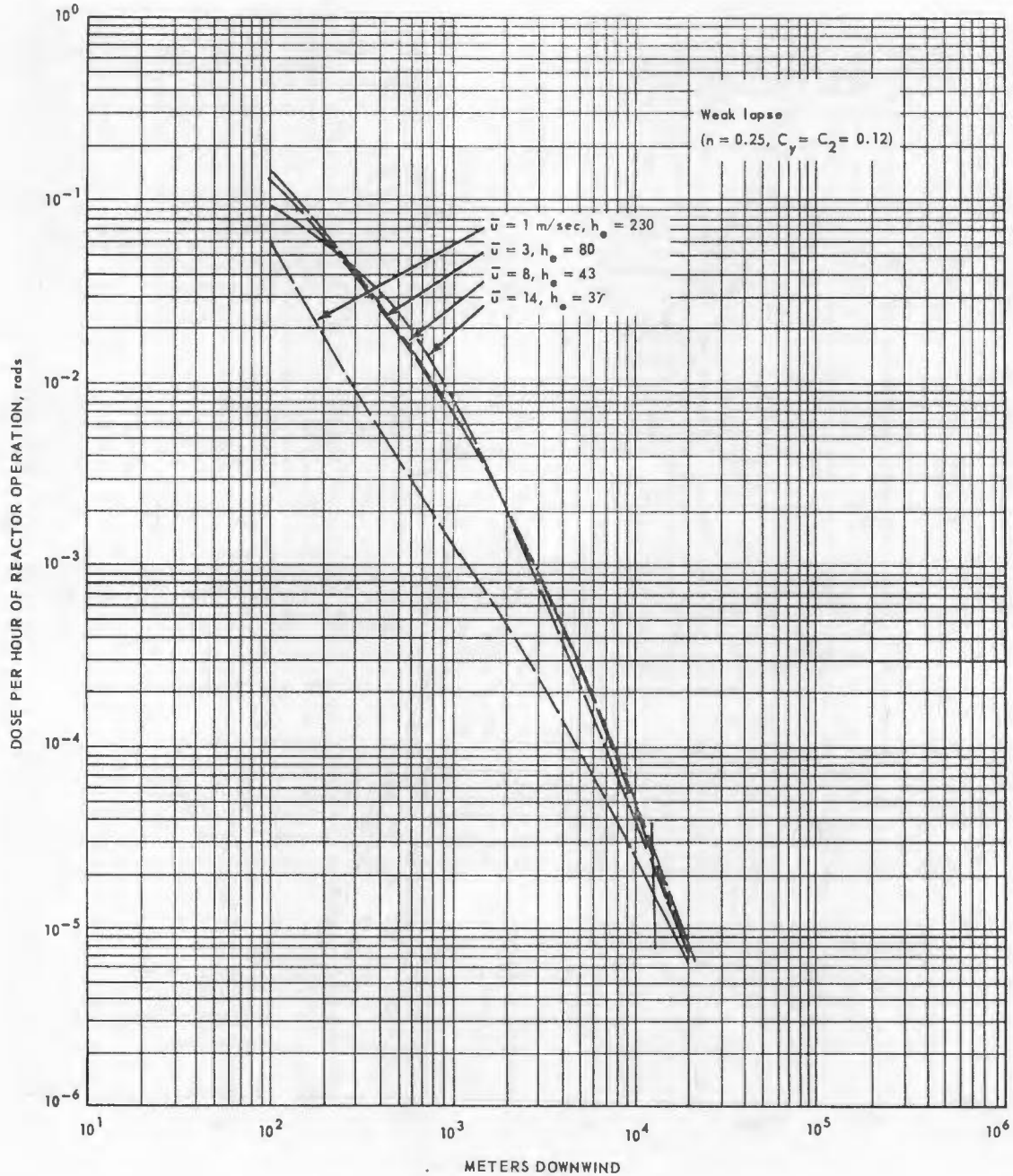


Fig. 6.12 - External dose from continuous release cloud in sector $\theta = 0.393$ for weak lapse

SECRET
CONFIDENTIAL

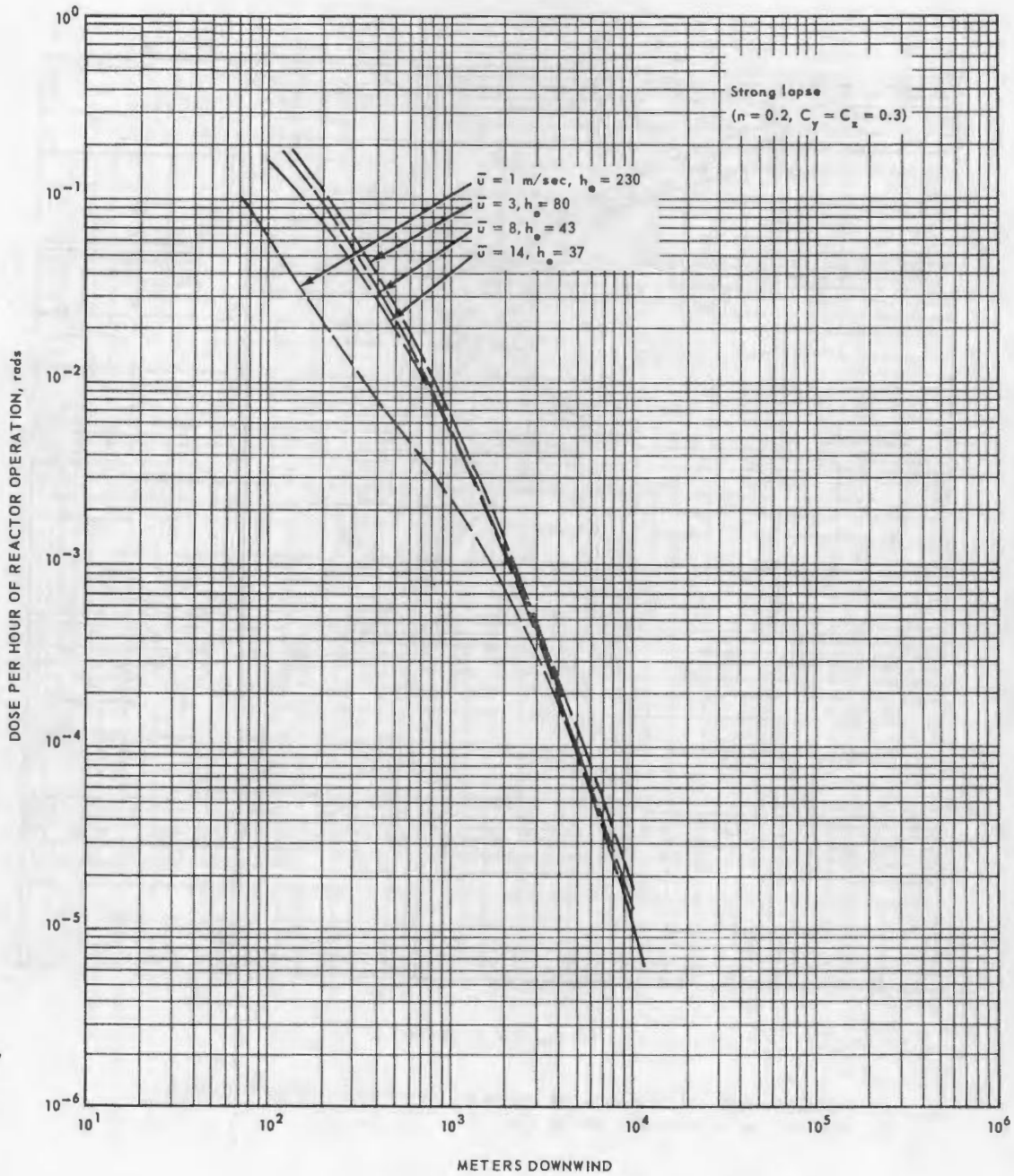


Fig. 6.13—External dose from continuous release cloud in sector $\theta = 0.393$ for strong lapse

CONFIDENTIAL
SECRET

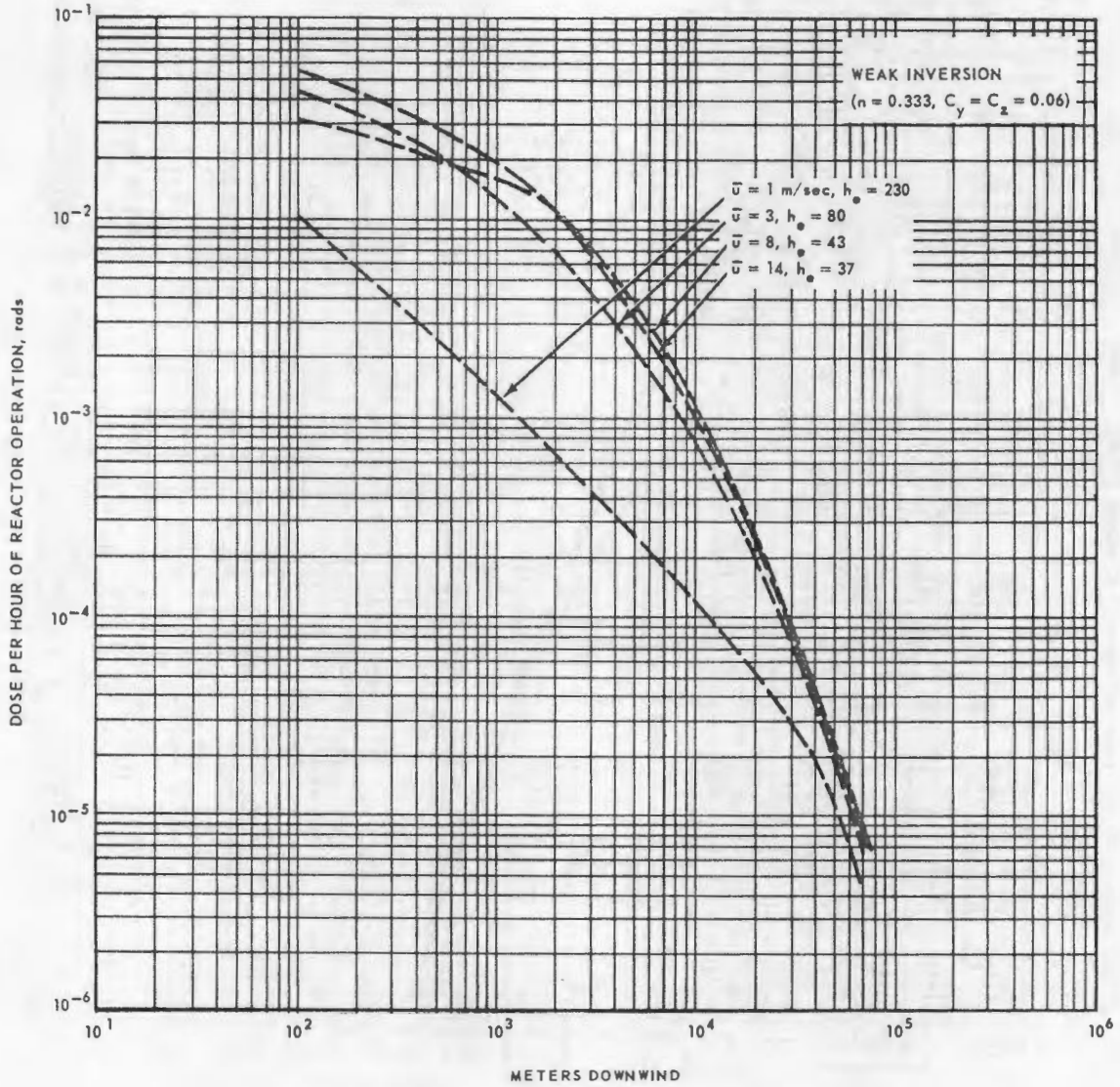


Fig. 6.14— External dose from continuous release cloud in sector $\Theta = 0.393$ for weak inversion, steady wind

SECRET
CONFIDENTIAL

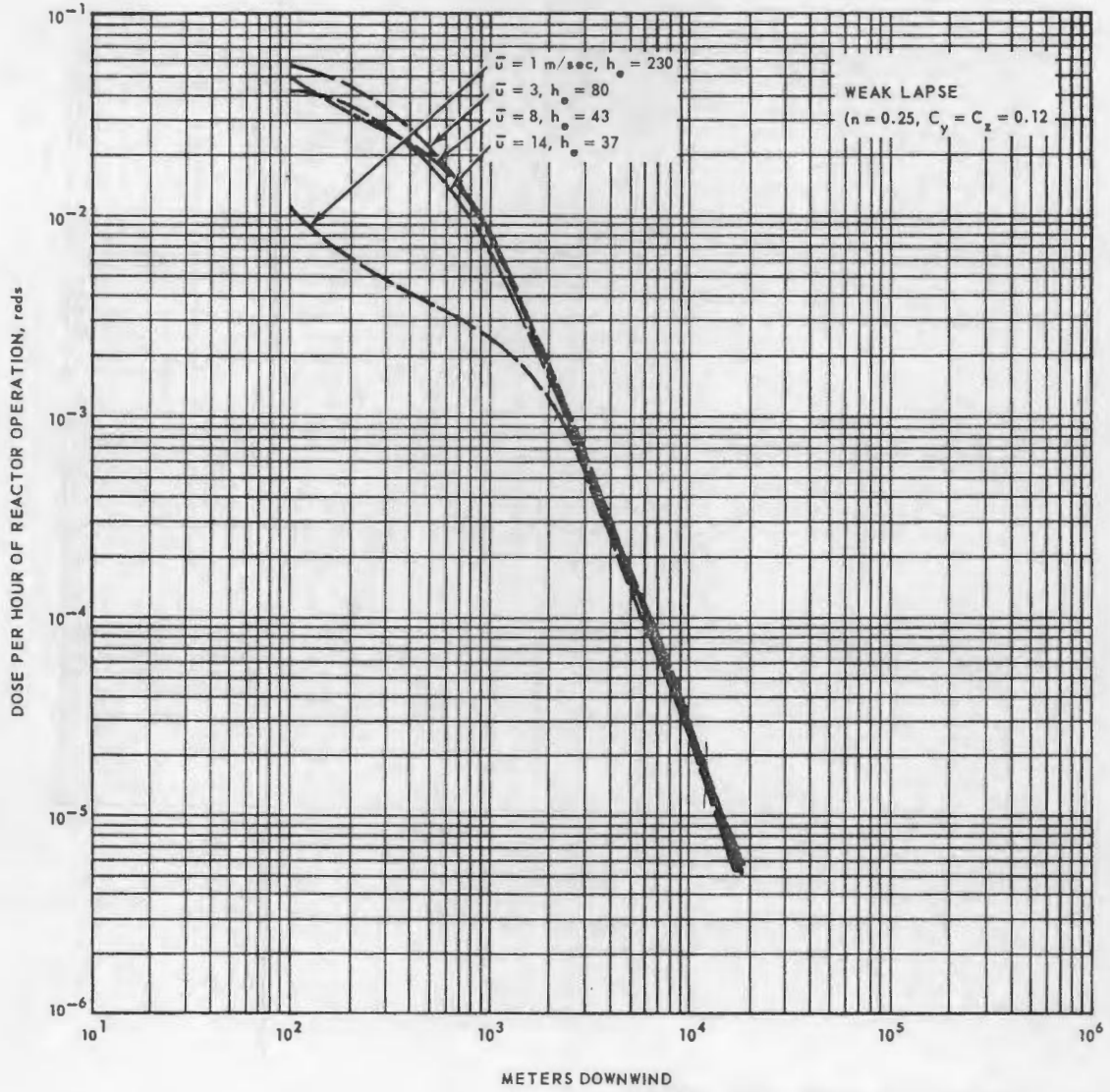


Fig. 6.15 - External dose from continuous release cloud in sector $\theta = 0.393$ for weak lapse, steady wind

~~CONFIDENTIAL~~
SECRET

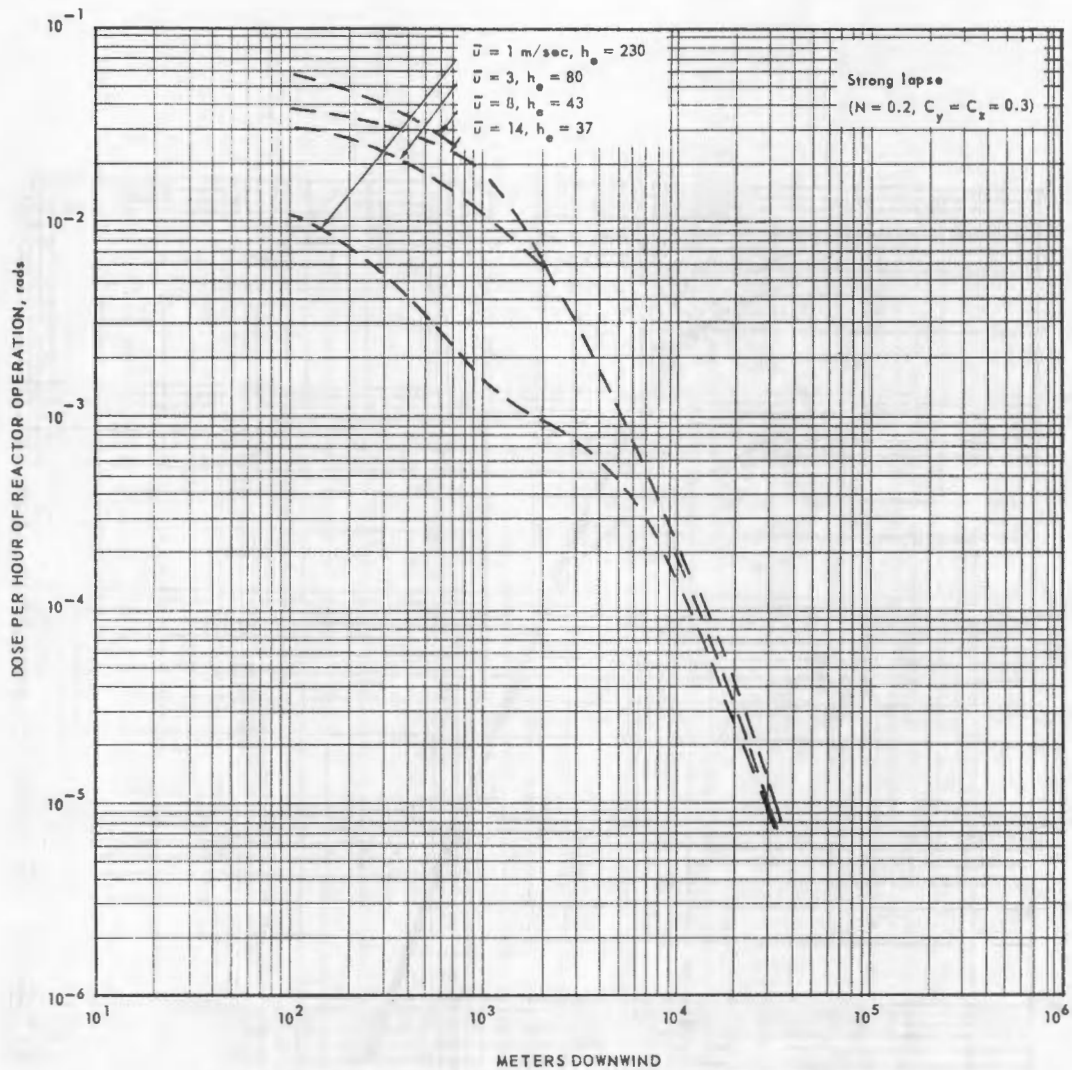


Fig. 6.16 - External dose from continuous release cloud in sector $\theta = 0.393$ for strong lapse, steady wind

6.3 ESTIMATED OFF-SITE DOSE

6.3.1 GENERAL

Doses to the people who inhabit the area surrounding the test site can be controlled during normal operation by operating the reactor during the time when the most favorable meteorological conditions for effluent dilution exist. The main factors to consider in this minimization of the hazard are the direction and distances to inhabited areas, the dilution of the effluent provided by the atmosphere, and the direction of the winds carrying the fission products.

The latest available data and techniques were used in estimating the degree of hazard that could exist when meteorological control is utilized for minimization of off-site hazard during normal operations. The analysis in general estimates the maximum dose to the

~~CONFIDENTIAL~~
SECRET

thyroid due to inhalation over given time periods by considering the relationship of the areas of nearest population, the wind distribution at the reactor site to 16 points of the compass as well as different stability classifications, and atmospheric dilution of the effluent utilizing a modification of Sutton's* diffusion equations.

6.3.2 INHABITANTS AND DAIRY CATTLE

6.3.2.1 Population Distribution in the NRTS Area

There are no inhabitants within 7 miles of the FET. Up to 20 miles, there are about 1200 residents. In the area between 20 and 35 miles from the FET, there are somewhat less than 6000 inhabitants. Table 6.4 gives the population, distance, and direction from the FET for all the inhabited communities within 35 miles.

A population distribution map is shown in Figure 6.17. The areas between communities may be considered to have less than one person per square mile.

Exclusive of personnel at the ANPD site, the maximum number of people within the boundaries of the NRTS during the day is 3000. This number drops below 1500 at night. These people are essentially all between 17 and 28 miles from the FET.

The region of southeastern Idaho within 100 miles of the site has a population of approximately 200,000. The major population area is located about 50 miles to the southeast.

6.3.2.2 Distribution of Dairy Cattle in the NRTS Area

The county agent of Jefferson County, Idaho, has estimated that the 1560 dairy cattle in the area near the ITS are distributed as follows:

Roberts	360
Hamer	490
Montevew	330
Mud Lake	380

For the most part, these cattle are fed on the previous year's crop of locally grown hay, which has been stored in stacks outdoors. About 10 percent of the dairy cattle are estimated to be fed by grazing, mostly in the Roberts area where some pasture exists.

Some additional information has been accumulated by Idaho AEC personnel who report that the Montevew - Mud Lake area contained 91 farms with one or more cows, the total number of cows being 583. Fifty of the 91 farms sold their milk to two creameries, Kraft's at Ririe and Challenge at either Rexburg or Idaho Falls. Since no grade A milk is produced in this area, the creameries use the grade B milk for cheese. Persons on 41 farms produce milk for their own consumption. Milk from 20 farms is sold to neighbors. There are approximately 111 families in the area consuming locally produced milk.

Forty-one farms pastured 221 cows on 367 acres for an average of 1.7 acres per cow. Only six farms supplemented pasture with hay. In August and September there may be some pasturing in harvested grain and hay (alfalfa) fields. Since alfalfa - particularly when covered with dew - causes bloat, pasturing in alfalfa is probably restricted to certain periods during the day.

6.3.3 DOSE DISTRIBUTION BY SECTORS

6.3.3.1 Analysis of Wind Distribution

From records of observed data taken at the 20-foot level of the meteorology tower at the IET installation, the distribution of winds was determined by 22.5-degree sectors

*O. G. Sutton, Micrometeorology, New York, McGraw-Hill Book Co., 1953.

~~CONFIDENTIAL~~
~~SECRET~~

TABLE 6.4
NATIONAL REACTOR TESTING STATION POPULATION DATA IN 1958

	Population ^a	Distance From FET, miles
Terreton - Mud Lake Area	500	10
Montevue Area	500	10
Howe Area	200	15
Winsper	5	20
Hamer Area	70	27
Atomic City	50	28
Butte City	150	29
Roberts	750	30
Lewisville	500	30
Menan	530	30
Dubois Area	500	30
Arco	1,850	31
Moore	850	35
Idaho Falls	28,400	40
Ucon	550	40
Rigby	2,500	40
Shelly	2,100	40
Iona	600	42
South End of NRTS (MTR, CPP, CFA, SPERT, EBRI Area)	Day shift Total	1600 2600
Naval Reactor Facility	Day shift Total	600 1100
Total Work Force at NRTS (Operations and construction)	All shifts	6000

^aPopulation data from R. Rossi, AEC-LAROO
Source: IDO. Populations include nearby ranches.

with the 16 points of the compass centered in the sectors. Wind speed and stability (lapse and inversion) classifications were determined for the winds in each sector. The wind roses are given in the appendix of this report. The data are the most representative information available for the GE-ANPD site and are considered to be representative of the wind conditions that prevail at the heights at which the effluents are released.

These data by sector, wind speed class, and season of the year were further separated by stability classifications of strong lapse, weak lapse, and weak inversion. The assumptions given in Table 6.5 were obtained by consideration of average temperature soundings and other climatological data given in IDO-10020* and IDO-12004[†] (see appendix).

The resulting information, presented in Figure 6.18, shows the number of hours each season that a particular stability condition may be expected to occur.

*D. A. Humphrey and E. W. Wilkins, (U. S. Weather Bureau), "The Climatology of Stack Gas Diffusion at the NRTS," IDO-10020, USAEC, March 1952.

†G. A. DeMarrais (U. S. Weather Bureau), "The Engineering Climatology of the NRTS," IDO-12004, USAEC, November 1958.

~~SECRET~~

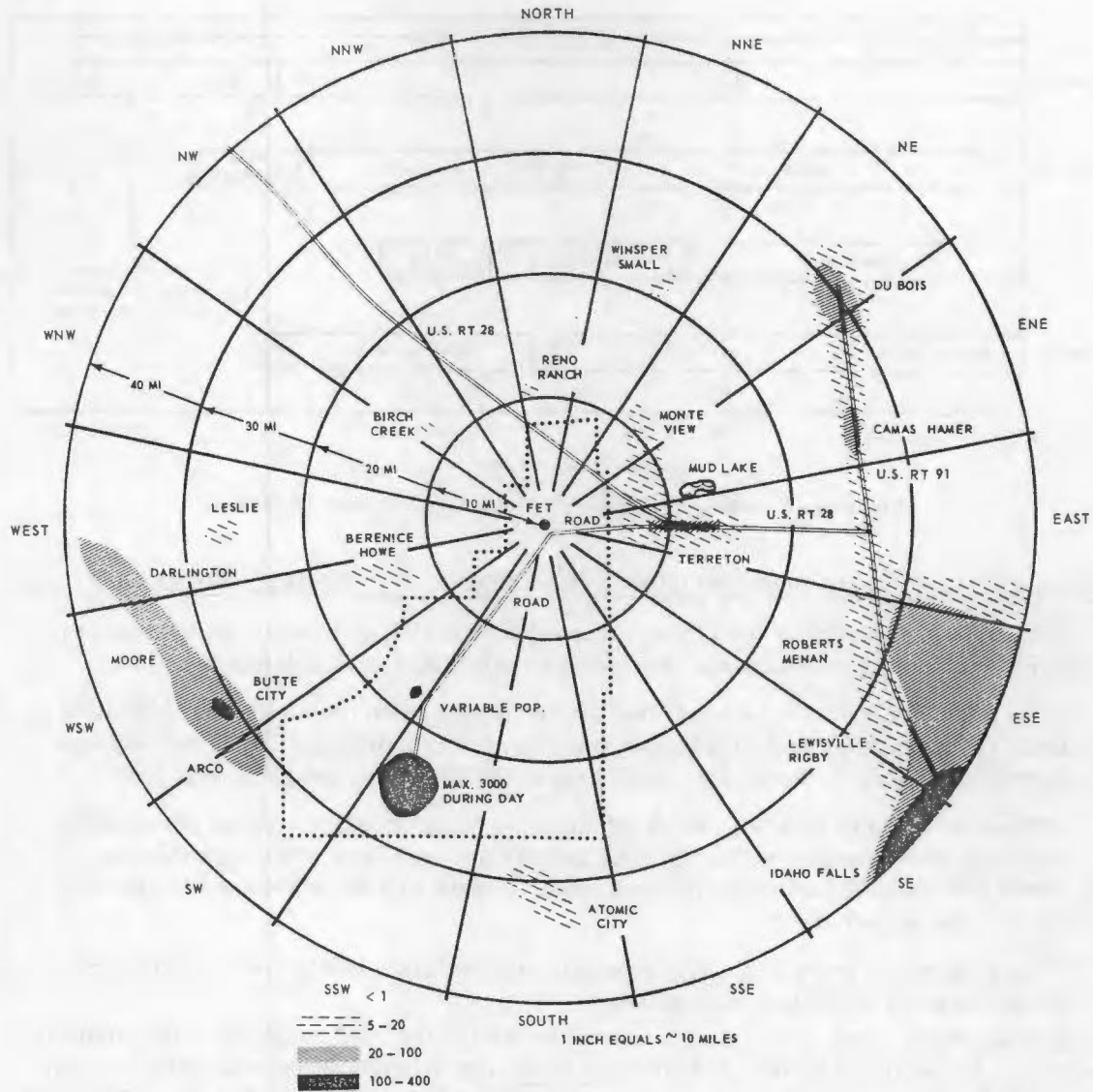


Fig. 6.17 - Population density around Flight Engine Test facility

TABLE 6.5

ESTIMATED HOURS PER DAY OF DIFFERENT STABILITY CLASSIFICATIONS FOR THE SEASONS OF THE YEAR AT THE GE-ANPD SITE AT NRTS

Season	Meteorological Stability Conditions, hours/day		
	Strong Lapse	Weak Lapse	Weak Inversion
Spring	6	9	3
Summer	9	4.5	2
Fall	7	3.8	2
Winter	4	6.5	6

~~CONFIDENTIAL~~
~~SECRET~~

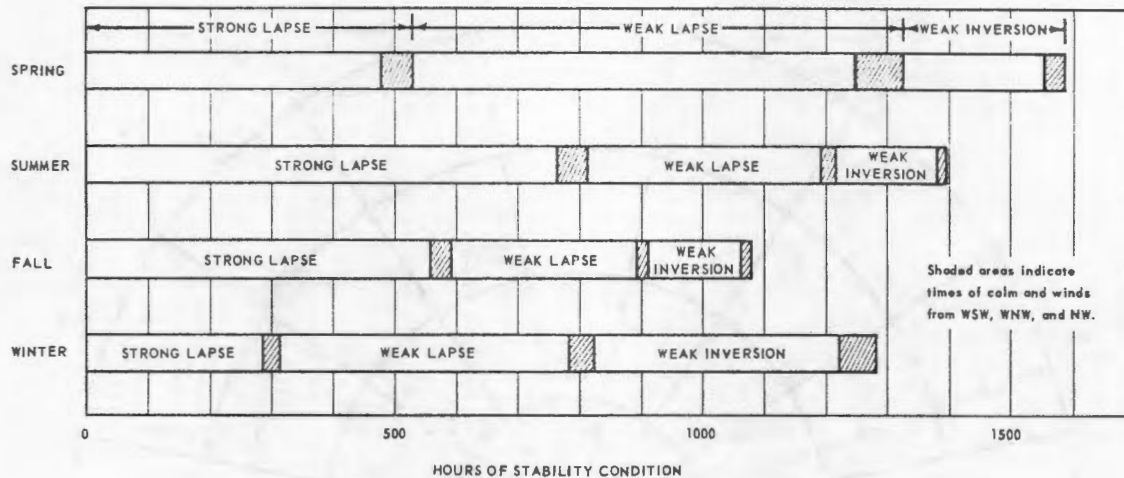


Fig. 6.18 - Possible meteorologically stable operating hours by season

6.3.4 ESTIMATION OF DOSE TO OFF-SITE PERSONNEL - NORMAL OPERATION

Operation of reactors at the ITS is governed by a series of general operating rules. The rule pertaining to continuous or expected evolution of radioactivity is stated:

"The power plant will not be operated above standby when the actual dose resulting from any continuous evolution of radioactivity, or the calculated dose from any expected release of radioactivity, would exceed the limits for the particular test.

"These dose limits will be some fraction of the occupational maximum permissible exposure for personnel within the ANP monitoring area. For other locations on NRTS and off-site, the exposure limit for ANP tests will be established by the AEC on a calendar year basis.

"The expected release of activity refers to any operation in which a deliberate release of radioactivity is contemplated."

For locations other than those monitored by ANPD, the AEC establishes the limits for estimated dose to personnel. The AEC currently has allotted 100 percent of the annual permissible off-site radiation exposure as specified in ID-0500 - 7 - 071 for ANPD operations. The current limitation is therefore 3.0 rem to thyroid or skin, 1.5 rem to other critical organs, and 0.5 rem to the external whole body.

From preceding meteorological data, it is apparent that satisfactory meteorological conditions for reactor operation can be expected to prevail for more than 1000 hours in any given season. A 200-hour reactor test program can therefore be easily completed in any given season by operating the reactor less than 20 percent of the time during which the diffusion conditions are adequate.

In estimating the doses to the thyroid from inhalation of radioactive material by off-site personnel, the 200 hours of reactor operation was assumed to be accomplished in each of the four seasons. The frequency of the stability classifications (strong lapse, weak lapse, and weak inversion) satisfactory for operation, the wind speed classes, and the wind directions during the 200 hours were selected to be proportional to those existing during the season considered. Measured values for the fractional release of fission products and air cleaning efficiency were used, and doses were calculated for the nearest off-site personnel in the various sectors around the ITS monitoring areas. The results of these calculations are shown graphically in Figures 6.19 through 6.22.

~~SECRET~~
~~CONFIDENTIAL~~

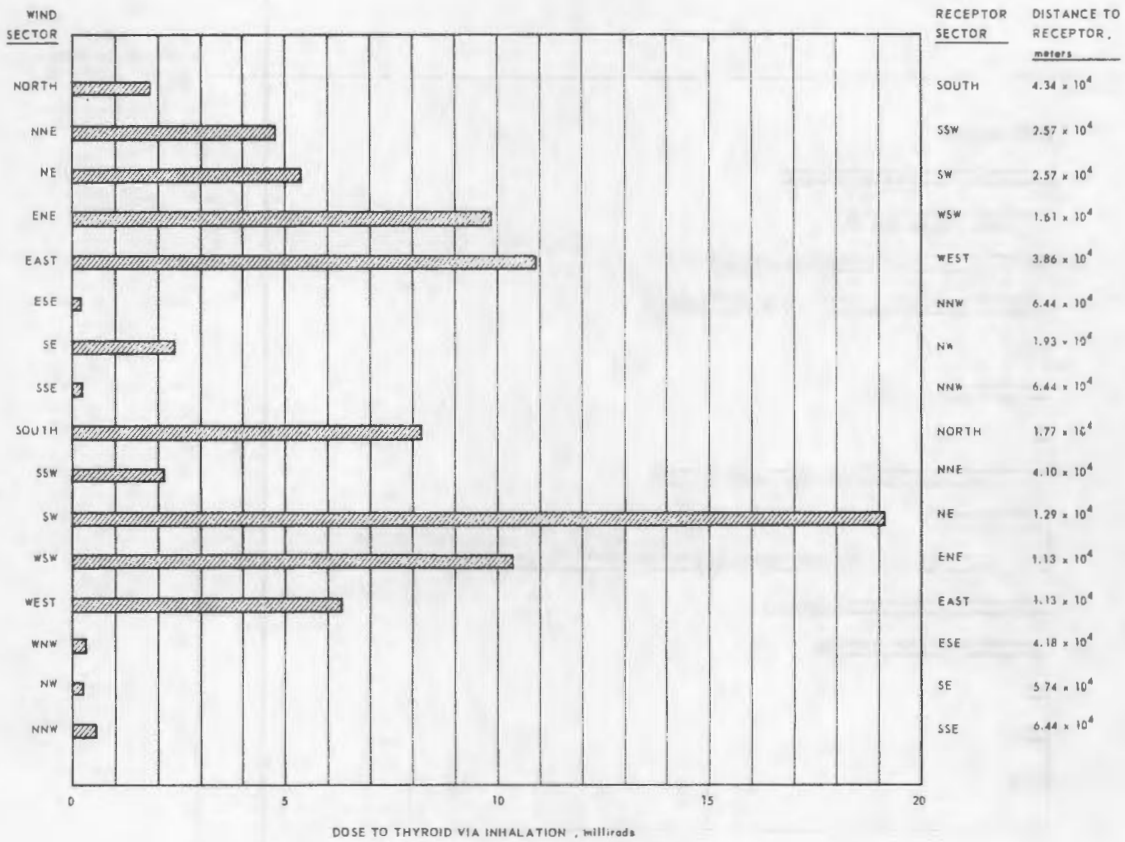


Fig. 6.19 - Dose to thyroid from inhalation after 200 hours of operation at 50 megawatts with no air cleaning during typical spring meteorological conditions

~~CONFIDENTIAL~~
SECRET

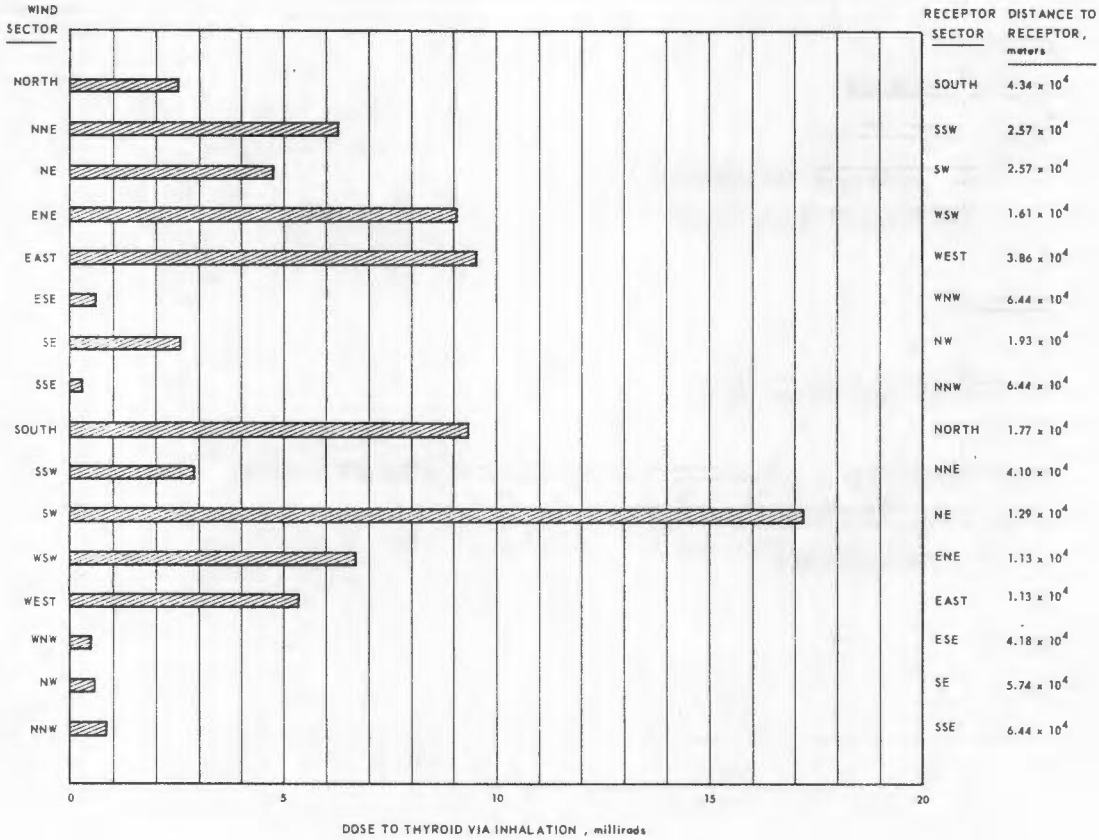


Fig. 6.20 - Dose to thyroid from inhalation after 200 hours of operation at 50 megawatts with no air cleaning during typical summer meteorological conditions.

~~CONFIDENTIAL~~
SECRET

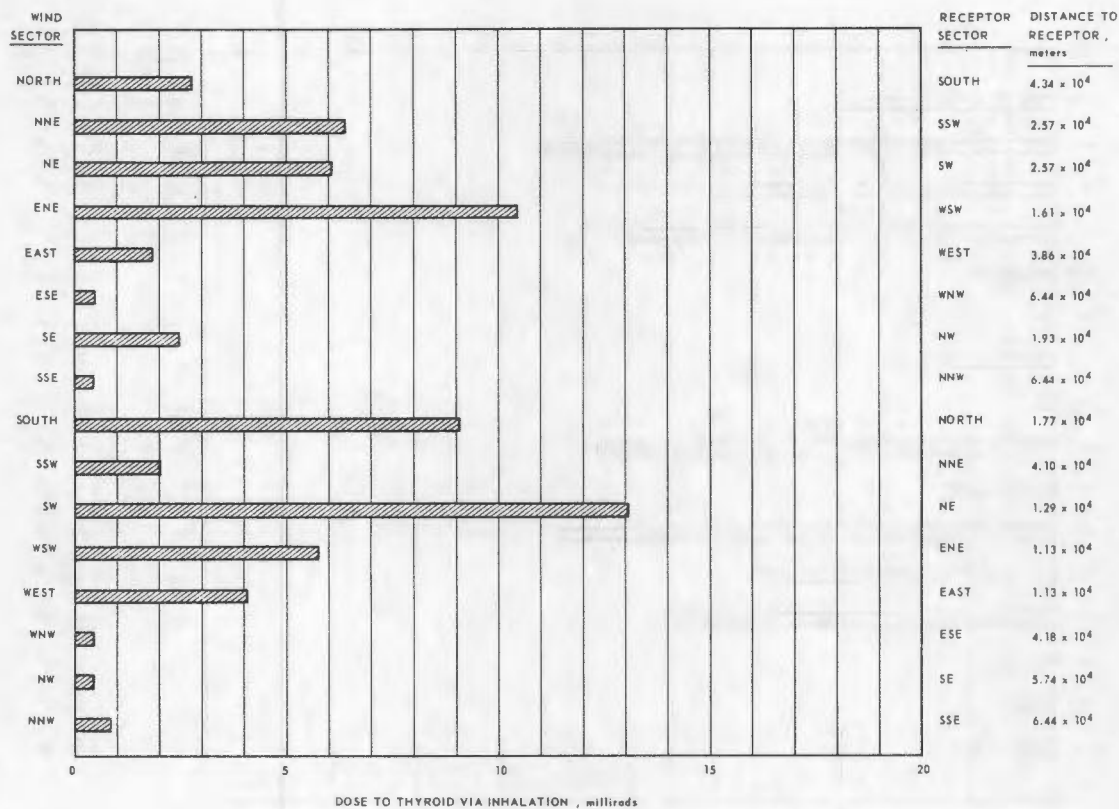


Fig. 6.21 - Dose to thyroid from inhalation after 200 hours of operation at 50 megawatts with no air cleaning during typical fall meteorological conditions

CONFIDENTIAL
SECRET

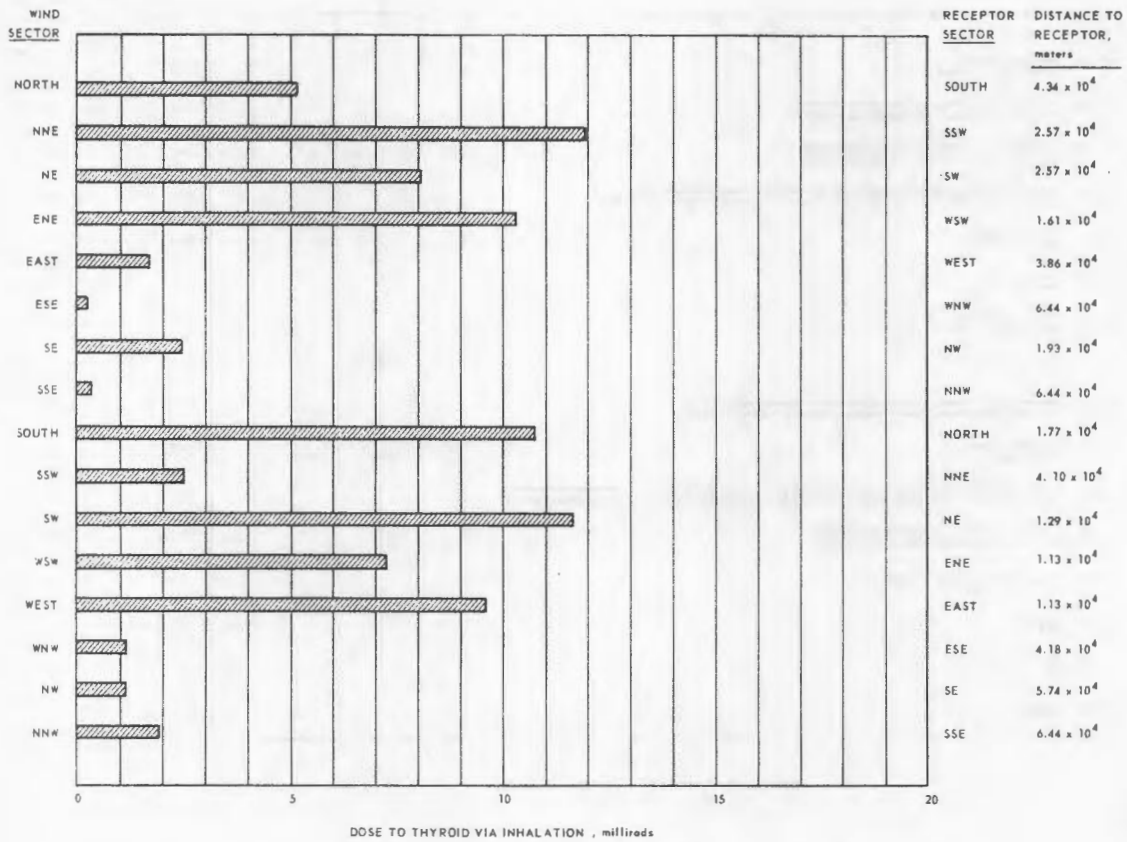


Fig. 6.22—Dose to thyroid from inhalation after 200 hours of operation at 50 megawatts with no air cleaning during typical winter meteorological conditions

SECRET
CONFIDENTIAL

Figures 6.19 through 6.22 indicate that 200 hours of reactor operation during "typical" meteorological conditions for any season will result in doses of less than 20 millirads to the thyroid of nearest off-site personnel from inhalation when no air-cleaning device is used in the effluent stream. The graphs indicate the doses for the various wind sectors, receptor sectors, and distances to the nearest receptors with respect to the FET.

Calculations for the thyroid inhalation doses made use of representative meteorological parameters for the seasons without regard to on-site G-E facilities. Winds from the WSW, WNW, and NW sectors may carry the effluent over G-E facilities on the site. These facilities are all monitored by G-E health physics personnel, and exposure of personnel is readily evaluated and controlled. If it appears desirable to avoid these sectors, operation can be controlled without undue operational hardship since these winds prevail a relatively small fraction of the time.

6.4 CALCULATED DOSES FOR MAJOR ACCIDENTS

Analysis of various kinds of major accidents including startup accidents and after-shutdown meltdown indicates that they may all end up as nuclear excursions with a total energy release during the excursion of about 2.8×10^{10} watt-seconds and with the vaporization of about 4 percent of the reactor core material. Small-scale laboratory experiments with molten fuel indicate the release of about 75 percent of the iodine from the melt and less than 10 percent of the gross activity and bone seekers. Since the shutdown mechanism is violent, it is expected that some small particles of the core may be airborne in addition to those released to the air as vapor. While the calculations assume complete melting, there must be some portion of the disrupted core that will not melt. In addition, because of the violence of the disruption the unvaporized portions will be scattered in relatively small masses, which will not remain molten for very long. Thus, it would appear pessimistic to assume that half of the total iodine and a tenth of the gross activity would be released.

Dose calculations are based on this assumption and the assumption of an operating power level of 50 mw during a series of 18 ten-hour operating periods spaced 4 days apart, followed by a 25-hour continuous operation.

Most operating periods will normally take place during daylight hours when lapse conditions prevail; however, since there is a possibility that a major accident may take place during an inversion, meteorological parameters of $n = 0.333$, $c = 0.06$, and a low wind speed of 1 m/sec were selected for calculating the dosages downwind. While allowance is made for decay of fission products, no correction was made for any reduction of dose because of depletion of the cloud by deposition on the ground or vegetation. The doses to the thyroid, lung, and bone as a function of distance from the source are given in Figure 6.23, and the results for cloud gamma and deposited gamma doses for both infinite exposure and during the first day are given in Figure 6.24.

At the distance to the nearest inhabited area (about 1.1×10^4 meters) and assuming evacuation within 24 hours, the total dose to the thyroid is about 2900 rads and total doses to both the lung and bone are about 800 rads. If the accident took place during weak lapse, the doses would be less by a factor of 10. If the accident took place during a strong lapse, they would be less by a factor of 100. Doses would also be reduced if the wind speed were increased.

The calculated correction factors for other possible operating times are given in Table 6.6.

CONFIDENTIAL
SECRET

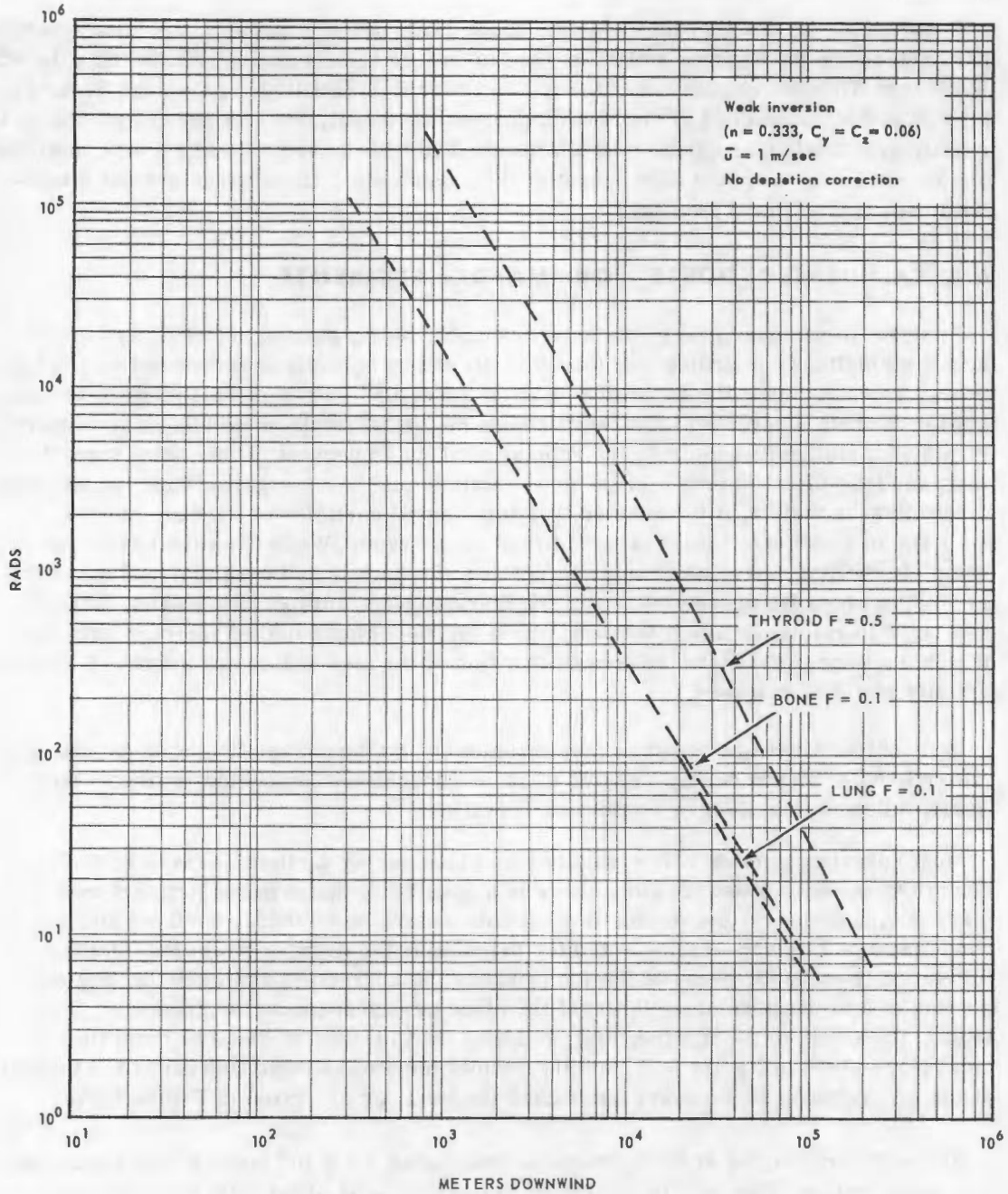


Fig. 6.23—Doses to thyroid, lung, and bone as a function of distance from the source

SECRET
CONFIDENTIAL

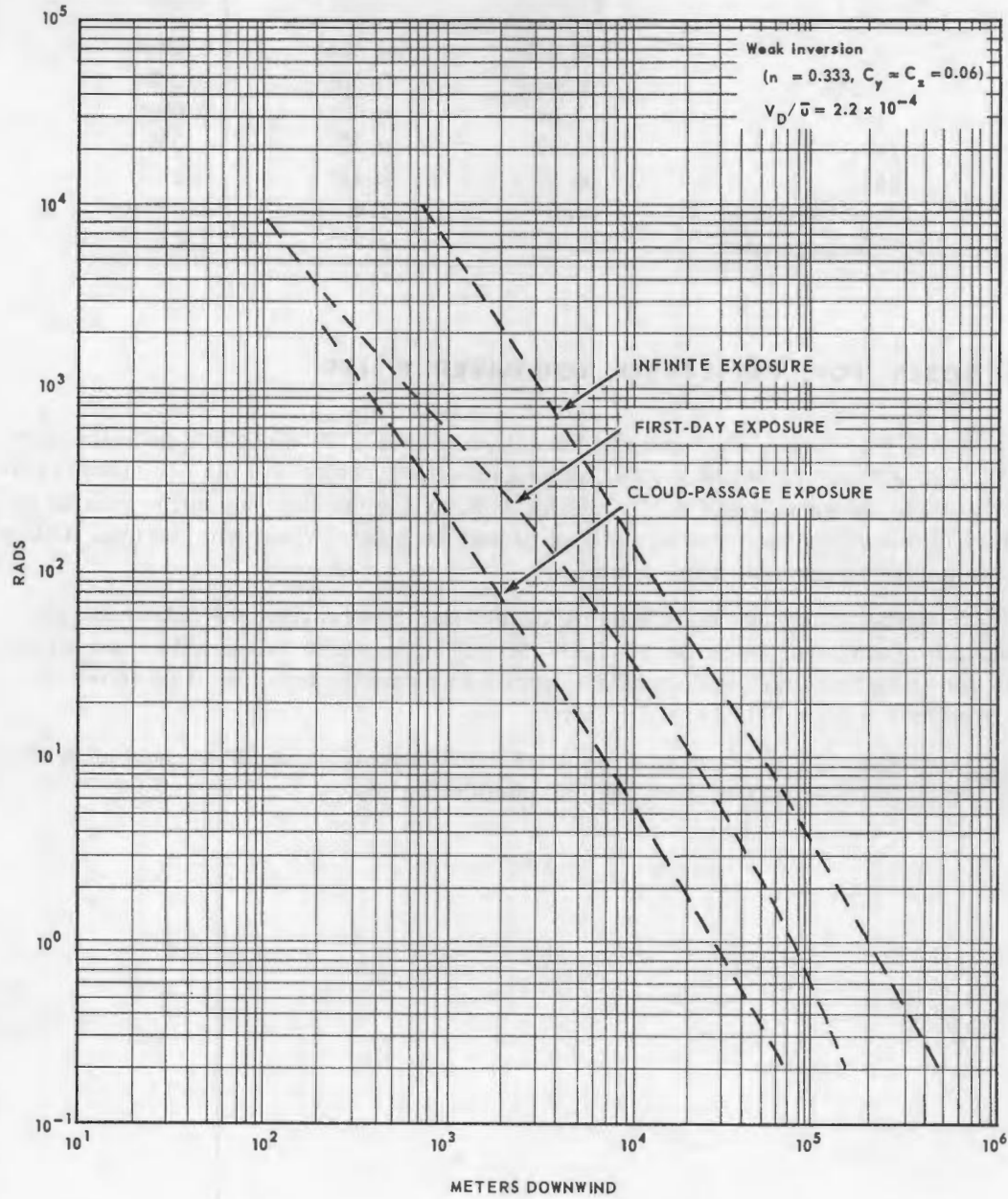


Fig. 6.24—Cloud and deposited external gamma doses after first-day and infinite exposures

CONFIDENTIAL
SECRET

TABLE 6.6

DOSE CORRECTION FACTORS FOR OTHER OPERATING TIMES
FOR NEAREST POPULATED AREA ($X = 1.1 \times 10^4$ m)

Time, hr	Thyroid	Lung	Bone
0	0.009	0.004	0.0014
0.167	0.018	0.008	0.0028
1	0.06	0.031	0.0095
10	0.37	0.22	0.083
25	0.67	0.46	0.21
205 accumulated	1.0	1.0	1.0
1000 accumulated	2.0	3.2	3.75

6.5 DOSES FOR DETECTABLE LOCALIZED MELTS

The LIME experiment indicated that the effluent from a 19-tube blockage in the ACT would be detectable above the normal continuous activity release. This detection is primarily due to the short-lived fission products. Since the melting may occur with an inventory of older fission products, the hazard may be greater than would be indicated by the comparative readings on the detectors.

Since 19 tubes represent about 0.08 percent of the total reactor, the maximum dose downwind should never be more than 0.08 percent of the doses calculated for the complete core meltdown case and should be appreciably smaller than this if shutdown of the reactor is accomplished expeditiously.

On this basis, then, the thyroid dose at 1.1×10^4 meters should be no more than 2.3 rads, which is less than the allowable maximum of 3 rads.

SECRET**CONFIDENTIAL**

~~CONFIDENTIAL~~
~~SECRET~~

7. CONCLUSIONS

A testing program for the direct-cycle reactor operating a total of 200 hours per season on nuclear power with coated ceramic fuel elements may be completed with negligible exposure to inhabitants of the areas surrounding the Idaho Test Station. The maximum dose to the thyroid of the nearest inhabitants will probably be less than 20 millirads as a consequence of inhalation of the fission products if no air cleaning device is used, and doses to other critical organs and the whole body will be considerably less than 20 millirads. Use of an air cleaning (electrostatic) device of the type currently being tested might be expected to lower this thyroid dose by a factor of about 10.

Doses to the thyroids of children in the area that result from iodine in the milk cycle could approach 3-rad yearly limit if the testing is accomplished during the summer season, unless the operating periods are controlled. However, extensive field monitoring will generate the data necessary to provide operational controls needed to assure that the 3-rad limit will not be exceeded.

Localized-melting accidents caused by interference with normal cooling airflow to small portions of the reactor are detectable because of increased fission product emission. Melting can be limited so that such accidents do not degenerate into large meltdowns.

Major reactor excursions caused by either control malfunction or complete core meltdown are possible only with the concurrent failure of multiple safety systems and have a very low probability of occurrence. The doses to off-site inhabitants in the event of such an accident may be significant but should not be lethal.

~~SECRET~~

~~CONFIDENTIAL~~

8. APPENDIX

8.1 SITE AND FACILITIES

8.1.1 GENERAL DESCRIPTION

The ANPD test site is located in the northeastern part of the National Reactor Testing Station (NRTS), Idaho Falls, Idaho. The NRTS lies on the west side of the semi-arid Snake River Plain in southeastern Idaho and is bounded by mountain ranges about 10 to 15 miles to the northwest, approximately 30 miles to the north, and roughly 50 miles to the east. The mountains to the north form an unbroken barrier of the Snake River Plain, while the ranges to the northwest and southeast, which form the sides of the Plain, are penetrated by deep valleys oriented northwest-southeast. It has an average elevation of 5000 feet above mean sea level. The location is remote from heavily inhabited sections. There is no agriculture within the NRTS and very little immediately outside the boundaries. Figure 8.1 shows the location of the NRTS and its relation to the surrounding terrain. The ANPD site, other major installations, and main highways at the NRTS are shown in Figure 8.2.

The ANPD area is generally a valley floor, which rises gradually toward the northeast. It has the lowest elevation of the NRTS and was at one time the site of end points, or sinks, of several rivers or creeks originating in the mountains to the northwest. Diversion of water upstream for irrigation has resulted in dryness in the lower reaches of the channels for many years. Surface drainage is good. The entire area is underlaid by a series of lava flows, and outcroppings are numerous. The region is semi-arid, and desert-like characteristics prevail. The ground is sparsely covered with vegetation, predominantly sagebrush and other desert plants. Figure 8.3 shows typical ground cover.

8.1.2 TEST FACILITIES

The reactor system is to be tested in the Flight Engine Test (FET) facility. The location of the FET and the other test and supporting facilities at the ITS are shown in Figure 8.4. The FET area (lower left in Figure 8.4) has a four-rail track system for movement of test apparatus between the maintenance and test buildings. A shielded locomotive provides power for movement of equipment on the rail system. A road to the facility for trucks and automobiles will be provided that has a branch that is shielded for safe access to the control and equipment building during reactor operation. An illustration of the facility is shown in Figure 8.5. Figure 8.6 and 8.7 show the floor plan and vertical section of the installation.

The FET facility roof is a reinforced concrete arch with exterior ribs. The clear interior span is 320 feet, and the interior length is 234 feet. The enclosed area is 74,880 square feet. The roof rises from 24 feet at the spring line to a clear height of 99 feet at centerline of the building. The front wall is closed by rolling doors, remotely operated from the control room and covering a width of 240 feet. The remaining portion of the rear wall is closed by steel framing and metal panels. The power plant coupling station is lo-

~~CONFIDENTIAL~~
~~SECRET~~



Fig. 8.1—N.R.T.S. and its relation to surrounding terrain

~~SECRET~~
~~CONFIDENTIAL~~

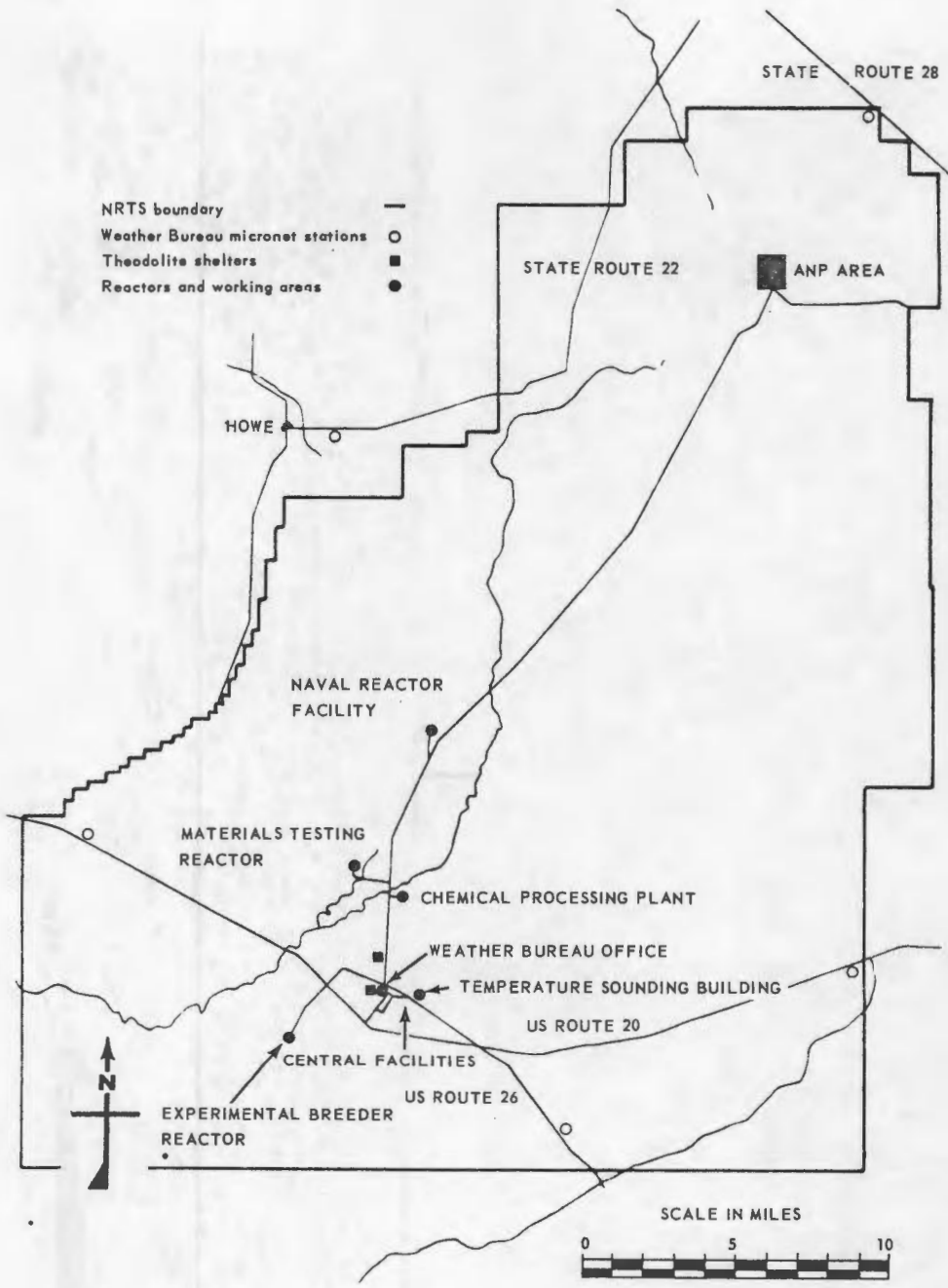


Fig. 8:2—Location of ANPD area at NRTS

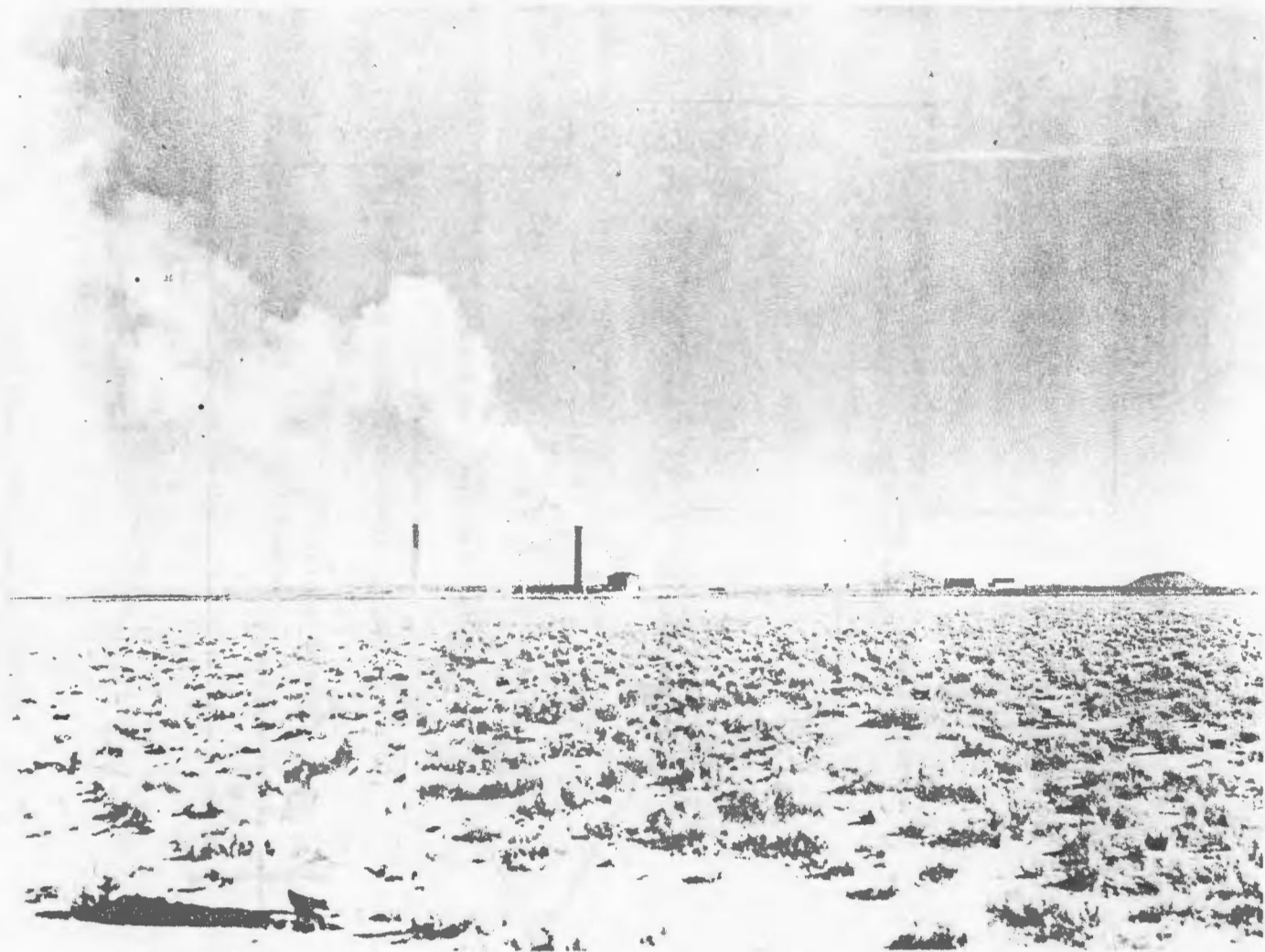


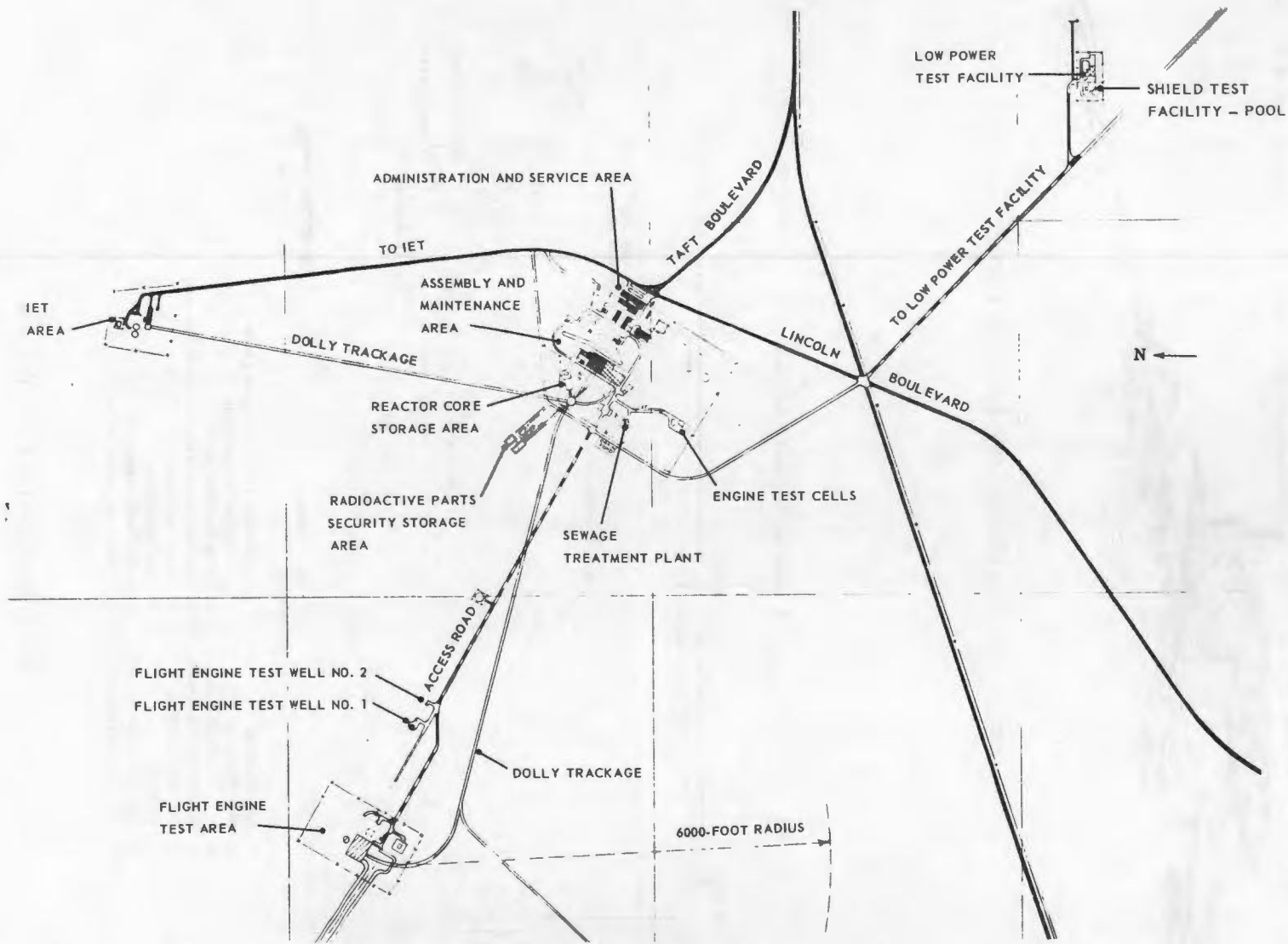
Fig. 8.3 - Typical vegetation covering the ANPD site at NRTS (cinder buttes are visible in background)

~~CONFIDENTIAL~~
SECRET

~~CONFIDENTIAL~~
SECRET



SECRET
CONFIDENTIAL



CONFIDENTIAL
SECRET

Fig. 8.4 - Idaho Test Site layout

~~CONFIDENTIAL~~
SECRET

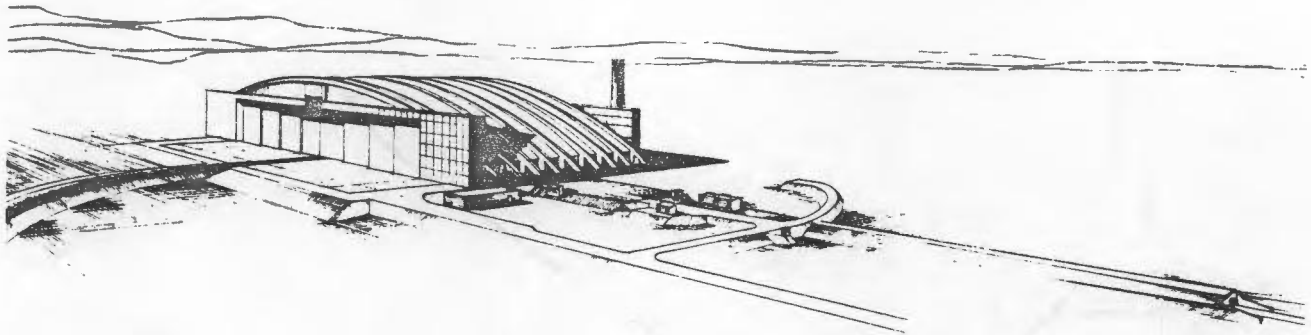
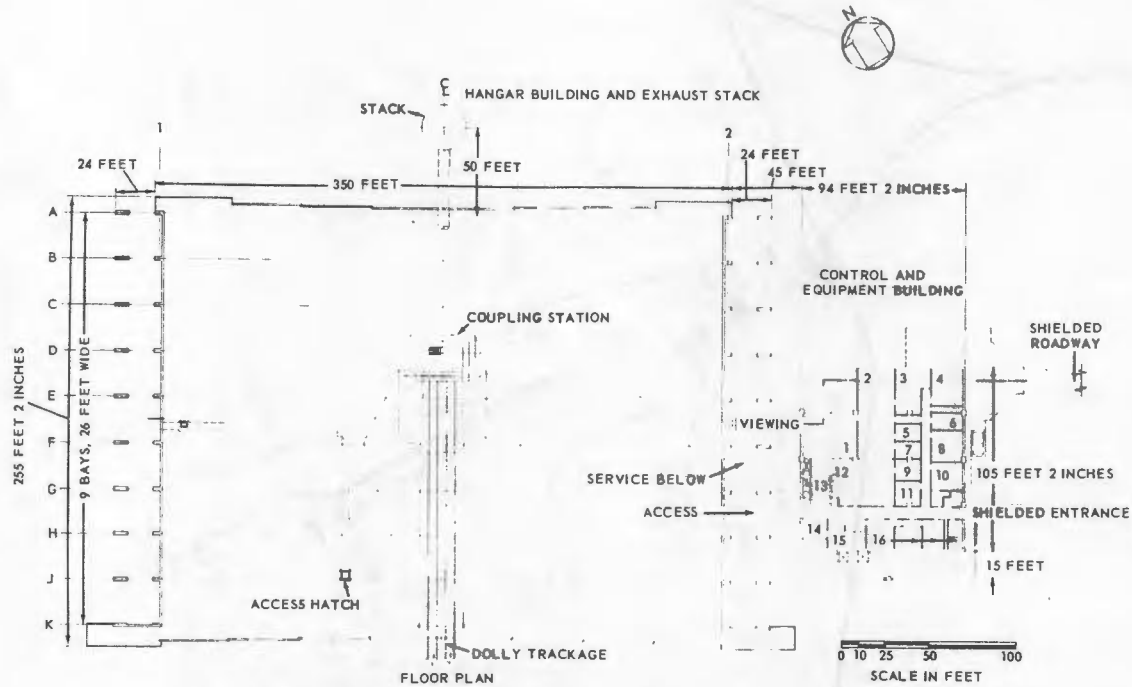


Fig. 8.5 - Illustration of Flight Engine Test facility building



- | | |
|---------------------------|--|
| 1 CONTROL ROOM | 9 INSTRUMENTATION SUPERVISOR'S ROOM |
| 2 DATA ROOM | 10 TECHNICAL BRIEFING ROOM |
| 3 DATA REDUCTION ROOM | 11 HEALTH PHYSICS ROOM |
| 4 FLIGHT OPERATIONS ROOM | 12 INSTRUMENTATION REPAIR AND HOLDING ROOM |
| 5 DATA ANALYSIS ROOM | 13 COUNTING ROOM |
| 6 KITCHEN | 14 UNDRESSING ROOM |
| 7 CONTROL OPERATIONS ROOM | 15 WASH AND SHOWER ROOMS |
| 8 PLANT OPERATIONS OFFICE | 16 LOCKER AND TOILET ROOMS |

Fig. 8.6 - Flight Engine Test facility floor plan

SECRET
~~CONFIDENTIAL~~

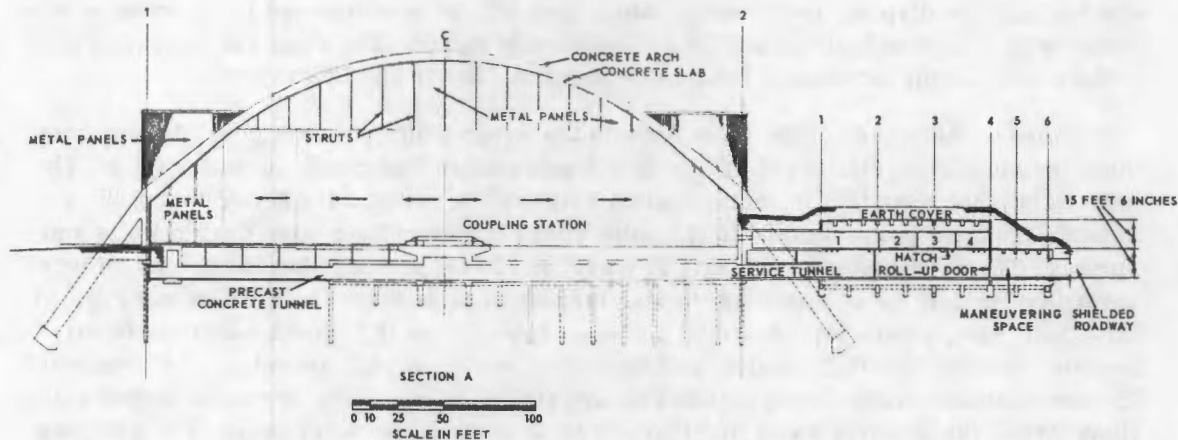


Fig. 8.7 - Cross section of Flight Engine Test facility

cated near the center of the structure and is connected to the control and equipment building by a tunnel. The building will be heated and ventilated with package-type units.

The control and equipment building is an underground two-level reinforced-concrete structure, shielded by its concrete structure and a covering earth embankment.

The control, data-processing, counting, and shielded-enclosure rooms will be air conditioned year-around. The cable, water-pump, and fuel-pump rooms will be heated and ventilated. The remainder of the building will be heated and evaporative cooled.

8.2 GEOPHYSICAL CHARACTERISTICS AT NRTS

8.2.1 HYDROLOGY AND DISPOSITION OF LIQUID WASTES

The water table is at a depth of about 200 feet at the northern boundary of the IET site and about 550 feet at the southern boundary. It is believed that at least 1500 second-feet constitutes the underflow beneath much of the NRTS area and that about 300 second-feet flow under part of eastern and southwestern portions. The rate of flow is estimated at an average velocity of one-half mile per year. It is believed that the nearest point of surface discharge is along the banks of the Snake River below the American Falls Reservoir, 75 miles from the site, where numerous springs issue from porous lava beds.

Surface drainage at NRTS is southerly toward a low area in which Big Lost River, Little Lost River, and Birch Creek formerly disappeared. Construction of dams at the headwaters of these streams and irrigation diversions has moved the disappearance points upstream. Although the area slopes vary moderately, the site has good drainage because of the limited rainfall and the permeability of most areas. Surface water is rapidly absorbed after rainfall. With the exception of Mud Lake, located northeast of the site, the land is well drained and devoid of swampy areas.

Since the fuel element materials are not to be reprocessed at this installation, the only liquid wastes to be disposed of are minor amounts of contaminated liquids from the shield, solutions used in the clean-up of contamination in the hot shop, and small amounts of chemical wastes from the inspection cubicle and laboratory. The contaminated fluids from the hot shop will be filtered to remove the particulate activity; and, if the activity levels

~~CONFIDENTIAL~~
~~SECRET~~

are too high for disposal to the water table, they will be concentrated in the waste evaporator in the hot shop building and then permanently stored. The same concentration procedure is available for wastes from the inspection cubicle and laboratories.

Because of the nature of the water flow in the water table, it is not possible to depend upon any significant dilution of radioactive liquid wastes that reach the water table. The only significant reduction in contamination arises from radioactive decay during their passage from the point of entry to the point where they may be removed from wells and springs. The estimated average rate of travel is 33 feet per day, but there may be local variations so that the recommended value for use in calculations is 330 feet per day. At this "fast" rate, wastes introduced to the water table at the IET would reach the Naval Reactor Facility site in 272 days. Radiochemical analyses will, therefore, be required for those mildly contaminated liquids that are above the maximum permissible concentrations (MPC) for drinking water and that are to be put into the water table. The analyses will have to be complete enough to identify the radioactive elements so that calculations can be made to determine the expected concentrations at a future time when these waste liquids will have traveled in the water table to a point where withdrawal and consumption is possible.

8. 2. 2 GEOLOGY

The entire area is underlaid by a series of Pleistocene lava flows, which are covered in places by soil or alluvium from a few inches to more than 100 feet in thickness. The flows, which range in thickness from about 35 feet to 150 feet, are frequently separated by layers of sand, gravel, or clay.

The lava, whenever exposed, is very uniform in appearance and character and is very porous and vesicular in composition. The lava is very fluid when hot and is thought, in general, to have issued from fissures rather than volcanoes. Its fluid character accounts for the large nearly flat level surfaces found in these areas. In addition to its vesicular character, which accounts for part of its porosity, lava flows frequently contain tunnels and cavities as the result of the top cooling and forming a stationary crust while the hot interior portion continues to flow, leaving a tunnel or cavity.

In places the surface of the lava is covered by gravel that apparently was deposited by former streams. This gravel is 1 to 2 inches in size, and the pebbles are mainly fine-grained limestone with some igneous stones.

Near the sinks in the northern portion of the tract, the covering over the lava is fairly fine silt of unknown thickness. The log of the U. S. G. S. Well No. 7 in Section 27 T6N R31E shows a depth of 126 feet before basalt was encountered. Most of this 126 feet is sand, silt, and clay.

8. 2. 3 SEISMOLOGY

Although many recorded earthquakes have been felt in Idaho, none were of sufficient intensity to cause more than minor damage to buildings. Of the 24 recorded earthquakes with epicenters within the state, seven had their epicenters within approximately 100 miles of the FET site. One of these, which was of unrecorded intensity, was at Arco. The seismic map of the United States shows that most of Idaho, including the site, is in zone 2, a zone where earthquakes of intensity to cause moderate damage may be expected.

Although the lava plain of the Snake River is geologically young, the surrounding mountains are mostly of great age. Some geologically recent faults appear to cross the plain beneath the lava beds, although their traces are not evident on the surface. None of these show indication of historically recent movement outside the lava plain. It may be expected

~~SECRET~~

~~CONFIDENTIAL~~

that earthquake shocks will continue to be felt in the site area, but a prediction as to their intensity cannot be made with assurance.

It is believed that no serious damage is probable to structures soundly designed to resist shocks of moderate intensity. Movements may be sufficient to break underground pipe connections at faces of buildings since this damage has been of frequent occurrence in moderate intensity earthquakes. Some magnification of shocks may result in those portions of the site that are deeply covered with alluvium.

On August 18, 1959, a very damaging earthquake occurred near West Yellowstone, Montana, about 100 miles from the NRTS. The intensity of this quake was variously reported at from 7.2 to 7.8 on the Richter scale of magnitude, where 7.0 is the approximate lower limit of a major earthquake and 8.5 represents the greatest intensity ever observed. Damage at the NRTS, nevertheless, was limited to a few minor cracks in some concrete structures.

8.2.4 CLIMATOLOGICAL DATA

8.2.4.1 General Climatic Regime

The climatic data and summary given here have been obtained primarily from measurements taken by the U. S. Weather Bureau at the NRTS and documents* issued by them that discuss the climatic factors in greater detail.

Since measurements have been taken for a limited number of years at the ANP site, longer periods of record of nearby U. S. Weather Bureau stations have been adjusted to compare with the shorter period of record of the ITS to achieve a more representative compilation. In most cases the normal values are based on the period 1921 to 1950 and are means adjusted to represent observations taken at the present standard location.

The location of the NRTS in a broad flat valley with the surrounding mountain ranges, its altitude above sea level, and its latitude all have a definite effect upon the climate. Since all air masses entering the Snake River Plain must first cross over a mountain barrier and in so doing precipitate a large percentage of their moisture, the rainfall is light and the region has desert-like characteristics. The local northeast-southwest orientation of the plain and its mountain range walls tend to channel the prevailing west winds of this latitude so that a southwest flow predominates over the NRTS. The second most frequent winds come from the northeast. The relative dryness of the air and the infrequency of low cloudiness, particularly during the summer, permit intense solar heating of the surface during the day and rapid radiational cooling at night. These factors combine to give a large diurnal range of temperature near the ground. Because of the moderating influence of the Pacific Ocean, most of the air masses flowing over this area are usually warmer during winter and cooler in summer than those at a similar latitude in the more continental climate east of the Continental Divide. The mountains to the north and east act as an effective barrier and keep most of the shallow but intensely cold winter air masses that push southward from Canada over the Great Plains from entering the Snake River Plain. Occasionally, however, the cold air can spill over the mountains. When this happens, the cold air is held in the valley by the surrounding mountains and NRTS experiences low temperatures for periods lasting a week or longer.

*G. A. DeMarrais (U. S. Weather Bureau), "The Climatology of the NRTS," IDO-12003, USAEC, Idaho Falls, Idaho, June 1958.

U. S. Weather Bureau, "Local Climatological Data - Idaho Falls 42, NW, Idaho," U. S. Government Printing Office, Washington, D. C., 1958.

G. A. DeMarrais (U. S. Weather Bureau), "The Engineering Climatology of the NRTS," IDO-12004, USAEC, Idaho Falls, Idaho, November 1958.

D. A. Humphrey and E. W. Wilkins (U. S. Weather Bureau), "The Climatology of Stack Gas Diffusion at the NRTS," IDO-10020, USAEC, Idaho Falls, Idaho, March 1952.

~~CONFIDENTIAL~~
~~SECRET~~

Temperature inversions based at the surface are present for at least a few hours almost every day of the year and for the lower 250 feet are present for about half of the total time for the year as a whole. The average maximum depth has been estimated to be about 2000 feet.

The annual precipitation is extremely light, being 7.35 inches per year, and varies considerably throughout the year. Snowfall varies from practically no snow at all to the opposite extreme in which snow has covered the entire NRTS to a depth of 1 to 2 feet. Despite these extremes, the annual totals do not vary greatly from year to year.

Destructive winds have not been a problem. Tornadoes have never been reported in the region although funnel-shaped clouds have been sighted over the NRTS.

Four to six thunderstorms can be expected during each summer month, and some of these produce hail. Lightning protection is a must for man-made structures since the lack of natural targets makes them vulnerable.

Super-cooled fog occurs occasionally in winter with a snow cover and may last several days. These conditions permit the accumulation of considerable rime icing on power and telephone lines.

The dust content of the air is very small while the ground is snow covered. Dust-favoring winds (gusts of 20 mph or more) occur on the average for 6 hours during 13 windy days per month. Dust concentrations have varied from a low of 0.014 milligram per cubic meter over snow cover to a high of 0.77 milligram per cubic meter on a day when dust devils were present near the sampling station. Concentrations vary widely from place to place. Average daytime concentrations during the warmer months run about 0.7 milligram per cubic meter.

The average annual pressure is about 25 inches of mercury.

8.2.4.2 Individual Elements

Tables 8.1 and 8.2 give significant temperatures and humidities on a monthly basis. It is of interest to note that the maximum daily range of temperature for the NRTS is 58°F.

Because of its relationship to temperature, relative humidity has a large diurnal range. The small amount of water vapor in the air causes low daytime readings, often below 15 percent in summer, and the large drop in temperature at night gives humidities near 100 percent.

Table 8.3 presents monthly precipitation normals for the GE-ANP site, and Table 8.4 gives the average number of days of precipitation by months. It is of interest to note the wide ranges that occur and the maximum amounts that have occurred in 24 hours. Other data compiled by the U. S. Weather Bureau at NRTS show that the ANP area has the minimum normal annual precipitation for the NRTS (7.35 inches).

The relatively small number of days with precipitation occurring along with the low average monthly precipitation indicates that conditions that permit rainout of reactor effluents occur infrequently.

The winds observed at NRTS are strongly influenced by the major topographic features of the Snake River Valley. The prevailing westerly winds of this latitude are channeled by the mountains upon entering the western part of the Valley and become southwesterly at the south end and south-southwesterly at the north end of the NRTS. This channeling within the confines of the mountain walls not only affects the direction but increases the speed. A similar phenomenon occurs at the north end when the flow above the mountains is from the north or northwest. The northwest corner of the NRTS then experiences strong chan-

~~SECRET~~
~~CONFIDENTIAL~~

TABLE 8.1
MONTHLY TEMPERATURE NORMALS IN °F

Month	Average	Average	Extreme	Extreme	Average	Daily Range	
	Daily	Daily				Average	Maximum ^a
	Maximum	Minimum	High	Low	Monthly		
January	25.3	-0.7	46	-30	12.3	26	50
February	31.2	5.8	55	-35	18.5	25	53
March	41.0	16.4	67	-14	28.7	25	48
April	56.9	27.9	80	10	42.4	29	57
May	67.3	36.6	93	16	52.0	31	55
June	76.1	43.0	97	25	59.6	33	51
July	87.9	48.3	102	32	68.1	40	58
August	85.3	45.3	99	28	65.3	40	57
September	74.7	36.0	99	19	55.4	39	58
October	62.5	26.1	83	5	44.3	36	58
November	42.7	15.1	67	-20	28.9	28	48
December	30.3	5.3	50	-26	17.8	25	43
Annual	56.8	25.4	102	-35	41.1	31	58

^aApril 1950 through September 1958.

TABLE 8.2
AVERAGE RELATIVE HUMIDITY AT CENTRAL FACILITIES STATION
JANUARY 1950 THROUGH DECEMBER 1957

Month	Average	Average	Average	Extreme
	Daily High, %	Daily Low, %	Daily Mean, %	
January	92	57	79	20
February	93	51	77	24
March	94	42	71	9
April	86	26	55	6
May	82	24	53	6
June	77	21	48	6
July	59	15	35	4
August	59	13	33	4
September	58	15	34	4
October	65	24	49	3
November	88	39	67	14
December	93	57	80	23
Annual	79	33	57	3

CONFIDENTIAL
SECRET

TABLE 8.3
MONTHLY PRECIPITATION NORMALS IN INCHES

Month	Rainfall			Snowfall ^a		
	Average Monthly	Maximum Monthly	Minimum Monthly	24-Hour Maximum	Mean Total	24-Hour Maximum
January	0.53	0.84	0.19	0.42	7.8	8.5
February	0.37	0.89	0.08	0.70	4.4	6.5
March	0.45	1.00	Trace	0.41	4.6	5.8
April	0.59	1.10	0.01	0.42	1.9	5.0
May	1.04	3.00	0.10	0.88	0.5	3.1
June	1.08	1.84	0.09	1.31	Trace	Trace
July	0.51	1.33	0.14	1.33	0.0	0.0
August	0.80	1.81	0.06	0.70	0.0	0.0
September	0.59	1.18	0.00	1.00	Trace	0.1
October	0.47	1.01	0.00	0.43	0.3	1.6
November	0.31	0.55	0.09	0.48	1.3	1.8
December	0.61	1.82	0.10	0.52	4.2	3.0
Annual	7.35	3.00	0.00	1.33	25.0	8.5

^aData applicable to observing station at Central Facilities.

TABLE 8.4
AVERAGE NUMBER OF DAYS WITH
PRECIPITATION BY MONTH FOR ANP
AREA FOR PERIOD
JANUARY 1950 THROUGH DECEMBER 1957

Month	Days With Precipitation
January	8.7
February	5.3
March	5.2
April	5.1
May	8.3
June	5.8
July	4.6
August	4.6
September	2.3
October	4.0
November	4.6
December	10.0

SECRET

neled northwest winds. Other important local effects occur that influence the wind structure and result in the frequent occurrence of northerly winds, particularly at night during inversion conditions. (These local wind effects are discussed in greater detail in previously referenced documents.)

The normal or fair-weather pattern, then, shows the winds to principally blow from the southwest quadrant during the day and the north quadrant during the night. Passing storms, however, can alter this situation so that winds from any direction may be experienced.

Considerable wind-speed and direction data have been compiled for locations on and near the NRTS by the U. S. Weather Bureau. Figure 8.8 shows annual wind roses for 13 locations on or near the NRTS with the period of record noted. It is of considerable interest and importance from the standpoint of waste disposal by atmospheric processes to note the predominant up-down valley flow. Stations Birch Creek, Y, and Howe significantly show the effect of wind channeling by mountain valleys that are oriented northwest-southeast.

More detailed studies of the wind structure have been made, and others are being conducted for the ANP site from data obtained on a 200-foot meteorological tower. Monthly seasonal and annual wind roses for the 20-foot level separated according to lapse or inversion conditions for the period 1953-1956 comprising 30,012 total hours are given in Figures 8.9 through 8.13. A wind rose summary by season and lapse-inversion separation for the 150-foot level of the ANP tower is presented in Figure 8.14 for the period of May 1956 through April 1957. Examination of these wind roses shows that in general the wind flow pattern at the 150-foot level is quite similar to the wind structure at the 20-foot level. The 20-foot level data were selected for utilization in the off-site-dose study presented in another section of this report because of the greater period of record and the similarity in the general pattern as noted. Future wind studies at the higher levels on the meteorological tower are planned to be utilized in similar analyses since they would be more representative of the wind structure at the height at which reactor effluents are released.

On the average the speed of the wind through a 24-hour period follows a fairly regular pattern regardless of season. Wind speeds reach their maximum during the afternoon and gradually decrease to a minimum in the early morning hours. Table 8.5 gives average wind speeds by month for the 20-foot level of the ANP tower for the period of record November 1952 through December 1957 as well as maximum hourly average and peak gusts for the 20-foot level July 1950 through December 1957. It is of interest to note that the maximum winds are primarily channeled winds with up-valley flow predominant.

The atmospheric pressure at the NRTS is lower than sea-level pressure by approximately 5 inches of mercury. Over the 8 years of observations at Central Facilities, with a barometer elevation of 4,939 feet above mean sea level (ANP 4790 feet MSL), the mean station pressure (not reduced to sea level) has been 25.0 inches of mercury. The probable extreme limits of pressure are 24 and 26 inches. The mean daily range is 0.160 inch, varying from near 0.110 inch in the summer to slightly over 0.200 inch in winter. The largest pressure change for the 8 years on 1 day was recorded as 0.496 inch in December.

The objective of the atmospheric dust program at the NRTS is to determine for expected meteorological conditions the concentrations of dust by weight per unit volume of air, the particle size, distributions, the chemical nature, the abrasiveness of particles, and the variations of dustiness, with respect to location on the NRTS and with respect to height of air intake. Observations so far have been confined mostly to the ANPD area. The sampling began July 22, 1952. Concentration and particle size analyses are performed by

CONFIDENTIAL
SECRET

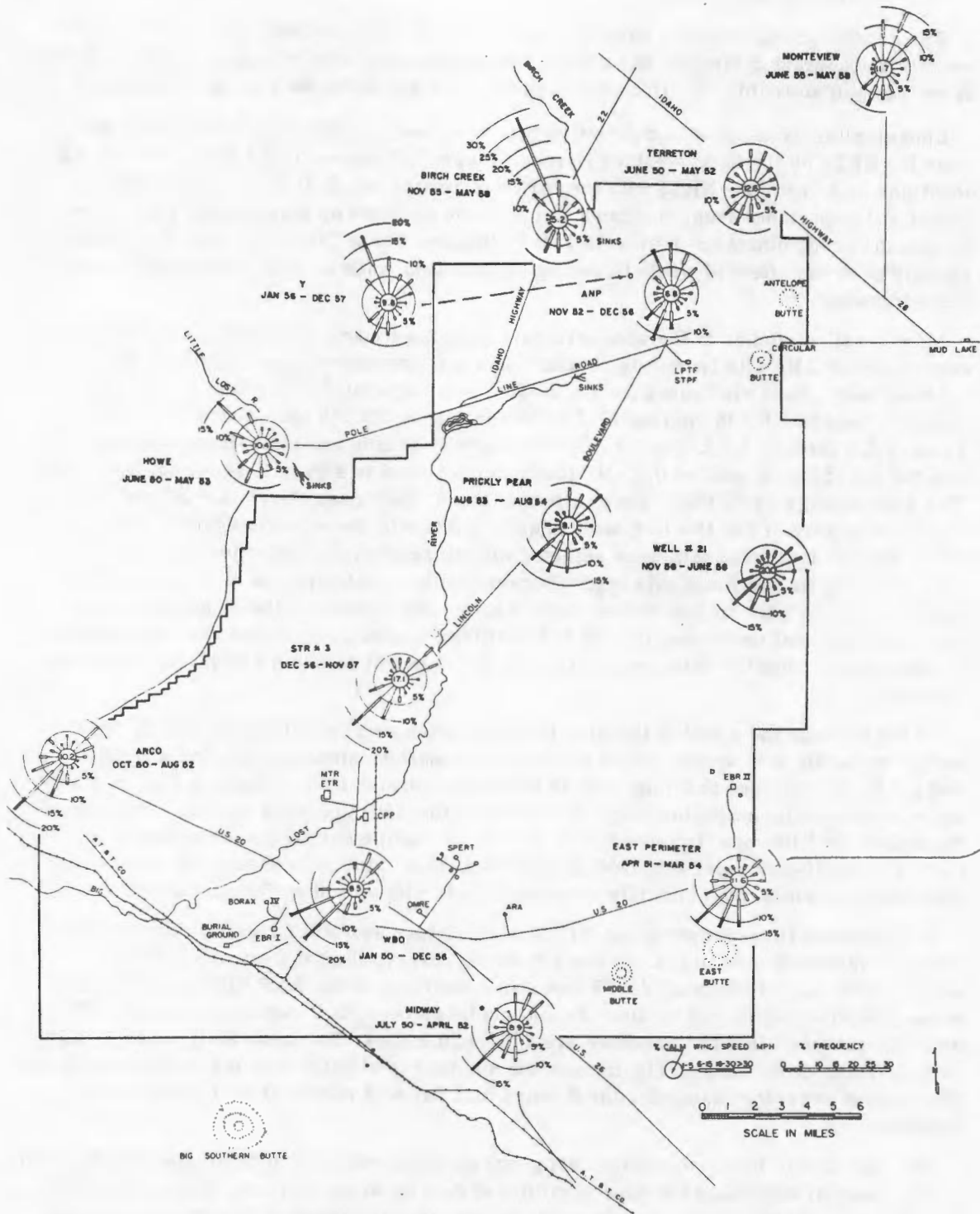


Fig. 8.8 - Annual wind roses for NRTS at 20-foot level

SECRET
CONFIDENTIAL

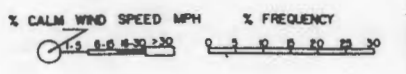
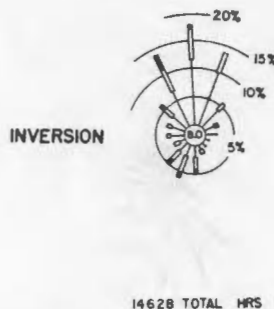
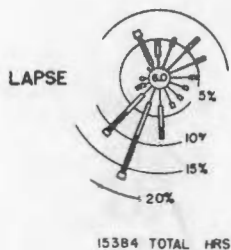
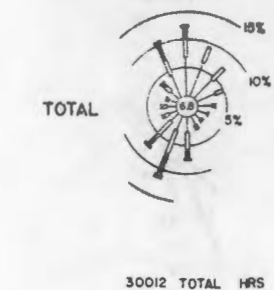


Fig. 8.9 - Composite wind roses for ANPD-IET site at 20-foot level for period of record 1953 - 1956

the Weather Bureau Office, Idaho Falls, Idaho, and spectrographic analyses are performed by the Public Health Service, Cincinnati, Ohio. High-volume air samplers with Mine Safety Appliance fluted filters are used for concentration measurements and to obtain dust samples for spectrographic analysis. A Millipore filter and a rotary pump is used to obtain samples for particle size analysis.

Dust concentrations measured in the ANPD area thus far have varied from a low of 0.0369 milligram per cubic meter on a summer day with light winds to a high of 0.1513 milligram per cubic meter during a period when dust devils were present in the vicinity of the sampling station. The average concentration over 1759 sampling hours (most of which were during the windiest parts of the days) was 0.0726 milligram per cubic meter.

~~CONFIDENTIAL~~
SECRET

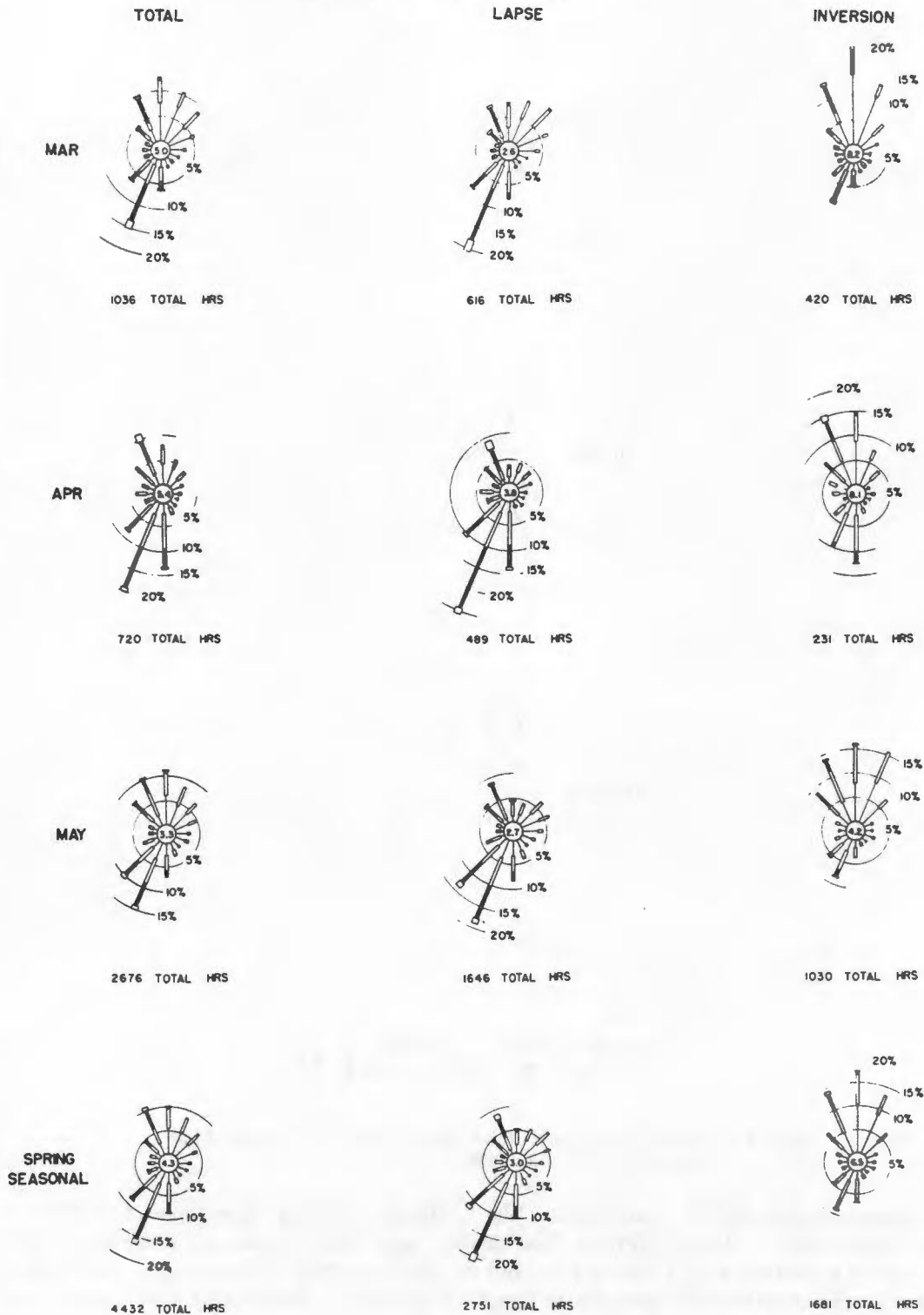


Fig. 8.10 - Spring season and monthly wind roses for ANPD-IET site at 20-foot level for period of record 1953-1956

SECRET
~~CONFIDENTIAL~~

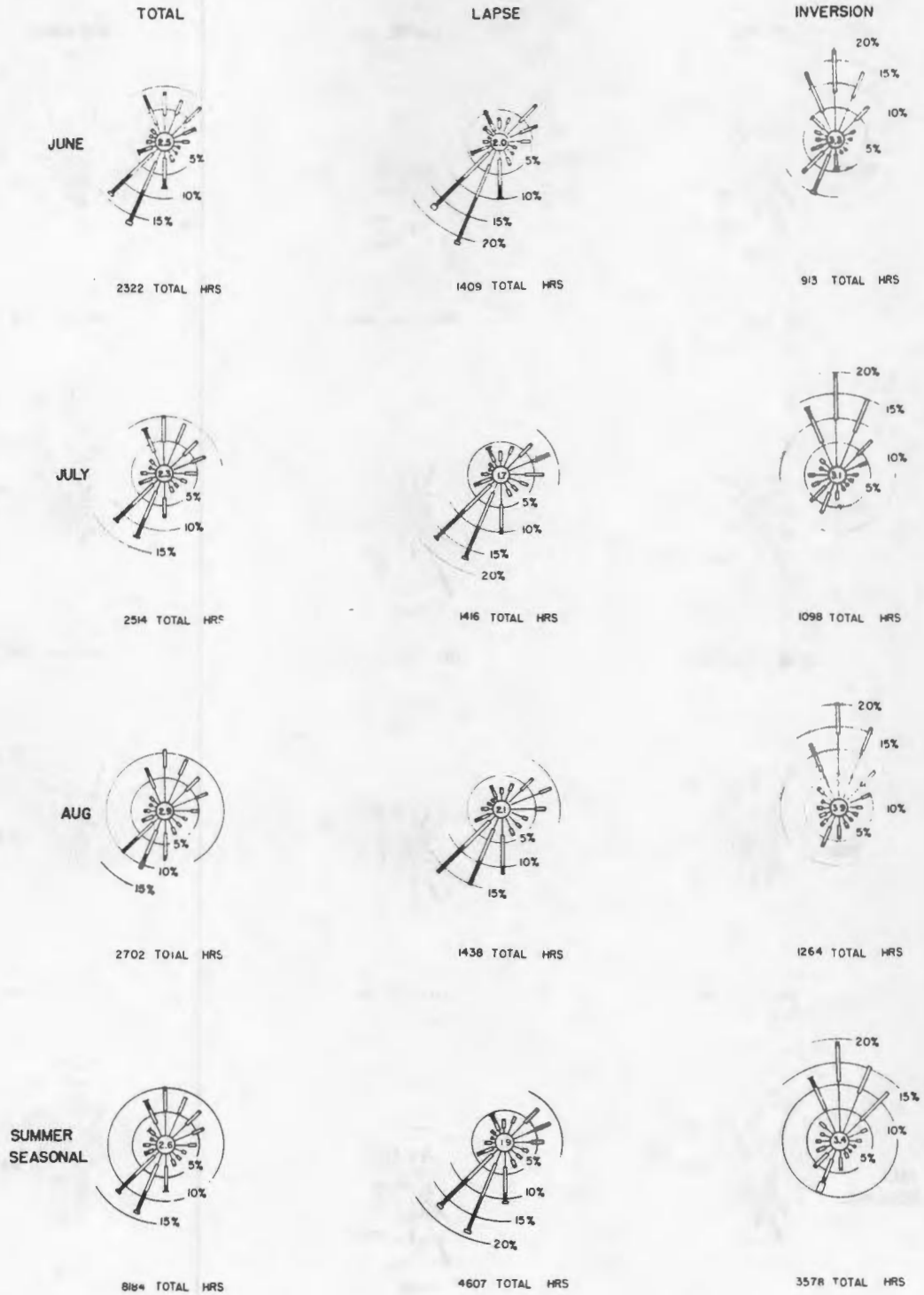
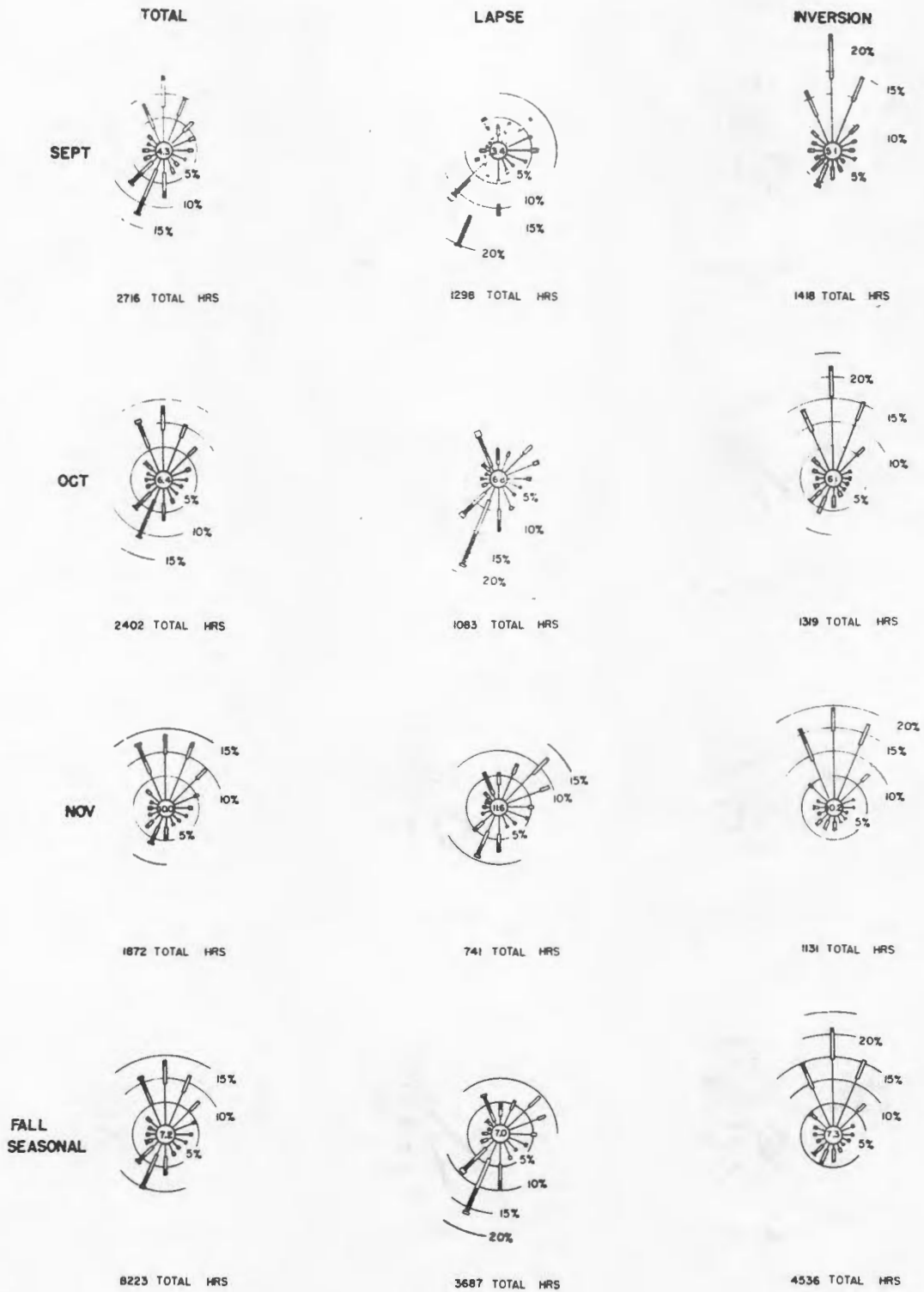


Fig. 8.11 - Summer season and monthly wind roses for ANPD-IET site at 20-foot level for period of record 1953 - 1956

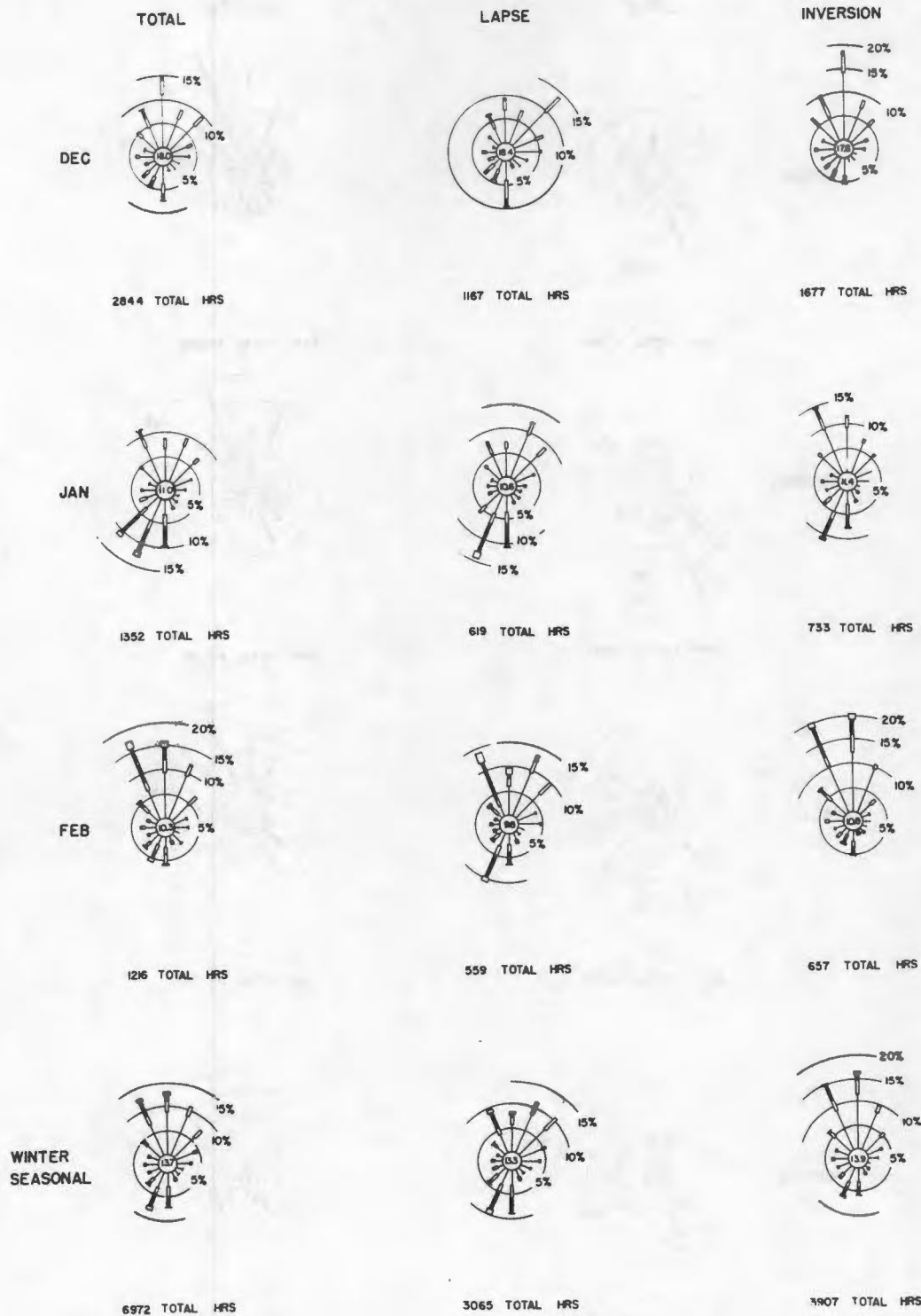
CONFIDENTIAL
~~SECRET~~



% CALM WIND SPEED MPH % FREQUENCY
 0 5 10 15 20 25 30 0 5 10 15 20 25 30

Fig. 8.12—Fall season and monthly wind roses for ANPD-IET site at 20-foot level for period of record: 1953-1956

SECRET
CONFIDENTIAL



% CALM WIND SPEED MPH % FREQUENCY
0-5 5-15 15-20 20-30 0 5 10 15 20 25 30

Fig. 8.13 - Winter season and monthly wind roses for ANPD-IET site at 20-foot level for period of record 1953 - 1956

CONFIDENTIAL
SECRET

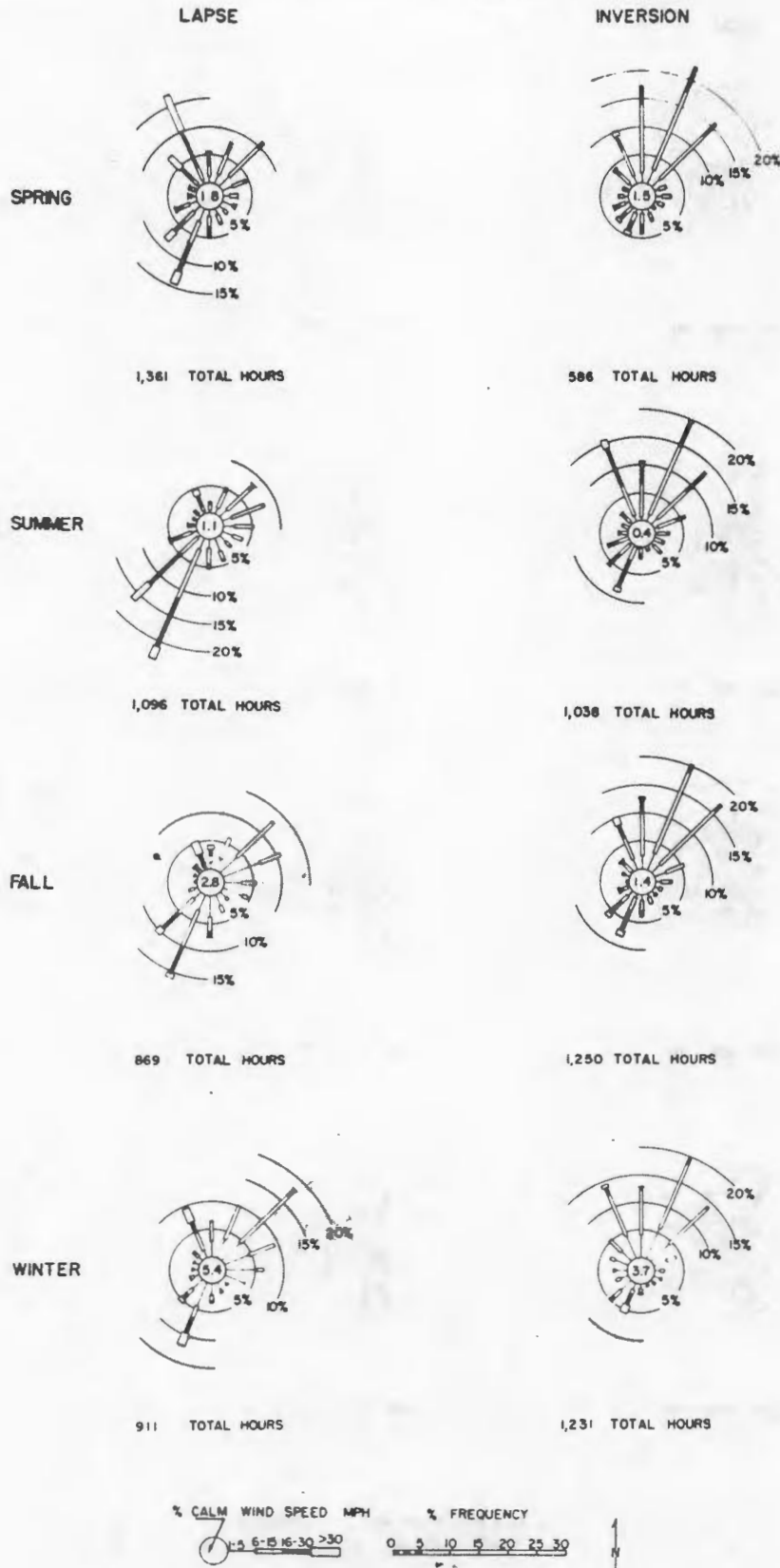


Fig. 8.14 - Seasonal wind roses for ANPD site at 150-foot level for period May 1956 through April 1957

SECRET
CONFIDENTIAL

TABLE 8.5

AVERAGE WIND SPEED AND MAXIMUM WIND VELOCITY DATA FOR THE 20-FOOT
LEVEL OF THE ANP TOWER BY MONTH OF THE YEAR

Month	Average Speed, mph	Maximum Hourly Speed, mph	Average Direction	Peak Gust	
				Speed, mph	Direction
January	5.7	41	SSW	59	WSW
February	7.7	46	SSW	62	N and WSW
March	9.1	50	S	68	S
April	10.3	50	NW	61	NW
May	9.4	43	S	64	NNW
June	9.9	40	SW	65	SW
July	8.4	38	SSW	55	SW
August	7.9	34	SSW	64	SSW
September	7.4	36	SW	54	SSW
October	7.4	40	NW	63	NNW
November	5.5	37	NNW	61	NNW
December	5.2	41	SSE	61	S
Annual	7.8				

During July and August the concentrations ran between 0.04 and 0.05 milligram per cubic meter, but with the beginning of road construction and increased vehicular traffic, they rose to 0.05 - 0.13 milligram per cubic meter in November.

Dust sampling at Central Facilities gave a concentration of 0.7720 milligram per cubic meter at the same time that the high concentration of 0.1315 was measured at the ANPD site. This also is indicative of the increased dustiness resulting from human activity and points out that the ANPD site can be expected to have higher dust concentrations as construction develops.

Particle sizings from four samplings during a variety of wind and dustiness conditions in August and November gave similar size distributions. Median sizes ranged from 0.330 to 0.385 micron, and standard deviations ranged from 1.94 to 2.75 microns. In all samples, less than 1 percent of the particles was greater than 1 micron. A few of the particles collected were as large as 80 microns.

The results of the spectrographic analysis of five fluted filters are given in Table 8.6. Each of the filters had about 0.04 milligram of dust per cubic meter of air pulled through them. All were exposed during the windiest part of summer afternoons, and dust devils were present during the sampling period for all but filter No. 1-0. Spectrometric tests were made for each element listed in Table 8.6, and the concentrations present in a control filter (which was not used in sampling) were subtracted out of the concentrations found in the sampling filters. Calcium and silicon are the major constituents on the average. Comparatively large concentrations of aluminum and iron were present when filter No. 5-0 was exposed.

An analysis of surface soil in the ANPD area gives an idea of the composition of the dust that may be raised locally when the crusted surface is pulverized by increased human activity. For this purpose four representative samples of topsoil were selected for spectrographic analysis, and the results are given in milligrams per gram of soil in Table 8.7. The concentrations in the four samples were averaged, since they differed only slightly in their chemical contents.

~~CONFIDENTIAL~~
~~SECRET~~

TABLE 8.6

CONCENTRATIONS OF VARIOUS CHEMICAL CONSTITUENTS IN FILTERED DUST
IN THE ANPD AREA

(milligrams per cubic meter of air filtered)

Element	Filter 1-0	Filter 5-0	Filter 7-0	Filter 13-0	Filter 15-0	Average
Ca	1.11×10^{-4}	7.84×10^{-4}	6.50×10^{-4}	0.82×10^{-4}	0.83×10^{-4}	3.42×10^{-4}
Mg	0.17	0.33	0.17	0.11	0.16	0.19
Ni	0.04	0.11	0.06	0.03	0.04	0.06
Cu	0.11	0.33	0.26	0.11	0.16	0.19
Al	0.34	2.04	0.77	0.56	0.67	0.88
Zn						
Mo		trace	trace	0.006	trace	trace
Mn		0.06	0.03	0.02	0.02	0.03
Cr	0.03	0.15	0.15	0.02	0.07	0.08
Fe		1.39		0.48	0.36	0.45
Sb						
As						
Ba	0.02	0.04	0.03	0.02	0.02	0.03
Co						
Pb	0.02	0.02	0.08		0.04	0.03
Si	0.59	> 3.00	1.03	> 1.13	0.39	> 1.23
Sn	0.04	0.06	0.06	0.02	0.04	0.04
Ti	trace	0.11	0.08	0.06	0.04	0.06
Hg						
Bi						
Cd			Insufficient Sample			
Be			Insufficient Sample			
W						
V		0.006	trace	0.002	trace	0.002
U						
Na		trace		trace		
Sr				present		

TABLE 8.7

AVERAGE CONCENTRATIONS OF VARIOUS CHEMICAL CONSTITUENTS
IN SURFACE SOIL IN THE ANPD AREA

(milligrams per gram of soil)

Element	Concentration	Element	Concentration	Element	Concentration
Ca	65.6	Sb		Cd	
Mg	12.0	As		Be	
Ni	0.18	Ba	> 0.9	W	> 1.0
Cu	0.31	Co	0.05	V	0.23
Al	22.7	Pb		U	
Zn	0.32	Si	major	Te	
Mo		Sn		Na	present
Mn	1.38	Ti	8.1	K	present
Cr	0.62	Hg		Sr	present
Fe	31.2	Bi			

~~SECRET~~

Silicon was the major constituent, but strontium, sodium, and potassium were also present. Uranium possibly was present in two of the samples. Calcium, iron, aluminum, and titanium were present in appreciable quantities.

Petrographic examination of samples of airborne dust at the ANPD site was performed by the Harvard University School of Public Health. The examination indicated that approximately half of the particles was crystalline minerals, and the rest oxides or organic matter. The crystalline minerals were principally silicates, but some quartz was also present, indicating that the dust is moderately abrasive.

The maximum dustiness can be expected during the warmer months. During colder months, the presence of snow cover and frozen or moist ground will lower the frequency of dusty conditions. Observations of the state of the ground (recorded twice daily at the NRTS) show that the ground is in a condition favoring dustiness a little less than half of the time during the year.

It has been found that with wind speeds averaging 16 mph or more at the NRTS, there will be gusts of 20 mph or more and visible dustiness often results. Dust-favoring winds occur about 10 percent of the time during the year for an average of 6 hours of 13 windy days per month. The frequency of dusty conditions is then about 5 percent, since the state of the ground favors dustiness only about half of the time. In general, the afternoons of the warmer months provide most of the dusty conditions that occur. Dust devils are often seen over the area in summer, and these raise dust locally when wind speeds are too light to raise dust on a large scale.

8. 2. 4. 3 Diffusion Parameters and Conditions

Because of the excessive temperature and velocity of the exhaust gases from this reactor, the height to which the effluent rises before leveling off may well be significantly above the physical height of the stack. The empirical formula of Bryant-Davidson* estimates this rise and seems best suited for this computation. It is written:

$$h = d \left(\frac{v}{u} \right)^{1.4} \left(1 + \frac{T}{T_s} \right)$$

where h = increase in stack height in feet

d = stack diameter in feet

v = stack draft velocity in feet/sec

u = mean wind speed in feet/sec

$T = T_s - T_a$ excess temperature of stack gas in $^{\circ}$ Rankine, where T_a is ambient temperature

T_s = absolute temperature of stack gas in $^{\circ}$ Rankine

The above relationship has been used for computations of effective heights in the dose equations discussed elsewhere in this report.

The diffusion parameters used in the modified forms of Sutton's diffusion equations,† which are the basis for calculation of the radiation hazard levels in this report, are given

*L. W. Bryant, "The Effects of Velocity and Temperature of Discharge on the Shape of Smoke from a Funnel or Chimney: Experiments in a Wind Tunnel." National Physical Laboratory, Great Britain, Administrative 66, January 1949.

†W. F. Davidson, "The Dispersion and Spreading of Gases and Dusts from Chimneys." Transactions of Conferences on Industrial Wastes, Fourteenth Annual Meeting, Industrial Hygiene Foundation of America, November 18, 1949, pp. 38-55.

†R. E. Baker, C. C. Gamertsfelder, and R. F. Gentzler, "Final Report First Meltdown Experiment (Operation Boot)," APEX-445, General Electric Co., January 1959.

~~CONFIDENTIAL~~
~~SECRET~~

in Table 8. 8. These values are consistent with those suggested by Sutton and for the NRTS are considered to be conservative. Some evidence exists that indicates that the parameters given in Table 8. 8 for strong lapse overpredicts observed values.

The mean wind speeds utilized in calculations were obtained from the wind-rose data for the 20-foot level for the ANP meteorological tower previously given. The values were selected on the low side of each wind-speed class and represent conservative values.

TABLE 8. 8

DIFFUSION PARAMETERS

Stability Condition	$C_z = C_y$ (meters ^{n/2})	n (dimensionless)
Strong Lapse	0. 30	0. 20
Weak Lapse	0. 12	0. 25
Weak Inversion	0. 06	0. 333

The analysis of the wind-rose data by different stability classifications, wind-speed class, sector, and season of the year (presented previously) was accomplished by estimating the number of hours per day per season that classification of strong lapse, weak lapse, and weak inversion would be expected to occur. The estimates are given in Table 8. 9 and were based on average temperature change with height data given in Figures 8. 15 through 8. 20, ratios of lapse and inversion to total hours from the 20-foot level wind-rose data, average hours of daylight during the various seasons, and other climatological data pertinent to NRTS.

TABLE 8. 9

ESTIMATED HOURS PER DAY PER SEASON THAT CONDITIONS OF STRONG LAPSE, WEAK LAPSE, OR WEAK INVERSION OCCUR

Season	Strong Lapse	Weak Lapse	Weak Inversion
Spring	6	9	3
Summer	9	4. 5	2
Fall	7	3. 8	2
Winter	4	6. 5	6

While the data supporting these estimated hours per day of particular conditions are limited, they are considered to be representative and may underestimate the strong-lapse classification. Further studies in diffusion climatology are presently being conducted and compiled by the U. S. Weather Bureau at NRTS.

The effect of the stability conditions of strong lapse, weak lapse, and weak inversion on smoke plumes is shown schematically in Figure 8. 21. Type A occurs with superadiabatic (very unstable) temperature lapse rates. The stack effluent, if visible, appears to loop because of thermal eddies in the wind. Gases diffuse rapidly, but sporadic puffs having strong concentrations are occasionally brought to the ground near the base of the stack for a few seconds during light winds. Type B occurs with a gradient from dry adiabatic to isothermal. The effluent stream is shaped like a cone with axis horizontal. The

~~SECRET~~
~~CONFIDENTIAL~~

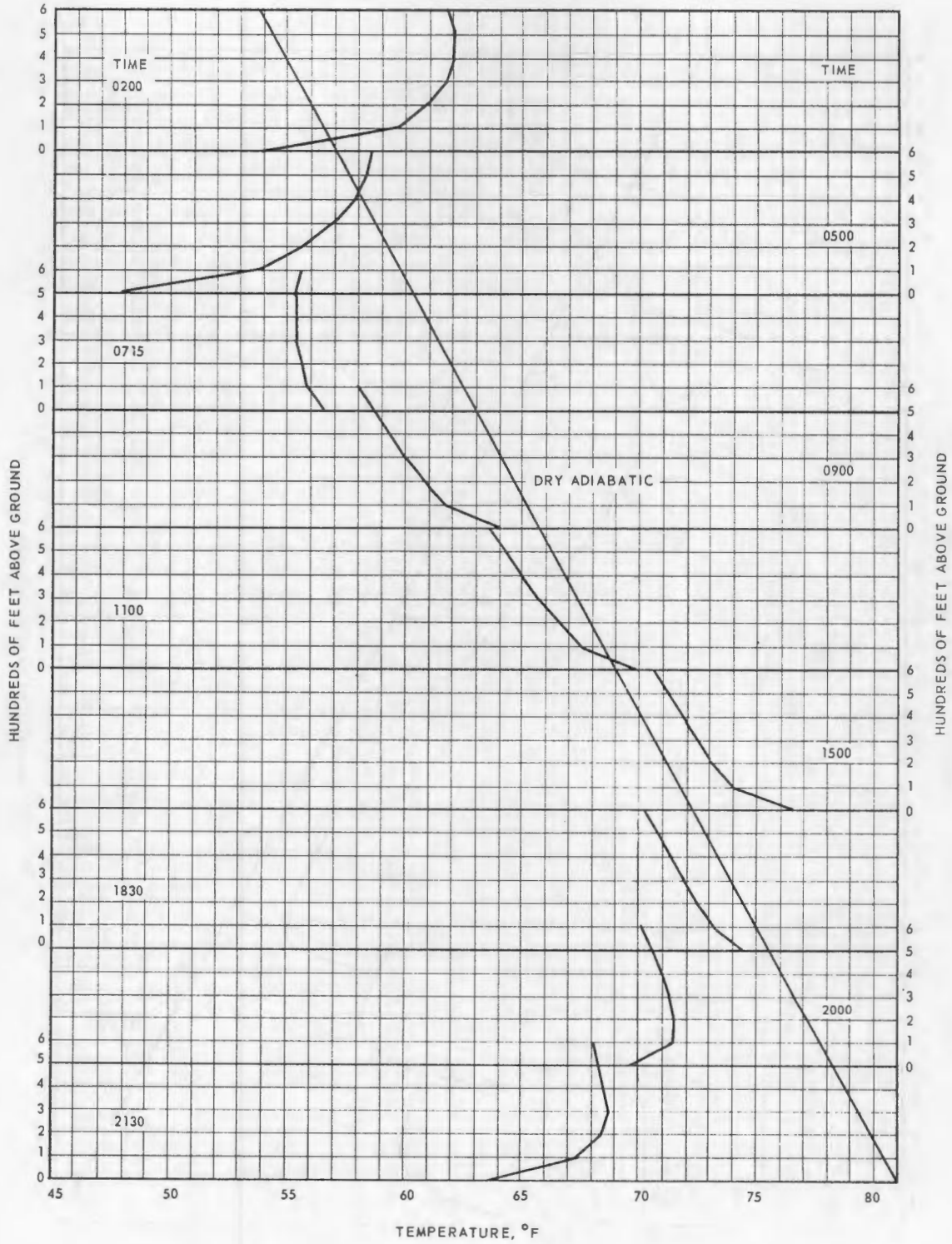


Fig. 8.15— Average temperature soundings for June, July, and August 1951

~~CONFIDENTIAL~~
~~SECRET~~

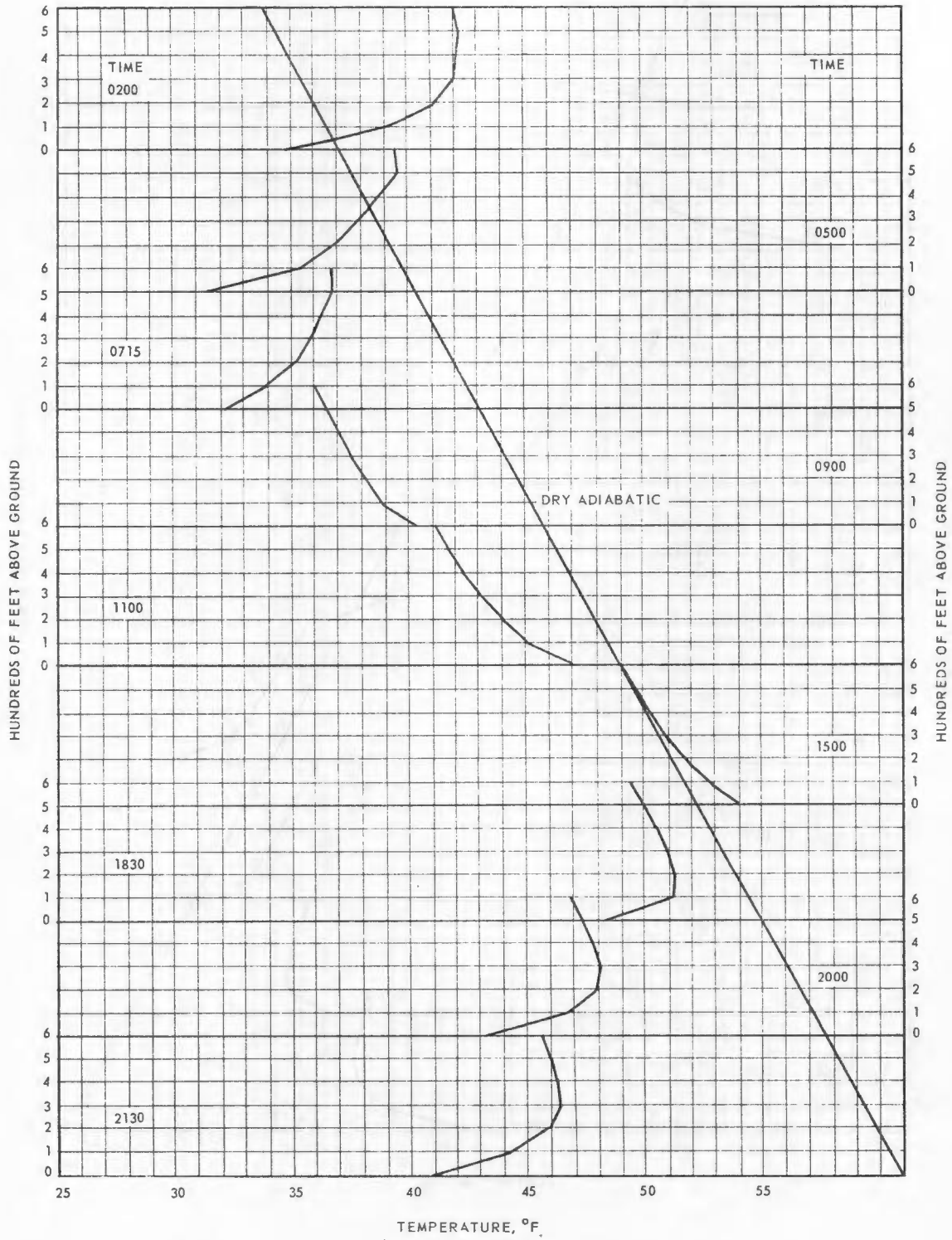


Fig. 8.16 - Average temperature soundings for September, October, and November 1951

~~SECRET~~
~~CONFIDENTIAL~~

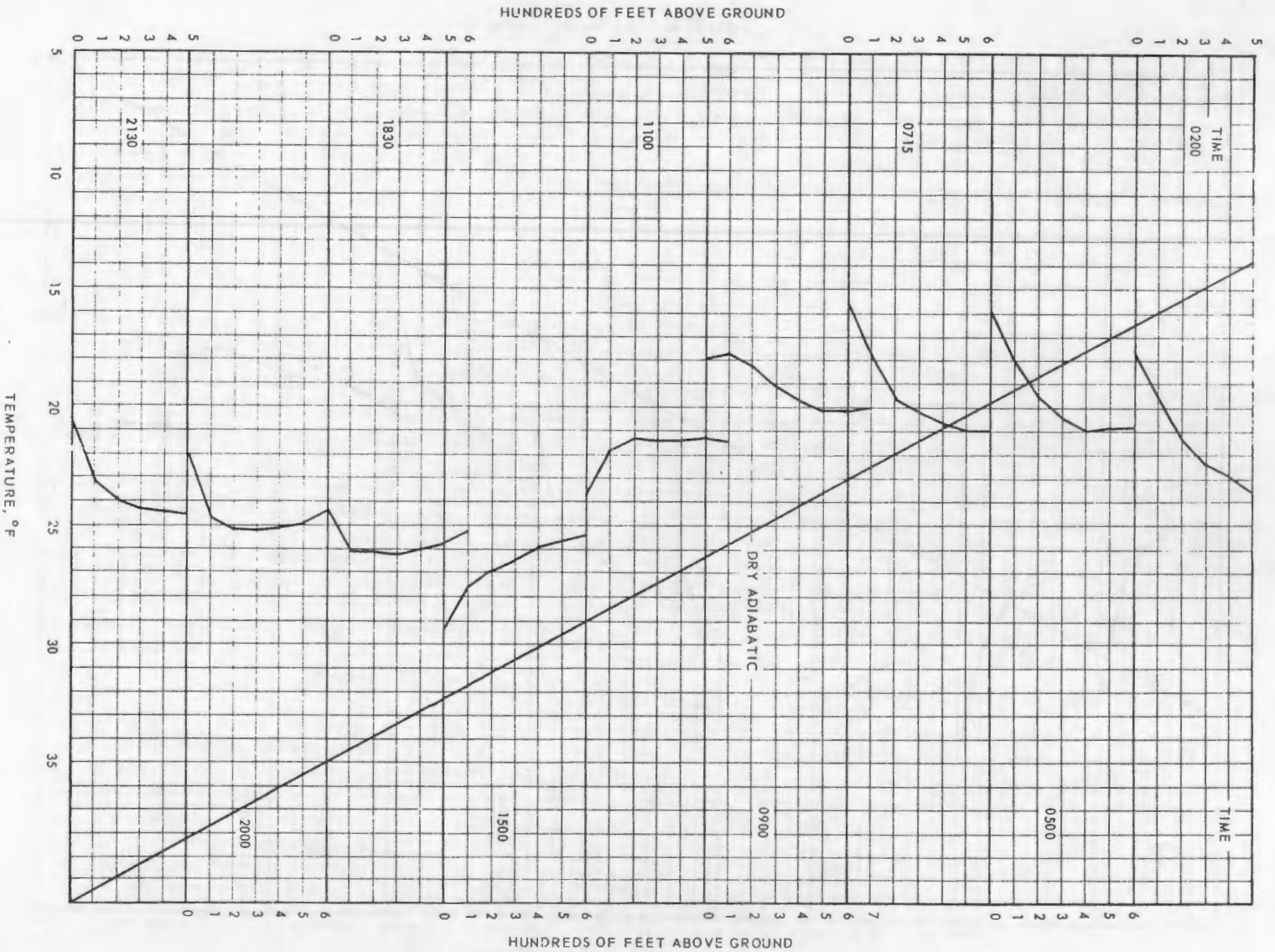


Fig. 8-17 - Average temperature soundings for December 1950, January, and February 1951

UNCONFIDENTIAL
SECRET

CONFIDENTIAL
~~SECRET~~

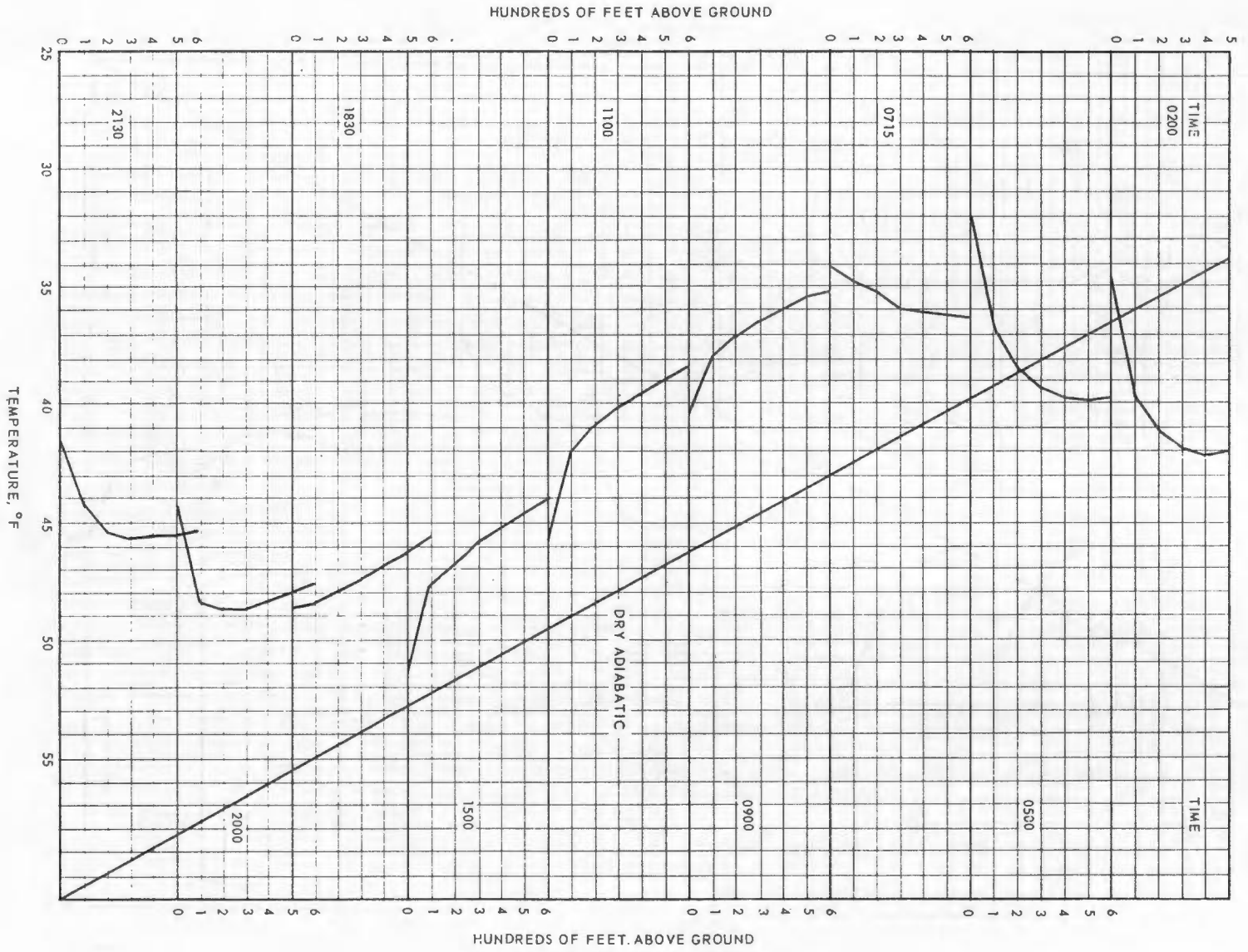


Fig. 8.18 - Average temperature soundings for March, April, and May 1951

CONFIDENTIAL
~~SECRET~~

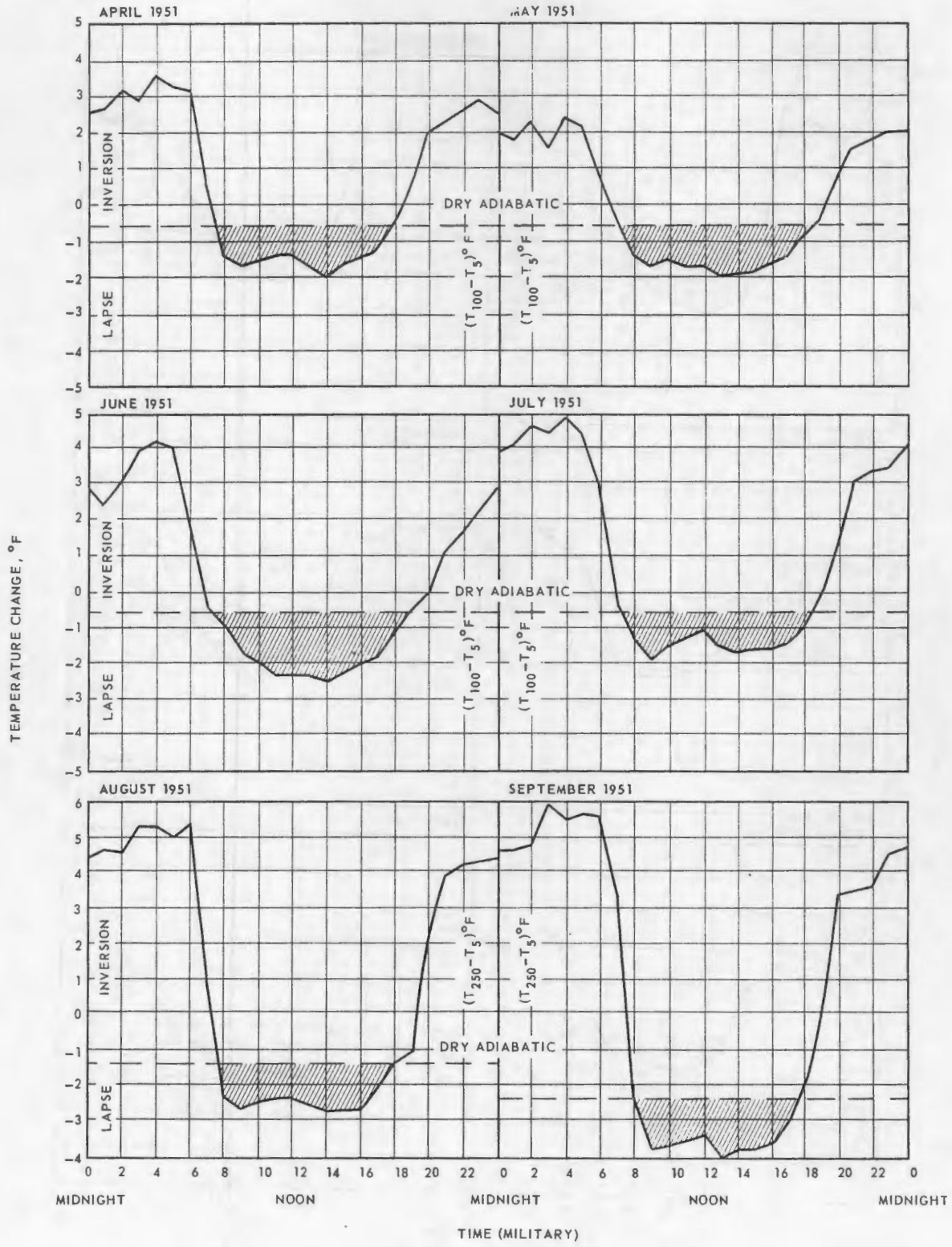


Fig. 8.19 - Average hourly vertical temperature gradients for period April through September 1951

CONFIDENTIAL
SECRET

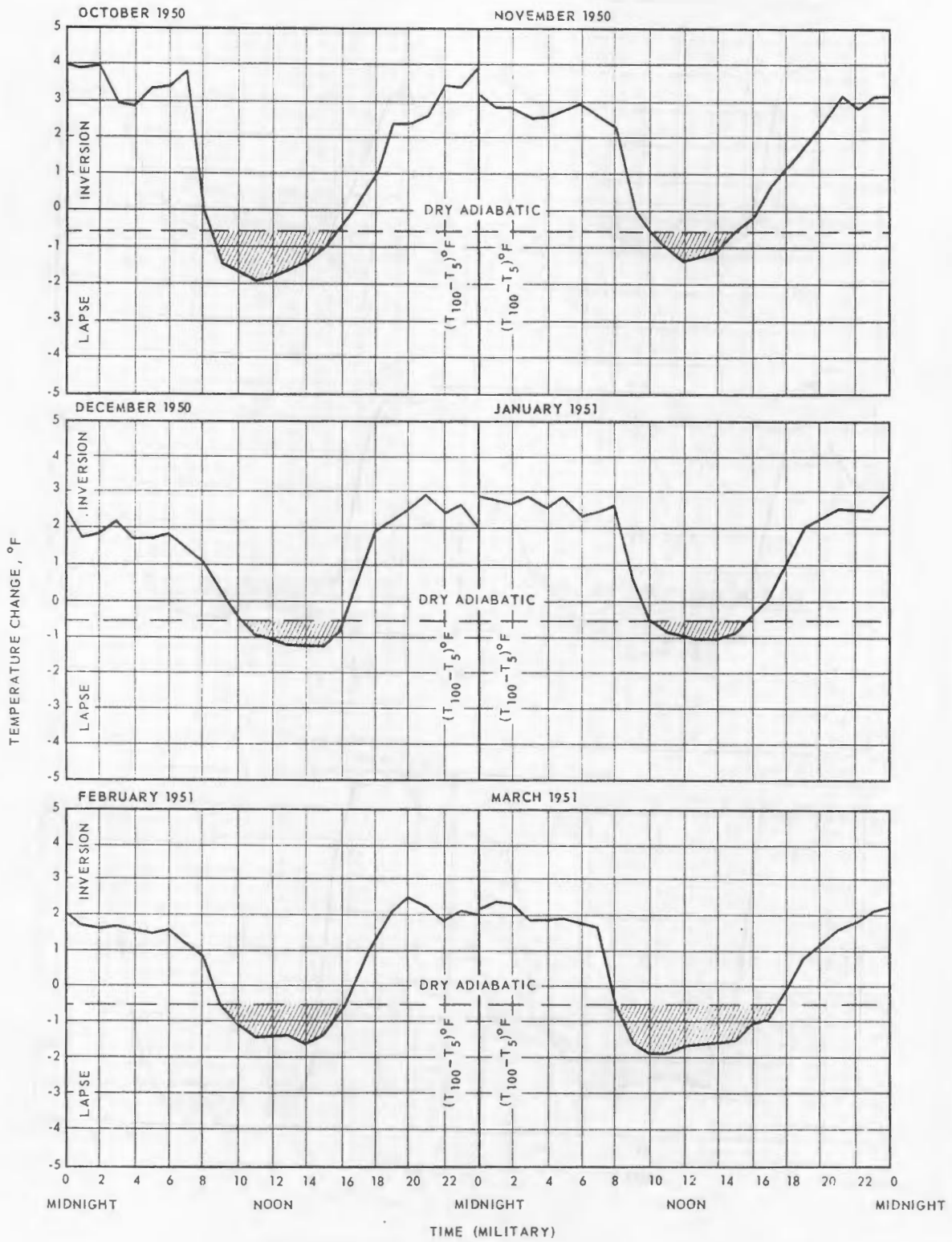


Fig. 8.20 - Average hourly vertical temperature gradients for period October 1950 through March 1951

CONFIDENTIAL
SECRET

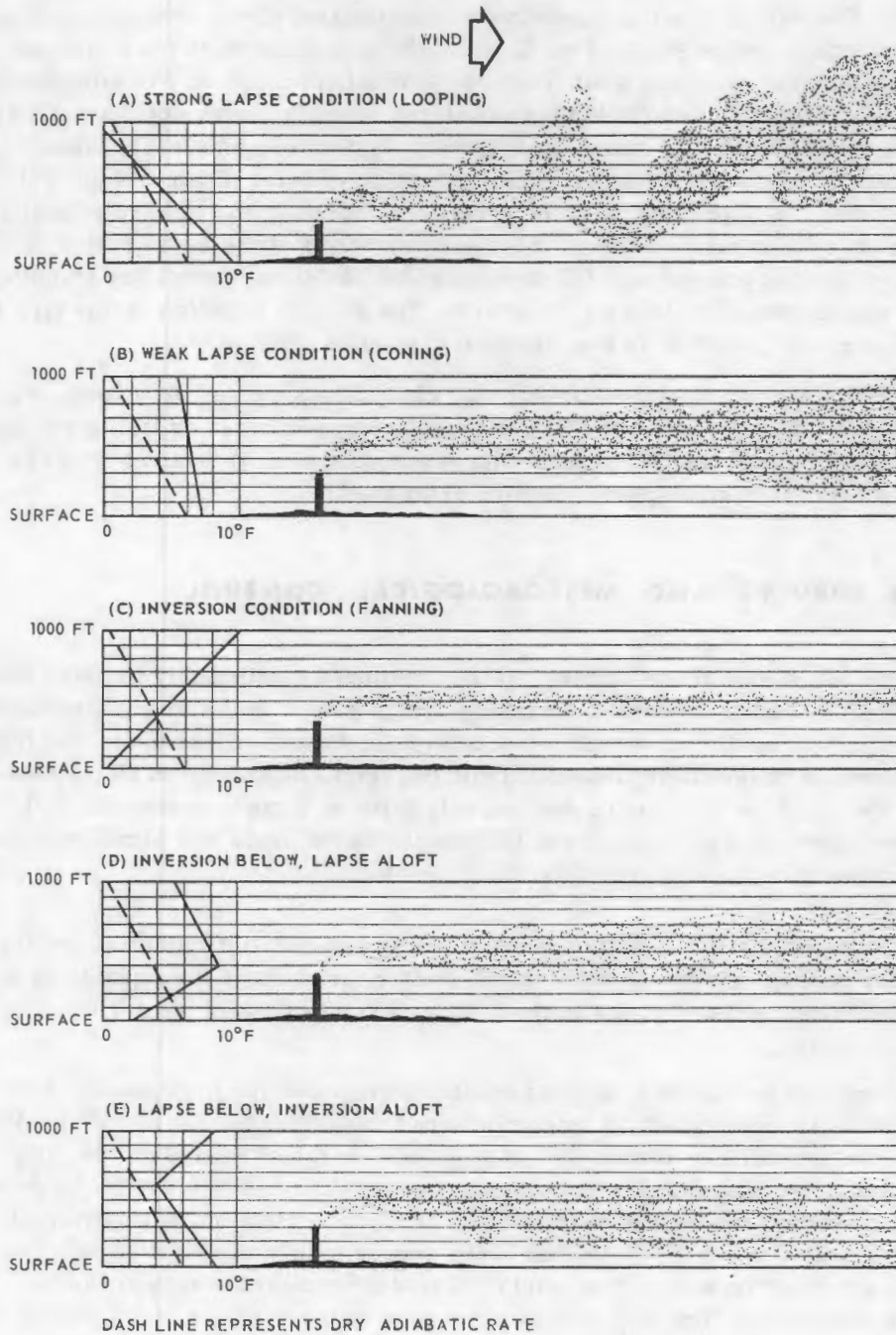


Fig. 8.21 - Schematic representation of stack-gas behavior under various conditions of vertical stability

CONFIDENTIAL
SECRET

distance from the stack that the effluent first comes to the ground is greater than with Type A because thermal turbulence, and hence vertical motion, is less. Type C occurs with a temperature inversion (stable flow) condition. The stack effluent diffuses little in the vertical. The effluent trail may resemble a meandering river, widening very gradually with distance from the stack. Type D is usually associated with the transition from lapse to inversion but may persist at times for several hours. It may be considered the most favorable diffusion situation to be encountered since the inversion prevents effluent reaching the ground and at the same time allows it to dilute rapidly in the lapse layer. Type E occurs at the time that the nocturnal inversion is being dissipated by heat from the morning sun. The lapse begins at the ground and works its way upward rapidly in summer but slowly in winter. In the event that the inversion is above the effective stack height, the effluent is trapped and diffuses in the shallow lapse layer. The trapping process gives strong concentrations on the ground. The average duration of this type is short, however, and proceeds in the direction of greater dilution.

In the analysis of wind-rose data by stability classification given previously, only Types A, B, and C were considered since they will represent a major fraction of the possible operating time. The schematics and description are presented here to give a qualitative concept of atmospheric dilution processes.

8.3 AREA SURVEYS AND METEOROLOGICAL CONTROL

All reactor operations above standby will be monitored continuously by stack monitors. Standby is defined as: 30 percent of maximum design power; fuel element temperatures below two-thirds of maximum design temperatures in degrees Fahrenheit; less than 10 curies per hour of radioactivity released from the stack, as measured 10 minutes after formation. One of these monitoring devices will serve as a rupture detector that will give an automatic signal causing shutdown of the reactor in the event of a significant, sudden increase in radioactive material released from the stack.

During all operations in which the expected release of radioactivity exceeds 10 curies in any 1-hour period (referenced at 10 minutes after formation), the capacity is maintained to make dose measurements in the field as a verification of the accuracy of the calculated exposure.

Before startup of the reactor, dose calculations are made for the continuous release of fission products from the stack by using measured values for the source term. At a point downwind from the stack, a mobile unit is positioned in the cloud and an air sample of 12 or more minutes is obtained. The accuracy of the prediction is determined by forming the ratio of the predicted concentration to the measured concentration. If this ratio does not lie between 1 and 10 and a re-evaluation of the source term and observed diffusion regime does not improve the accuracy, the reactor is shut down until the reason for the discrepancy can be discovered. The verification procedure is repeated for every significant weather-diffusion type that occurs during an operating period.

In addition to the dose-verification measurements, a 25-station system for radiation telemetering, with stations located at the periphery of the GE-ANP monitoring area, telemeters integrated lung dose and whole-body dose information for any preassigned averaging interval up to 1 hour to the control center in the Assembly and Maintenance area. Any integrated exposures can be summed on an hourly basis as the test progresses. Spectral analysis of the air filters for iodine-isotope content will make it possible to determine

SECRET

a ratio between the thyroid seekers and the gross activity from which the integrated thyroid exposure can be calculated.

Four outlying stations for meteorological telemetering with anemometers mounted 140 feet above the ground telemeter the weighted wind direction and wind speed averaged for for 6, 15, 30, or 60 minutes to the control center in the A and M area. Lapse-rate information consisting of the most recent 5-minute average of the temperature difference between the 5- and 140-foot levels is also telemetered to the control center for the same call-in periods. A fifth meteorological-telemetering station located at the source provides the same information as the outlying stations along with standard deviation of the wind direction. This meteorological information is used in calculating cloud trajectories, accurately determining decay-time intervals, and warning of impending wind shifts or shear zones that may establish themselves across the monitoring area and complicate the diffusion regime.

Figure 8.22 shows the GE-ANP monitoring area with the telemetering stations in their respective locations. Each radiation-telemetering station contains a fixed-filter air sampler and a low-range (0.01 to 10 mr) and high-range (0.1 to 100 mr) ion chamber. Four-wheel-drive mobile units equipped with scintillation detectors and air-sampling equipment are used to obtain supplementary information, as required, from areas where station separations are large.

Radiation monitoring inside the ANP monitoring area is under the jurisdiction of LAROO-ITD. Off-site radiation monitoring is the responsibility of IDO. During each test, General Electric, IDO, the U. S. Public Health Service, and the U. S. Weather Bureau will be in constant contact with each other.

8.4 CURRENT HAZARD STUDIES

With the philosophy that hazards should be evaluated as realistically as possible before they have an opportunity to occur during operation, a continuing experimental hazard-evaluation program has been an integral part of the GE-ANPD development effort.

8.4.1 REACTOR EFFLUENT DILUTION

In addition to standard monitoring of normal operations and the accompanying program of verification of predicted downwind doses, a continuing experimental program is conducted to secure data about reactor-effluent dilution. The experiments have three principal objectives: (1) determination of fission product release factors for normal and abnormal conditions; (2) determination of hazard levels for various methods of isotope reception (inhalation, iodine intake in milk, etc.) for particular isotopes at specified distances downwind from the point of effluence; and (3) correlation of the observed field data with meteorological parameters, to improve prediction capability.

During instantaneous or continuous conditions a measurable amount of fission products is released from an operating reactor during either normal or abnormal operation, and the levels of activity at specified distances over a specially designed field grid are determined. Measurements of meteorological parameters for correlation with dilution rates of the effluent are made. Sampling for vertical distribution of the effluent and deposition on vegetation are planned, and consideration is being given to the placement of dairy cows to determine parameters for iodine in milk.

Present capabilities permit experiments to be conducted at distances as great as 4 miles from the point of effluence on a 60-degree grid northeast of the ANPD site at the Idaho Test Station, and plans are under way for measurements over greater distances on

~~CONFIDENTIAL~~
~~SECRET~~

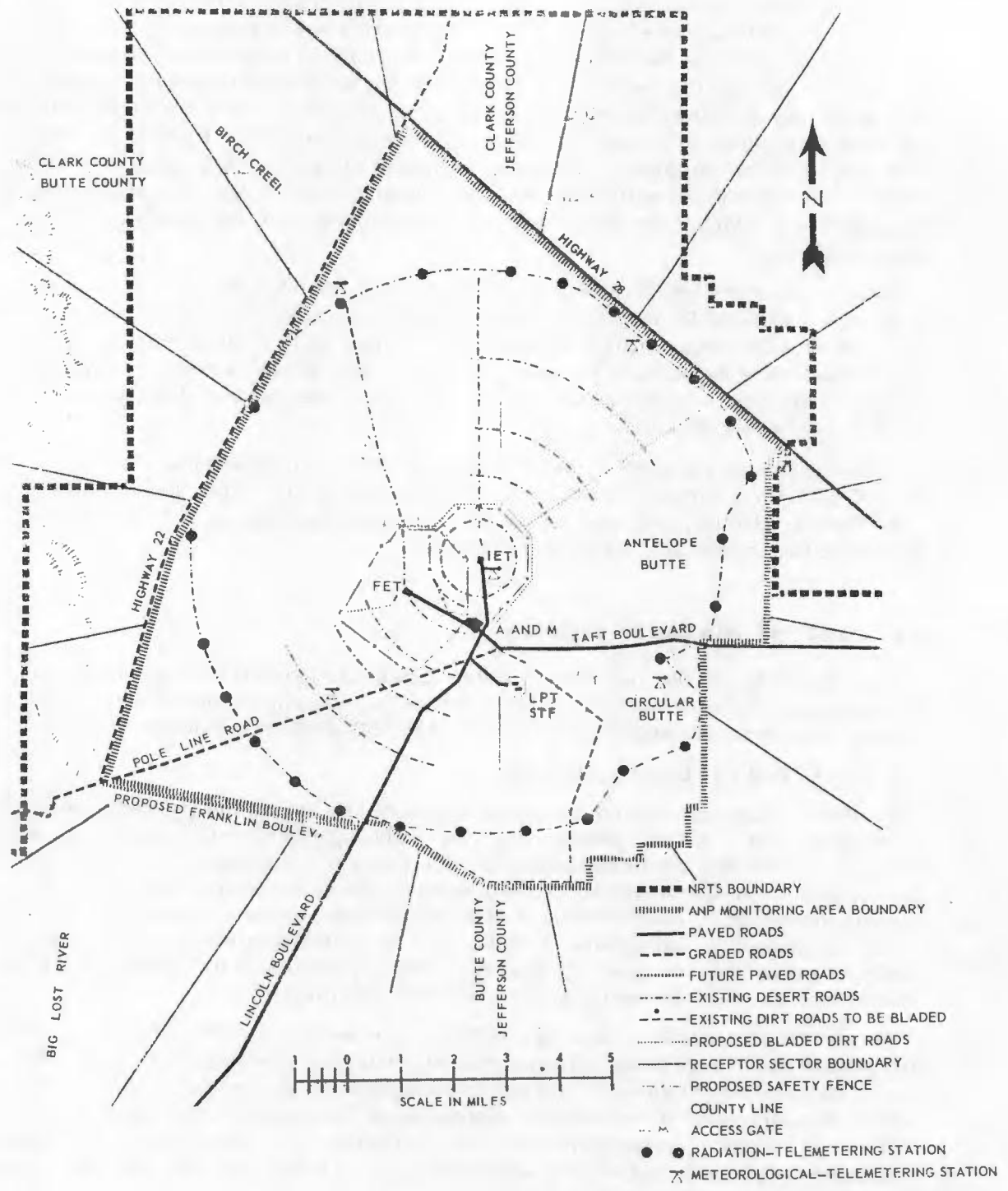


Fig. 8.22 - GE-ANPD monitoring area

~~SECRET~~

a grid southwest of the site. In addition, equipment to permit dispersal experiments using fission product simulants to obtain atmospheric dilution data has been installed. Such experiments will provide needed information on atmospheric processes, but do not adequately represent a fission product cloud or provide data on release fractions, radioactive-cloud composition, etc.

A program is being conducted to develop instrumentation for the direct measurement of parameters necessary to predict the dilution of reactor effluents and the degree of hazard resulting. The measured parameters would be incorporated into a complete measurement and data-processing system.

8.4.2 LIMITED-MELT EXPERIMENTS

The first limited-melt experiment with ceramic fuel elements, LIME I, was performed at ITS on August 25, 1960. The experiment was performed in a very smooth, routine manner; and although the analysis of the available data is not yet complete, the data appear to be consistent and valuable.

8.4.2.1 Purpose of Experiment

LIME I was designed primarily to provide information about the physical characteristics of ceramic fuel elements made molten by nuclear heating in a reactor environment and secondarily to provide a concentrated source of airborne fission products suitable for testing an electrostatic air-cleaning device and for conducting an atmospheric diffusion study.

8.4.2.2 Description of Reactor

The limited-melt experiment was designed for the CTF using the HTRE No. 2 parent reactor and a specially designed insert cartridge (L2E-4). The cartridge contained (1) ceramic fuel elements, (2) a buffer zone of unfueled BeO tubes, and (3) an insulation boundary layer. A cross-sectional drawing of the insert indicating the fuel, thermocouple, and insulation arrangements is shown in Figure 8.23. The air-coolant channels of the central bundle of 18 fuel elements in the insert were completely blocked, and the surrounding fuel elements were orificed to permit only partial cooling. Thus melting temperatures were assured when the reactor system was operated at full power.

8.4.2.3 Method of Operation

The reactor system was operated at reduced power on August 22 and 23 for a total of 8.15 megawatt-hours to establish the desired premelt fission product inventory for the tracer aspects of the experiment. About 1.83 percent of the total power was provided by the insert. After sufficient decay of short-lived fission products (to reduce the potential hazard), the reactor was operated at full power (10 megawatts) on August 25 for 10 minutes to melt a significant portion of the ceramic fuel elements and to release fission products.

8.4.2.4 Preliminary Results

Approximately 10 percent of the effluent was diverted through the side loop to the precipitator during the melting, and very early estimates of the removal efficiencies are 87 percent for I^{135} , 97 percent for I^{134} , and 96 percent for gross gamma emitters.

The cloud containing the melt effluent was monitored throughout the 20,000-foot sampling sector and beyond the site boundary. The approximate width of the cloud is indicated in Figure 8.24. The approximate maximum external gamma dose rates monitored under the cloud during passage are given in Figure 8.25. Milk samples collected from farms in the path of the cloud indicated some iodine activity in the milk from four farms. The maximum concentration was 0.5 picocuries* (pc) per milliliter, which is far below acceptable limits.

*Picocuries = micro-microcuries.

~~CONFIDENTIAL~~
~~SECRET~~

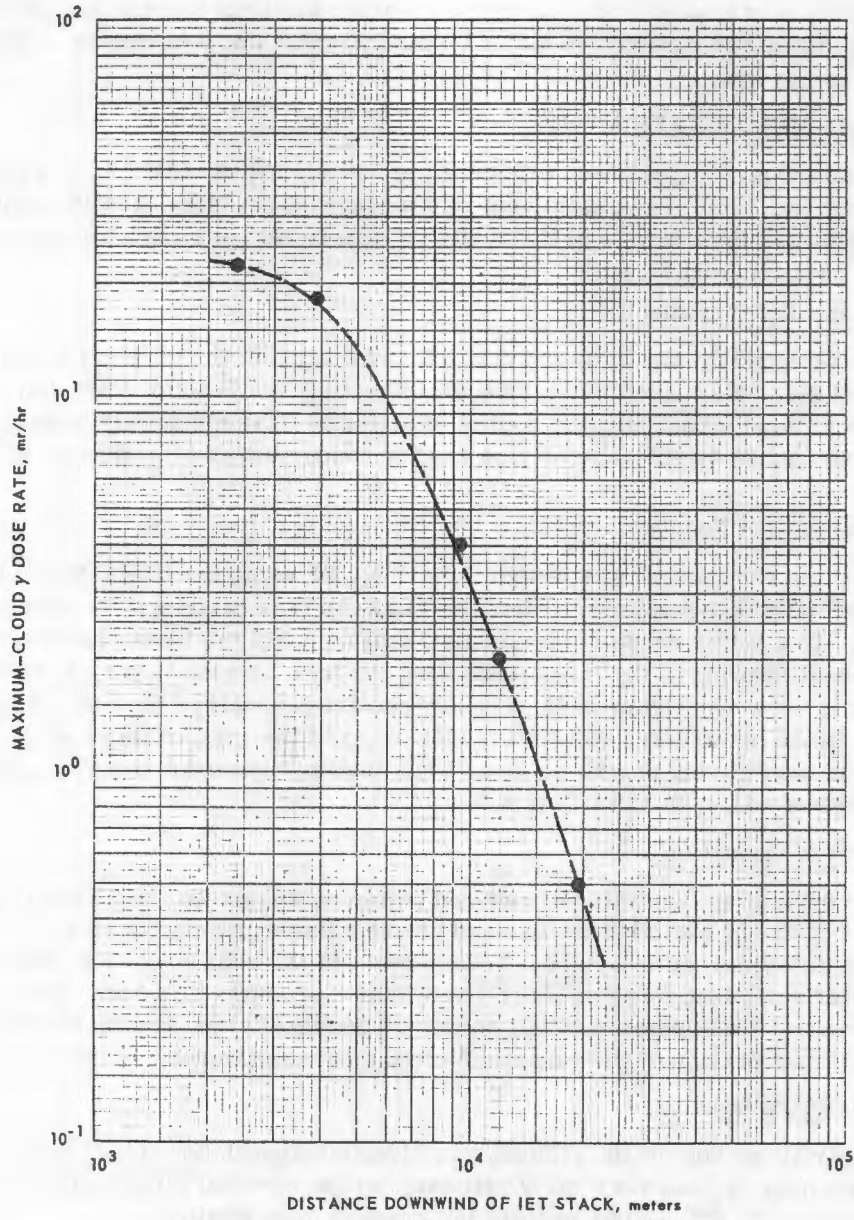
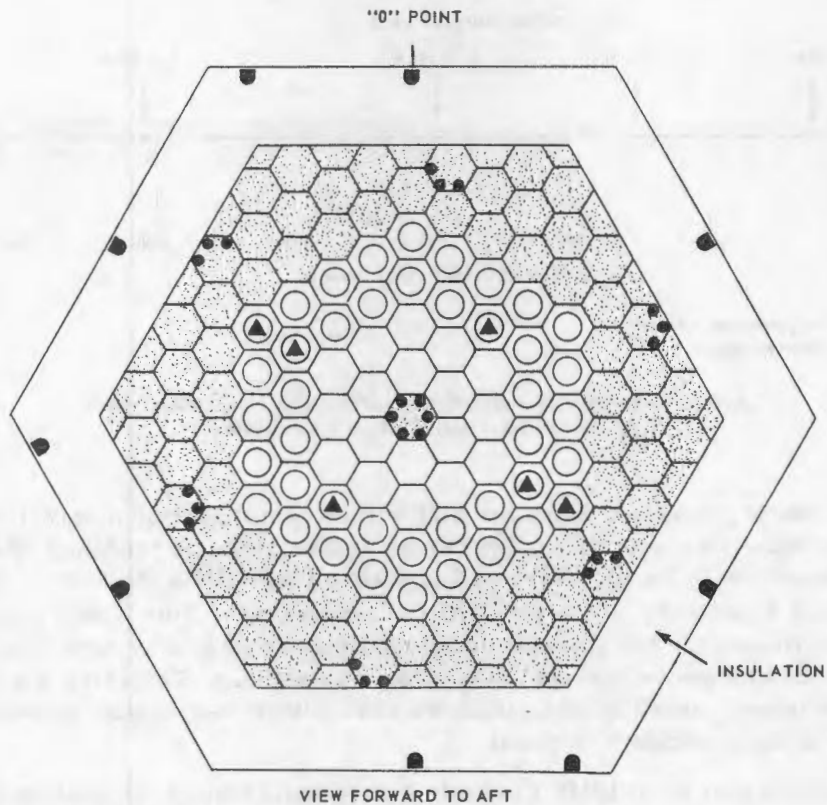


Fig. 8.25 - Maximum-cloud gamma dose rates downwind of the IET stack, based upon preliminary LIME I data

~~SECRET~~
~~CONFIDENTIAL~~



- | | |
|--|--|
| Thermocouples: | |
|  Fueled tubes, plugged |  Unfueled region |
|  Fueled tubes, orifices |  Fueled region |
|  Unfueled tubes |  Insulation liner |
| |  Exit air |

Fig. 8.23 - Layout of Insert L2E-4 showing thermocouple locations

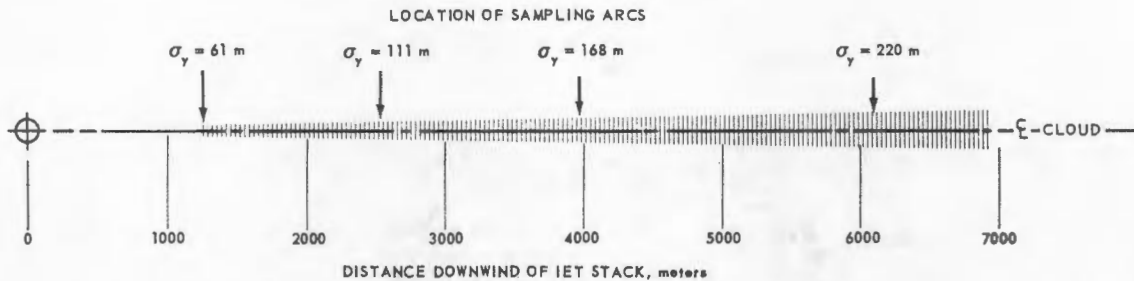
This was the first release from GE-ANPD operations that was sufficiently large to obtain measurable iodine activity in the milk from off-site farms.

8.4.2.5 Significance of Results

Analysis of LIME I permits a more realistic evaluation of the possible consequences of core damage resulting from severe coolant airflow maldistributions in the unlikely event that they occur.

Before the LIME I experiment there was some question as to whether a localized-melt region could be detected early enough in a full-size ceramic core to prevent its growth into a major accident. The fission product release rate from LIME I was a factor of 15 to 20 times that encountered during the testing of Insert 2B. During the later phase of the Insert 2B testing program the insert was operated at relatively high ($\sim 3000^{\circ}\text{F}$) temperatures. At that time the insert was operated at 1 megawatt and continuously released about 0.01 of

~~CONFIDENTIAL~~
~~SECRET~~



Cloud width is given as σ_y measured in meters.
 $2\sigma_y^2 = C_y^2 X^{2-n}$ in the Sutton equation

Fig. 8.24 - Approximate width of cloud from LIME I preliminary data, indicated by total activity from air samples

the fission products generated. Since the ACT will be operated at 50 megawatts and is expected to continuously release only 0.0008 of the fission products produced, the advent of a local-melt region in the ACT core will produce an immediate increase in air activity a factor of about 4 (or more) above the continual release rate. This timely warning mechanism will be sufficient for the operator or automatic systems to shut down or scram and thus prevent more extensive damage to the other core regions. Therefore if a localized-melt region is indeed caused by some unknown and unlikely mechanism, preventive actions will not allow a major accident to result.

The preliminary data from LIME I indicate a successful test. A completely successful experiment of this type can yield much valuable information concerning the radiological aspects of fission product release. Vegetation and fallout samples collected throughout the sampling sector will permit a better evaluation of potential thyroid doses through the milk cycle. These data coupled with the first measurable concentrations of I^{131} in milk as a result of the controlled release are the first significant applicable data on what is presently the most limiting parameter of biological consequences.

Dual filters used on the air samplers (a standard filter paper backed by carbon-impregnated fibers) will provide better information concerning doses resulting from inhalation of the cloud than any previously available data. The meteorological conditions selected for the release were favorable for a study of atmospheric diffusion, which will be supplemented by fallout data over the entire range of the sampling network.

8.4.3 SUB-LIME TEST

LIME I was not intended to be representative of a classical blockage in an ANPD reactor. Instead, it was designed to insure melting so that the spread of damage could be studied. Another insert design (L2E-6) being considered would reasonably approximate complete blockage of a 19-tube bundle in the ACT during operation at approximately 50 megawatts. The complete blockage of a bundle of 19 tubes in the ACT operating at approximately 50 megawatts with full airflow in adjacent tubes results, according to thermodynamic calculations, in a marginal melt condition wherein the heat from the molten fuel is in equilibrium with the heat removed by adjacent coolant channels and the molten region does not spread. This experiment would be a reasonably good check on the adequacy of the thermodynamic theory to predict core damage as well as an interesting experimental mockup of ACT blockage consequences.

8.4.4 AIR-CLEANING MEASUREMENTS

A side loop has been installed in the 76-inch duct leading from the Core Test Facility to the stack. This side loop has been used to study the efficiency of an electrostatic air-

~~SECRET~~
~~CONFIDENTIAL~~

cleaning device for removal of the various fission products from the reactor effluent. Some measurements taken to date are given in section 6.1 of this report. The relatively low concentration of fission products in the effluent during normal operation has made determination of the efficiency very difficult. An insert has been built to permit greater concentrations by operation at above-normal temperatures. Effluent from other inserts will also be used whenever possible to determine the air-cleaning efficiency.

8.4.5 TREAT TESTING OF FUEL ELEMENTS

A series of experiments has been proposed to investigate damage to ceramic fuel elements as a consequence of an excursion. This study will make use of the Argonne National Laboratory TREAT facility, which is capable of pulse operation to produce heating rates very similar to those expected during an excursion of the ACT reactor.

The initial testing phase of this program will begin early in October. Results of the initial phase will determine the advisability of similar, more extensive testing to determine fission product release as a function of fuel element damage resulting from a transient excursion.

8.4.6 IMPACT-DEFORMATION EXPERIMENTS

A theoretical approach to crash deformation of a nuclear reactor was evaluated in an impact test performed at the General Electric Missile and Space Vehicle Department with a simplified model. The model, a 10-pound cylindrical object alternately hollow and solid and represented analytically as a double spring-mass system, was impacted axially at 300 feet per second by a 50-pound slug. Displacements, accelerations, and strains were measured directly. The measurements corresponded approximately with theoretical predictions, except that dynamic critical buckling strengths were greater than estimated. Further tests are planned at lower energies, with the intentions of increasing the volume of information gathered from oscillograph readings and strain measurements.

Larger-scale experiments are planned in which controlled crashes will be made of models having mechanical characteristics of design reactors. Equipment now in existence at various sites will be used in these high-velocity impact tests. The object will be to determine the probable modes of deformation and their nuclear consequences.

8.5 METHODS AND FORMULAE FOR HAZARDS CALCULATIONS

8.5.1 HAZARDS FORMULAE

The equations to be used when winds are steady or when the source is instantaneously produced are

For inhalation:

$$D = \frac{0.114 C_Z F_T P_0}{\bar{u} C_y} \sum \frac{f_a \bar{E} \gamma (1 - e^{-\lambda T}) e^{-\lambda t} e^{-\frac{h^2}{\sigma_z^2}}}{f_c g \lambda_e} e^{-\frac{h^2}{\sigma_z^2}} \quad \text{rads}$$

For gammas from deposited fission products:

$$D = 13.7 \frac{V_D}{\bar{u}} e^{-\frac{h^2}{\sigma_z^2}} e^{-\frac{2 V_D}{\pi^{1/2} \bar{u}} \int_0^x \frac{e^{-\frac{h^2}{\sigma_z^2}}}{\sigma_z} dx} F_T J(t_e) \rho \mu_a \left[G_1 + \frac{k}{2} G_2 \right] \quad \text{rads}$$

~~CONFIDENTIAL~~
~~SECRET~~

For gammas from airborne fission products:

$$D = 27.4 F_T P_\gamma(t_e) \frac{\rho \mu_a}{\bar{u}} [I_1 + KI_2] \quad \text{rads}$$

When the instantaneous emission of fission products at the time of formation is considered, in using the above equations and in calculating $J(t_e)$ and $P_\gamma(t_e)$, the value of T in the expression $\sum [f_a \bar{E} \gamma (1 - e^{-\lambda T}) e^{-\lambda t_e}]$ is assumed to be 1 second. The total dose is the product of this dose rate per second and the reactor operating time.

For the thyroid dose due to iodine-contaminated milk when winds are steady

$$D' = 2080 \frac{V_D}{\bar{u}} \frac{C_Z}{C_Y} \frac{m}{M} a f_m e^{-\frac{2 V_D}{\pi^{1/2} \bar{u}} x - \frac{h^2}{\sigma^2}} \int_0^x \frac{e^{-\frac{h^2}{\sigma^2}}}{\sigma} dx$$

$$F_T P_0 \sum \left(\frac{f_a \bar{E} \gamma \lambda e^{-\lambda t_e}}{f_c g \lambda_e} \right) e^{-\frac{h^2}{\sigma_Z^2}} \quad \text{rads per second of operation.}$$

When varying wind directions are involved, the average dose in any sector of angle Θ (radians) is

For inhalation:

$$D = \frac{0.202 F_T P_0}{\bar{u} x} \sum \frac{f_a \bar{E} \gamma \lambda e^{-\lambda \frac{x}{\bar{u}}}}{f_c g \lambda_e} e^{-\frac{h^2}{\sigma_Z^2}} \quad \text{rads per second of operation.}$$

For gammas from deposited fission products:

$$D = \frac{24.3 V_D}{\Theta \bar{u}} F_T J(t_e) e^{-\frac{2 V_D}{\pi^{1/2} \bar{u}} x - \frac{h^2}{\sigma^2}} \int_0^x \frac{e^{-\frac{h^2}{\sigma^2}}}{\sigma} dx$$

$$\frac{e^{-\frac{h^2}{\sigma^2}}}{\sigma} \frac{\mu_a}{x} \left[\bar{G}_1 + \frac{K}{2} \bar{G}_2 \right] \quad \text{rads per second of operation.}$$

For thyroid dose due to contaminated milk:

$$D = \frac{3680 V_D}{\Theta \bar{u}} \frac{m a f_m F_T P_0}{M \sigma} \sum \left(\frac{f_a \bar{E} \gamma \lambda e^{-\lambda \frac{x}{\bar{u}}}}{f_c g \lambda_e} \right)$$

$$e^{-\frac{2 V_D}{\pi^{1/2} \bar{u}} x - \frac{h^2}{\sigma^2}} \int_0^x \frac{e^{-\frac{h^2}{\sigma^2}}}{\sigma} dx e^{-\frac{h^2}{\sigma^2}} \quad \text{rads per second of operation.}$$

~~CONFIDENTIAL~~
~~SECRET~~

Explanation of symbols used in the preceding equations:

- a equivalent area of grass eaten by a cow in one day. When applied to wind scale data, a is 11.3 square miles, obtained by assuming the daily feed intake of the cows is 30 pounds and a total of 1200 grams of vegetation per square mile.

- C_y, C_z virtual diffusion parameters in y and z directions

- D dose, rads

- \bar{E} effective energy per disintegration, Mev

- f_a fraction of inhaled isotope that reached a critical organ

- f_c fraction of organ in which the isotope is deposited

- f_m fraction of iodine that cow eats and thus has in its milk

- F_T product of fractions that affect the release of fission products

- g mass of critical organ, grams

- G_1, G_2 integrals for converting ground concentrations into doses

- h_e effective stack height

- I_1, I_2 integrals for determining dose from cloud

- $J(t_e)$ energy remaining in emitted fission products at time t_e , watt-second

- K $\frac{\mu - \mu_a}{\mu_a}$

- m amount of milk drunk per day, 10^3 cc.

- M amount of milk produced per day per cow, 10^4 cc.

- n dimensionless diffusion parameter

- P_0 power level of reactor, watts

- $P_\gamma(t_e)$ gamma power of emitted fission products at time t_e

- Q amount of Be emitted per second

- t_e time after emission that exposure occurs (usually t_e is equal to $\frac{x}{\bar{u}}$), seconds

- T time reactor operates at power P_0 , seconds

- \bar{u} wind velocity, miles per second

- V_D deposition velocity of airborne contaminants

- x, y, z position coordinates; point (0, 0, 0) is at the base of the stack, x is measured in the direction of the wind, and z is the vertical distance from ground.

- σ fission yield of fission product isotope

- γ subscript indicating gamma radiation

- θ angular width of sector, radians

- ρ specific gravity of air (ρ is 1 for normal temperature - pressure conditions)

- λ radioactive decay constant

- λ_e $\lambda + \lambda_b$, the effective elimination constant

~~CONFIDENTIAL~~
~~SECRET~~

λ_b	biological elimination constant
μ	total absorption coefficient (m^{-1})
μ_a	energy absorption coefficient (m^{-1})

8.5.2 METHODS AND ASSUMPTIONS USED IN RUNAWAY ANALYSIS

The first step in determining the shutdown mechanism for the unchecked runaway was choosing a realistic model that would readily lend itself to available analysis techniques.

The model used operates in the following manner. A controls failure or operator action causes the withdrawal of all control rods at their nominal rate that adds reactivity to the system at a rate of $6.0 \times 10^{-4} \Delta k$ per second. The resulting runaway generates enough energy to completely melt the reactor and to bring the reactor temperature to the vaporization point. Fundamental flux modes are assumed to apply throughout the runaway. Therefore, because of the flat radial power distribution, vaporization starts uniformly across the radius at the longitudinal midplane. Vapor pressures that accelerate the reactor apart longitudinally and terminate the runaway are then built up. In the model, two limiting cases of vapor release were considered. One case assumed that there was no vapor escape because all free-flow passages were blocked from the melting. The other case assumed no vapor-flow blockage; the vapor was allowed to escape from the reactor at sonic velocities.

The analysis of the coupled nuclear-thermodynamic-mechanical system was performed in two integrated phases. The first phase involved reactor kinetics calculations in which the time-dependent power and energy were calculated up to the point when vaporization started.

In the second phase, by utilizing the power- and energy-generation rates from the kinetics calculations of the first phase as input, the mechanics and thermodynamic calculations were performed to describe the physical events occurring after vaporization started. The fuel element vaporization and resulting core separation that was calculated in the second phase was used to calculate a negative reactivity effect due to core separation.

A second iteration was then performed to obtain the power turnover resulting from the reactivity effect of core separation. The new power- and energy-generation rates were then used in the second iteration of phase two to determine final values for the fraction of the core that was vaporized and for the accelerations that were obtained.

The reactor kinetics analysis and the mechanics and thermodynamics analysis that were used are described on the following pages.

Reactor Kinetics Analysis

The reactor kinetics analysis of the runaway involved, as a function of time, the solution of the coupled equations for off-critical fission power, the concentrations of six delayed neutron emitters, and the reactivity, both causing and caused by the runaway.

The numerical solution utilizing the Runge-Kutta technique for the following equations was performed by the IBM 704 computer with ANPD Program 129, which is described in detail in APEX-457. *

$$\frac{dP(t)}{dt} = \frac{k_{ex}(1-\beta_e) - \beta_e}{l} P(t) + \frac{1}{lc} \sum_{i=1}^6 \lambda_i E_i r_i(t) \quad (1)$$

*F. W. Mezger, "Simple Reactor Runaway Analysis," Technical Information Service, APEX-457, 1959.

~~SECRET~~

$$\frac{dr_i(t)}{dt} = \beta_i c \nu P(t) - \lambda_i r_i(t), \quad i = 1 \dots 6. \quad (2)$$

$$k_{ex} = k_{ex, T} + k_{ex, i} \quad (3)$$

Where

- β_e = effective delayed neutron fraction
- $P(t)$ = power at time t
- l = neutron generation time
- $c = 3.1 \times 10^{10}$ fissions per second per watt
- $\nu = 2.46$ = neutrons per fission
- λ_i = decay constant of i^{th} delayed group
- E_i = ratio of effective-to-actual fraction of i^{th} neutron group
- $r_i(t)$ = Concentration of i^{th} neutron group at time t
- $k_{ex, i}$ is excess reactivity that induces the runaway
- $k_{ex, T}$ is excess reactivity caused by the runaway

In the program, four distinct stages of a runaway, the end of each of which can be terminated by either time, power level, or energy that is generated, are allowed. In the first three stages, any arbitrary combination of different step, linear, and accelerational reactivity changes can be inserted, and, in all four stages, different reactivity coefficients can be defined.

The equations of $k_{ex, i}$ and $k_{ex, T}$ have the following general form for the first time stage.

$$k_{ex, i} = S_1 + l_1 + \frac{a_1}{2} t^2; \quad \text{for } 0 \leq t < t_1 \quad \text{and} \quad (4)$$

$$k_{ex, T} = \gamma_1 \int_0^t P(t') dt'; \quad \text{for } 0 \leq t < t_1.$$

In subsequent time stages, cumulative equations of a similar form are used for the reactivity.

The negative temperature coefficient in runaway B was expressed in the program as a coefficient proportional to the total energy released. Figure 8.26 shows the results of thermodynamic analysis in which the relationship between temperature rise and energy release during a runaway is shown. When the data on Figure 8.26 are combined with the data from the bottom curve in Figure 2.14, which shows $\Delta k/k$ versus temperature, a value of reactivity versus energy is obtained. This value was $-9.1 \times 10^{-12} \Delta k/k$ per watt-second and was assumed to apply to 5.0×10^9 watt-seconds (the melting point).

For the analysis showing reactor scrams, a nominal -2 percent Δk was assumed as the scram worth. In each case, it was used as a linear negative change over a 300-millisecond time interval. The actual ACT controls system will have larger scram capability than this. In all cases of power or period scrams, a scram initiation delay of 140 milliseconds was assumed.

For runaways terminated by core separation due to fuel vaporization, the negative reactivity effect causing shutdown used in the analysis was a negative reactivity co-

CONFIDENTIAL
~~SECRET~~

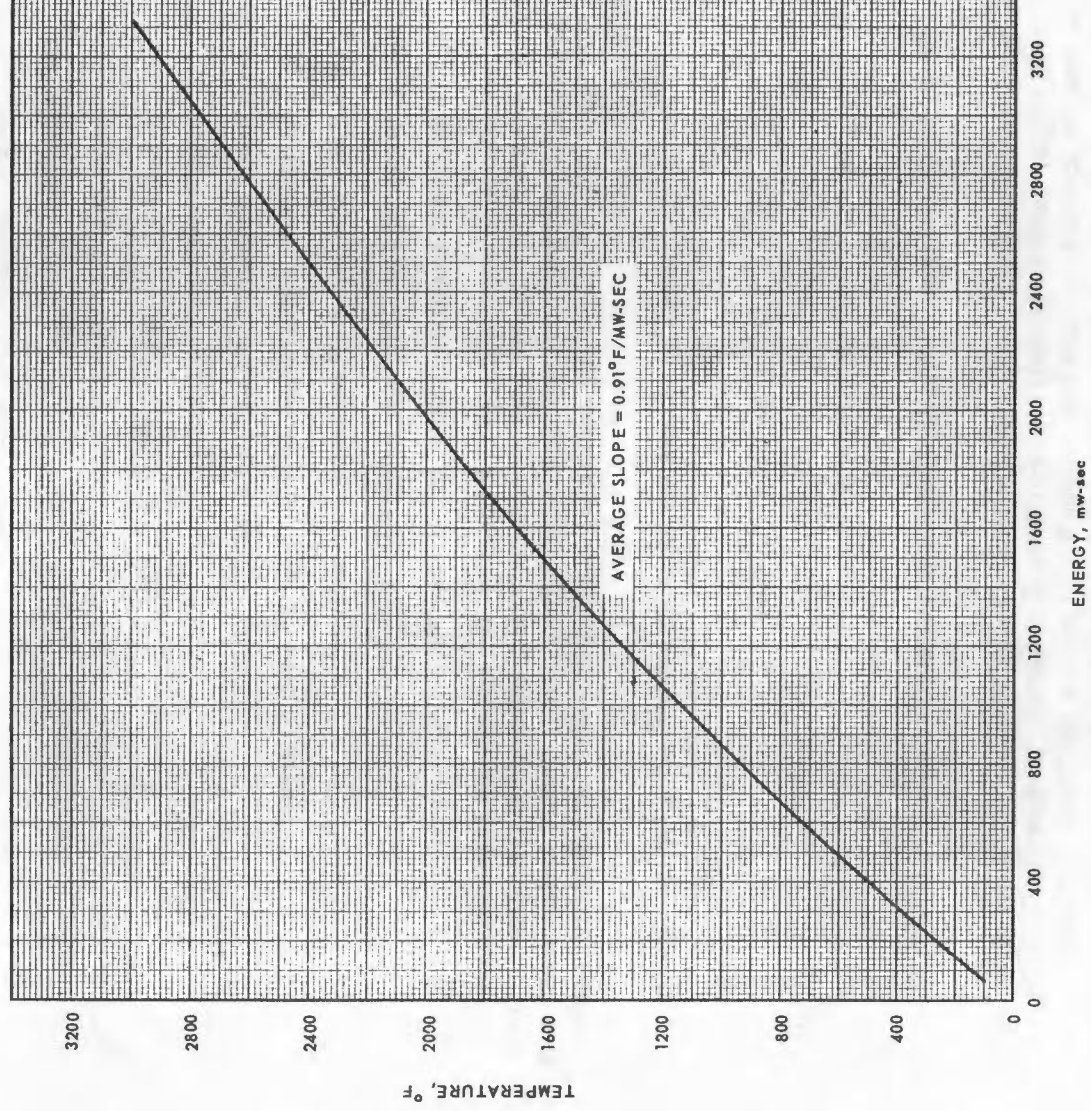


Fig. 8.26 -- Temperature rise versus energy evolved during runaway

CONFIDENTIAL
~~SECRET~~

8. 6. 3 SPECTRA

The prompt fission spectrum used for both U²³⁵ and U²³⁸ is a modification* of the original Watt spectrum and is given by

$$S(E) = 0.45270463 e^{-E/0.965} \sinh \sqrt{2.29 E},$$

where E is in Mev and S(E) is normalized to one neutron.

8. 6. 4 DELAYED NEUTRONS

The delayed neutrons are lumped into six delay groups. The spectra are based on data of Batchelor, Hyder, and Bonner and are described in APEX-458.† The delay fractions, β_j , and decay constants ω_j , contained in APEX-458 have been revised to an average of values due to fissions induced by slow neutrons and by fast neutrons.‡

Group	β_j	$\omega_j, \text{sec}^{-1}$
1	0.00023	0.0126
2	0.00142	0.0311
3	0.00126	0.1134
4	0.00264	0.3060
5	0.00080	1.253
6	0.00022	3.381

$$\beta = 0.00657$$

*L. Cranberg, G. Frye, N. Nereson, and I. Rosen, "Fission Neutron Spectrum of U²³⁵, Phys. Rev. 103, No. 3, August 1, 1956, 662.

†B. H. Duane, R. E. Reid, and D. S. Selengut, "Off-Critical Reactor Theory," APEX-458, October 1956.

‡G. R. Keepin, T. F. Wimett, and R. K. Ziegler, "Delayed Neutrons from Fissionable Isotopes of Uranium, Plutonium, and Thorium," Phys. Rev. 107, 1957, 1044.

1951
1000

1000
1000

1000
1000

1000
1000

1000
1000

Year	Value	Year	Value
1951	1000	1952	1000
1953	1000	1954	1000
1955	1000	1956	1000
1957	1000	1958	1000
1959	1000	1960	1000

1000
1000

1000
1000

1000

efficient proportional to the total energy evolved after 2.67×10^{10} watt-seconds. This is the total evolved energy necessary to raise the core temperature to the point when vaporization starts ($\sim 8000^\circ\text{F}$). Detailed nuclear analysis showed the effect of longitudinal core separation to be $-6.4 \times 10^{-3} \Delta k$ per centimeter of separation. From the energy evolved and the thermal characteristics (heat of vaporization) of the materials, a relationship between energy and core separation was obtained. Combining the reactivity versus separation and energy versus separation relationships yielded a curve of $-\Delta k$ versus energy evolved. This is shown in Figure 8.27. The two average values over the indicated energy ranges, shown in Figure 8.27, were used in the analysis.

As explained earlier in the report, the assumption of vaporization starting as a disk at the longitudinal peak-power point seems justified. Once vaporization has started, following melting of the total core, it is difficult to say whether the vapor can initially leave the system. It would seem that, since all of the reactor is melted, the coolant channels would be sufficiently blocked and would prevent vapor losses. However, to bracket the value of the fraction of the core that is vaporized, calculations were made for the case of no vapor escape before core separation and for the case of vapor release until sonic velocity was reached and choking resulted. Thus there is a range between 2.5 and 4 percent vaporized core. Dose-rate calculations were based on the 4 percent figure.

In both the above cases, the vapor pressure is assumed to generate forces capable of accelerating the core apart. The calculated accelerations were 3 to 4 orders of magnitude greater than that required to overcome the structural integrity built into the system, i. e., capability of taking 8-G accelerations at the front and 2-G at the rear.

Mechanics and Thermodynamic Analysis

Mechanics and thermodynamic calculations were performed in the runaway analysis after the start of fuel element vaporization. The active core was assumed to have attained a constant temperature of 8000°F before vaporization started. Vaporization was then assumed to commence at the midplane of the active core.

Vapor buildup in the core was treated in two limiting cases.

1. Case 1 - No vapor escape from the core before separation.
2. Case 2 - The core remained intact (including flow area) up to the time of physical separation. The rate of vapor flow was related to the rate of vapor buildup by assuming sonic flow at the core exits.

Case 2 yields higher vaporization and was used to calculate the dose rates for the runaway. Equations will be given for case 2 only when the case of no vapor flow is considered a special case of case 2.

At the time the separation calculations were started, the data generated in kinetics analysis were assumed to apply, i. e.,

Power	5.2×10^{11} watts
Energy	2.67×10^{10} watt-seconds
Time	12.818 seconds.

The thermodynamic derivations pertinent to the calculations are:

1. Rate of vapor buildup = rate of vaporization - rate of vapor flow

$$\frac{dM_v}{dt} = \frac{dM}{dt} - W_f \quad (1)$$

~~CONFIDENTIAL~~
SECRET

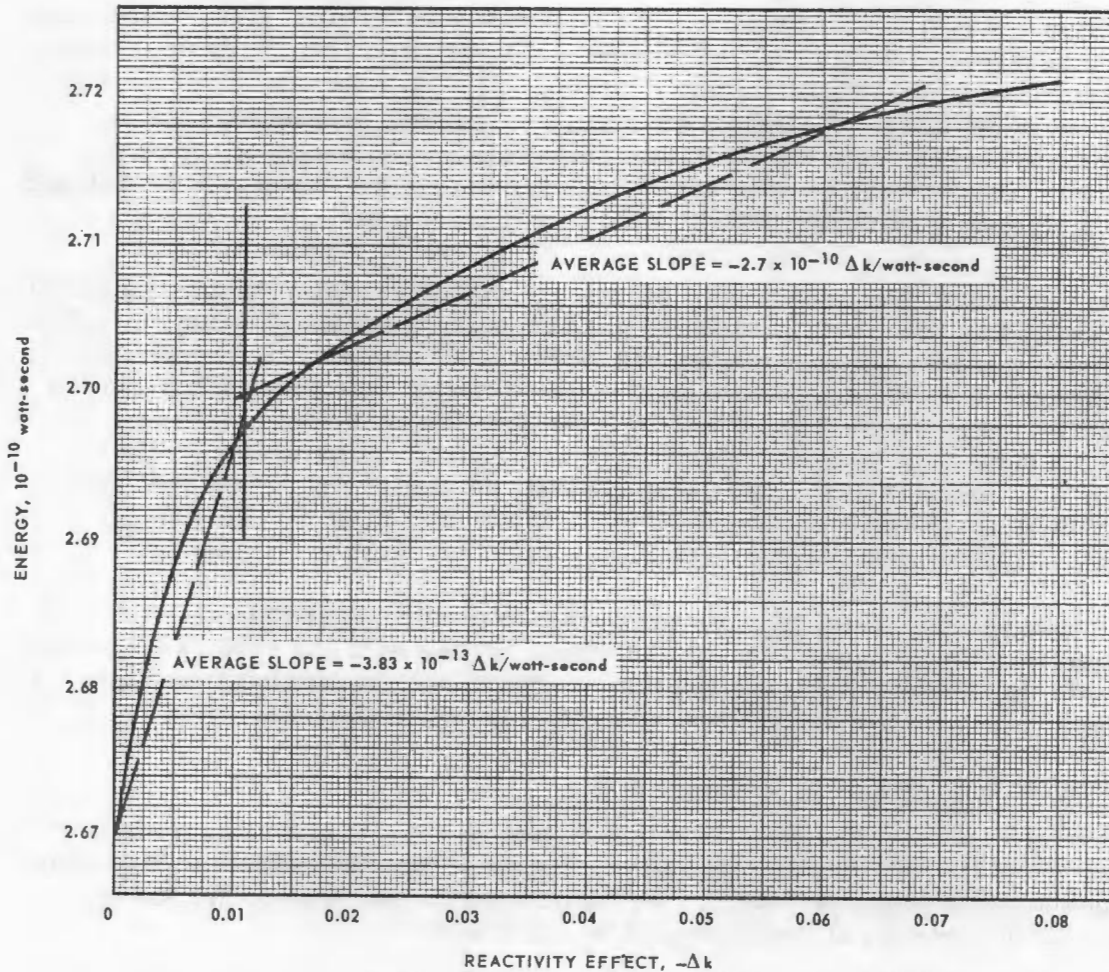


Fig. 8.27 - Evolved energy after start of vaporization versus reactivity effect of vaporization

2. W_f is related to M_v by assuming a mach number of 1 at the core exits. The relationship for maximum flow of a perfect gas under isentropic conditions is:

$$\frac{\left(\frac{W_f}{A}\right) \sqrt{\frac{R}{g_c} T_t}}{P_t} = \sqrt{k \left(\frac{2}{k+1}\right)^{\frac{k+1}{k-1}}} \quad (2)$$

3. The perfect gas law is assumed to apply

$$P = \rho RT = \frac{M_v}{V} RT \quad (3)$$

All vapor in the system is assumed to be contained in the active core void at a constant pressure, and this pressure and temperature are assumed to be equivalent to the total pressure and total temperature at the core exits.

SECRET
~~CONFIDENTIAL~~

4. Combining equations (2) and (3) gives

$$W_f = \sqrt{k \left(\frac{2}{k+1} \right)^{\frac{k+1}{k-1}}} \cdot \frac{A}{V} \sqrt{g_c RT} M_v \quad (4)$$

and by substituting $\alpha = \sqrt{k \left(\frac{2}{k+1} \right)^{\frac{k+1}{k-1}}} \cdot \frac{A}{V} \sqrt{g_c RT}$

$$W_f = \alpha M_v \quad (5)$$

The rate of vapor formation $\frac{dM}{dt}$ is related to power by assuming a single exponential function for power in the neighborhood of the time value at which the core has achieved vaporization temperature

$$\frac{dM}{dt} = \frac{P(t)}{\Delta H_{\text{vaporization}}} = K e^{\beta t} \quad (6)$$

Equation 1 becomes

$$\frac{dM_v}{dt} = \frac{dM}{dt} - \alpha M_v$$

or $dM_v = dM - \alpha M_v dt$ (7)

5. An exact solution to the differential equation is

$$d e^{\alpha t} M_v = e^{\alpha t} dM$$

$$e^{\alpha t} M_v = \int_0^t e^{\alpha t} dM \quad (8)$$

6. However, $dM = K e^{\beta t} dt$, substituting in equation (8) and integrating yields

$$M_v = K e^{-\alpha t} \int_0^t e^{\alpha t} e^{\beta t} dt$$

or

$$M_v = \frac{K}{\alpha + \beta} [e^{\beta t} - e^{-\alpha t}]_0^t \quad (9)$$

7. Pressure force is related to the translation of half the core

$$F = \frac{W_{c+r}}{g_c} \frac{d^2 x}{dt^2} \quad (10)$$

~~CONFIDENTIAL~~
~~SECRET~~

8. Taking $F = PA'$ and using the perfect gas law acceleration becomes

$$\frac{d^2x}{dt^2} = 2g_c \frac{A' RT M_V}{V W_{c+r}} \quad (11)$$

9. Then initially $M_V(t)$, $\frac{d^2x}{dt^2}$, $\frac{dx}{dt}$, $x(t)$, and $\int_0^t W_f dt$ can be readily evaluated. From the values of $x(t)$ and $\int_0^t W_f dt$ a new value for $P(t)$ was determined from reactor kinetic relationships previously discussed, and (6) was evaluated numerically in a stepwise manner.

$$M_V(t_n) = \frac{e^{-\alpha t_n}}{\Delta H_{\text{vaporization}}} \left[\sum_{n=1}^n \int_{t_{n-1}}^{t_n} e^{\alpha t} (a_n t + b_n) dt \right] \quad (12)$$

where

$$[P(t)]_{t_{n-1}}^{t_n} = a_n t + b_n \quad (13)$$

$M_V(t_n)$ was plotted and integrated to determine

$$\frac{dx}{dt}, \int_0^t W_f dt, \text{ and } x(t)$$

$$\Delta H_{\text{total}} = \Delta H_{\text{fusion}} + 60^\circ\text{F} \frac{\Delta H}{4500^\circ\text{F}} + 4500^\circ\text{F} \frac{\Delta H}{8000^\circ\text{F}} \quad (14)$$

10. Energy required to elevate the core to a vaporization temperature of 8000°F was computed by:

$$\frac{\Delta H}{T_1 T_2} = \int_{T_1}^{T_2} C_p dT \quad (15)$$

11. Molal heat capacity was assumed to be represented by

$$C_p = 8.45 + 4 \times 10^{-3} T - \frac{3.17 \times 10^5}{T^2} \quad (16)$$

and

$$\frac{\Delta H}{T_1 T_2} \text{ becomes } \frac{W_c}{M.W.} \int_{T_1}^{T_2} \left[8.45 + 4 \times 10^{-3} T - \frac{3.17 \times 10^5}{T^2} \right] dT \quad (17)$$

Thermochemical data for heats of vaporization, fusion, and decomposition were estimated from the Kistiakowsky equation for latent heat of vaporization,

$$\frac{\lambda}{T_b} = 8.75 + 4.575 \log_{10} T_b \quad \text{and}$$

from Brewer.[†]

λ = Latent heat of vaporization, cal/mole.

T_b = Normal boiling point, °K.

*K. K. Kelley. "Contributions to the Data on Theoretical Metallurgy." Bulletin 584, Bureau of Mines, 1960.

†L. Brewer. "Thermodynamic Properties of the Oxides and Their Vaporization Processes." Chemical Reviews, 52, 1953.

~~SECRET~~

A summary of the thermochemical properties of the fuel element materials is given in Table 8.10.

TABLE 8.10
THERMOCHEMICAL PROPERTIES OF FUEL ELEMENTS MATERIALS

Component	Weight Fraction	Normal Boiling Point (T_b), °K	Latent Heat of Vaporization (λ), cal/g	Decomposition Energy (D_0), cal/g	Heat of Vaporization ($\Delta H_{\text{vaporization}}$), Btu/lb
BeO	0.738	4860	4860	5000	17,740
Zr O ₂	0.073	4570	948	2930	7,000
UO ₂	0.085	-	-	-	3,370
Y ₂ O ₃	0.104	4570	516	710	2,210
Fuel Composition	1.00	4860	-	-	14,127

Thermodynamic properties for the vapor were calculated on the assumption that BeO (the most important component) exists as atomic specie in vapor form. The gas constant (R) and the ratio of specific heats (k) are based on this assumption.

Nomenclature

<u>Symbol</u>	<u>Description</u>	<u>Units</u>	<u>Value Used</u>
M_v	Weight of Vapor contained	lb	
M	Weight of Vapor formed	lb	
W_f	Rate of Vapor flow	lb/sec	
t	Time	Seconds	
A	Flow Area (one end)	ft ²	3.855
R	Gas constant for vapor	$\frac{\text{ft-lb}}{\text{lb-}^\circ\text{R}}$	93.5
g_c	Gravitational acceleration	ft/sec ²	32.2
T	Temperature of Vapor	°R	8460
P	Pressure	lb/ft ²	
k	Ratio of specific heats for vapor	--	1.52
ρ	Density of vapor	lb/ft ³	--
V	Volume of Vapor (Core Void)	ft ³	9.96
P(t)	Power as a function of time		
F	Force	lb _{force}	--
W_{c+r}	Mass of Core and End Reflectors	lb mass	3935

~~CONFIDENTIAL~~
~~SECRET~~

Nomenclature

<u>Symbol</u>	<u>Description</u>	<u>Units</u>	<u>Value Used</u>
W_c	Mass of Core only	lb mass	2860
x	Separation distance from midplane	ft	--
A'	Pressure Area of Core (Frontal Area)	ft ²	9.427
α	Constant	sec ⁻¹	2.683×10^3
$\Delta H_{\text{vaporization}}$	Heat of Vaporization	Btu/lb	14,127
$(M.W.)_v$	Molecular Weight Vapor	lb/mole	16.54
K	Constant		34.82×10^3
β	Constant		19.44
$\Delta H_{\text{fusion}}^*$	Heat of fusion	Btu/lb	1224
$M.W.$	Molecular Weight Core	lb/mole	32.
ΔH_{total}	Total Energy required to elevate core to vaporization temperature	watt-seconds	2.67×10^{10}
C_p	Specific heat, active core	Btu/mole - °F	--

The results of the separation analysis for case 2 are given in Table 8.11.

TABLE 8.11

RESULTS OF SEPARATION ANALYSIS FOR CASE 2

Time (t), sec	Weight of Vapor in System (M_v), lb	Weight of Vapor Outside Reactor, lb	Weight of Vapor Formed (M), lb	Total Separation Distance, in.	Acceleration, ft/sec ²
0	0	0	0	0	0
5×10^{-4}	9.81	16.99	26.8	0.339	11.3×10^4
1×10^{-3}	12.8	34.3	47.1	1.77	14.7×10^4
1.5×10^{-3}	13.6	53.6	67.2	4.37	16.2×10^4
2×10^{-3}	13.2	60.7	73.9	7.3	15.2×10^4
2.5×10^{-3}	13.	82.5	95.5	11.2	14.95×10^4

For both cases 1 and 2 the total elapsed time from the completion of melting to the start of vaporization was 0.04 second. For case 1, after an additional time interval of 0.0018 second, the reactor had separated 30 inches and the rate of separation attained was 161 feet per second. Vaporization was assumed to have stopped after 30 inches separation.

8.5.3 REACTIVITY EFFECTS OF MELTED FUEL REDISTRIBUTION

To fully evaluate the hazards associated with any particular melting situation, it is necessary to account for the reactivity effect of the melted fuel redistribution. How fast and in what manner the melted fuel redistributes itself become the important factors.

*O. Kubachewski and E. Evans, "Metallurgical Thermochemistry," Pergamon Press, 1958.

~~SECRET~~

~~CONFIDENTIAL~~

The heating source distribution determines the rate and direction of melt progression and thus give the best clue to which model to assume for a given melting situation. From Figure 2.19 in section 2.1.1.3 it can be seen that the fission distribution is almost flat radially. The secondary heating radial distribution is similarly flat. From this it can be determined that, for any melt situation (from air loss at power or after shutdown), the melting will start uniformly across the radius and then progress longitudinally from the peak-power position toward the ends of the core. Since the reactor is to be operated horizontally, the molten material will sag to form something similar to a half-disk that will grow lengthwise with increased melting.

From this basic model two different curves of excess multiplication constant resulting from active core melting were obtained. In the first curve it is assumed that the radial reflector collapses into the void left by the redistributed fuel. These data were obtained from a one-dimensional, two-group slab calculation. The physical and nuclear model is shown in Figure 8.28. The transverse buckling in region B was adjusted to give the leakage corresponding to the new dimensions as shown in region B of the physical model. Figure 8.29 shows the excess multiplication constant resulting from the melting.

For the case of no reflector collapse a two-dimensional, two-group diffusion calculation was made with Program CURE. Rectangular geometry was assumed since it is the only geometry capable of mocking up this condition. The dimensions, other than length, were adjusted to give the same leakage as the radial leakage from a cylindrical reactor. The transverse dimension (W) in the void region was adjusted to approximate the transverse leakage that would occur if the void region were adjacent to the radial reflector.

Figure 8.30 shows the model, and Figure 8.31 shows the reactivity effects of the melt.

8.6 REACTOR PHYSICS

8.6.1 INTRODUCTION

The following data on neutron cross sections, fission neutron spectra, and delayed neutron data were incorporated in the nuclear analyses that are the basis for much of the nuclear design data and reactor characteristics reported. An attempt has been made to summarize the aspects of these data that would be of interest to those interpreting or evaluating this report.

8.6.2 CROSS SECTIONS

Thermal Group

All thermal group cross sections are represented by a one-group Maxwellian average of the cross sections between 10^{-4} and 10 ev. The averaging has been done using a Maxwellian distribution of neutron velocities for 68°, 500°, 1000°, 1500°, 2000°, 2500°, and 3000° F.

Beryllium - ANPD Nuclear Data Tape Designation: RBE (N, 2N)

The cross sections for beryllium came from BNL-325* and NDA-36†. One of the two neutrons from the (n, 2n) reaction is considered to be inelastically scattered; the other is considered to be a fission neutron (spectrum is independent of incident-neutron energy).

*D. J. Hughes and R. B. Schwartz, "Neutron Cross Sections," Supplement Number 1, BNL-325, January 1, 1957.

†A. Benton and M. Fleishman, "Comparison of Calculations and Critical Experiments for NDA Compact Core Reactor," NDA-36, January 31, 1957.

~~CONFIDENTIAL~~
~~SECRET~~

As used in reactor calculations, the spectrum of the fission neutron is assumed to be the same as for U^{235} fission neutrons. The appropriate relations are:

$$\sigma_s = \sigma_{s, \text{elastic}} + \sigma_{n, 2n}$$

$$\xi\sigma_s = \xi_{\text{elastic}} \sigma_{s, \text{elastic}} + \xi_{\text{inelastic}} \sigma_{n, 2n}$$

$$\sigma_{tr} = (1 - \overline{\cos \Theta}_{\text{elastic}}) \sigma_{s, \text{elastic}} + \left(1 - \frac{2}{3A}\right) \sigma_{n, 2n}$$

$$\sigma_a = \sigma_{n, \gamma} (\text{assumed } 1/v) + \sigma_{n, \alpha}$$

$$\nu\sigma_f = \sigma_{n, 2n}$$

The effect of high-energy elastic scattering anisotropy, (n, 2n) and (n, α) reactions are included within the approximations of the relations given above.

Uranium-235 (REV U 235)

The cross-section data came from the following sources.

σ_{total} : 10 Mev to 1.9 Mev, BNL-250*

1.9 Mev to 35 ev, BNL-325

Below 35 ev, from resonance parameters given in CWR-478† and an empirical

$$\text{curve of } \eta(E) = \frac{\nu\sigma_f(E)}{\sigma_a(E)}$$

σ_{fission} : 10 Mev to 14 kev, LA-2114‡

14 Kev to 35 ev, BNL-325

Below 35 ev, BNL-250

The variation of $\eta(E)$ was fit to Los Alamos 16-group values of $\frac{\nu\sigma_f(E)}{\sigma_a(E)}$ by the empirical relation

$$\eta(E) = 1.35 + (0.05646 + 1.257 \times 10^{-5} (E \text{ ev})^{0.4894}) \log_e (E \text{ ev}).$$

The variation of $\nu(E)$ was taken from ANL-5800§, where $\nu(E) = 2.47 + 0.145 E(\text{Mev})$.

The values of $\eta(E)$ and $\nu(E)$ together with σ_{total} and σ_{fission} determine σ_a and σ_s , except where resonance parameters were used, below 35 ev.

The absorption integral to cadmium cutoff (0.44 ev) is 472 barns, and the corresponding fission integral is 325 barns. Both of these values are higher than those reported by Westcott**.

Inelastic scattering at high energies has been included in $\xi\sigma_s$ using the statistical model to determine the distribution of the inelastically scattered neutrons. Elastic scattering anisotropy is contained in σ_{tr} .

*M. D. Goldberg, D. J. Hughes, J. A. Harvey, and V. E. Ralcher, "Neutron Cross Sections," BNL-250, August 1, 1954.

†D. L. Kavanagh, "Uranium Cross Sections from a Breit-Wigner Analysis," CWR-478, Vol. I, June 10, 1957.

‡R. L. Henkel, "Summary of Neutron-Induced Fission Cross Sections," LA-2114, May 8, 1957.

§"Reactor Physics Constants," ANL-5800.

**C. H. Westcott, "Effective Cross Section Values for Well-Moderated Thermal Reactor Spectra," CRRP-787, August 1, 1958.

~~SECRET~~

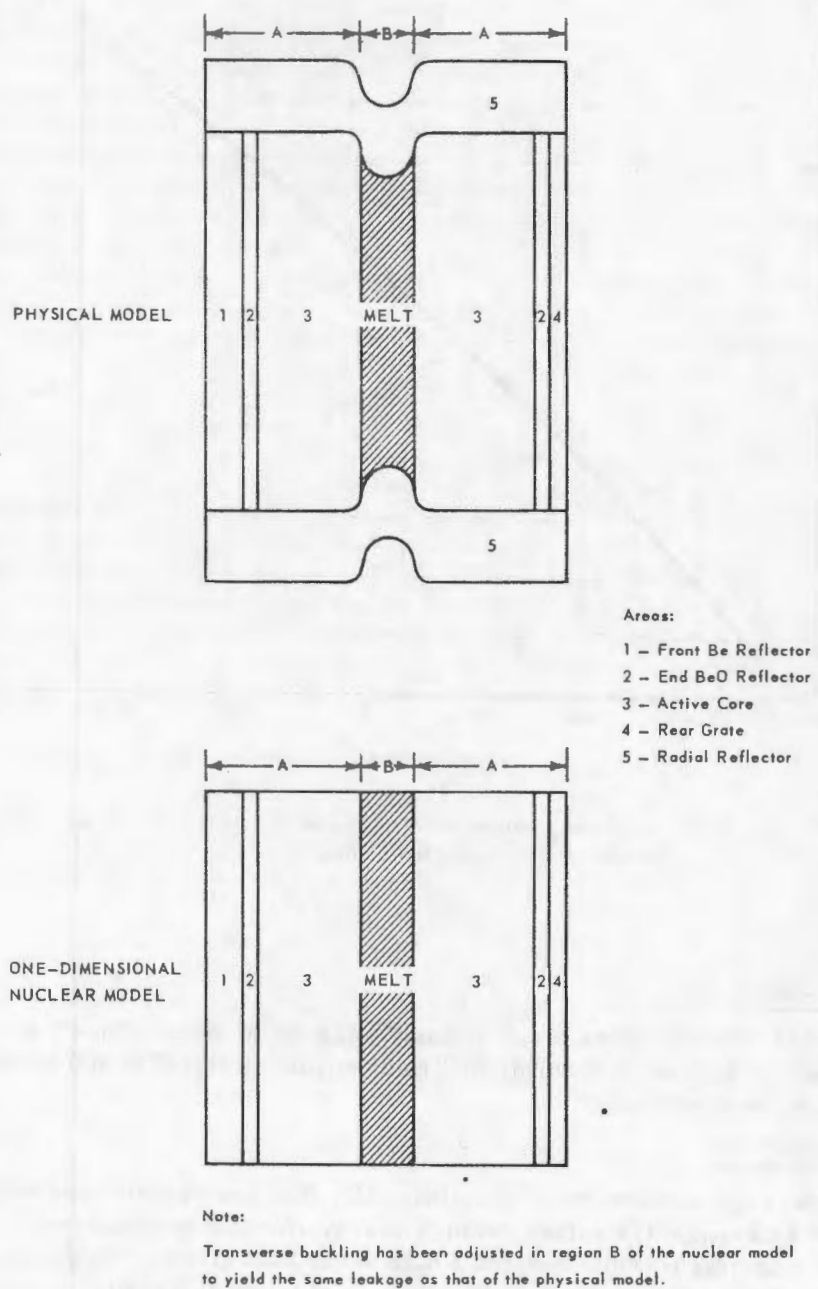


Fig. B.28 - Physical and nuclear models for calculating reactivity effects of melting with collapse of radial reflector

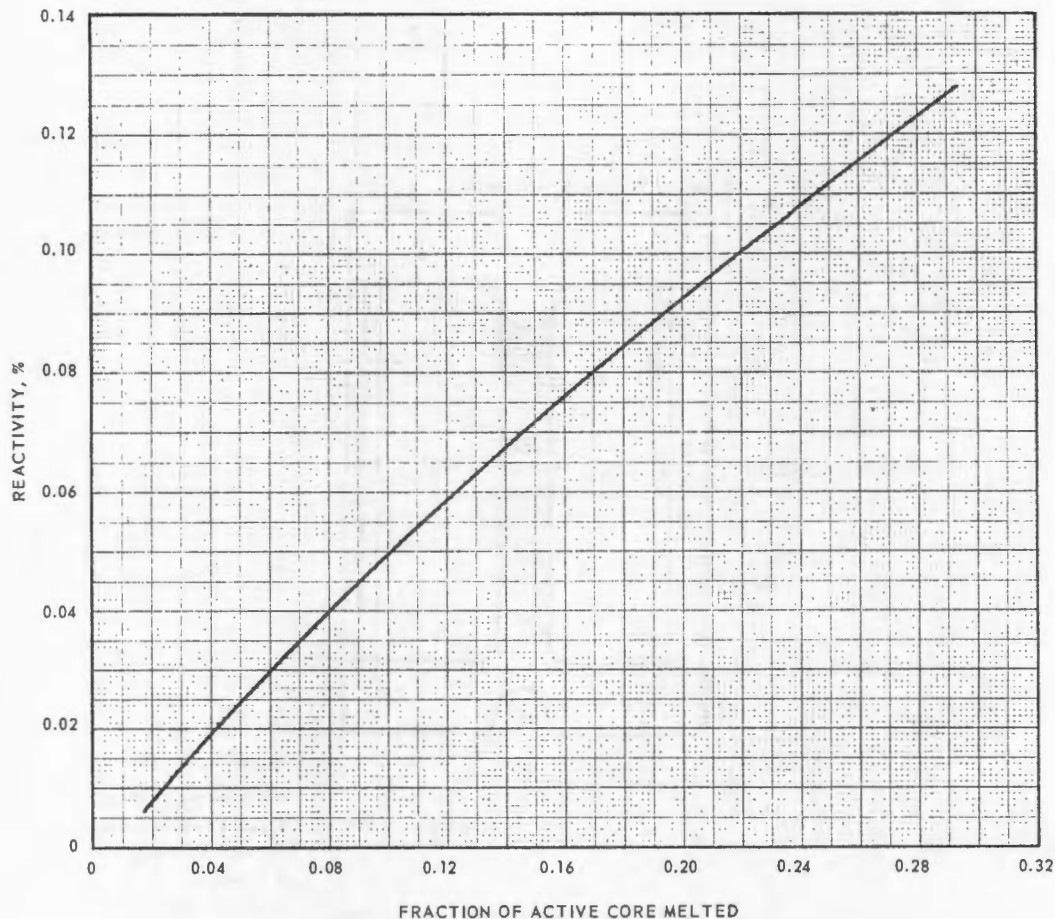
~~SECRET~~

Fig. 8.29 - Reactivity addition resulting from melting of active core and collapse of radial reflector onto melted fuel

Uranium-238 (U 238)

These are cross sections based on early attempts to include the effects of inelastic scattering and resonance absorption. The absorption integral is 500 barns as compared with 290 barns measured.

Yttrium (REV Y)

The total cross section came from BNL-325. The absorption cross section is taken to be $1/v$ with $\sigma_{2200} = 1.2$ barns. No high-energy effects are accounted for. The scattering cross section near thermal is about 1 barn lower than given in the second edition of BNL-325. Some resonance absorption is present (about 0.3 barns), which is ignored in these cross sections.

Oxygen (O)

This compilation assumes σ_a is $1/v$ and has no high-energy inelastic, anisotropic, elastic, or (n, α) absorption effects, all of which are present physically. The effect of ignoring these high-energy oxygen cross sections in BeO-moderated critical experiments has been found to reduce the calculated multiplication constant by about 1 percent.

~~SECRET~~~~CONFIDENTIAL~~

TOP SECRET

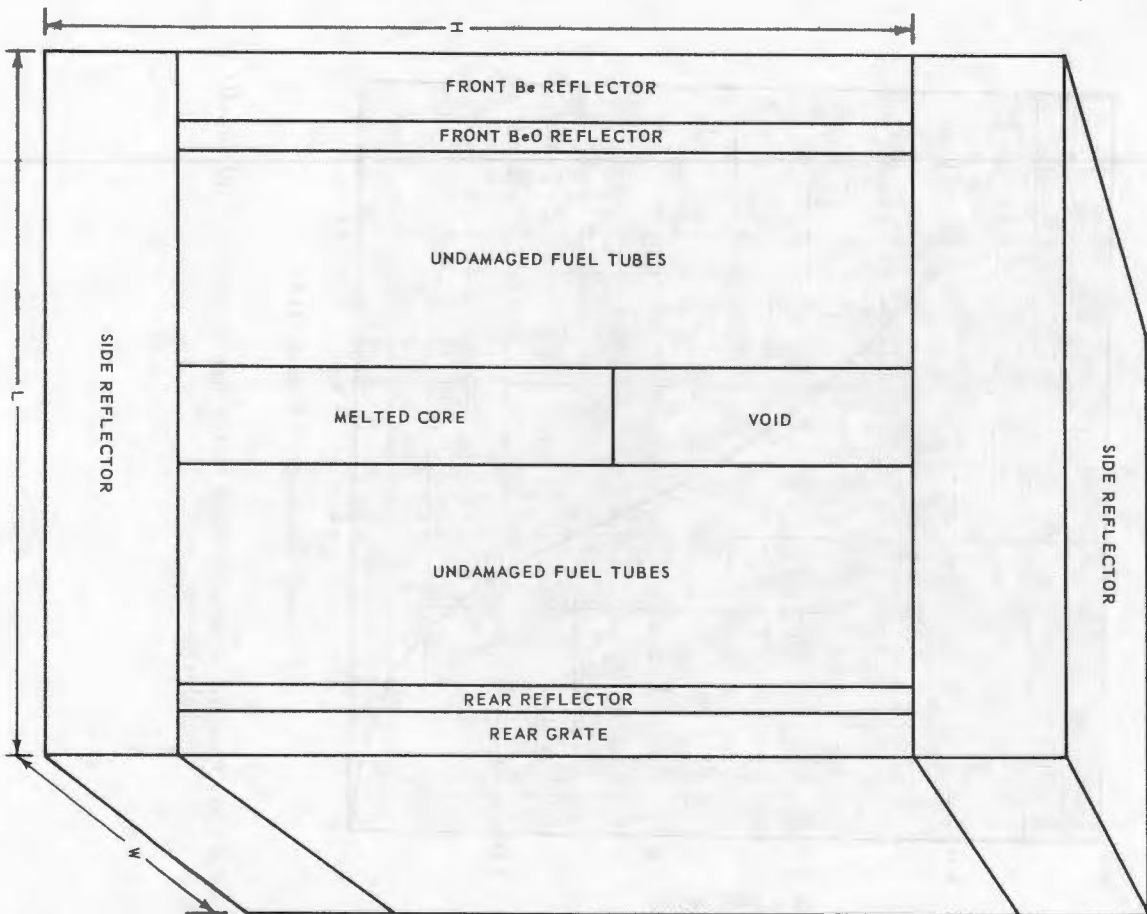


Fig. 8.30 - Nuclear model for no-collapse melt analysis

TOP SECRET

~~CONFIDENTIAL~~
~~SECRET~~

DECLASSIFIED

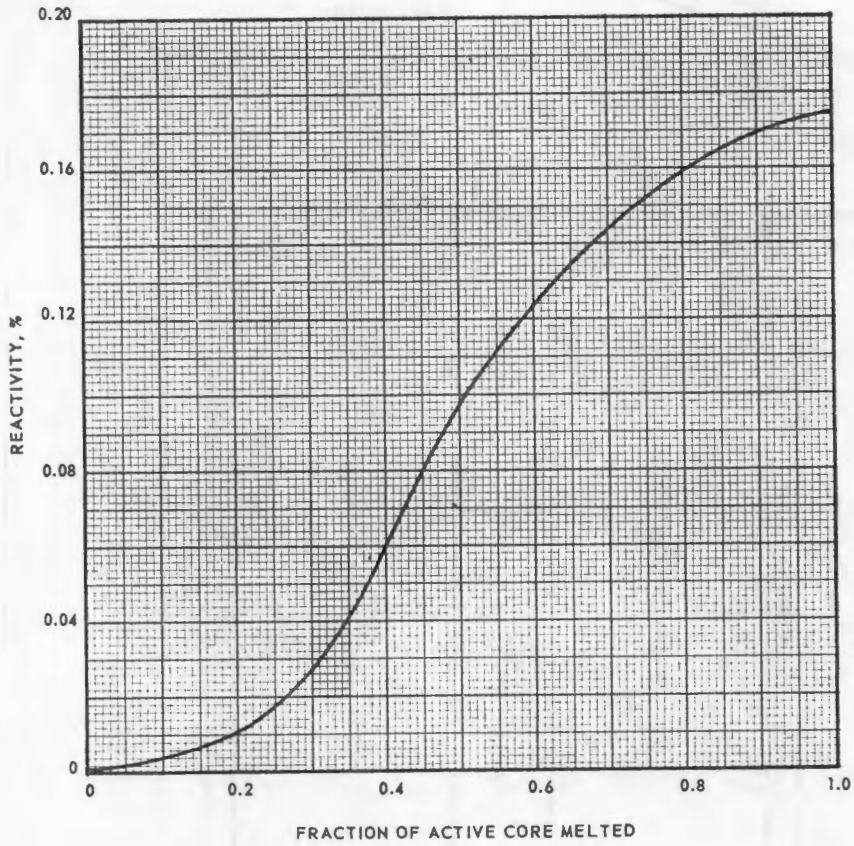


Fig. 8.31 - Reactivity addition resulting from melting of active core without collapse of radial reflector

DECLASSIFIED

SECRET

~~CONFIDENTIAL~~

8.6.3 SPECTRA

The prompt fission spectrum used for both U²³⁵ and U²³⁸ is a modification* of the original Watt spectrum and is given by

$$S(E) = 0.45270463 e^{-E/0.965} \sinh \sqrt{2.29 E},$$

where E is in Mev and S(E) is normalized to one neutron.

8.6.4 DELAYED NEUTRONS

The delayed neutrons are lumped into six delay groups. The spectra are based on data of Batchelor, Hyder, and Bonner and are described in APEX-458.† The delay fractions, β_j, and decay constants ω_j, contained in APEX-458 have been revised to an average of values due to fissions induced by slow neutrons and by fast neutrons.‡

Group	β _j	ω _j , sec ⁻¹
1	0.00023	0.0126
2	0.00142	0.0311
3	0.00126	0.1134
4	0.00264	0.3060
5	0.00080	1.253
6	0.00022	3.381

$$\beta = 0.00657$$

*L. Cranberg, G. Frye, N. Nereson, and L. Rosen, "Fission Neutron Spectrum of U²³⁵, Phys. Rev. 103, No. 3, August 1, 1956, 662.

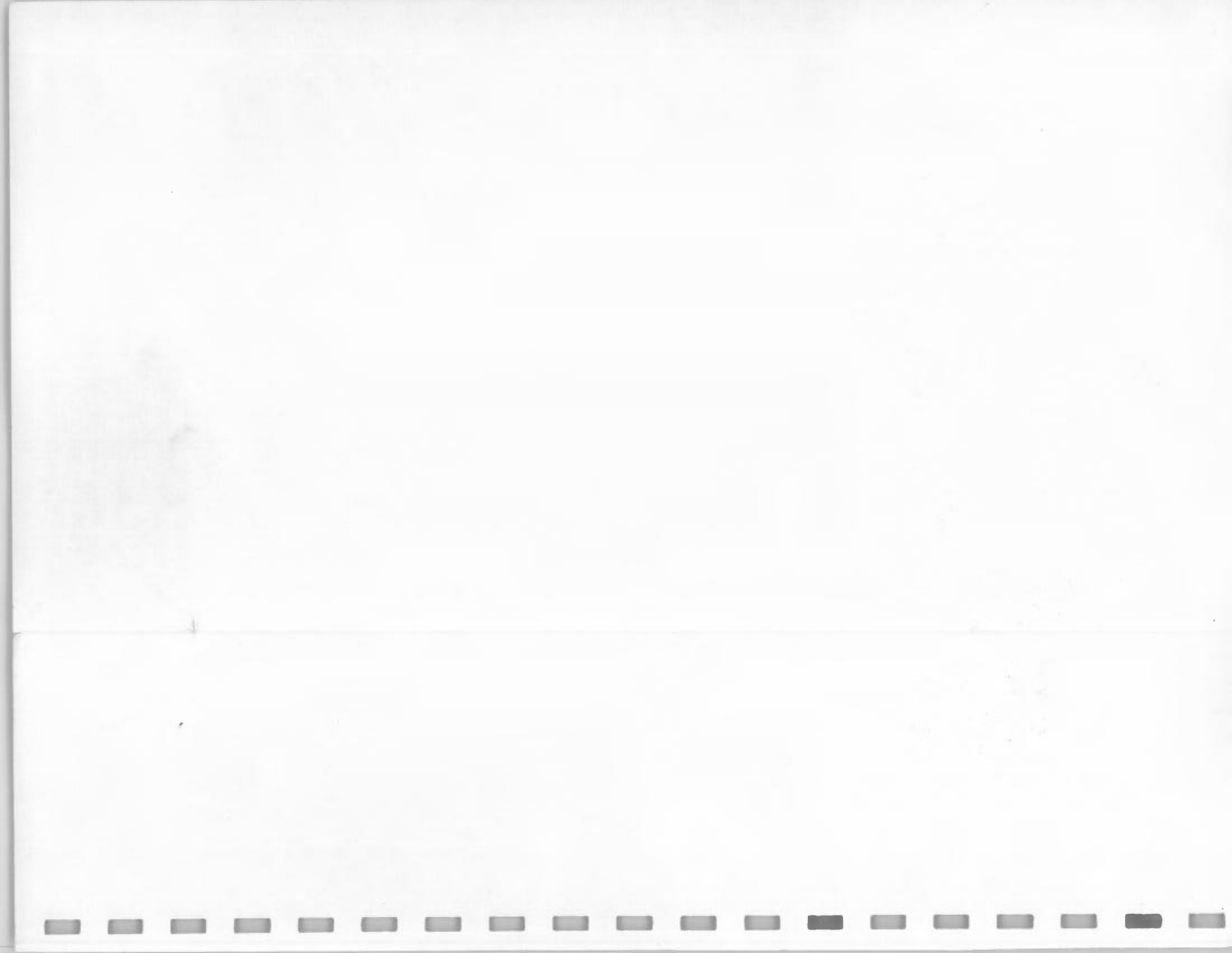
†B. H. Duane, R. E. Reid, and D. S. Selengut, "Off-Critical Reactor Theory," APEX-458, October 1956.

‡G. R. Keepin, T. F. Wimett, and R. K. Ziegler, "Delayed Neutrons from Fissionable Isotopes of Uranium, Plutonium, and Thorium," Phys. Rev. 107, 1957, 1044.

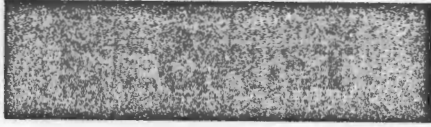
SECRET

CONFIDENTIAL

SECRET



~~CONFIDENTIAL~~

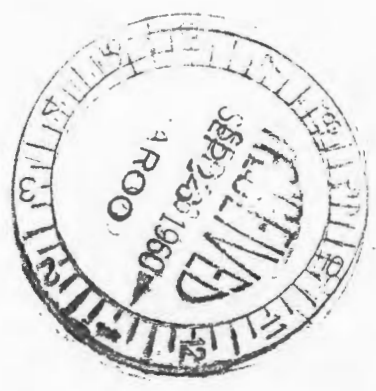


DECLASSIFIED

APEX-573

ATOMIC ENERGY COMMISSION

GENERAL INVESTIGATIVE DIVISION



DECLASSIFIED



~~CONFIDENTIAL~~